The application of ion mobility mass spectrometry to molecules of pharmaceutical significance

BY

Cristian Lewis Lapthorn (BSc)

A thesis submitted in partial fulfilments of the requirements of the University of Greenwich
for the degree of Doctor of Philosophy

April 2016

Department of Pharmaceutical, Chemical & Environmental Sciences
Faculty of Engineering & Science,
University of Greenwich, Medway Campus,
Chatham Maritime, Kent ME4 4TB, UK

UNIVERSITY
of
GREENWICH

DECLARATION

"I certify that this work has not been accepted in substance for any degree, and is not concurrently being submitted for any degree other than that of Doctor of Philosophy being studied at the University of Greenwich. I also declare that the work is the result of my own investigations except where otherwise identified by references and that I have not plagiarised the work of others."

Signed ………………………………………… Cristian Lewis Lapthorn (Candidate)

Date …………………………………………

MPhil/PhD Supervisors

Signed .... Prof. Frank. S. Pullen

Date ………………………………………….

Signed .... Prof. Babur. Z. Chowdhry

Date …………………………………………..

ACKNOWLEDGEMENTS

This thesis is dedicated to Jiyun and to my mother; words are not enough to express my feelings for everything you have given. This thesis is in honour of my departed and much missed father, who strove every day to give me and my siblings everything he could, and encouraged us to be the best we could be, supported with unconditional love.

ABSTRACT

Ion mobility-mass spectrometry experiments have been conducted to measure the drift-time and calculate collision cross-sections (CCSs) using travelling wave ion mobility spectrometry, and determine the CCS using drift-tube ion mobility spectrometry systems of analytes. The aim of the study was to identify if predictive approaches could facilitate rapid and definitive assignment of charge location sites and chemical structure. Molecular modelling was conducted to determine the energy minimised/geometry optimised structures and charge distribution of the protonated molecules studied. The geometry and charge distribution data were utilised in subsequent ion mobility calculations using two main methods 1) projection approximation and 2) trajectory method.

Fluoroquinolone antibiotics were investigated as previous literature had postulated the ion mobility separation of charge location isomers differing only by their protonation site with little expected difference in their geometry (see **Chapter 2**). Projection approximation prediction of theoretical CCSs (tCCSs) for the singly protonated molecules of norfloxacin (with the proton assigned to all possible oxygen or nitrogen-containing protonation sites to generate candidates) revealed <2 Å^2 difference in tCCSs based on molecular modelling. In stark contrast the experimental CCS (eCCS) demonstrated >10 Å^2 difference between different components. The product ion spectra are consistent with the hypothesis of charge location isomer mobility separated components. Investigations with other fluoroquinolones, with both drift-tube ion mobility and travelling wave ion mobility, and using the trajectory method, remain consistent with the hypothesis of charge location isomers (see **Chapter 3**).

A larger scale study sought to probe the accuracy of tCCSs over a large number of small molecule drug structures. If tCCSs accurately predict eCCSs, then tCCSs could be used to identify compounds and isomers based on their CCSs (see **Chapter 4**).

Finally, software was developed to considerably accelerate the calculation of trajectory method tCCSs from 8-100 times faster than existing published approaches depending on available computing infrastructure (see **Chapter 5**). In summary this research project has explored whether eCCSs and tCCSs may be useful as a key structural tool alongside other traditional measurements including chromatographic retention time and *m/z*.

CONTENTS

TABLE OF FIGURES

VIII

X

TABLES

ABBREVIATIONS

Abbreviation	Meaning
ACN	Acetonitrile
ADC	Analog-to-digital converter
CCS	Collision cross-section
CI	Chemical ionisation
CID	Collision-induced dissociation
CRM	Charge residual model
CV	Compensation voltage
Da	Dalton
DART	Direct analysis in real-time ionisation
DC	Direct current
DDA	Data directed analysis
DFT	Density functional theory
DOE	Design of experiment
DTIMS	Drift-time ion mobility spectrometry
DV	Dispersion voltage
eCCS	Experimental collision cross-section
EHSS	Exact hard sphere scattering
EI	Electron impact
EM	Electron multiplier
ESI	Electrospray ionisation
eV	Electron volts
h	hour
HPLC	High performance liquid chromatography
(g)	Gas
IEM	Ion evaporation model
IM	Ion mobility
IMS-MS	Ion mobility mass spectrometry
IMS	Ion mobility spectrometry
IR	Infra-red spectroscopy
LC	Liquid chromatography
MALDI	Matrix-assisted laser desorption/ionisation
MCA	Multi-channel acquisition
MCP	Microchannel plate
MD	Molecular dynamics
mg	Milligram
min	Minutes
mL	Millilitre
MRM	Multiple reaction monitoring
MS	Mass spectrometry
MS/MS	Tandem mass spectrometry
m/z	Mass-to-charge ratio
NMR	Nuclear magnetic resonance
oa-TOF	Orthogonal acceleration time-of-flight
PA	Projection approximation
PDB	Protein databank

PSA	Polar surface area
Q	Quadrupole
RF	Radio frequency
RMS	Root mean squared
SFC	Supercritical fluid chromtography
SIM	Selected ion monitoring
SRIG	Stacked ring ion guide
tCCS	Theoretical CCS
TDC	Time-to-digital converter
TICC	Total ion current chromatogram
T.M.	Trajectory method
TOF	Time-of-flight
T_R	Retention time
T-Wave	Travelling-wave
TWIG	Travelling-wave ion guide
TWIMS	Travelling-wave ion mobility spectrometry
UHPLC	Ultra high performance liquid chromatography
UPLC	Ultra performance liquid chromatography
V	Volts
XIC	Extracted ion count
μL	Microlitre

Other abbreviations are explained, where appropriate, in the text.

PUBLICATIONS

1. Published

Ion mobility spectrometry-mass spectrometry (IMS-MS) of small molecules: Separating and assigning structures to ions. *Mass Spectrom. Rev.,* 32, 43-71 (2013). Lapthorn, C., Pullen, F. and Chowdhry, B. Z.

Can ion mobility-mass spectrometry and density functional theory help elucidate protonation sites in 'small' molecules? *Rapid Commun. Mass Spectrom.,* 27 (21), 2399-2410 (2013). Lapthorn, C., Pullen, F., Chowdhry, B. Z., Dines, T., and Perkins, G.

How useful is molecular modelling in combination with ion mobility mass spectrometry for 'small molecule' ion mobility collision cross-sections? *Analyst*, 140, 6814-6823 (2015). Lapthorn, C., Pullen, F., Chowdhry, B.Z., Wright, P.A., Perkins, G. and Heredia, Y.

POSTERS PRESENTATIONS

1. **British Mass Spectrometry Society annual meeting,** Cardiff, Wales. 11-14 September 2011.

"How hot do you like it? Study of ripening processes and components in chilli peppers using DART ambient ionisation mass spectrometry", Cris Lapthorn, Babur Z. Chowdhry, Frank Pullen, and Pete Ryan.

2. **British Mass Spectrometry Society Ion Mobility Mass Spectrometry Special Interest Group inaugural meeting,** UCB Celltech, Slough, England. 16 April 2013.

"Ion mobility mass spectrometry of β-cyclodextrin and amino acid complexes: a study of inclusion complexes and electrostatic adducts", Yanira Ruiz Heredia, Cris Lapthorn, Frank Pullen, Babur Z. Chowdhry and George Perkins.

3. **British Society Mass Spectrometry Society annual meeting,** Eastbourne, England. 9 - 11 September 2013.

"Ion mobility mass spectrometry of β-cyclodextrin and amino acid complexes: a study of inclusion complexes and electrostatic adducts", Yanira Ruiz Heredia, Cris Lapthorn, Frank Pullen, Babur Z. Chowdhry and George Perkins.

4. **Schools of Engineering and Science, Medway School of Pharmacy and NRI Faculty Research Symposium,** University of Greenwich at Medway, Chatham, England. 13th June 2013.

"Ion mobility mass spectrometry of β-cyclodextrin and amino acid complexes: a study of inclusion complexes and electrostatic adducts", Yanira Ruiz Heredia, Cris Lapthorn, Frank Pullen, Babur Z. Chowdhry and George Perkins.

5. **EPSRC UK National Service for Computational Chemistry Software User Meeting,** Imperial College, London, England.

   11 December 2013.

"Integrating ion mobility mass spectrometry and molecular modelling for 'small' molecules", Cris Lapthorn, Frank Pullen, Babur Z. Chowdhry, Yanira Ruiz Heredia and Trevor Dines.

6. **British Mass Spectrometry Society annual meeting**, Astrazeneca, Alderley Edge, England.

   31 March-02 Apr 2014.

"The effect of charge location in ion mobility mass spectrometry for small molecule analytes", Cris Lapthorn, Mike McCullagh, Frank Pullen, Babur Chowdhry, Trevor Dines and George Perkins.

7. **American Society of Mass Spectrometry annual conference**, Baltimore, USA.

   15-19 June 2014.

"The effect of charge location in ion mobility mass spectrometry for small molecule analytes", Cris Lapthorn, Mike McCullagh, Frank Pullen, Babur Chowdhry, Trevor Dines and George Perkins.

8. **American Society of Mass Spectrometry annual conference**, St. Louis, USA.

   01-02 June 2015.

"Investigation of Ion Mobility Mass Spectrometry Analysis of Electrochemically Generated Oxidation Products of Opiates and Comparison with Theoretical CCS Value", Cris Lapthorn, Mark Taylor, Russell Mortishire-Smith, Jayne Kirk, Andrew Baker, Stefania Torres.

9. **American Society of Mass Spectrometry meeting**, St. Louis, USA.

   01-02 June 2015.

"The importance of charge isomers in quantitation; ion mobility mass spectrometry of fluoroquinolone antibiotics", Cris Lapthorn, Mike McCullagh, Sara Stead, Martin Palmer, Keith Richardson, Kevin Giles, Jasper Boschmans, Frank Sobott, Babur Chowdhry, George Perkins.

ORAL PRESENTATIONS

1. **Waters Innovations in Separation Science,** Leicester, England 21-22 June 2011.

 "New approaches to old problems: analysis of peptides, proteins, antibodies and oligonucleotides in Open Access"

2. **Waters Global Metabolite Identification Executive Technology Forum,** Milford, USA 20–22 September 2011.

"Innovation and the application of ion mobility-mass spectrometry to 'small-molecule' challenges"

3. **Waters Ion Mobility-MS future technology requirements and Ion Mobility-MS Knowledge Transfer and Networking meeting,** Manchester, England. 24-25 September 2013.

"How can 3D structure help you obtain a deeper understanding of MSMS pathways?"

4. **Waters Users meeting at the American Society for Mass Spectrometry meeting**, St. Louis, USA.
31 May 2015.

"Using 'small molecule' CCS from ion mobility mass spectrometry for ID and prediction"

5. **Waters Users breakfast meeting at the American Society for Mass Spectrometry meeting**, St. Louis, USA.
02 June 2015.

"The transformation of ion mobility and CCS technology into a core decision making tool"

6. **British Mass Spectrometry Society IMS-MS Special Interest Group meeting,** Liverpool, England.

07 July 2015.

"The importance of charge isomers in quantitation; ion mobility mass spectrometry of fluoroquinolone antibiotics"

7. **British Mass Spectrometry Society Annual Meeting,** Birmingham, England.

16 September 2015.

"'Using 'small molecule' CCS from ion mobility mass spectrometry for identification and prediction"

Chapter 1: Ion mobility spectrometry-mass spectrometry (IMS-MS) of small molecules: separating and assigning structures to ions

Based on the publication: *Lapthorn, C., Pullen, F. and Chowdhry, B. Z. Ion mobility spectrometry-mass spectrometry (IMS-MS) of small molecules: Separating and assigning structures to ions.*

Mass Spectrom. Rev., 32, 43-71 (2013)

1.1.   INTRODUCTION TO ELECTROSPRAY IONISATION

In 1882 Rayleigh postulated that as solvent evaporated the density of charges on the surface of a droplet reached a critical limit at which Coulombic repulsion would overcome the surface tension and smaller droplets would be formed from an explosion.[1] Theoretical and experimental studies of charged droplets from 1914-1917 demonstrated that charged droplets did break up as predicted.[2,3] Photographs show the breakdown in more detail, including the formation of a conical meniscus at the tip of the capillary predicted in 1964.[4] Electrospray ionisation (ESI) was first coupled to mass spectrometry in 1968[5,6] and developed to analyse macromolecules in the 1980s[7–10] The application of pneumatically-assisted electrospray further supported the use of LC-MS[11,12] enabling a wide range of compatible flow rates from liquid chromatography. In 1988 the observation of multiply charged ions in samples of polyethylene glycols[13] highlighted the potential for electrospray to be used to analyse large molecular weight species on an instrument with a relatively narrow *m/z* data acquisition range.

In typical modern uses of ESI an electric potential is applied between the capillary tip and the mass spectrometer interface and charged droplets are emitted when the charge repulsion exceeds the surface tension of the liquid at the Taylor Cone.[14] Charged droplets are typically attracted by an electric field potential or pulled by a vacuum towards the entrance of the mass spectrometer. The droplets undergo solvent evaporation and droplet fission until gas-phase analyte ions are produced (see Figure 1-1). There are two dominant theories proposed to explain how charged droplets become gas-phase ions called the Charge Residue Mechanism (CRM) and the Ion Evaporation Model (IEM).

In the CRM, the droplet size is believed to decrease as solvent evaporation occurs and charge repulsion increases. When the charge repulsion inside the droplet exceeds the surface tension, or the Rayleigh limit, then droplet fission occurs resulting in the formation of smaller droplets. This process continues until the analyte exists alone in droplets and the solvent evaporates.[5] The CRM is believed to be the primary mechanism for the creation of gas-phase ions from high molecular weight analytes.[15]

In the IEM, the droplet size is believed to decrease as solvent evaporation occurs and charge repulsion increases. The charge repulsion inside the droplet is believed to be sufficient to eject the analyte ions from the droplet into the gas-phase.[16–18] The IEM is believed to be the primary mechanism for small inorganic and organic ion production.[19–22]
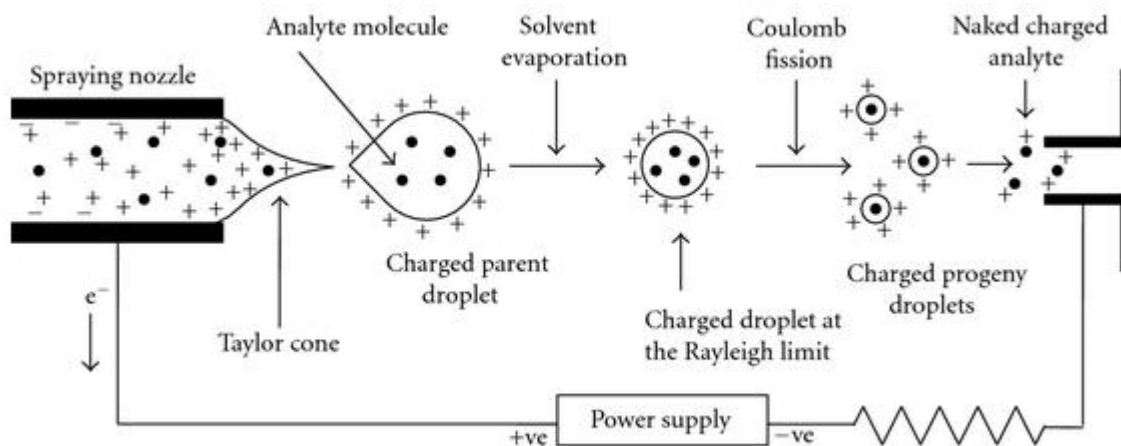
Figure 1-1. Schematic representation of the electrospray ionisation process (adapted from reference 14).

ESI –MS can be used to analyse polar analyte molecules from <100 Da to a 100 MDa virus capsid[23] using the ability to generate a distribution of multiply charged ions. Typically computer software is now used to transform multiply charged ion distributions to the zero charge state. ESI is a soft ionisation method so little fragmentation is typically observed and selective fragmentation is typically performed using collision-induced dissociation (CID) to aid structure elucidation.[24]

The sensitivity using ESI-MS includes attomole-level detection limits[25] for large molecules and reduced flow rates are often advantageous in reducing sample consumption and further increasing sensitivity.[26] Quantitative measurements are usually carried out using hyphenated mass spectrometry approaches including high performance liquid chromatography, capillary electrophoresis and supercritical fluid chromatography and by measuring the relationship between the instrument response and the analyte concentration.[27] Fortunately there are a number of methods to improve sensitivity and selectivity[27] and ESI-MS is commonly used to record quantitative measurements in forensic toxicology,[28] pharmacokinetic studies,[29] proteomics[30,31] and in food and environmental screening.[32]

1.2 INTRODUCTION TO IMS

The existence of ions in the gas-phase was first discovered when investigating changes in the electrical conductance of air[33] which had previously been thought to be an electrical insulator. Further work established the generation of ions by UV emissions and X-rays from work by Thomson and Rutherford[34], Roentgen[35] and Rutherford[36]. The rudimentary scientific tools available at the time did not allow a comprehensive understanding of ion behaviour but the behaviour of simple gas-phase ions in a weak electric field was further elucidated by Langevin[37], who demonstrated that air was a mixture of gases and developed models that described these simpler systems remarkably well.

Thomson and Aston later developed the first mass spectrometer[38] and further research focussed on low pressure studies of ion-molecule systems that, although not directly involving typical ion mobility pressure regimes, accrued knowledge in the behaviour of ion motion in a partial vacuum.

The rapid uptake of ion mobility spectrometry (IMS) in military and forensic applications[39] benefited from the relatively high proton affinity of the analytes (chemical warfare agents, explosives and illicit drugs), low detection limits and miniaturisation of IMS instrumentation. IMS instrumentation was re-designed for the field, using internal calibrant standards and simplified user interfaces, which allowed their use by non-scientist military and security personnel. IMS instrumentation is now ubiquitous in handheld forensics, cleaning validation and military applications (from border control to explosive testing in war zones).

Separation in IMS occurs rapidly, in milliseconds, rather than seconds as in chromatography, so IMS is now beginning to be recognised as a powerful separation step which can be utilised post-ionisation using a range of equipment. It also benefits from robust day-to-day operation and allows size and shape separation and measurement of analytes that cannot easily be derived using other techniques. Miniaturisation, primarily demonstrated so far in overtone IMS and microfabricated Field Asymmetric IMS (FAIMS), is a highly attractive feature and IMS typically has a low detection limit of nanograms and does not require expensive and environmentally damaging solvents.

1.3. INTRODUCTION TO IMS-MS

The most important aspect of the combination of an IMS separation (typically occurring in the millisecond time-frame) and MS detection (typically occurring in the microsecond time-frame) is that it allows an additional separation step to be obtained on a MS time-frame (*e.g.* in addition to liquid chromatography), without compromising the speed of MS detection.

The work of McDaniel and Martin[40], Kebarle and Hogg[41], Albritton *et al.*,[42] and later Crompton and Milloy[43] developed the recognisable configuration of linear drift-tube IMS (DT-IMS). The combination of ion mobility and mass spectrometry allowed more complex studies to be conducted in order to develop models of ion mobility.

IMS was first hyphenated to a mass spectrometer by Barnes, McDaniel and Martin[44] using a magnetic sector mass spectrometer; subsequently McAffee and Edelson[45] described hyphenation to a time-of-flight (TOF) MS. The coupling of IMS with a TOF mass spectrometer is particularly appropriate because the TOF mass spectrometer has the fastest data acquisition rate of any mass spectrometer and can acquire many spectra on the microsecond scale whilst the IMS analytes arrive in a millisecond timescale.

A review by Hill *et al.*[46] describes the early development of IMS-MS with significant contributions and discoveries including those from Bowers, Kemper, Clemmer and Kebarle. IMS has since been interfaced to quadrupole mass spectrometers[47,48], quadrupole ion traps[49] linear ion traps and Fourier-transform ion cyclotron mass[50] which is beneficial in terms of a wider linear dynamic range and increased mass spectral resolution. Clemmer *et al.*,[51] and Creaser *et al.*,[49] also reversed the stages to produce a MS-IMS design that traps and stores ions in an initial quadrupole ion trap for subsequent ion mobility measurements which has the advantage of pre-concentrating low abundant components.

Recently IMS has been hyphenated to mass spectrometry systems, and the availability of commercially supported instrumentation has arguably led to a rapid increase in the number of publications on IMS-MS, as shown in Figure 1-2. FAIMS, a type of differential mobility spectrometry, originated in Russia in the early 1980s[52] emerged as an analytical tool[53] and was later commercialised by Ionalytics (Selectra, 2003), as a front-end accessory for MDS Sciex (Concord, Ontario, Canada) mass spectrometer systems (2004), Thermo FAIMS, (2007) and Owlstone Nanotechnologies FAIMS. Waters Inc. (Milford, MA) introduced the first generation Synapt Triwave travelling wave IMS system in 2006 and updated with a second

generation instrument with improved resolution (G2, 2009), improvements to sensitivity (G2S, 2011) and new data acquisition and informatics (G2S*i*, 2013). Sciex launched the SelexION ion mobility device in 2011 for their triple quadrupole mass spectrometer and quadrupole-trap mass spectrometer and Agilent brought out the 6560 IMS-MS system in 2013. In 2015, Waters Inc. launched their Vion IMS-MS system with an alternative configuration with the quadrupole following the IMS cell.
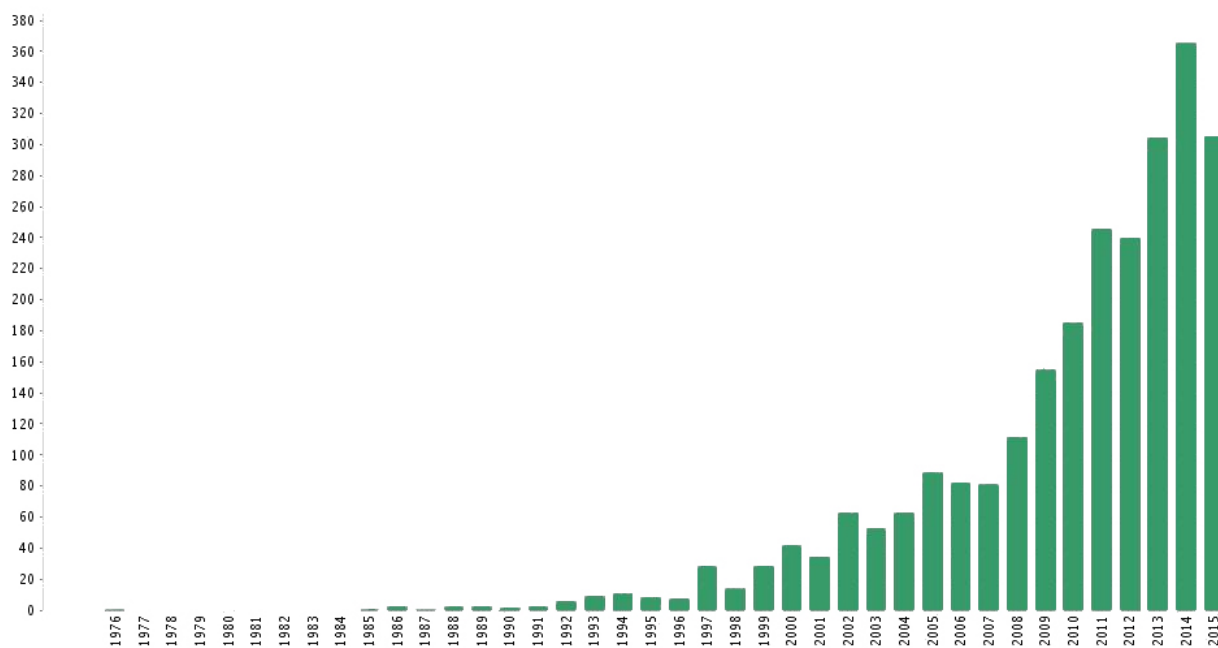
Figure 1-2. Chart showing the published items each year including the term "ion mobility" and "mass spectrometry" in the topic from Thomson Reuters Web of Science.

There has been limited recognition of the potential of IMS-MS analysis for Lipinski's 'rule-of-5' small molecules[54] instead of traditional IMS analyte classes (*e.g.* explosives, chemical warfare and illicit drugs). The historical lack of interest and sporadic periods of development in IMS-MS for small molecule applications seems most likely to be due to perceived poor resolution, strengths in competing chromatographic techniques and weaknesses in the robustness of IMS regarding a poor linear range[55], "memory effects" from contamination[56] and interference from matrices.

In contrast IMS-MS has been applied to biomolecules including peptides[57], proteins (60 kDa-150 kDa) and large protein complexes (1- 4 MDa)[58] particularly after the application of non-covalent mass spectrometry conditions to IMS-MS. The use of these especially gentle electrospray ionisation conditions is believed to maintain the weak (cooperative) molecular

interactions present in many biomolecular structures and thus avoid fragmentation. Whilst IMS-MS typically lacks the resolution (1% error or 10 nm^2) of X-ray crystallography or NMR spectroscopy for large molecular weight biomolecules it does enable analysis of smaller amount of material, it also allows analysis of structures >100 kDa that are difficult to analyse by NMR spectroscopy and is, arguably, as realistic an environment as X-ray crystallography structures due to lattice effects present. IMS-MS has, therefore, been utilised as a tool to probe the stabilisation of proteins in the presence of ligands and metals (as a unique method of metal speciation),[59] protein-protein-interactions, protein mutants and their structural consequences, as well as protein unfolding *via* various means of ion activation.[60] In addition to detailed understanding of individual biomolecular systems, IMS-MS has also been applied to more high-throughput analytical approaches including screening of phosphorylated peptides[61], identification and separation of chemically cross-linked peptides[62] and combining topology in protein substructures with proteomics data .[63] This review focuses on small molecule applications.

1.4.   DIFFERENCES IN PERFORMANCE OF IMS-MS AND IMS

1.4.1. The ion efficiency and resolution challenge

Some of the key differences between IMS and hyphenated IMS-MS include the pressure regime in the ion mobility cell, the size of the instrument and the typical ionisation source. Whilst specifications and performance in IMS may be indicative of those in IMS-MS there are some technical reasons why this may not follow. It is critical to note that the results may well be different in IMS-MS compared to IMS due to sensitivity issues and pressure regime changes from IMS to MS stages.

In IMS-MS there are often two main challenges, (i) to utilise all the ions from the ionisation source, (especially in a pulsed IMS separation such as drift-time IMS, but not a challenge in DMS or FAIMS which typically have a 100% duty cycle if a single transmission voltage is selected) and (ii) elimination of all neutral species whilst ensuring transmission of ions to the MS stages to maintain sensitivity. Traditionally DT-IMS-MS sensitivity has been estimated to be inversely proportional to the IMS resolving power squared; ion losses at the IMS exit aperture ranging from 99 to 99.9%[64] and ion introduction losses being between 99.6 to 99.9% [65]. The desire to increase the gas pressure in the DT-IMS cell to increase resolution must therefore be balanced with the possibility that it may well reduce ion transmission by

requiring a reduction of the aperture size in the interface from IMS to MS. The different pressure regimes in IMS systems are described in Table 1-1.

Table 1-1. A comparison of required resolving power in theoretical plates for various types of IMS compared to typical chromatographic conditions.

Type of IMS system	Pressure regime	Typical operating pressure
Ambient DT-IMS	Ambient pressure	1000 mbar[46]
Reduced pressure DT-IMS	Reduced pressure	10^{-5} to 1.3 mbar[66,67]
FAIMS or DMS	Ambient pressure->ambient pressure	400 to 1571 mbar[68]
Travelling wave IMS	Reduced pressure	0.5 mbar (Waters Synapt G1) to >3 mbar (Waters Synapt G2) [69]
Differential mobility analysis	Ambient pressure	1013 mbar

For DT-IMS-MS the drift gas pressure must be increased proportionally to electric field strength in order to maintain a low E/N ratio ($<2 \times 10^{-17}$ Vcm^2), required to obtain field-independent mobilities for which the simplified Mason-Schamp equation[70] holds:

$$K = (3q/16N)(2\pi/\mu kT)^{1/2} 1/\Omega \qquad (1)$$

Where K is the ion mobility, q is the ionic charge, N is the buffer gas density, μ is the reduced mass of the buffer gas and the ion, k is the Boltzman constant, T is the temperature and Ω is the collision cross-section (CCS).

For Travelling Wave Ion Mobility-MS (TWIMS-MS) the gas pressure must also be increased proportionally to the electric field, such that:

$$K = K_o N_o / N = K P_o T /(P T_o) \qquad (2)$$

where K is the ion mobility, N is the buffer gas density, N_o is the Loschmidt number (the value of N at standard temperature (T_o = 273K) and pressure (P = 1 Atm)) and K_o is the reduced ion mobility.

Approaches to maximise IMS-MS sensitivity include utilising quadrupole and octopole ion traps[49,71,72] and electrodynamic ion funnels[73] to accumulate and introduce ions efficiently from the ion source to increase the sensitivity of DT-IMS. Multiplexing approaches including Hadamard[74] and Fourier-type[75] gating techniques have also been utilised for increasing the sensitivity of DT-IMS, by increasing the frequency of ion injection events and thus increasing the quantity of ions injected into DT-IMS by up to 50%. Most of these approaches have been integrated into full IMS-MS systems with dramatic improvements in sensitivity.

There is some uncertainty in the identification of the ions in their transmission through the IM cell and it seems clear that hyphenating IMS and MS allows a more comprehensive understanding of the ionisation processes and fragmentation pathways in IMS. For example, when using a radioactive ^{63}Ni cell, proton transfer to the analytes should lead to protonated monomer and dimer ions; however, without a mass spectrometer as the detector, the identification of the ions in the ion cell cannot be unambiguously ascertained. Indeed, a comparison of limonene and 2-nonanone by IMS and IMS-MS resulted in a variety of unexpected fragments and ions, resulting in a non-trivial IMS spectrum and making interpretation of the results difficult[76]. Any unambiguous identification of ions in IMS will be important both in structural measurements (size, shape and topology) and for comparison of related IMS techniques (*e.g.* TWIMS-MS) that often use historical DT-IMS-MS data as calibration standards in ion mobility and CCS calculations.

1.5.   FEATURES OF IMS TECHNIQUES UTILISED IN IMS-MS

IMS-MS potentially provides a number of advantages over and above IMS including:

1. A rapid gas-phase separation step before mass spectrometry analysis.

2. Identification of ions subsequent to characteristic drift times by comparison with data acquired under comparable conditions.

3. Measurements of CCSs and derivation of further information about size and shape, either by comparison with computational modelling or by analysis within a series of compounds.

4. Better characterisation of ion and ion-neutral ion mobilities by simultaneous acquisition of mass spectrometry data.

5. Better characterisation of ionisation[77] and fragmentation pathways *via* a better understanding of gas-phase ion structures.

IMS has been hyphenated to high performance liquid chromatography, gas chromatography[78,79], supercritical fluid chromatography[80,81], ions produced *via* matrix-assisted laser desorption/ionisation[82], desorption electrospray ionisation[83], pulsed corona discharge ionisation[84] (Hill and Thomas, 2003) and miniaturised to microchip scale[85].

IMS-MS systems are typically composed of four stages (Figure 1-3):

1. An ion source (*e.g.* matrix-assisted laser desorption ionisation (MALDI) or electrospray (ESI)) that generates ions.

2. An IMS cell, where charged particles migrate under the influence of an electric field.

3. A mass analyser, typically a time-of-flight (TOF) mass spectrometer which is designed to allow a fast acquisition rate and large mass detection range.

4. An ion detector.
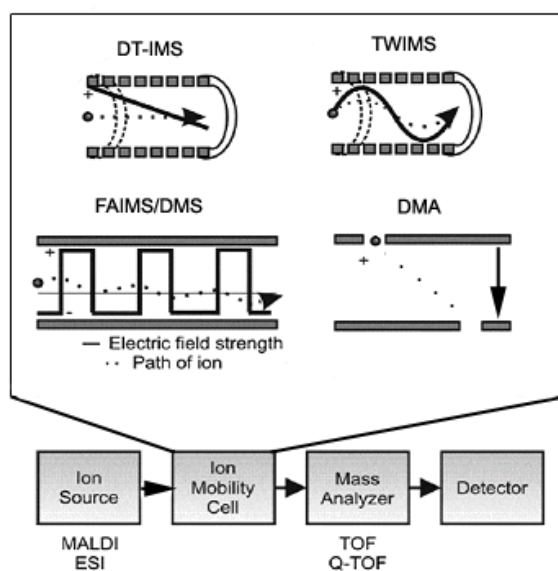
Figure 1-3. Overview of typical ion-mobility mass spectrometer configurations (adapted from reference 86).

There are four main types of IM cell utilised in IMS-MS.

1. Drift-time IMS (DT-IMS) is the simplest configuration where CCS can be directly calculated without calibration and provides the highest resolving power. A tube is filled with a buffer gas (or mixture) and a low voltage field is applied, typically from 5 to 100 Vcm⁻¹. The ions collide with neutral buffer gas molecules, exit *via* a detector, and the CCS Ω_T, at a temperature T can be obtained by measuring the velocity of the ions and solving the Mason-Schamp equations at intermediate electrical fields (5-100 Vcm⁻¹):

$$V_d = KE \qquad (3)$$

where V_d is the drift velocity of the ion, K is the ion mobility, E is the imposed electric field, and:

$$\Omega_T = \left(\frac{3ze}{16N} \right) \left(\frac{2\pi}{\mu kT} \right)^{1/2} \left(\frac{1}{K} \right) \qquad (4)$$

where z is the numerical charge, e is the elementary charge, N is the number density of the buffer gas, μ is the reduced mass of the ion-buffer gas neutral pair, k is the Boltzmann constant and T is the temperature in Kelvin.

DT-IMS suffers from an inherent lack of sensitivity, due to a pulsed analysis (where ions are measured in packets), and the subsequent loss in duty cycle, as the time between packets of ions is not utilised. A review of IMS[87] discusses the history of IMS, the chemistry and physics of ion behaviour and reflects on the potential future development and applications of IMS.

In linear DT-IMS, illustrated in Figure 1-4, the sample is introduced to an ionisation region where ionisation can take place by a number of methods including β-emission from a ⁶³Ni corona discharge, photo-ionisation, electrospray *etc*. Ions are allowed through an electric shutter grid, whilst neutrals remain in the ionisation source and the measurement time is initiated. The drift tube can vary in length from 5 centimetres to

11

3 metres or more. An electric field gradient, typically from 10-100 Vcm^{-1}, from the ionisation source to the detector causes the ions to traverse the drift tube at a constant velocity. A drift gas is introduced counter-current to the flow of ions keeping the drift-tube free of neutrals which could participate in ion-neutral clusters.

Ionisation region   Drift region   Detector

Drift Gas
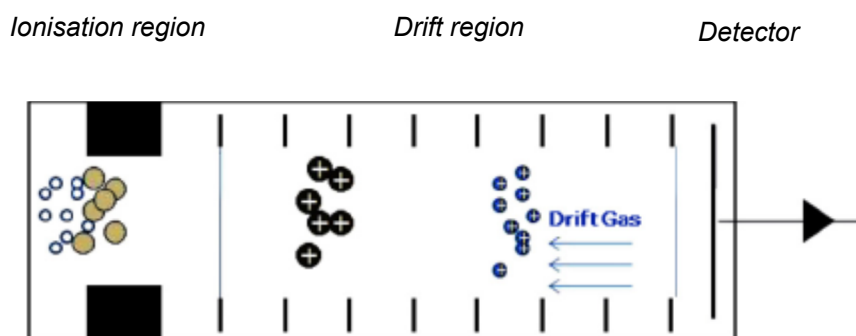
Figure 1-4. Illustration of DT-IMS where a voltage gradient is applied to the ions from left to right (adapted from reference 87).

The total ion signal is detected and plotted with respect to time to form an ion mobility mobilogram, *e.g.* (see Figure 1-5) for a mixture of amphetamines analysed by ESI-DT-IMS-MS.[88] Smaller ions travel faster through the drift region and have shorter drift times, compared to higher molecular weight ions that drift slower and possess longer drift times.
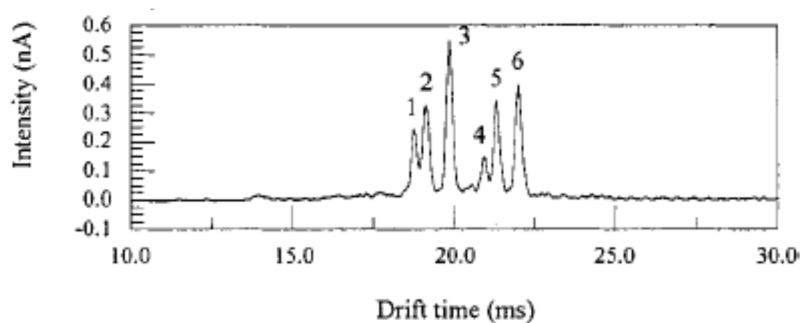
Figure 1-5. ESI-DT-IMS-MS mobilogram of a mixture of 1) amphetamine, 2) methamphetamine, 3) ethylamphetamine, 4) 3,4-methyldioxyamphetamine, 5) 3,4-methylenedioxy methamphetamine, and 6) 3,4-methylenedioxyethylamphetamine (adapted from reference 88).

Another complementary approach to classical DT-IMS-MS was the use of the second quadrupole (Figure 1-6) in a triple quadrupole mass spectrometer as an ion mobility device; while this approach was never commercialised it did open up opportunities in hyphenation of IMS and MS. In the triple quadrupole energy loss method an incident ion is transmitted to the second quadrupole of a triple quadrupole mass spectrometer where the ion will experience a drag coefficient and generate a stopping curve; from the stopping curve the ion mobility can be measured and a CCS determined. Indeed, Covey and Douglas were the first to measure CCSs for some biomolecules using this method[89] and also later reviewed collision dynamics in quadrupole systems including an assessment of the internal energy of the $C_6H_5^+$ ion by measuring the increase in CCS after collisional activation[90].
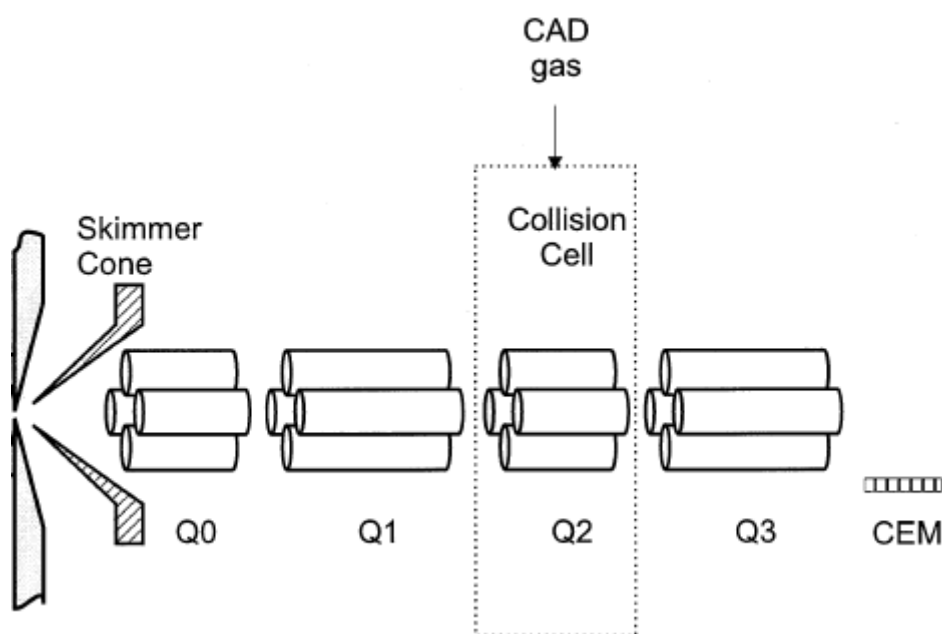
Figure 1-6. Schematic of the triple quadrupole configuration that can be used to obtain ion mobility measurements *via* an energy loss method (adapted from reference 91).

This triple quadrupole energy loss method was further developed to utilise segmented collision cell rods separated by small 1 mm gaps that enabled a radio-frequency only quadrupole drift cell to be used to reduce ion losses due to diffusion and enable mass selection before or after the drift cell, and a DC gradient that moved the ions in an axial direction (see Figure 1-7). Unfortunately this configuration was outside the typical low-field IMS range and may have resulted in field-heating of ions. This configuration was

later improved to possess an increased gas pressure and lower field concentration that resulted in minimal internal excitation of the ions[92].
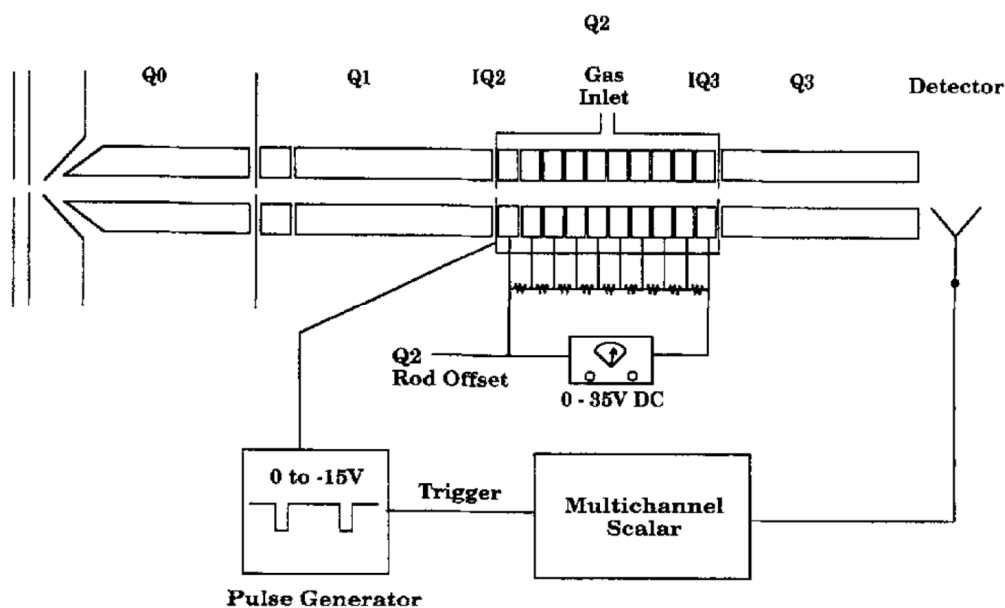
Figure 1-7. Schematic of a segmented triple quadrupole configuration that can be used to obtain ion mobility measurements (adapted from reference 91).

2. Differential mobility IMS (DMS) or FAIMS uses a sequence of intermediate and high field regimes where the behaviour of ions is described empirically by the Mason-Schamp equation[70] under a high-field regime, which can be expanded to an infinite series of E/N:

$$K_0(E) = K_0(1 + a(E/N)^2 + b(E/N)^4 + c(E/N)^6 + ...) \qquad (5)$$

where K_0 is the reduced ion mobility, E is the electric field intensity and N is the buffer gas number density. However, under a typical FAIMS electric field the mobility can be approximated by using the first two factors as the importance of the sixth order and higher are insignificant (the fourth order is two orders of magnitude smaller than second order, and the second order is three to five orders of magnitude smaller than one[93].

The basic principle of operation is that ions are introduced to a region with electrodes and a stream of gas acts as a transport medium. An asymmetric waveform is passed across the electrodes, which consists of a high potential electric field for a short time followed by a low potential electric field for a longer time; this typically fixed dispersion voltage (DV) waveform is superimposed with a variable compensation voltage (CV) to maintain a stable trajectory for the analyte ion. This process will effectively select ions and act as an ion filter, as shown in Figure 1-8. A cylindrical electrode configuration has usually been designated FAIMS, whereas parallel plate configurations have typically been designated as DMS.
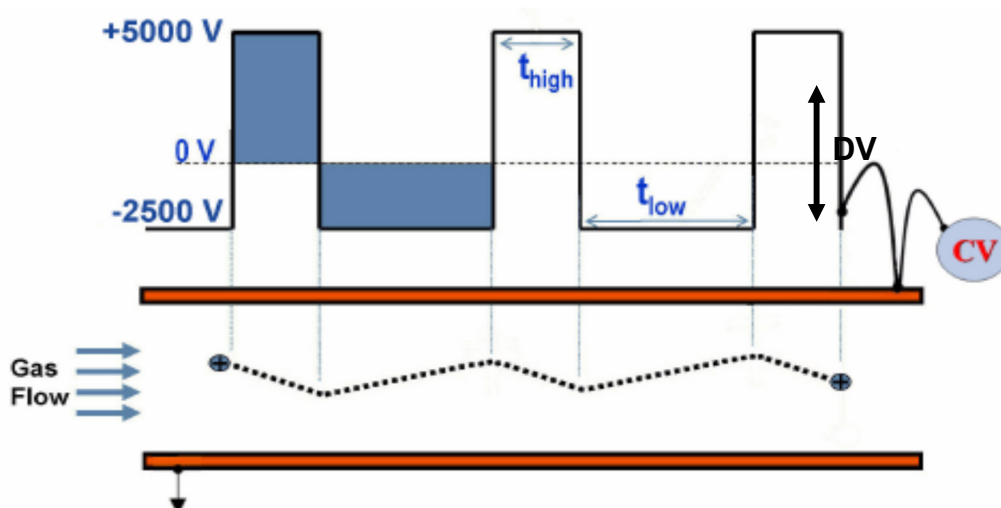
Figure 1-8. Illustration of an example of a parallel plate DMS with compensation voltage applied showing ion transmission (adapted from reference 94).

A compensation voltage scan measurement (Figure 1-9) shows a typical profile attained by optimising the effect of inner and outer electrode temperatures on peak profile for morphine and its 3-β-D-glucuronide metabolite.[95] Optimising the separation of morphine whilst maintaining sensitivity was reported to enable the metabolite interference to be effectively filtered out, and significantly improve the quantification of morphine.

15
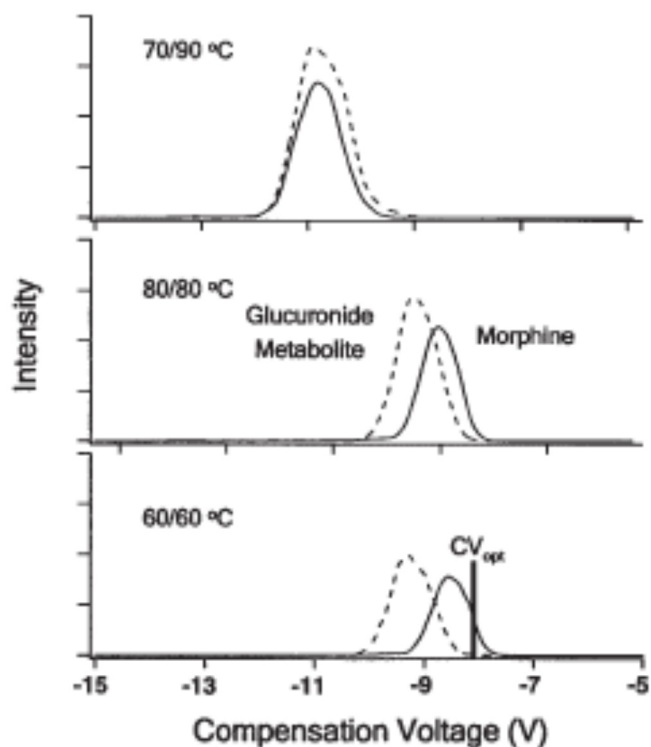
Figure 1-9. Compensation voltage scans of morphine and the glucuronide metabolite (adapted from reference 95).

The use of compensation voltage optimisation to select an analyte ion can result in a clear difference in the mass spectrum observed resulting in an increased S:N ratio for the analyte and a reduction in other signals as shown in the use of ESI-FAIMS-MS with cisplatin and its hydrolysis products[96] shown in Figure 1-10.

(a)   (b)
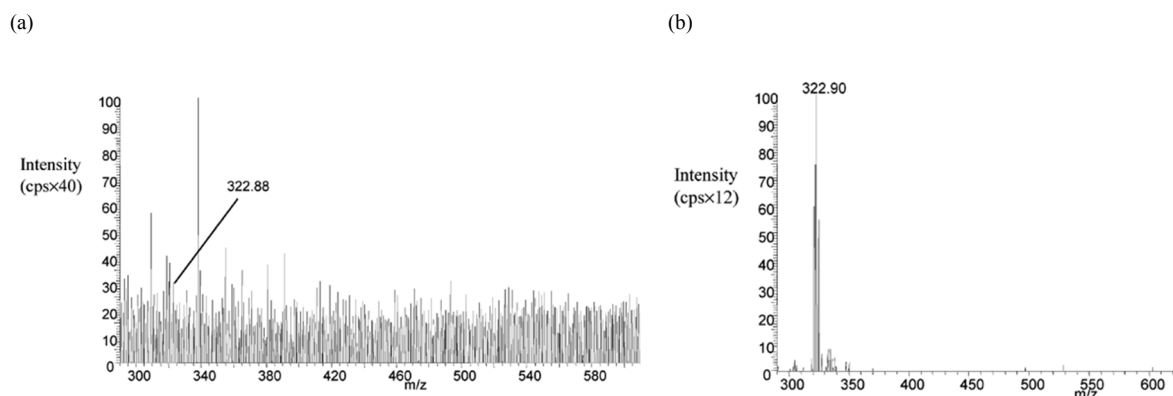
Figure 1-10. Positive ion mass spectra showing the reduction in background noise and increase in signal:noise from (a) ESI-MS to (b) ESI-FAIMS-MS (adapted from reference 96).

Currently the factors determining the separation mechanism in FAIMS or DMS and factors governing peak width as well as transmission remain relatively difficult to predict.[93] The parameters influencing performance include field intensity, ion path length, gas properties (composition, temperature, pressure), shape and width of electrodes, the profile and frequency of asymmetric waveform, compensation voltage scan speed and gas flow. The separation of trace level impurities by combining experimental observation with a Design of Experiment (DOE) statistical treatment indicated important factors in the optimisation of the values of the compensation voltage, signal intensity, separation, peak asymmetry and peak width[97]. However, a study of tetraalkylammonium ions found standard conditions were often suitable for selecting ions with a range of *m/z* 100-700 units[98]. The simulation of ion motion in planar electrode FAIMS and cylindrical electrode FAIMS, provided insights into design, experimental variables and interpretation[99] and some of the key molecular and instrumental parameters affecting performance have been reviewed.[100,101]

Whilst there are several novel geometries[102], there are two main forms of field asymmetrical waveform ion mobility spectrometers: 1) those with planar electrode geometry and 2) those with curved electrode geometry. Both planar geometry and the curved geometries of FAIMS and DMS evolved during the 1990s, and in the early 1990s the term differential mobility spectrometry (DMS) became generally synonymous with planar electrodes and the term FAIMS became synonymous with curved geometries, although there are multiple examples of overlapping usage of the terms DMS and FAIMS. One of the primary differences relates to the use of polar transport gas modifiers. Planar devices create homogeneous electric fields which enables the use of transport gas modifiers without resolution losses whereas curved geometries tend to create inhomogeneous fields which lead to a loss in resolution when using transport gas modifiers. However, curved geometries have been shown to provide some degree of ion focusing at atmospheric pressure resulting in higher sensitivity.[103,104] Planar line-of-sight analysers enjoy the convenience of transmitting all ions when the RF voltages are turned off, so that operation without mobility separation can be achieved simply by turning off the fields. Curved geometry/non line-of-sight FAIMS, in contrast, require the device to be removed for operation without mobility separation.

A comprehensive review discussed the applications of FAIMS for drinking water analysis, pharmaceutical metabolite identification and separation of isomers and isobaric peaks.[68] In addition a detailed account of the fundamentals of DMS and FAIMS has been written.[105]

3. Travelling wave ion mobility spectrometry (TWIMS) is a method whereby ions are separated according to their mobility in a series of voltage pulses in a travelling wave (T-wave) mobility cell utilising RF ion guides.[106] The resolving power is relatively low; however, CCSs can be derived by calibration with known standards. This ion mobility approach has been successfully interfaced to a conventional time of flight mass spectrometer and, due to the trapping gates and fast data acquisition rate of the TOF, good sensitivity is achieved. Despite attempts[99,107] the motion of ions in TWIMS is not fully understood and calibration is typically used to calculate CCS values. The commercial technical and software support has arguably reinforced attempts to utilise IMS-MS in separation, characterisation and measurement applications, for example, *via* the routine use of multidimensional data in Waters Driftscope software[108] and additional software to process complex data such as time-aligned parallel fragmentation.[109]

In travelling wave ion mobility spectrometry a transient DC voltage pulse is applied in order to create an electromotive force *via* a series of sequentially opposite polarity RF-only rings to create a travelling wave which propels ions through the device, as shown in Figure 1-11. Ions with high ion mobility slip behind the wave less often (or spend more time surfing) than ions of low ion mobility thus enabling separation based on relative ion mobility.
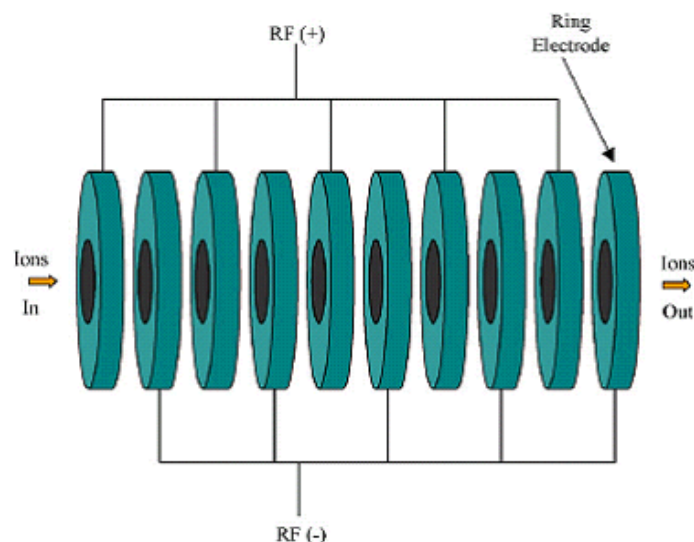
Figure 1-11. Illustration of a stacked ring ion guide used in traveling wave ion mobility spectrometry (TWIMS) (adapted from reference 110).

Visualising data obtained using the proprietary Driftscope software enables a range of options for understanding the data including 3D visualisation, 2D plots and intensity views *etc.* The data can be interactively processed if desired, for example, to show data that only contains a certain component using various geometric selection tools such as lasso and square area.

4. The Differential Mobility Analyser (DMA) was originally developed to generate particles in order to calibrate aerosol instruments, later expanded to describe the mobility of non-diffusing particles[111] and recently to describe the mobility of diffusing particles.[112] The DMA consists of a combination of electric field mobility in addition to a fast gas stream, only ions with a well-defined electrical mobility are transmitted into an outlet slit leading to the mass spectrometer inlet (see Figure 1-12). The DMA vacuum regime means that the measured ions do not experience a vacuum interface or ion guide so may be less prone to structural modifications[113] and, as the separation technique is a space-dispersion rather than a time-dispersion technique, the ions can be continuously transmitted to a mass spectrometer.
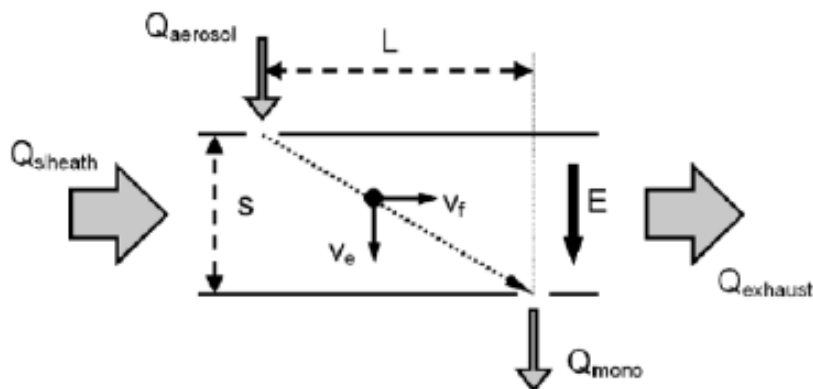
Figure 1-12. Schematic of the operation of a differential mobility analyzer. Ion are injected at the top left and move downwards and to the right, over a distance S, under the influence of an electric field E (adapted from reference 114).

The DMA technique may be considered a hybrid of DT-IMS and DMS as the separation process is based on the low electric field mobility like DT-IMS, however the sampling is continuous as in DMS. DMA-MS has been most widely explored for large molecules; however, discussion on multiple charged polyethylene glycol ions[115] illuminated structures from approximately *m/z* 300-3000 units describing configurations for long straight chain molecules. One of the advantages of DMA is that it can, theoretically, be easily added to existing mass spectrometry stages without complex interfaces due to operation at atmospheric pressure[116]. A DMA was coupled to an existing Sciex QStar MS (Concord, ON, Canada) enabling separation of L-alanine and an isomer, sarcosine[117], which are proposed to be small molecule biomarkers from urine in the progress of prostate cancer.

IMS covers a range of different techniques and unfortunately some gross simplifications have resulted in terminology that may be confusing.

1. DT-IMS is also known as Classical IMS, Conventional IMS, Standard IMS, Drift-Tube IMS, Time of flight IMS, Traditional IMS, Plasma Chromatography and Ion Chromatography.

2. DMS includes High Field Asymmetric Waveform IMS (FAIMS), Field Ion Spectrometry and Ion Mobility Spectroscopy and is commercialised in the Ionalytics Selectra, Thermo FAIMS, Owlstone Nanotechnologies and AB Sciex Selectra systems.

3. Travelling wave ion mobility spectrometry (TWIMS) is commercialised in the Waters Synapt and Vion systems.

4. Differential Mobility Analysers (DMA) have been developed by several groups at Yale (USA), CIEMAT (Madrid) and RAMEM (Madrid).

Comparison of key benefits and challenges of IMS-MS methods

There is currently a wealth of IMS-MS systems available both commercially and being used and developed in academic institutions, a summary of advantages and disadvantages is shown in Table 1-2.

Table 1-2. A comparison of the advantages and disadvantages of different types of ion mobility spectrometry

	Drift-time IMS	**Travelling-wave IMS**	**FAIMS**
Collision cross section determination	Direct through Mason-Schamp equation[70]	Only after calibration using relevant samples[107]	None
Orthogonality of separation to *m/z*	Low	Low	High
Resolving power	>100 $\Omega/\Delta\Omega$[73]	~45 $\Omega/\Delta\Omega$[69]	~100 $\Omega/\Delta\Omega$[118]
Pressure	10^{-5} to 1000 mbar[46,66,67]	0.5 mbar (Waters Synapt G1) to >3 mbar (Waters Synapt G2)[69]	400 to 1571 mbar[68]
Field strength	<1000 V/cm[119]	Varies during motion, typically <1000 V/cm[120]	>10 000 V/cm[121]
Typical gases utilised	He, Ar, N_2	He, Ar, N_2, CO_2	He, Ar, N_2, CO_2, H_2

DT-IMS-MS has been most widely used in academic institutions and provided some of the highest resolving powers. An advantage of DT-IMS-MS is that the ion mobility can be determined experimentally and collision cross-section determined without requiring calibration. A key challenge is that the pulsed analysis leads to an inherent loss of duty cycle and hence reduction in sensitivity.

An advantage of both DMS-MS and FAIMS-MS is that it operates as a continuous device when the compensation voltage is selected so does not have the inefficient sampling issues of DT-IMS and TWIMS. The separation appears to be orthogonal to *m/z* and sometimes size so that separations may be uniquely tuned to select a chosen analyte and thus be used as a powerful separation technique. A key challenge is that it has proven difficult to definitively assign structural properties and changes to DMS measurements as several factors appear to contribute to the clustering/de-clustering mechanism and analyte drift times thus it appears to be best utilised as a separation device.

An advantage of TWIMS-MS is that it is commercially supported and that the ion mobility can be determined experimentally and CCS determined with suitable calibration. Whilst the resolution obtained in TWIMS is typically lower than dedicated DT-IMS-MS and some FAIMS/DMS the software to interpret and process the complex data is well supported.

Advantages of DMA-MS include operation in the low electric field regime that typically means less structural distortions and determination of CCSs, a continuous sampling rate that should mitigate sensitivity losses (with reported transmission efficiencies of up to 50%[117] and the theoretical ability to add the device as a front-end to many existing mass spectrometer systems. However DMA-MS has not been fully commercialised yet or utilised for the multitude of small molecule applications explored in DT-IMS-MS, FAIMS-MS, DMS-MS and TWIMS-MS though it shows significant promise.

1.6.   UNDERSTANDING IMS-MS RESOLVING POWER AND SELECTIVITY

IMS can separate analytes based on their ion mobility including closely related species such as isomers,[122] isobars and isotopomers[123]. The key parameters affecting a useful separation are 1) the resolving power and 2) the selectivity.

Resolution and peak capacity in IMS

The combination of ion mobility and mass spectrometry in IMS-MS offers a technique that is able to distinguish components based on their size to charge ratio (Ω/z for IMS) and mass to charge ratio (*m/z* for MS), thereby enabling orthogonal specificity. Even with expensive high-resolution mass spectrometer systems affording mass resolution of over 400,000 it is still analytically challenging to differentiate between isomeric components and often complex MS[n] experiments are required to achieve selectivity for unambiguous assignment. Ion mobility can provide extra resolving power, however IMS used alone is currently unable to unambiguously identify an unknown molecular component without *a priori* knowledge of the measured drift time.

It is possible to measure the resolving power of ion mobility using a single quotient definition[124];

$$R = dt \, / \, wh \qquad (6)$$

where *R* is the resolving power of the IMS, *dt* is the drift time of the ion of interest and *wh* is the full peak width measured at half height. Resolving power is a measure of the efficiency of an instrument to separate two peaks. The Waters Synapt G2 IMS system has been developed to encompass a resolving power of up to 40; FAIMS resolving powers of up to 100[118] have been achieved, and several reports of resolving powers of up to 225 with DT-IMS have been reported[125–127]. Developments including higher pressure trapping and focussing.[128] overtone ion-mobility[129] and circular instruments[130] are expected to exceed these current limitations.

The number of theoretical plates is a mathematical concept, relevant in any chromatographic technique, which is often used to describe column efficiency and is an indirect measure of the peak width for a peak at a specific retention time:

$$N = 5.545 \left(\frac{t_R}{W_h} \right)^2 \qquad (7)$$

where N = number of plates, t_R = retention time and W_h = peak width at half height (in units of time). The number of theoretical plates is typically used to compare chromatographic systems and the data in Table 1-33 compares various types of IMS with typical traditional chromatographic techniques.

Table 1-3. A comparison of required resolving power in theoretical plates for various types of IMS compared to typical chromatographic conditions.

Approximate number of theoretical plates	Required resolving power of equivalent IMS	Comparative chromatography conditions
20000	60	High performance liquid chromatography (HPLC)
80000	120	Ultra high performance liquid chromatography (UHPLC)
125000	150	Gas chromatography (GC)
222000	200	High resolution IMS[48]
887000	400	Capillary electrophoresis (CE)

Therefore, a current high-resolution IMS resolving power of 200 is roughly equivalent to a chromatographic efficiency of >200,000 theoretical plates.

Peak capacity of IMS-MS

Complex samples require high efficiency to achieve separation and, even in early stage drug discovery, having a high efficiency affords a good opportunity to separate degradants and process impurities away from the desired product. Peak capacity is defined as the maximum number of peaks that can fit in any two-dimensional method.[66] A two-dimensional method will have a high peak capacity if the resolution of each dimension is high and the difference in their separation mechanism (orthogonality) is high. The peak capacity will also be defined by the complexity of the sample and the properties of the analytes in the sample. For example, complex biological samples with a range of retention times will provide larger peak capacities for a technique than that of the analysis of a mixture of analytes of a specific class.

Peak capacity is therefore a better, but highly molecule dependent, indicator of the separation power compared to measuring resolution alone.

In an ideal situation the peak capacity of a two-dimensional method is the product of the first and second dimensions,[131] but corrections can be made for cases where the two dimensions are not 100% orthogonal. Whilst the separation based on their size to charge ratio (Ω/z for IMS) and mass to charge (m/z for MS) ratio is, to some extent, orthogonal there is a well-known correlation between mobility (approximately proportional to size) and mass.[132]

The corrected peak capacity, P_c, in IMS-MS can theoretically be estimated[133] using the relationship:

$$P_c = R_{IMS} \times R_{MS} \times \textit{fraction of orthogonality} \qquad (8)$$

where R_{IMS} is the average resolving power of the ion mobility spectrometer, and R_{MS} is the average resolution of the mass spectrometer.

An example of increased peak capacity in IMS-MS was observed in a study of various classes of metabolites in blood[133] (including amino acids, organic acids, fatty acids, purines *etc.*) using a DT-IMS-MS system. In the range of m/z 23 – 830 units, the drift time spread of ~14.3 ms results in ~28% of the total 2D space, or an average deviation in drift time of ±14% along the theoretical trend. With an average IMS resolving power of 90, average MS resolution of 1500, and ±14% orthogonality, the estimated peak capacity, Pc, for the instrument is 90 x 1500 x 14% = 18,900. The relatively low MS resolution of 1500 (peak width is 0.27 *m/z* at an average *m/z* value of 404) in this study resulted in an estimated peak capacity of MS alone of 2989. A six fold increase in the peak capacity was therefore observed (~19,000) in IMS-MS compared to MS alone (~3000).

Reversed phase chromatographic columns are routinely used to separate small molecules and the peak capacity for gradient elution high performance liquid chromatography[134] was found to be typically up to 300 and up to 400 for gradient elution ultra-performance liquid chromatography.[135] Comparing the peak capacity for different types of IMS with typical traditional chromatography peak capacities (Table 1-4) shows that the extra dimension of IMS is potentially a powerful separation tool.

Table 1-4. Approximate separation peak capacity for various analytical separation methods, where ion mobility and hyphenated techniques are italicised.

Technique	Approximate peak capacity
FAIMS[136,137]	*8.9-44*
DT-IMS[133]	*90*
HPLC[134]	300
UHPLC[135]	400
MS[133]	3000
IMS-MS[133]	*19000*
HPLC-MS	900000
HPLC-IMS-MS[133]	*11340000*

It is conceivable that HPLC-IMS-MS may become a standard addition or replacement for HPLC-MS systems due to the ease of configuration and the increase in separating power. Indeed many proteomic applications are increasingly using HPLC-IMS-MS to separate complex peptide mixtures, leading to unprecedented extensive proteome maps.[138,139] HPLC-IMS-MS often does not require careful configuration, demanding sampling rates and does not appear to suffer from robustness issues compared to many two-dimensional techniques such as LC x LC, GC x GC *etc*.

Modifying selectivity in IMS

The selectivity of ion mobility can be modified by increasing the electric field in DT-IMS,[48] the use of covalent shift reagents[140] to derivatise[141] or use non-covalent adducts/shift reagents[142–144] to form complexes with analytes and effect a selective shift in ion mobility relative to coincident analytes, using drift gas modifiers[145] (sometimes called clustering agents in DMS-MS[137]) by altering the composition of the drift gas[88,144] and by the use of different reagent gases in GC-IMS-MS.[146] Currently there does not appear to be a consensus on useful and well characterised selectivity modifiers so method development is presently not fully predictable; however some of these changes are trivial and can be considered analogous to changing the stationary or mobile phases in liquid chromatography.

The use of covalent shift reagents[140], as shown in Figure 1-13, effectively derivatises molecules, potentially creating lower density analogues of the precursor species with a marked increase in the CCS relative to a smaller increase in mass. This is clearly illustrated by deviations to larger cross-sections compared to the general trend in mass-mobility correlation for carbohydrates. Compared to the underivatised species, it was reported that covalent derivatisation afforded three distinct advantages: (i) tuneability was increased for isobaric species difficult to identify and/or resolve by mass spectrometry alone, (ii) an enhanced sensitivity of 2x more signal intensity was observed and (iii) the derivatised species could be used as tags or fragment labels in CID and as IR active species in IRMPD studies.
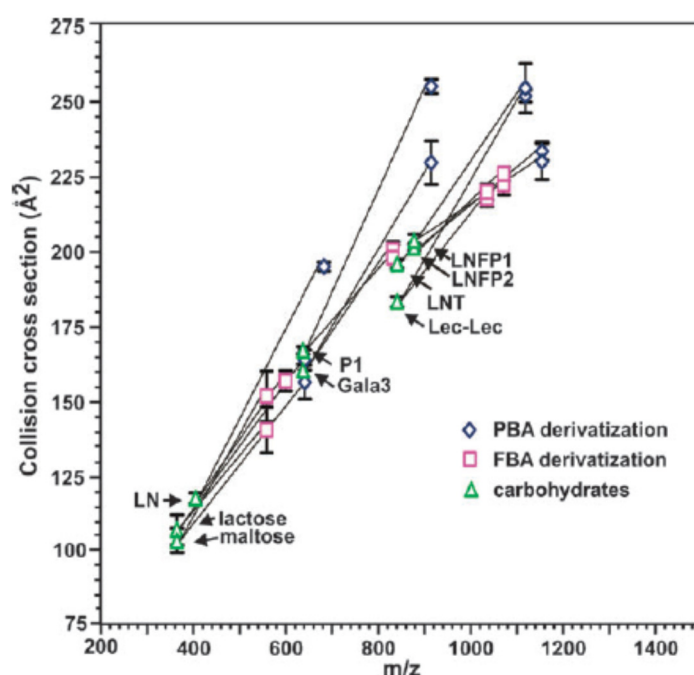
Figure 1-13. Effect of derivatisation of carbohydrate species with boronic acid on CCS (adapted from reference 140).

For small molecules the effect of the dipole interaction is typically far more significant than for larger molecules (>m/z 500) so that using drift gas modifiers or mixtures can be a powerful method to alter selectivity (elution order of analytes). Indeed for small molecules such as amino acids the polarisability has been found to be a critical factor affecting separation of analytes, whereas in large molecules the collision cross-section term appears to dominate.[147,148] Thus, for small molecules exploiting polarisability to probe structural details and maximise separation has immense future potential.

An example of the potential of exploiting polarisability to separate analytes is given by the different slopes of calculated ion radii for iodoaniline and chloroaniline with different drift gases, helium (0.205×10^{-24} cm^3), argon (1.641×10^{-24} cm^3) and carbon dioxide (2.911×10^{-24} cm^3), indicating that it should be possible to separate any analytes with different slopes (Figure 1-14) by choosing an appropriate drift gas composition.
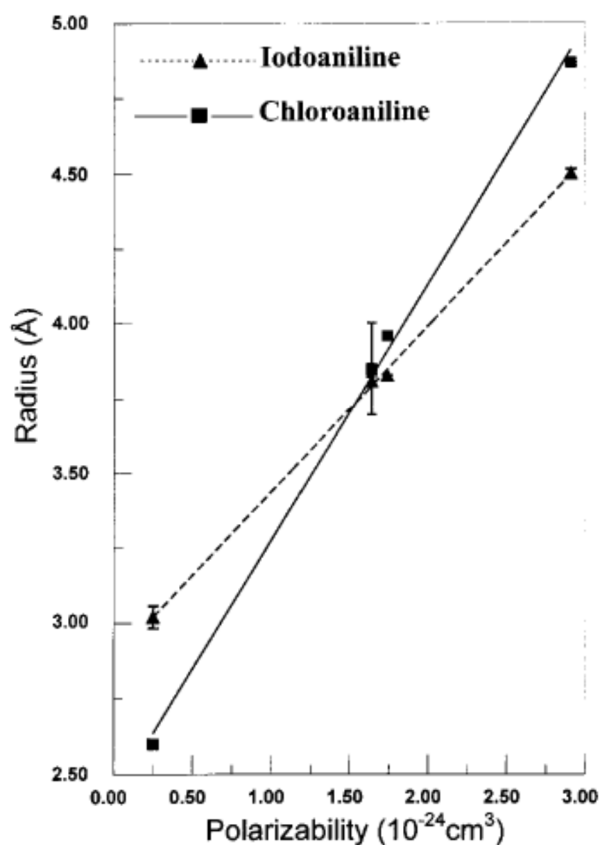
Figure 1-14. Calculated ion radii as a function of drift gas polarisability (adapted from reference 149).

The use of vapour modifiers added to the drift gas in planar DMS-MS has been widely explored[87,101] although the full mechanism of the interactions has not been elucidated enough to enable predictable separations in mixtures. A series of publications exploring cluster/declustering[137,150–153] further explored the possibility of predicting analyte shifts in response to changes in drift gas modification and provide a powerful route to optimising separations.

The 'cluster/declustering effect' that addition of vapour modifier induces appears to have dramatic effects on the peak capacity in a planar electrode configuration[137], improving the peak capacity for a 70 component mixture from 13 in pure nitrogen to 44 in 2-propanol doped nitrogen (see Figure 1-15), although this had the disadvantage that 10/70 components were depleted in intensity by 20-fold or more due to them having a lower proton affinity than the dopant.
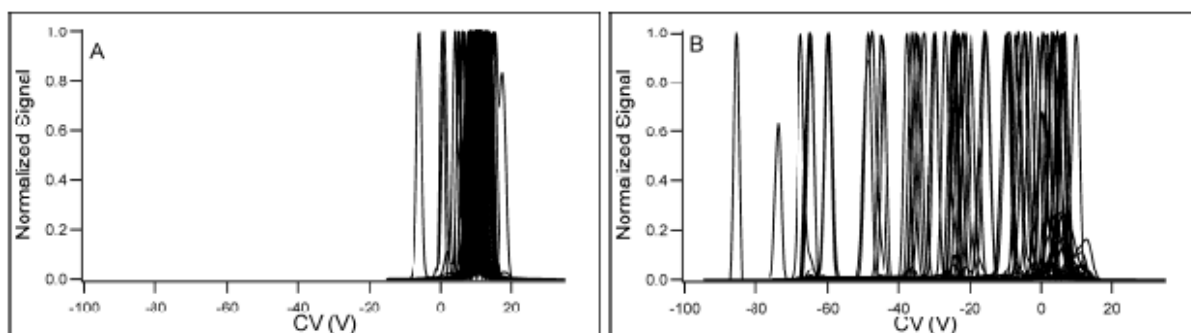
Figure 1-15. Separation of a 70-compound mixture with (A) nitrogen transport gas and (B) nitrogen with 1.5% 2-propanol in parallel plate FAIMS configuration (adapted from reference 137).

Changes to the temperature, composition[154] and pressure of a single drift gas is commonly used to change selectivity and IMS gases including nitrogen, air, helium, carbon dioxide and sulphur hexafluoride have been evaluated. The use of binary gas mixtures[141], shown in Figure 1-16, results in excellent selectivity enhancements over single gas composition IMS separations and demonstrates that this selectivity is tunable by altering the binary gas composition.
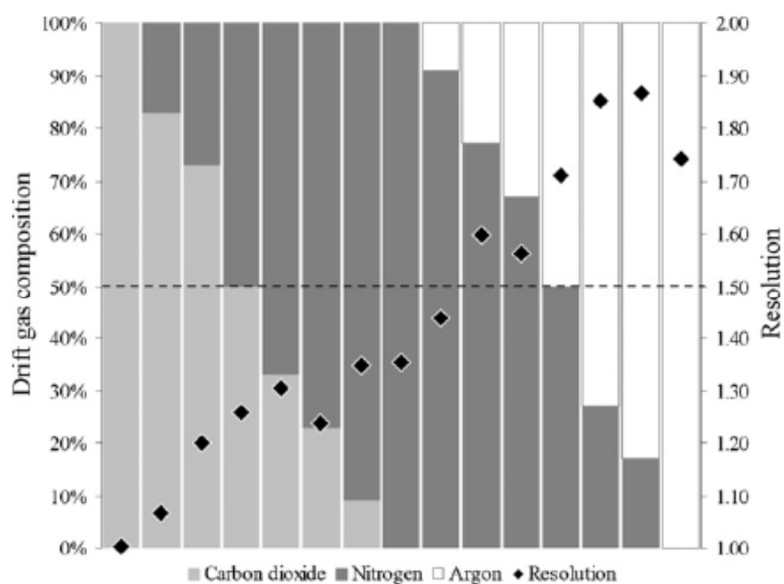
Figure 1-16. Effect of drift gas composition on the ion mobility resolution of the drugs rosiglitazone and lamotrigine $[M + H]^+$ ions in binary drift gas mixtures in TWIMS. The composition of the binary drift gas mixtures are represented by shaded bars indicating the percentage of each gas in the mixture (left hand axis). Resolving powers greater than 1.5 indicate full separation of components and this threshold is indicated by the dashed line at a resolution of 1.5. The resolution of lamotrigine and rosiglitazone is indicated by the right hand axis (adapted from reference 141).

1.7. APPLICATIONS OF IMS AND IMS-MS SEPARATIONS IN SMALL MOLECULE ANALYSIS

IMS has been investigated for the analysis of a wide range of small molecule applications including active pharmaceutical ingredients,[155–158] veterinary drugs,[159] metabolites,[160] pesticides,[161–163] prescription and illicit drugs,[164,165] combinatorial libraries[166], autonomous health diagnostics[167,168] and immunoassay detection.[169,170] Here some highlights of small molecule analysis using IMS-MS systems are outlined.

1.7.1. Low abundance metabolite and small molecule identification using IMS-MS

A novel use of LC-IMS-MS was demonstrated for a 5HT$_3$ antagonist, ondansetron, and its aromatic hydroxyl isomeric metabolites[171] that are typically generated *in vivo* and *in vitro*. Using conventional UHPLC-MS-MS the unambiguous characterisation of the hydroxyl metabolites would not be possible as they can produce identical MS/MS spectra. Using UHPLC-MS in a biological matrix system ondansetron and metabolites display different

retention times but could not be assigned without using purified standards as a reference. Using an IMS separation, shown in Figure 1-17[71], and *in silico* methods the components were identified based on their ion mobility. For these components a low number of rotatable bonds are present so the computational method is rapid, interpretation of complex NMR spectra is not required and isolation or synthesis is unnecessary to create primary standards. In this case the identity of metabolites with smaller than 1Å^2 difference between their CCS was distinguished using a Waters Synapt TWIMS by comparison with CCS values obtained using computational methods.
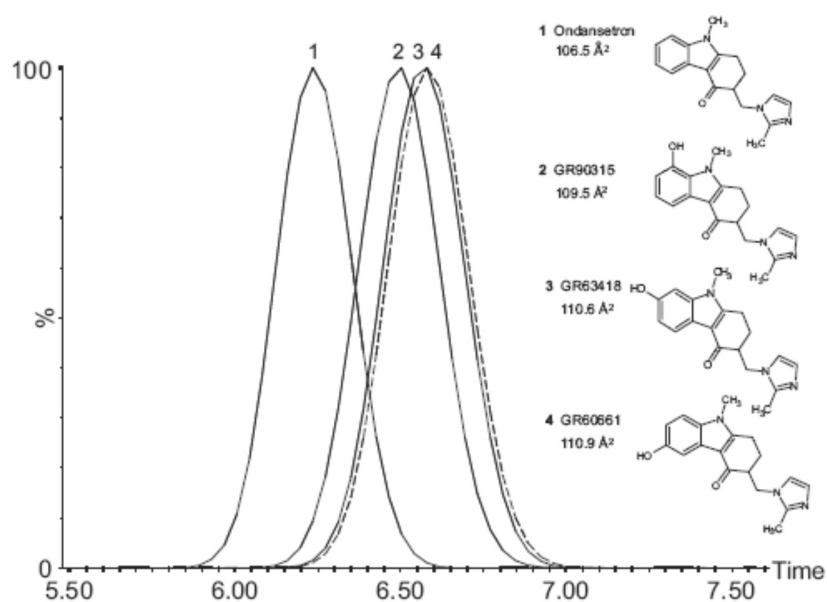
Figure 1-17. TWIMS ion mobility arrival time distributions for ondansetron and the 6-, 7- and 8-hydroxyl metabolites (adapted from reference 171).

The subsequent use of product ion mobility as a tool for assignment of positional isomers[172] was also demonstrated for both model compounds and a real-case example, emphasizing the possibilities of structural determination by both parent ion and product ion mobility where mass spectra alone appear indistinguishable and cannot be used to confidently assign a candidate structure. For example two different product ion mobilities for 11 *ortho-*, *meta-* and *para-* substituted hydroxyl metabolites with a phenylethylamine substructure were sufficient to assign their structures.

1.7.2. Rapid, portable and sensitive analysis using miniaturisation of IMS and IMS-MS

One of the advantages of FAIMS is that it does not require complicated vacuum equipment or large analyser tubes, thus it may be easily hyphenated to a portable mass spectrometer system[173]. Microfabricated FAIMS chips can increase the speed of separation by 100-10,000 times, filtering ions on the microsecond timescale enabling rapid monitoring of species at low level concentrations.[174] Current microfabricated FAIMS units, example shown in Figure 1-18, enables integration with an air sampler, ionisation source and detector for applications such as gas analysis, chemical monitoring and autonomous health diagnostics[167].
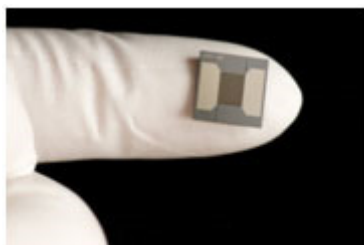
Figure 1-18. Illustration of the size of microfabricated FAIMS chip, courtesy of Owlstone Nanotechnologies and Pacific Northwest National Laboratory.

1.7.3. Increased selectivity in ambient and surface analysis mass spectrometry using IMS-MS

The direct and rapid analysis of substances using ambient ionisation mass spectrometry sources allows mass spectrometry data to be obtained with little or no sample preparation required for a variety of surfaces and matrices from tissue samples to intact tablet or liquid formulations. Application areas have included quantitative and qualitative measurements in pharmaceutical analysis, forensics, bioanalysis, *in vivo* imaging, proteomics *etc*. Whilst MALDI has been widely adopted in biological applications, for the analyses of biomolecules, there is currently a great deal of interest in ambient mass spectrometry approaches and there are now at least thirty methods documented[175].

The introduction of an additional IMS stage adds a further separation step to ambient ionisation mass spectrometry analysis without the need for rigorous sample preparation. Indeed for most surface analysis mass spectrometry methods the fact that the surface is

sampled and ions are generated in a single step means that the only viable method of separation and selectivity before the mass detector is to use a gas-phase separation method such as IMS. This extra dimension in selectivity maybe particularly useful in imaging applications. For example, in the case of whole-body imaging of rats, rats were dosed with 6 mg/kg *iv* with the anticancer drug vinblastine and the removal of interfering isobaric ions from endogenous lipids helped increase confidence in the MALDI imaging data[82] by removing 'false positives' which, by mass spectrometry imaging alone, could be interpreted as containing a high concentration of the active drug, as shown in Figure 1-19. The extra dimension of separation could also prove useful in removing any matrix-related isobaric ions. The datasets from the Driftscope imaging platform were transferred to Biomap 3.7.5.5 for visualisation enabling facile interpretation.
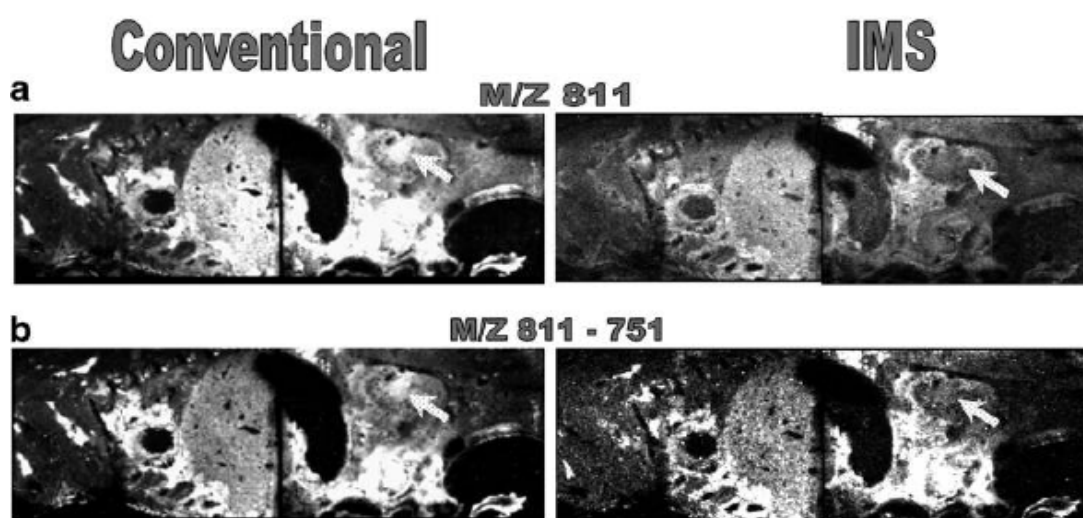
Figure 1-19. MALDI-IMS-MS image showing distribution of ions in whole-body sections and the arrow points to the area where specificity increased with application of IMS (adapted from reference 82). A lighter colour indicates increased abundance of the selected ion(s).

1.7.4. Chiral analysis using IMS-MS

A chiral modifier at 10 ppm of (S)-(+)-2-butanol was added to the buffer gas and enantiomers of a β-blocker, atenolol, were separated[176], as shown in Figure 1-20. It is proposed that selective interactions occur in the gas-phase between the enantiomer ion and the chiral modifier, to temporarily form a diastereomeric pair, so that the mobilities of the enantiomers

are altered and can be separated in time. Chiral ESI-DT-IMS-MS is now commercialised *via* the Excellims Corp IMS-quadrupole-MS system. A smaller, portable chiral IMS detector is now being developed by Excellims Corp for fast, on-site analysis including pesticide residues and environmental samples. The advantages of chiral IMS-MS compared to competing analytical techniques such as chiral SFC and chiral HPLC include rapid method development and high sensitivity, enabling rapid determination of enantiomeric excess (e.e.) for use in QA/QC environments or in broader applications including biomarker and metabolite identification.
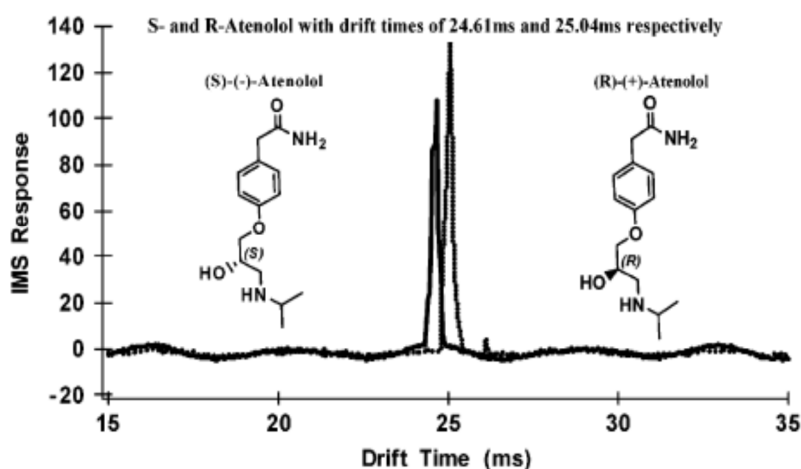
Figure 1-20. DT-IMS-MS separation of atenolol enantiomers showing the superimposed spectrum of the *R* and *S* enantiomers (adapted from reference 176).

Chiral resolution using FAIMS-MS has also been reported for six pairs of amino acid enantiomers separated as metal-bound complexes of divalent metal ion with an L-form amino acid[177] shown in Figure 1-21. The method employed a range of additional divalent metal cations and reference amino acids. Screening with different metal cations and reference compounds compares favourably with chiral HPLC and SFC screening times and can be automated using automated sample preparation platforms.
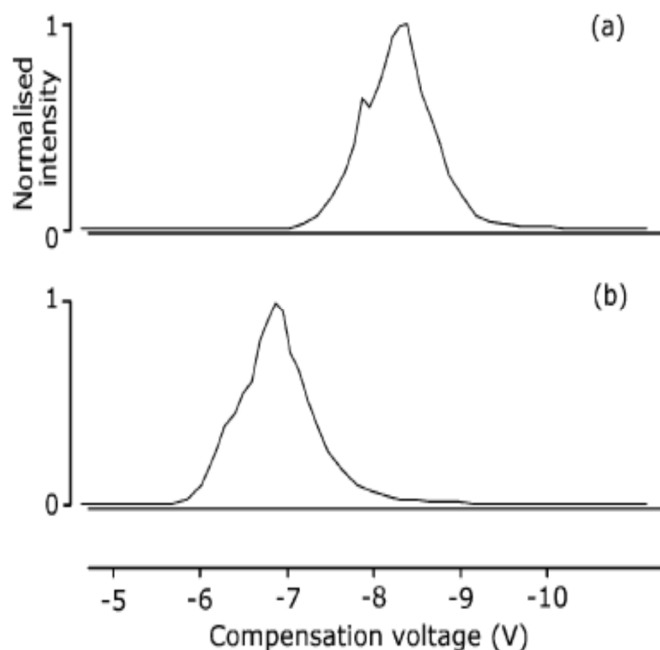
Figure 1-21. Separation of D/L-valine as $[Cu^{II}(L\text{-}Trp)_2(D/L\text{-}Val) - H]^+$. (a) D-Val; (b) L-Val using ESI-FAIMS mass spectrometry (adapted from reference 177).

An example of epimer separation where the diastereomers differ by only one chiral carbon, was achieved for β-methasone and dexamethasone.[178] The separation of the two epimers correlated well with differences observed in the calculated B3LYP/6-31G++(d,p) electrostatic potential surface. Whilst baseline separation is achievable by HPLC[179], the mass spectra of these compounds is very similar so the rapid separation and correlation with molecular modelling quickly identify this pair of compounds.

1.7.5. Resolution of isobars and isomers in complex mixtures using IMS-MS

Over 1100 metabolites were detected from methanolic extracts of 50 μL of blood samples including separation of over 300 isobaric/isomeric components, achieved without pre-concentration,[133] shown in Figure 1-22. The peak capacity compared to mass spectrometric analysis alone was increased by ~6 times and a broad range of metabolites were detected including lipids, carbohydrates, isoprenoids and estrogens. Interpretation of the data is further enabled by examining characteristic mobility-mass correlation data to identify similar classes of metabolites. In addition a reduction in the background noise due to selective ion filtering enabled detection and identification of low abundance components. A key advantage of the increased peak capacity of ion mobility mass spectrometry is that the rich data generated may

be utilised as a data repository and reviewed at a later date if required, *e.g.* later stage projects in a drug discovery environment may benefit from reviewing earlier studies.[180]
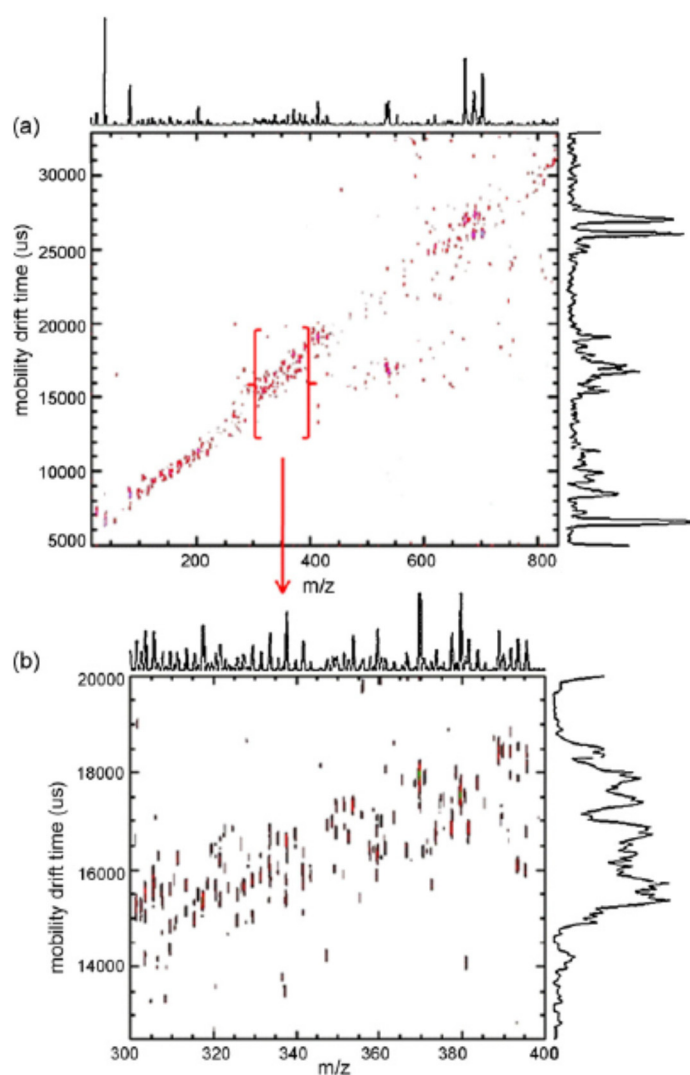
Figure 1-22. (a) Two-dimensional spectra of metabolic features measured in methanolic extract of human blood (b) a zoomed in region of the DT-IMS-MS spectrum illustrating peaks detected at the same nominal mass with different mobilities showing separation of isomers and isobars (adapted from reference 133).

1.7.6. Real-time reaction monitoring and process monitoring using IMS-MS

Reaction-monitoring in real-time has the potential to enable understanding of when reactions can be terminated at a suitable, rather than arbitrary, endpoint. By monitoring a process regularly throughout the reaction time, knowledge may also be accrued of the reaction, intermediates and product formation that could not be understood by irregular, sparse sampling alone and enable optimisation of experimental parameters *via* chemometrics. The

products formed by deprotonation of 7-fluoro-6-hydroxy-2-methylindole with sodium hydroxide were monitored by TWIMS-MS[181] and showed complementary and extra information from TWIMS-MS compared to MS alone, with shape selectivity information obtained by sampling every several minutes over a timescale of several hours (Figure 1-23).
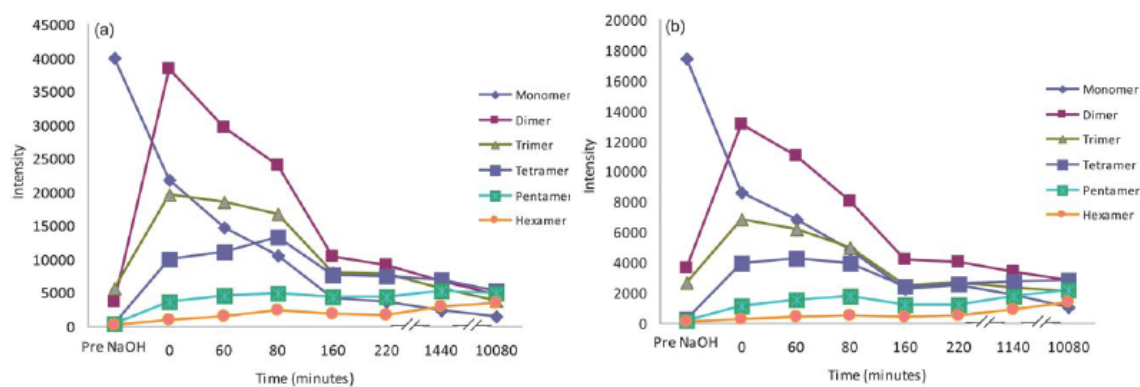
Figure 1-23. MS and TWIMS-MS analysis of the reaction of 7-fluoro-6-hydroxy-2-methylindole following the addition of aqueous sodium hydroxide. Signal response versus time in minutes for m/z 166 (monomer, I), m/z 311 (*O*-linked dimer, II), m/z 456 (*O*-linked trimer), m/z 601 (*O*-linked tetramer), m/z 746 (*O*-linked pentamer) and m/z 891 (*O*-linked hexamer) using (a) MS and (b) IM-MS (adapted from reference 181).

1.7.7. Rapid resolution of carbohydrate isomers using IMS-MS

Carbohydrate isomers including oligosaccharides are involved in numerous biological processes, such as cell-cell recognition and the development of embryos, but one of the main functions of carbohydrates is as oxidisable substrates in catabolism. However, to fully understand their different roles and functions it is necessary to understand both the linkage type and anomeric configuration whilst dealing with the challenge that, for example, in a mixture of sixteen D- and L-aldohexoses and eight D- and L-aldoses the total number of isomers with the same mass will be ninety six. The use of mass spectrometry as a tool is hindered by the similarity between fragmentation data obtained for different isomers; however, purification and determination of purity by NMR spectroscopy requires interpretation time and larger amounts of material. Separation of the metal ion adducts of anomeric methyl glycoside isomers (MeMan, MeGal and MeGlc) and isomeric forms of reducing sugars,[182] branch isomers, and very closely related isomers varying at a single stereochemical position[183] were addressed where MS[n] was not able to deliver solutions to the problem, as shown in Figure 1-24.
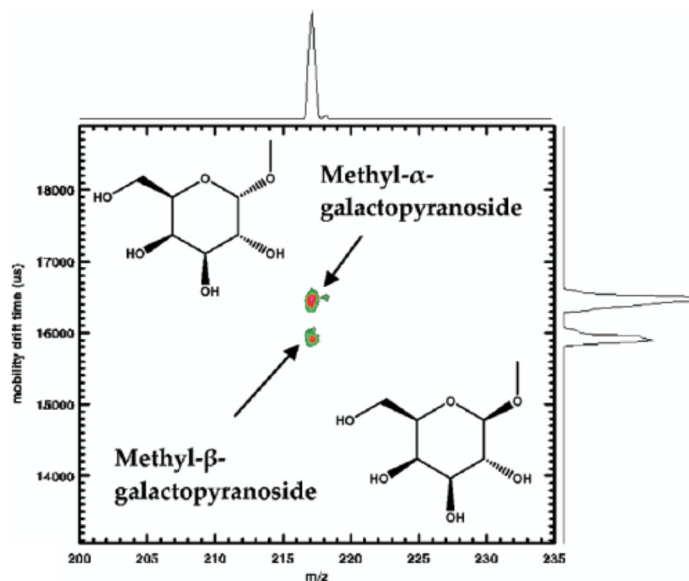
Figure 1-24. Two-dimensional DT-IMS-MS spectra of a mixture of methyl-α and β-D-galactopyranosides showing the separation (N_2 drift gas) of the sodium adducts at *m/z* 217 (adapted from reference 182).

1.7.8. Rapid analyte testing in complex drug formulations by IMS-MS

The combination of IMS-MS with ambient ionisation mass spectrometry may enable rapid analysis for complex mixtures including drug formulations without laborious method development and consumables required by other separation methods such as 2D LC-MS *etc*.

The complementary techniques of IMS and DART ambient ionisation operated separately has been demonstrated for AG-013736 in 1 mg Axitinib tablets[184] enabling a rapid analysis of AG-013736 in AG-013736 drug substances by DART ionisation and analysis of low-level limits for absence of the drug in placebo tablets by ion mobility spectrometry using a Model 400B IONSCAN-LS from Smiths Detection Scientific (Danbury, CT).

Hyphenated ambient ionisation IMS-MS and nano-electrospray has been used to analyse:

1. pharmaceutical formulations including tablets and creams containing one or more of ranitidine, paracetamol, codeine, anastrozole chlorhexidine and a nicotine-containing skin patch[83] using DESI.

2. pharmaceutical formulations from tablets containing one or more of timolol, paroxetine, paracetamol and codeine using nano-electrospray ionisation.[155]

38

3. pharmaceutical formulations containing one or more of paracetamol, ephedrine, codeine and caffeine from non-bonded reversed-phase thin layer chromatography (RP-TLC) plates by desorption electrospray ionisation (DESI).[185]

These examples demonstrate the wide applicability of analyses in various types of formulation illustrating that pre-treatment of samples is not required, rapid analyses can be conducted, whilst maintaining reproducible and robust results.

1.7.9. Analysis of supramolecular complexes using IMS-MS

The syntheses of supramolecular complexes that possess photo-optical properties are desired for solar energy capture and conversion, molecular machines, photochemical drugs and fluorescent-based sensors.
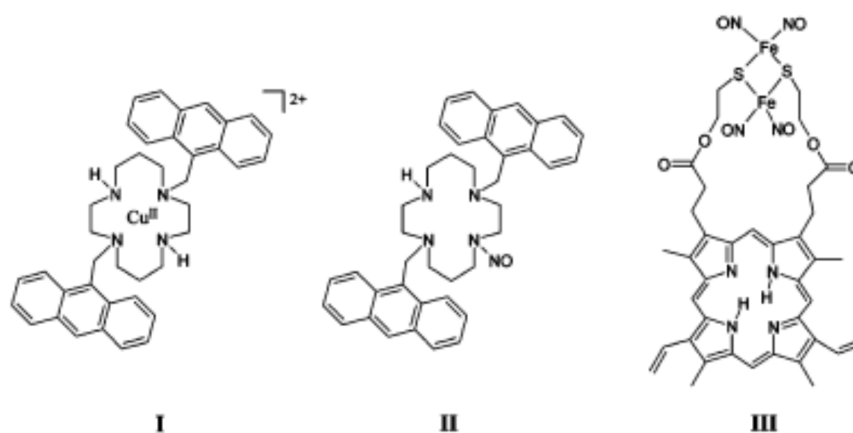
Figure 1-25. Schematic of $Cu^{II}(DAC)^{2+}$ (I), DAC-NO (II), and PPIX-RSE (III) (adapted from reference 186).

DT-IMS-MS was used to probe the structures of bichromophoric complexes in order to provide relevant data for sampling from *in situ* fluid data[186]. Complementary data to ^{1}H-NMR spectroscopy, X-ray crystallography and fluorescence measurements were obtained. For **I** the crystal structure agreed well with DFT structures and IMS-MS measurements, indicating that solid-state structures agreed well with gas-phase measurements. Only a single peak was observed in the ion mobilogram and calculation gave 161 Å^2 as the CCS, compared to 166 Å^2 ± 5 Å^2 predicted from the DFT structure. For **II** DT-IMS-MS measurements indicated two conformers by observation of two main bands in the ion mobilogram, by comparison with computational data this suggested two major families of Up-Up and Up-Down configuration,

as shown in Figure 1-26. The solution NMR spectroscopy data for **II** also suggested two conformers but the structures could not be unambiguously determined from the data.
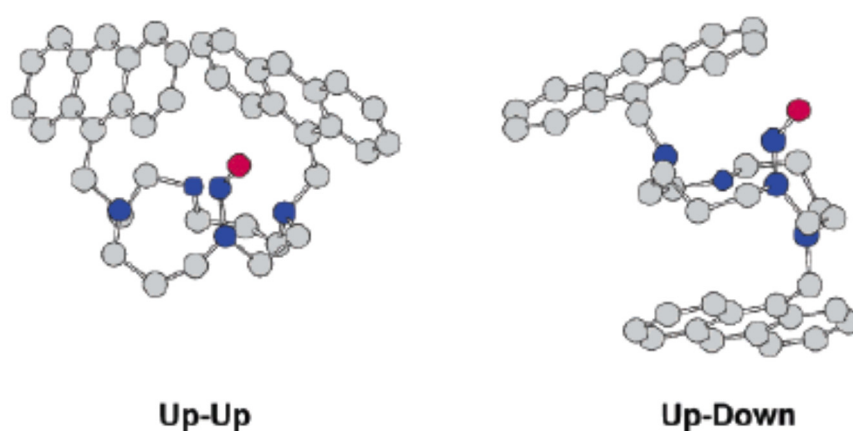
Figure 1-26. Examples of the two families predicted for $(II + H)^+$. The Up-Down family is the lower energy family, the Up-Up family has both anthracenyl groups on the same side as the cyclam (adapted from reference 186).

For **III** DT-IMS-MS measurements indicated two conformers which, in combination with DFT measurements indicated two compact structures, rather than folded structures, and correlated well with photo-physical features including a bimodal fluorescent decay and a residual emission in steady-state luminescence experiments. The proportion of the two conformers measured by IMS-MS, shown in Figure 1-27, agreed well with pre-exponential factors that indicated an approximate 80:20 ratio.
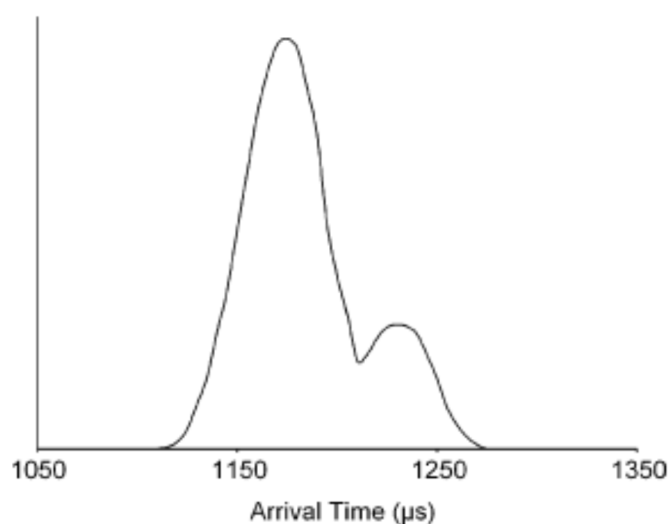
Figure 1-27. ATD for $[III + H]^+$ obtained at 80 K. Two distinct peaks indicate two conformers of $[III + H]^+$ are present (adapted from reference 186).

1.7.10. Hydration and desolvation of ligands and substrates

In drug design it is important to consider water molecules particularly in two situations: those water molecules that will be displaced during ligand binding in a receptor[187], and those water molecules that will be desolvated crossing the membrane environment.

Water in binding pockets in a receptor can provide surprising entropic and enthalpic contributions to structure and binding affinities.[188,189] If the key water binding sites and influence of small molecule ligands are known it may be possible to use this information in medicinal drug design, or to predict static hydration sites. It may be especially important to consider bridging waters that link ligand to protein *via* an extended hydrogen bond network.

Understanding membrane permeability is key to drug delivery and activity and is typically understood by hydrogen bond descriptors such as polar surface area (PSA) and surrogate measurements such as logD. These are considered important physicochemical parameters and modulated during lead optimisation. The reason that these parameters are important is that it is polar groups that are most involved in desolvation when molecules move from an aqueous extracellular environment to the lipophilic membrane environment. During this migration, molecules may change their conformation and lose water molecules in order to cross the membrane barrier. To further understand the effect of desolvation on ligands it is possible to add/remove water molecules one by one by changing the water vapour pressure of the DT-IMS-MS cell and gradually ascertain the ion mobility and conformation adopted from a hydrated ion towards a non-hydrated ion[190], shown in Figure 1-28(a). By measuring the energy change at different temperatures a van't Hoff plot can be generated, shown in Figure 1-28(b), thereby revealing the entropic and enthalpic contributions to hydration.
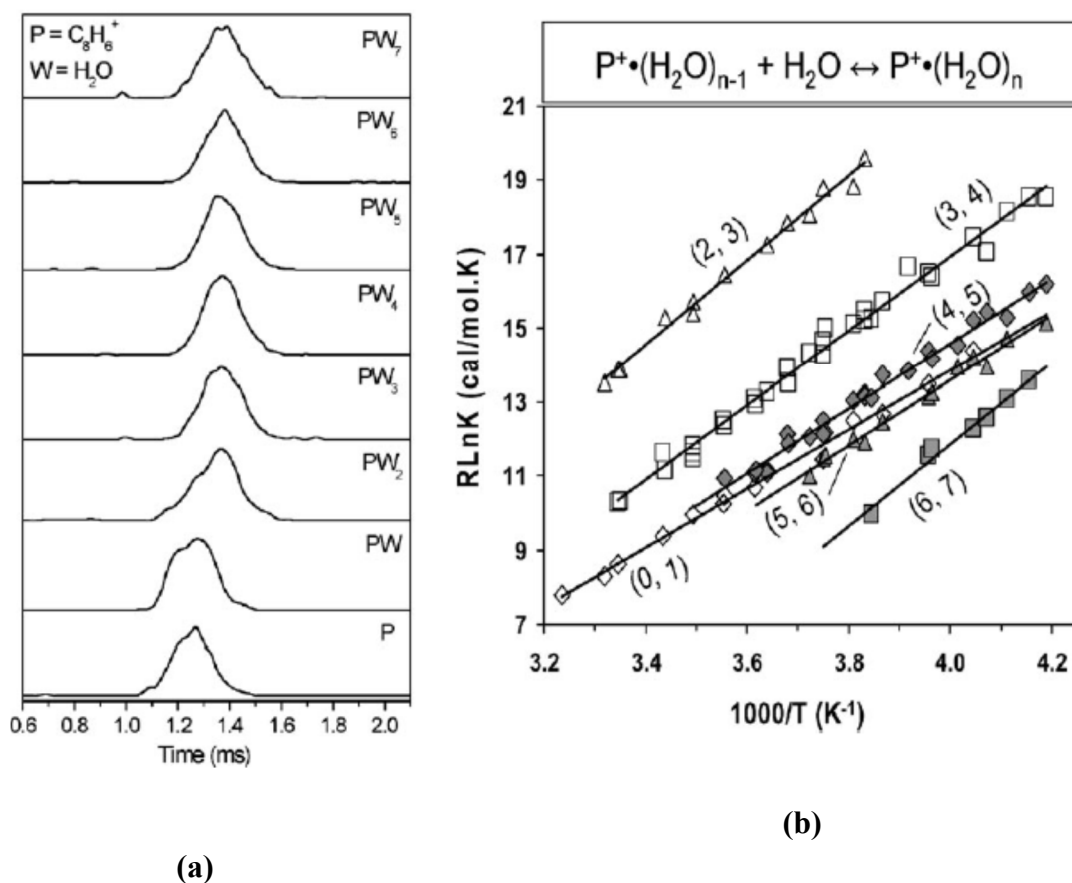
Figure 1-28. (a) ATDs of hydrated phenyl acetylene ions (PW$_n$) obtained following the injection of the phenyl acetylene ion $[C_8H_6]^+$ into 0.34 Torr of water vapour at 249 K (b) Van't Hoff plots for the equilbria $C_8H_6^{+•}(H_2O)_{n-1} + H_2O \Leftrightarrow C_8H_6^{+•}(H_2O)_n$ for n-1 and n as indicated (adapted from reference 191).

Hydration of small molecules has been studied for the phenyl acetylene ion, with stepwise hydration energies of 39.7 ± 6.3 kJ mol^{-1} from n=1 to 7; the entropy change for step 7 is larger, indicating a cyclic or cage like water structure.[191] For the benzene ion stepwise hydration energies were 35.6 kJ mol^{-1} from n=1 to 6. The binding energies were larger in the n=7 and 8 clusters indicating cyclic or cage like water structures.[192] For small protonated peptides[193] the hydration energy is largest for highly charged peptides and small non-arginine containing peptide and typically 30 to 60 kJ mol^{-1}; for pentapeptides AARAA, AARAA-OMe and Ac-AARAA the binding energies were typically ~41 kJ mol^{-1}.

The foregoing IMS-MS studies indicate hydration/desolvation studies of small molecule ions can provide structural information in the gas phase, this may be relevant to:

1. Understanding water and hydrogen bonded networks (including their entropic consequences) involving protein, ligand and water as part of molecular recognition systems,

2. Ligand desolvation on transport through membrane environments, and

3. Hydrogen/deuterium exchange experiments and how they are effected by molecular conformation.

Other methods to measure the hydration of small drug-like molecules include infra-red data recorded from a hydrated electrospray source or a droplet ion source[194] but these have not always provided unambiguous data, possibly due to the lack of energy required for proton transfer. The measurement of hydration/desolvation energies, described above, may provide a unique insight into the energy landscape of hydration/desolvation by conducting measurements over a range of temperatures.

1.8. OVERVIEW OF COLLISION CROSS-SECTION (CCS) MEASUREMENTS FOR SMALL MOLECULES

In DT-IMS-MS and TWIMS-MS, larger ions (with a larger CCS) tend to migrate slower through the gaseous medium in the IMS cell compared to smaller ions due to a higher number of collisions with the gas molecules (typically an inert gas such as nitrogen). The drift times through the IMS cell can also reveal structural information such as size, shape and topology; potentially including information relating to accessible conformations. Unfortunately DMS and FAIMS are, currently, not suitable for carrying out CCS measurements.

Understanding small molecule structure in the gas-phase may be advantageous for quality control or for a more detailed understanding of molecular structure in the gas-phase. For example in drug discovery the physicochemical and binding properties of small molecules depend on their 3D structure and at physiologically relevant temperatures a conformationally flexible small molecule is expected to be able to access a number of energetically feasible conformers, an example is shown in Figure 1-29.[95] The timescale of interconversion of conformers will define the structural information that can be obtained in solution and in the gas-phase. Understanding the energetics of small molecule conformers is currently largely carried out by generating potential conformers, known as conformational sampling, in computational studies.[195]
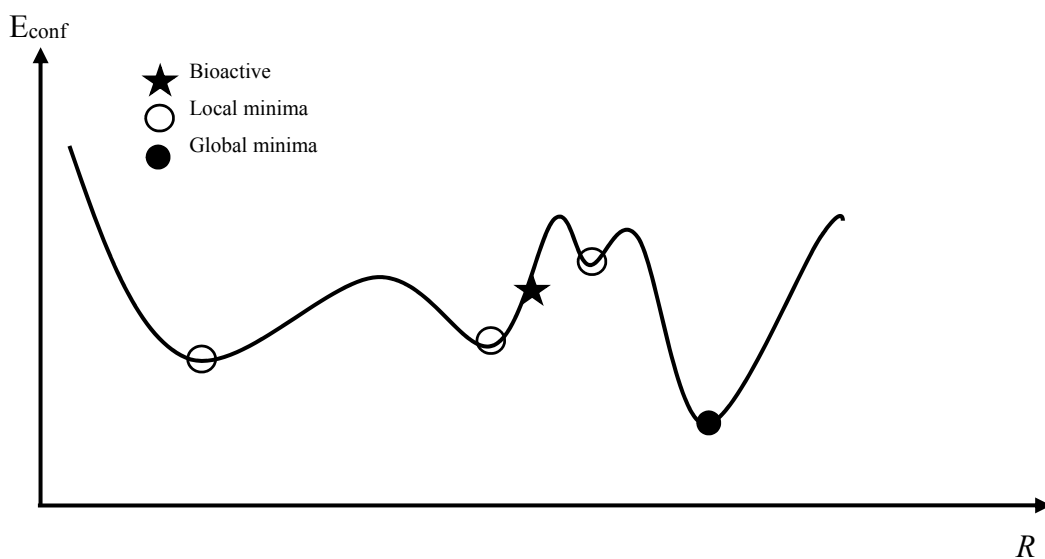
Figure 1-29. Hypothetical example of a one-dimensional molecular conformational potential energy surface. Conformational degrees of freedom (R) are shown on the X axis.

Computationally sampled models have been compared with X-ray crystallographic structures to understand how well the conformer models correlate with the bioactive conformation. Solution NMR spectroscopy can provide valuable information about the 3D structure; however the interpretation is often difficult due to the exchange between several conformations and typically requires molecular modelling to interpret results.

Rapid calculation of CCS by IMS-MS may be useful to decide which molecules in a library (series) could provide the optimum activity. This could be achieved coarsely by excluding molecules which are too rigid/flexible or too big/small.[196] These experiments potentially have the advantage of rapid speed of experiment and low consumption of sample relative to NMR spectroscopy and X-ray crystallography techniques. Understanding the conformation in the gas-phase may be a good indicator of the bioactive conformation. This may be especially relevant to compounds in drug discovery which are challenging to isolate and determine their structure. Mapping the conformational landscape defined *via* stereo-centres, intramolecular cyclisation *etc*., may help uncover a path to identification of new target compounds.

For protein structures there is now significant evidence that the gas-phase protein structure can reflect the native state solution phase structure under certain carefully controlled conditions. There have been several publications that demonstrate a good correlation between

X-ray crystallography, NMR spectroscopy and IMS studies for protein structures,[126,197–201] although there have also been some differences noted.[60] However, for small molecular weight molecules the evidence that gas-phase structures are similar to solution phase structures has been questioned; in a protein there are multiple co-operative interactions that maintain the 3D structure whereas for a small molecule there are typically fewer interactions resulting in a more flexible structure. Furthermore, a comparison of a range of gas-phase and X-ray crystallography molecular substructures for small molecules suggested that high-energy conformers were represented more in gas-phase, room-temperature Boltzmann distributions[202] than in crystal structures and broad peaks observed in IMS have generally been interpreted as indicating that multiple conformations are accessible and interconvert on the IMS measurement timescale.

Measurements using IMS-MS may not be the same as NMR spectroscopy (which are subject to solvent effects) or X-ray crystallography (which are subject to crystal lattice effects). In enzymes and membrane receptors, biomolecular recognition processes are likely to take place in hydrophobic 'binding pockets' of proteins where there will then be several interactions for a ligand including hydrophobic amino acids, with a large possibility (>0.8) of excluding most water molecules. The dielectric constant of a partial vacuum in IMS-MS (c.f. $\varepsilon_{vacuum} = 1$) is more similar to the immediate environment of a membrane receptor ($\varepsilon_{peptide/protein} = 2–4$) than for water ($\varepsilon_{water} = 80$).[203] It can be postulated therefore that the environment of a bioactive conformer will often be intermediate between aqueous and gas-phase (vacuum). Therefore the gas phase may be an appropriate medium in which to study the small molecule structures which in their active form are bound to a receptor located in a membrane, rather than in solution.

1.8.1. Study of an organoruthenium complex and its adducts with a DNA oligonucelotide

TWIMS-MS has been used to understand the binding of a "piano-stool" shaped organoruthenium complex with a single stranded oligonucleotide hexamer that shows promise as an anti-cancer agent. The illustration in Figure 1-30 shows examples of the protonated and deprotonated complexes, the doubly positive charged complex and the doubly negative charged complex. The single peak (A) suggests a single species, whereas multiple peaks in (B), (C) and (D) suggest either multiple binding of the Ru-drug fragment (confirmed

by interpretation of the mass spectra collected) or different conformers present in the mononucleotide due to different charge distributions along the phosphate backbone[196].
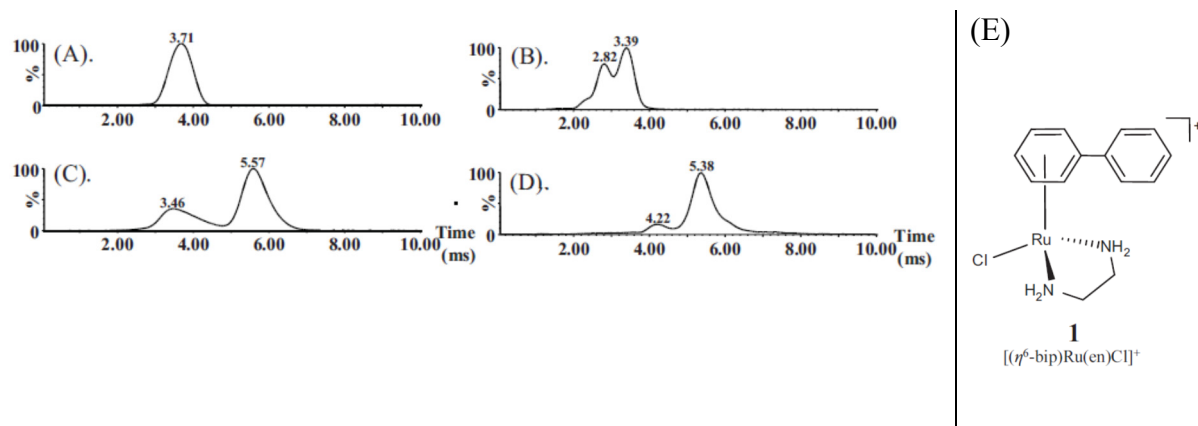
Figure 1-30. Arrival time distributions (ATDs) or drift times for (A) the $[M + 2H]^{2+}$ ion of d(CACGTG); (B) the $[M - 2H]^{2-}$ ion of d(CACGTG); (C) the complex $[CACGTG + 2[(\eta^6\text{-}bip)Ru(en)] - 2H]^{2+}$; and (D) the complex $[CACGTG + 2[(\eta6\text{-}bip)Ru(en)] - 6H]^{2-}$ and (E) structure of the organoruthenium anticancer complex $([(\eta^6\text{-}bip)Ru(en)])$ (adapted from reference 196).

The CCS values obtained for the *R*-based drug correlated well with those obtained by X-ray crystallographic data so that binding could be easily identified. Using MS/MS experiments, shown in Figure 1, subsequent to IMS separation, enabled the binding site to be determined by examining the resulting fragmentation pattern.
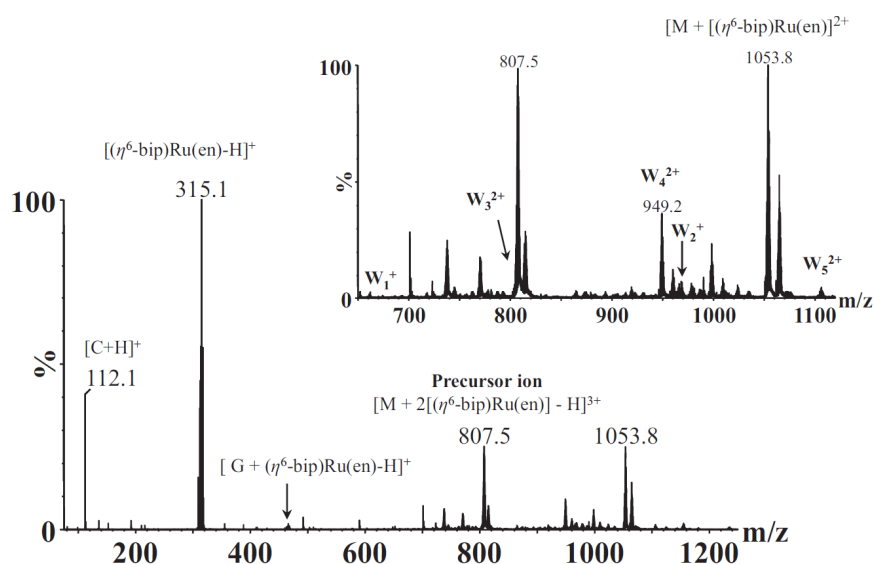
Figure 1-31. Electrospray ionisation MS/MS spectrum of the precursor ion of *m/z* 807.5 corresponding to $[CACGTG + 2[(\eta6\text{-}bip)Ru(en)] - H]^{3+}$ (adapted from reference 196).

46

1.8.2. Study of the in-flight epimerisation of a bis-Tröger base

The epimerisation pathway *via* the proposed alternatives of a) a proton catalysed ring opening or b) retro-Diels-Alder of a bis-Tröger base, shown in Figure 1-, were investigated using TWIMS-MS[204] as this could be important for the design of Tröger bases which, with their tweezer type structure, have been suggested as useful agents as molecular receptors, chiral solvating agents and inclusion complexes.[205]
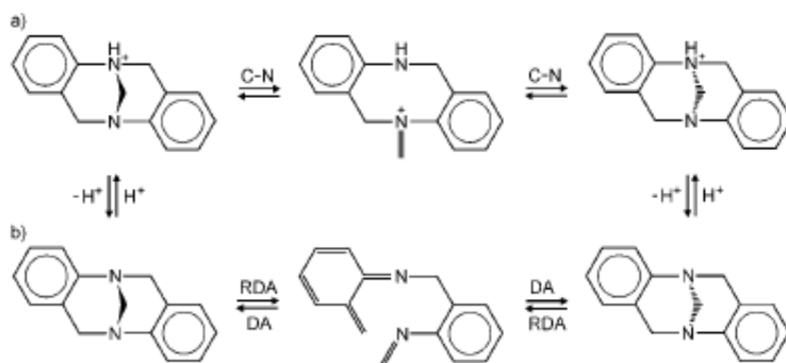
Figure 1-32. Proposed mechanism for epimerisation of a Tröger base by a) a proton catalysed ring opening or b) a retro-Diels-Alder mechanism (adapted from reference 204).

The two structures were separated well in the gas-phase TWIMS stage (Figure 1-) and activation of ions pre-TWIMS separation and post-TWIMS separation demonstrated that the anti-1H$^+$ isomer is the most thermodynamically favoured by measuring the intensity of each parent ion. The preferred mechanism was also concluded to be the proton catalysed ring opening as demonstrated by the lack of epimerisation when a Na$^+$ Tröger base was used a surrogate proton-like participant in the reaction, thus eliminating the possibility of a retro-Diels-Alder mechanism.
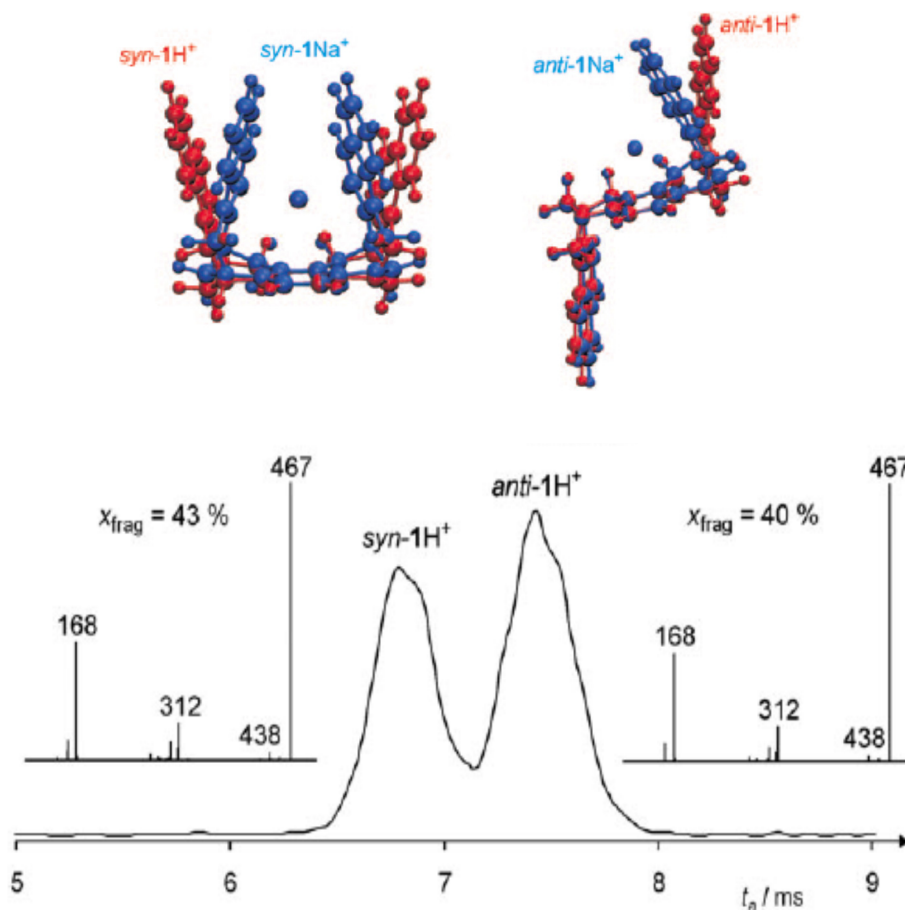
Figure 1-33. Ion mobility trace with associated mass spectra (shown inset) of the anti- and syn- isomers. The computationally calculated structures are shown above (adapted from reference 204).

1.8.3. Measurement of CCS for small molecules using DT-IMS-MS

The measurement of CCS in DT-IMS is simplified by the use of a static, uniform, electric field in which ion motion takes place; the physical principles are established and mobility values can be used to derive the CCS. Knowing the length of the drift region and the time that ions take to traverse it enables the ion's velocity to be determined:

$$v = KE \rightarrow \frac{L}{t_d} = K\frac{V}{L} \rightarrow K = \frac{L^2}{Vt_d} \tag{9}$$

where v is the ion's velocity, K is the ion mobility constant, E is the electric field, L is the length of the drift tube, t_d is the arrival time and V is the voltage across the drift region.

K should be corrected for temperature and pressure to obtain the reduced ion mobility, K_0 (corrected to 273 K and 760 Torr):

$$K_0 = K\left[\frac{273}{T}\right]\left[\frac{P}{760}\right] \tag{10}$$

The CCS, Ω_T, can then be derived directly:

$$\Omega_T = \left(\frac{3ze}{16N}\right)\left(\frac{2\pi}{\mu kT}\right)^{1/2}\left(\frac{1}{K}\right) \tag{11}$$

where Ω is the CCS, ze is the ionic charge, N is the background gas number density, μ is the reduced mass of the ion-neutral pair, k is Boltzmann's constant, T is the gas temperature and K is the mobility constant.

1.8.4. Calculation of CCS for small molecules using TWIMS

The measurement of CCS in TWIMS is not typically directly derived from the mobility of an ion[206] as the motion of the analyte in the travelling wave regime is complicated and, to date, is not fully understood. The TWIMS system is, therefore, usually calibrated using ions that have previously been measured by employing DT-IMS. A typical calibration regime[207] has been described based on the CCS values of oligo-glycine ions (available at http://www.indiana.edu/~clemmer/) which are currently accepted to be suitable as they are high mobility ions in the expected mobility range of small molecules, and have been measured previously using DT-IMS. Calibration with a static 4 V, wave gave more drift time values over a narrower range of CCSs than a wave ramp, potentially resulting in greater resolving power. Although changes can be made to the buffer gas used in the measurement, the larger the buffer gas molecules, the larger the CCS and it was noted that the buffer gas radius used in theoretical calculations must be indicative of the buffer gas used in the original

DT-IMS measurements (typically helium), even if the analysis of calibrants and analytes is carried out in a different buffer gas. The experimental resolving power was reported under these conditions for the isomeric amino acids isoleucine and leucine (131 g/mol), calculated the CCS at 68.95 Å^2 and 70.51 Å^2 respectively from the measured arrival time distributions (see Figure 1-).
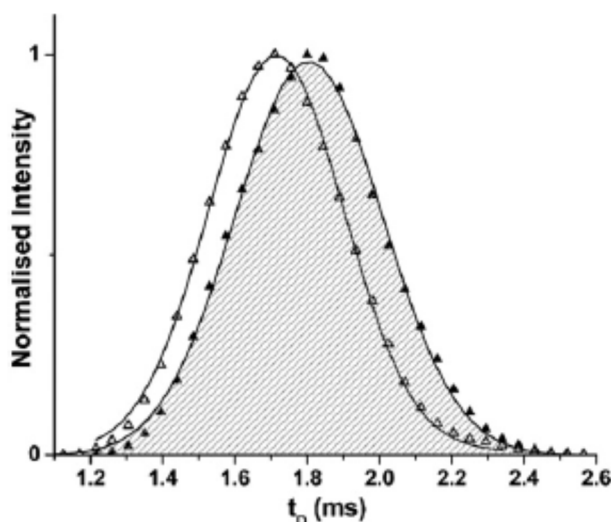
Figure 1-34. Overlaid mobility chromatograms of L-Ile (open) and L-Leu (filled) acquired using a static 4 V wave height. The ESI-TWIMS-MS experimental CCS values measured were 68.95 and 70.51Å^2, and the calculated CCS values were 70.81 and 72.03Å^2, for L-Ile and L-Leu, respectively (adapted from reference 207).

To understand the differences between solution state and gas-phase measurements the theoretical CCSs were calculated as a weighted average over multiple solution-phase rotameric states from a database of 5000 protein structures and compared to the experimentally measured gas-phase values (Table 1-5). Calculated CCS values for hydrophobic amino acids gave the best agreement with gas-phase TWIMS values, whilst more polar residues are experimentally found to be much smaller than calculated, mostly likely due to burying of polar and charged termini. The largest differences also appear to be correlated to the degrees of freedom in the amino acid side-chain.

Table 1-5. Comparison of measured and predicted CCS values for seven amino acids (adapted from reference 207).

Amino acid	Mw (g/mol)	Rotamers	TWIMS experimental CCS ($Å^2$)	CCS predicted from solution state ($Å^2$)	Difference ($Å^2$)	Notes
Pro	115.12	2	62.43	63.16	0.73	Hydrophobic
Val	117.15	3	64.81	64.82	0.01	Hydrophobic
Leu	131.12	4	70.51	72.03	1.52	Hydrophobic
Ile	131.12	4	68.95	70.81	1.86	Hydrophobic
Asp	133.11	5	62.93	69.81	6.88	Polar
Gln	146.15	5	62.85	75.08	12.23	Polar
Glu	147.13	7	63.35	76.69	13.34	Polar

This demonstrates that IMS-MS can distinguish between subtle changes in shape *e.g.* differentiating Leu and Ile and also has the potential to reveal structural information about the important interactions present in the gas-phase such as the burial of the polar groups in the examples Gln and Glu.

Recently calibration measurements have been acquired for a wider range of compounds including proteins,[208] phosphoric acid clusters,[209] glycans,[210] and using higher (CID) collision energies such as those used during un-targeted HDMS[E] data acquisition[211] in addition to the 'drug-like' set[178] and poly-(L/D)-alanine.[212] Mis-matching of charge state was found to introduce around 3.5% error in CCS determination, whilst mis-matching calibrant class was found to introduce errors of around only 1% (close to experimental error), whilst mis-matching both charge state and calibrant class was found to introduce errors of around 4.7%.[213]

1.8.5. Calculation of CCS for small molecules using overtone IMS-MS

Recently, overtone mobility spectrometry[129,214] where separation is achieved by applying time-dependent electric fields to sequential segments in a drift-tube thus eliminating ions that are not resonant with the applied field, has been used to demonstrate measurements of ion CCSs:

$$\Omega = \frac{(18\pi)^{1/2}}{16} \frac{ze}{(k_b T)^{1/2}} \left[\frac{1}{m_I} + \frac{1}{m_B} \right]^{1/2} \frac{E[\phi(h-1)+1]}{f(l_t + l_e)} \frac{760}{P} \frac{T}{273.2} \frac{1}{N} \quad (12)$$

where Ω is the CCS, k_b is the Boltzmann constant, z is the ionic charge, e is the charge of an electron, N is the buffer gas density, T is the temperature of the buffer gas, P is the pressure of the buffer gas, E is the electric field, m_I and m_B are the masses of the ion and the buffer gas. The overtone IMS specific parameters include f which is the application frequency, h is the harmonic index, I_t is the ion transmission length and I_e is the ejection length.

Reduced ion mobilities are reported to enable a comparison of DT-IMS-MS and overtone-IMS-MS measurements and are, in general, in good agreement. An especially interesting feature is the potential for overtone-IMS-MS to exclude different ion structures i.e. with different ion mobilities in the IMS stage. Typical IMS and TWIMS approaches are thought to measure an experimental average of all structures sampled within the IMS drift time, whereas overtone-IMS-MS appears to enable selection of particular structures over the IMS drift-time, potentially giving a better understanding of transitions on the IMS measurement timescale, in the order of a few ms. Current measurements are limited for small molecules but development is ongoing.

1.8.6. Using theoretical calculations to understand ion mobility data

The assignment of structural information is typically made by comparing theoretical, calculated CCS values with experimentally determined CCS values by using the following procedures:

1. Generate list of conformers,

2. Minimise structures to lowest energy structures,

3. Calculation of theoretical CCS, and

4. Comparison of theoretical CCS values with experimentally determined values.

1. Generate list of conformers

Initially the molecule must be transformed from a flat 2D to a representative 3D structure at physiological pH taking into account tautomerism, likely protonation site(s), bond lengths *etc*. The accessible conformations can be explored for small molecules[108,171] using methods including systematic search, molecular dynamics, random search and grid search tools but may be very computationally expensive if the number of rotatable bonds is high, requiring evaluation of thousands of potential structures for relatively simple structures.

2. Minimise structure to lowest energy structures

Molecular dynamics approaches have been applied to small molecules with success and computationally are far less demanding than for large molecules.[215–220] Methods have included force-field techniques including MMFF94 forcefield[171] and molecular dynamics[221] but quantum mechanical methods *e.g.*, density functional theory (DFT) is increasingly being used to understand small molecule structures in ion mobility.[220,222] Indeed DFT has almost become the 'norm' for calculating ion structures,[223] as it is more accurate than semi-empirical methods. Recent work has highlighted the potential for DFT to understand electron density in bond formation/cleavage and the effect of protonation on bond lengths[224–227] which makes DFT a potentially powerful tool in modelling ion structures in IMS-MS. Indeed the information obtained from DFT calculations may contribute to a better understanding of the ion structure for both the IMS separation and any tandem MS results.

3. Calculation of theoretical CCS

The main calculation protocols for obtaining theoretical CCS values in IMS include projection approximation (PA), trajectory method (TJ) and exact hard sphere scattering (EHSS). Whilst there has been some debate about which type of modelling is most appropriate, it is generally recommended to use the projection approximation (PA) method for small molecules of 20-100 atoms, for example using the Sigma software package or MOBCAL software. However, PA typically underestimates CCSs for polyatomic species, especially for different surfaces including concave structures, by up to 20%,[228] so is not typically recommended for larger molecular weight structures.

TJ typically works well for any size system, but calculations are computationally expensive. EHSS typically fails with small molecules because the ion-buffer gas interaction becomes important compared to the geometry of the ion and careful calibration of the relevant atomic radii is essential.[228] EHSS and TJ appear to provide better agreement for larger molecular weight ions as the parameterisation of EHSS is based on fullerenes and other large molecular weight ions.

There have been attempts to improve modelling, for large molecules[229] and small molecules,[207,230] by construction of new parameter basis sets with values for the carbon, oxygen, helium and nitrogen interaction radii calculated from suitable representative molecules. Further development of modelling and prediction techniques[231] and improvement in parameter basis sets may well provide closer agreement between calculated and measured CCSs. Recent improvements to a nitrogen based trajectory method[178] may help understand data generated in $N_{2(g)}$ (as the less polarisable $He_{(g)}$ is typically used) and create better calibrations for collision cross-sections (especially useful in TWIMS where $N_{2(g)}$ is the typical drift gas). The set of collision cross-sections for pharmaceutically relevant small molecule compounds appears self-consistent ($R^2 = 0.9949$) and covers a useful range of 124.5 to 254.3 $Å^2$ for nitrogen gas and a range of 63.0 to 178.8 $Å^2$ for helium gas.

4. Comparison of calculated CCS values with experimentally determined values

Typically validation is best achieved using known standards within experimental sets, either for relative ranking of results or to increase confidence in measurements. Structure co-ordination sets are widely available for some species *e.g.* at the RCSB Protein Data Bank and have been data based by Clemmer[212]. However, it should be noted that the co-ordination

structures from different sources may not agree as NMR spectroscopy structures are often subject to solvent effects, X-ray crystallographic structures subject to crystal lattice effects and measurements by ion mobility may be subject to gas-phase neutral contamination, activation, ionisation and solvent effects. Some publications describe the calculation of theoretical collision cross-sections using datasets obtained from NMR spectroscopy and X-ray crystallographic co-ordinate files (*e.g.* PDB files) as input without subsequent energy minimisation in the gas-phase which could result in erroneous estimates of CCS and further assignment; in such a case a better understanding *via* structure/energy minimisation may be important.

1.9. PREDICTION OF ION MOBILITY CONSTANTS

Whilst many approaches to IMS explicitly use or attempt to derive information on the 3D structure of the ion another approach is to use molecular descriptors to adequately describe an ion and predict the reduced mobility without any requirement to carry out computationally expensive geometry optimisation. A quantitative structure property relationship (QSPR) methodology[232] using five descriptors for a training set of 70 organic compounds and excluding three outliers gave a multi-linear regression (MLR) of $R^2 = 0.98$ and s = 0.047; the test set of seven compounds gave s = 0.047. Later, using six molecular descriptors on a training set of 135 compounds[233] and testing the model with 18 compounds gave an RMS error of 0.038. A more diverse set of 182 compounds and modification of two of the descriptors[234] correlated with an $R^2 = 0.80$. A subset of 159 of that data set was used to develop linear and non-linear models using MLR and progression pursuit regression to achieve R^2 values of 0.908 and 0.938 and s = 0.066 and 0.055, respectively.[235] The recent formulation of a linear equation for ion mobility in a series of polar aliphatic organic compounds resulted in ion mobility predictions that were typically >99% accurate.[236]

These molecular descriptor approaches are now widely used in predicting peptide IMS-MS drift times[237] to improve confidence in peptide identification. The same approach to prediction of small molecule IMS-MS drift times could well help refine models of drift time prediction and better understand important interactions affecting drift time and thus gas-phase structures, however this is currently not well understood.

1.10.   FUTURE DEVELOPMENTS

The adoption of IMS-MS both for small molecule as well as large molecule applications is likely to continue strongly, assisted by rapid developments in IMS design that marries the two stages of IMS and MS and mitigates the challenges of ion efficiency and resolution that has hindered their combination.

The resistive glass-IMS design recently invented to replace the traditional stacked-ring ion guides enables easier construction[238] and designs include a segmented RF quadrupole in the vacuum interface that improve sensitivity by over 2 order of magnitude[239]. The inverse ion mobility spectrometry technique that applies an inverted pulse to the shutter grid appears to increase resolution by 30-60% presumably by creating a gap in the charge cloud and thus reducing space-charging effects.[240]

A further hyphenation of a photoelectron spectrometer to a IMS-TOFMS shows promise as a complementary method to obtain further information on the structures of gas-phase ions by obtaining photoelectron spectra at three different detachment laser wavelengths,[241] and also hints at the possibilities for further information-rich data to be acquired and combined with IMS-MS by further hyphenation.

The adoption of IMS in hyphenated IMS-MS systems is continuing with important developments, for example, Agilent previously announced collaborations with Owlstone Nanotechnologies for an IMS-MS system and Bruker have investigated new modes of IMS.[242] There have been long-term research investments demonstrated in the launches of several updates to the Waters Synapt IMS-MS platforms with improved resolution and ion transmission and the new Waters Vion configuration with a quadrupole following the ion mobility cell. Sciex introduced the SelexION technology that is available for the Sciex Triple Quad 5500 and QTRAP 5500 Systems including selection of gas-phase dopants which can improve IMS separation and rapid 25 ms cycle time per MRM which matches cycle times with multi-component analysis and UHPLC time scales.

1.11.   CONCLUSIONS

Whilst IMS is a ubiquitous technique in airports as well as military and forensic applications, it is still the case that using IMS-MS for measuring structural information and for separations in small molecule applications there are subtle differences that can significantly affect the mobility and there is much more to be understood about how to measure the structures of gas-

phase ions reliably, the nature of the fundamental intra-molecular interactions that define their structures and what the effect of ion-neutral interactions are on ion mobility.

Many chemical classes have been investigated using IMS and IMS-MS and some of the main publications are listed in Table 1-6 to direct the reader to more detail on those classes.

Table 1-6. Applications of IMS-MS and IMS to small molecule classes.

Class	Year
Hydrocarbons[243]	1973
Halogenated benzenes and nitro benzenes (*o*-, *m*-substituted)[244]	1973
Dihalogenated benzenes (*o*-, *m*-substituted)[244]	1974
Benzoic and isophthalic and phthalic acids[244]	1975
Some *sec*-butylcholorodiphenyl oxides[244]	1976
o- and *p*- substituted chlorodiphenyl oxides[244]	1976
Ethyl butyl esters of maleic and fumaric[244]	1982
Succinic acids[244]	1982
Isomeric ketones[244]	1986
Isomeric alcohols[244]	1986
Substituted electrophilic olefins[244]	1988
Amides and amines[244]	1989 & 1994
Anilines[245]	1990
Simple monocyclic and dicyclic compounds [246]	1990
Aminoazoles[247]	1991
Ketones[248]	1991
Aminoalcohols[249]	1991
Benzodiazepines, amphetamines and opiates[244]	2001 & 2002
Amino acids[250]	2001
Amphetamines[88]	2002
Drug-like molecules[178]	2012
Sodiated *N*-linked glycans[251]	2013
Carbohydrates as group I adducts[252]	2013
N-glycans[253]	2014
Carbohydrates[254]	2014
Saxitoxins[255]	2014
Lipids, peptides, carbohydates and ammonium salts[256]	2015
Glycans, oligosaccharide standards and their fragments[257]	2015

Standardised calibration and measurement methods,[258] easily implemented and accurate predictive models and interpretation of results are still being developed but show great promise. The interchange between academia, vendors and industry is ensuring more options are available to potential users of IMS-MS. A range of current commercial manufacturers and IMS-MS types are listed in Table 1-7 for reference.

Table 1-7. Commercially available IMS systems or accessories able to interface to MS systems.

IMS-MS system	Type
Agilent 6560 IMS-MS	DT-IMS
Excellims IMS-MS	DT-IMS
Tofwerk IMS-MS	DT-IMS
Waters Synapt and Vion IMS-MS	TWIMS
Thermo FAIMS cylindrical electrode	FAIMS
Owlstone Nanotech	FAIMS
Sciex SelexION parallel plate	DMS
Sionex microDMx	DMS

Over the last decade there have been many novel applications and developments in IMS-MS involving new methods to generate ions, accumulate and focus ions, select ions preferentially, measure and process the multiplexed information and they have been used to solve problems ranging from hydration/desolvation in 'small' organic molecules to understanding the fundamental interactions in the building blocks of life, amino acids. IMS-MS is a novel method that can separate ions and use information on their mobility to assign structure on an unparalleled rapid timeframe and at high levels of sensitivity. In combination with a range of analytical equipment including ionisation sources, separation devices, solution chemistry and gas-phase chemistry; the use of IMS-MS offers a versatile and powerful approach to unique insights into complex mixtures and hitherto ambiguous structures.

1.12.   REFERENCES

1.   Rayleigh, L. On the equilibrium of liquid conducting masses charged with electricity. *Philos. Mag. Ser. 5* **14,** 184–186 (1882).

2.   Zeleny, J. The Electrical Discharge from Liquid Points, and a Hydrostatic Method of Measuring the Electric Intensity at Their Surfaces. *Phys. Rev.* **3,** 69–91 (1914).

3.   Zeleny, J. Instability of Electrified Liquid Surfaces. *Phys. Rev.* **10,** 1–6 (1917).

4.   Taylor, G. Disintegration of Water Drops in an Electric Field. *Proc. R. Soc. Lond. Ser. Math. Phys. Sci.* **280,** 383–397 (1964).

5.   Dole, M., Mack, L. L., Hines, R. L., Mobley, R. C., Ferguson, L. D. & Alice, M. B. Molecular Beams of Macroions. *J. Chem. Phys.* **49,** 2240–2249 (1968).

6. Mack, L. L., Kralik, P., Rheude, A. & Dole, M. Molecular Beams of Macroions. II. *J. Chem. Phys.* **52,** 4977–4986 (1970).

7. Yamashita, M. & Fenn, J. B. Electrospray ion source. Another variation on the free-jet theme. *J. Phys. Chem.* **88,** 4451–4459 (1984).

8. Fenn, J. B., Mann, M., Meng, C. K., Wong, S. F. & Whitehouse, C. M. Electrospray ionization for mass spectrometry of large biomolecules. *Science* **246,** 64–71 (1989).

9. Fenn, J. B. Electrospray wings for molecular elephants (Nobel lecture). *Angew. Chem. Int. Ed Engl.* **42,** 3871–3894 (2003).

10. Alexandrov, M. L., Gall, L. N., Krasnov, N. V., Nikolaev, V. I., Pavlenko, V. A. & Shkurov, V. A. Extraction of ions from solutions under atmospheric pressure as a method for mass spectrometric analysis of bioorganic compounds. *Rapid Commun. Mass Spectrom.* **22,** 267–270 (2008).

11. Bruins, A. P., Covey, T. R. & Henion, J. D. Ion spray interface for combined liquid chromatography/atmospheric pressure ionization mass spectrometry. *Anal. Chem.* **59,** 2642–2646 (1987).

12. Covey, T. R., Huang, E. C. & Henion, J. D. Structural characterization of protein tryptic peptides via liquid chromatography/mass spectrometry and collision-induced dissociation of their doubly charged molecular ions. *Anal. Chem.* **63,** 1193–1200 (1991).

13. Wong, S. F., Meng, C. K. & Fenn, J. B. Multiple charging in electrospray ionization of poly(ethylene glycols). *J. Phys. Chem.* **92,** 546–550 (1988).

14. Banerjee, S., Mazumdar, S., Banerjee, S. & Mazumdar, S. Electrospray Ionization Mass Spectrometry: A Technique to Access the Information beyond the Molecular Weight of the Analyte, Electrospray Ionization Mass Spectrometry: A Technique to Access the Information beyond the Molecular Weight of the Analyte. *Int. J. Anal. Chem. Int. J. Anal. Chem.* **2012, 2012,** e282574 (2012).

15. Winger, B. E., Light-Wahl, K. J., Ogorzalek Loo, R. R., Udseth, H. R. & Smith, R. D. Observation and implications of high mass-to-charge ratio ions from electrospray ionization mass spectrometry. *J. Am. Soc. Mass Spectrom.* **4,** 536–545 (1993).

16. Iribarne, J. V. & Thomson, B. A. On the evaporation of small ions from charged droplets. *J. Chem. Phys.* **64,** 2287–2294 (1976).

17. Nguyen, S. & Fenn, J. B. Gas-phase ions of solute species from charged droplets of solutions. *Proc. Natl. Acad. Sci. U. S. A.* **104,** 1111–1117 (2007).

18. Kebarle, P. & Tang, L. From ions in solution to ions in the gas phase - the mechanism of electrospray mass spectrometry. *Anal. Chem.* **65,** 972A–986A (1993).

19. Cole, R. B. Some tenets pertaining to electrospray ionization mass spectrometry. *J. Mass Spectrom.* **35,** 763–772 (2000).

20. Fernandez de la Mora, J. Electrospray ionization of large multiply charged species proceeds via Dole's charged residue mechanism. *Anal. Chim. Acta* **406,** 93–104 (2000).

21. Kebarle, P. A brief overview of the present status of the mechanisms involved in electrospray mass spectrometry. *J. Mass Spectrom.* **35,** 804–817 (2000).

22. Olumee, Z., Callahan, J. H. & Vertes, A. Droplet Dynamics Changes in Electrostatic Sprays of Methanol−Water Mixtures. *J. Phys. Chem. A* **102,** 9154–9160 (1998).

23. Tito, M. A., Tars, K., Valegard, K., Hajdu, J. & Robinson, C. V. Electrospray Time-of-Flight Mass Spectrometry of the Intact MS2 Virus Capsid. *J. Am. Chem. Soc.* **122,** 3550–3551 (2000).

24. Sleno, L. & Volmer, D. A. Ion activation methods for tandem mass spectrometry. *J. Mass Spectrom.* **39,** 1091–1112 (2004).

25. Valaskovic, G. A., Kelleher, N. L., Little, D. P., Aaserud, D. J. & McLafferty, F. W. Attomole-sensitivity electrospray source for large-molecule mass spectrometry. *Anal. Chem.* **67,** 3802–3805 (1995).

26. Wilm, M. & Mann, M. Analytical Properties of the Nanoelectrospray Ion Source. *Anal. Chem.* **68,** 1–8 (1996).

27. Wiley: Quantitative Applications of Mass Spectrometry. at <http://eu.wiley.com/WileyCDA/WileyTitle/productCd-0470025166.html>

28. Maurer, H. H. Current role of liquid chromatography–mass spectrometry in clinical and forensic toxicology. *Anal. Bioanal. Chem.* **388,** 1315–1325 (2007).

29. Jemal, M. & Xia, Y.-Q. LC-MS Development Strategies for Quantitative Bioanalysis. *Curr. Drug Metab.* **7,** 491–502 (2006).

30. Aebersold, R. & Mann, M. Mass spectrometry-based proteomics. *Nature* **422,** 198–207 (2003).

31. Ong, S.-E. & Mann, M. Mass spectrometry–based proteomics turns quantitative. *Nat. Chem. Biol.* **1,** 252–262 (2005).

32. Ortelli, D., Edder, P. & Corvi, C. Multiresidue analysis of 74 pesticides in fruits and vegetables by liquid chromatography–electrospray–tandem mass spectrometry. *Anal. Chim. Acta* **520,** 33–45 (2004).

33. Thomson, J. J. Conduction of Electricity through Gases. *Nature* **69,** 74–75 (1903).

34. Thomson, J. J. & Rutherford, E. On the passage of electricity through gases exposed to Röntgen rays. *Philos. Mag. Ser. 5* **42,** 392 (1896).

35. Röntgen, W. *Eine neue art von strahlen*. (Stahel'schen K.B. Hof und Universitätsbuch und Kunsthandlung, 1896).

36. Rutherford, E. The velocity and rate of recombination of the ions of gases exposed to Röntgen radiation. *Philos. Mag. Ser. 5* **44,** 422 (1897).

37. Langevin, P. *Ann. Chem. Phys.* **5,** 245 (1905).

38. Squires, G. Francis Aston and the mass spectrograph. *J. Chem. Soc. Dalton Trans.* 3893–3900 (1998).

39. Zolotov, Y. A. Ion mobility spectrometry. *J. Anal. Chem.* **61,** 519–519 (2006).

40. McDaniel, E. W. & Martin, D. W. *Drift tube-mass spectrometer for studies of thermal-energy ion-molecule reactions. Technical Report No. 3*. (1960).

41. Kebarle, P. & Hogg, A. M. Mass-Spectrometric Study of Ions at Near Atmospheric Pressures. I. The Ionic Polymerization of Ethylene. *J. Chem. Phys.* **42,** 668 (1965).

42. Albritton, D. L., Miller, T. M., Martin, D. W. & McDaniel, E. W. Mobilities of Mass-Identified H_3^+ and H^+ Ions in Hydrogen. *Phys. Rev.* **171,** 94 (1968).

43. Milloy, H. B. & Crompton, R. W. Momentum-transfer cross section for electron-helium collisions in the range 4-12 eV. *Phys. Rev. A* **15,** 1847 (1977).

44. Barnes, W. S., Martin, D. W. & McDaniel, E. W. Mass Spectrographic Identification of the Ion Observed in Hydrogen Mobility Experiments. *Phys. Rev. Lett.* **6,** 110 (1961).

45. McAfee, K. B. & Edelson, D. Identification and Mobility of Ions in a Townsend Discharge by Time-resolved Mass Spectrometry. *Proc. Phys. Soc.* **81,** 382–384 (1963).

46. Kanu, A. B., Dwivedi, P., Tam, M., Matz, L. & Hill, H. H. Ion mobility-mass spectrometry. *J. Mass Spectrom.* **43,** 1–22 (2008).

47. Karasek, F. W., Hill, H. H. & Kim, S. H. Plasma chromatography of heroin and cocaine with mass-identified mobility spectra. *J. Chromatogr.* **117,** 327–336 (1976).

48. Wu, C., Siems, W. F., Asbury, G. R. & Hill, H. H. Electrospray Ionization High-Resolution Ion Mobility Spectrometry−Mass Spectrometry. *Anal. Chem.* **70,** 4929–4938 (1998).

49. Creaser, C. S., Benyezzar, M., Griffiths, J. R. & Stygall, J. W. A Tandem Ion Trap/Ion Mobility Spectrometer. *Anal. Chem.* **72,** 2724–2729 (2000).

50. Bluhm, B. K., Gillig, K. J. & Russell, D. H. Development of a Fourier-transform ion cyclotron resonance mass spectrometer-ion mobility spectrometer. *Rev. Sci. Instrum.* **71,** 4078 (2000).

51. Clemmer, D. E. Injected-ion Mobility Analysis of Biomolecules. (1997). at <http://www.indiana.edu/~clemmer/Publications/pub%20042.pdf>

52. Gorshkov, M. P. Inventor's Certificate USSR No. 966583 in Russian. (1982).

53. Buryakov, I. A., Krylov, E. V., Nazarov, E. G. & Rasulev, U. K. A new method of separation of multi-atomic ions by mobility at atmospheric pressure using a high-frequency amplitude-asymmetric strong electric field. *Int. J. Mass Spectrom. Ion Process.* **128,** 143–148 (1993).

54. Lipinski, C. A., Lombardo, F., Dominy, B. W. & Feeney, P. J. Experimental and computational approaches to estimate solubility and permeability in drug discovery and development settings. *Adv. Drug Deliv. Rev.* **23,** 3–25 (1997).

55. Turner, R. B. & Brokenshire, J. L. Hand-held ion mobility spectrometers. *TrAC Trends Anal. Chem.* **13,** 281–286 (1994).

56. Gehrke, C. W. *Chromatography: a century of discovery 1900-2000 : the bridge to the sciences/technology*. (Elsevier, 2001).

57. Harvey, S. R., Macphee, C. E. & Barran, P. E. Ion mobility mass spectrometry for peptide analysis. *Methods San Diego Calif* **54,** 454–461 (2011).

58. Uetrecht, C., Rose, R. J., Duijn, E. van, Lorenzen, K. & Heck, A. J. R. Ion mobility mass spectrometry of proteins and protein assemblies. *Chem. Soc. Rev.* **39,** 1633–1655 (2010).

59. Souza Pessôa, G. de, Pilau, E. J., Gozzo, F. C. & Zezzi Arruda, M. A. Ion mobility mass spectrometry: an elegant alternative focusing on speciation studies. *J. Anal. At. Spectrom.* **26,** 201 (2011).

60. Jurneczko, E. & Barran, P. E. How useful is ion mobility mass spectrometry for structural biology? The relationship between protein crystal structures and their collision cross sections in the gas phase. *Analyst* **136,** 20–28 (2010).

61. Thalassinos, K., Grabenauer, M., Slade, S. E., Hilton, G. R., Bowers, M. T. & Scrivens, J. H. Characterization of Phosphorylated Peptides Using Traveling Wave-Based and Drift Cell Ion Mobility Mass Spectrometry. *Anal. Chem.* **81,** 248–254 (2009).

62. Santos, L. F. A., Iglesias, A. H., Pilau, E. J., Gomes, A. F. & Gozzo, F. C. Traveling-Wave Ion Mobility Mass Spectrometry Analysis of Isomeric Modified Peptides Arising from Chemical Cross-Linking. *J. Am. Soc. Mass Spectrom.* **21,** 2062–2069 (2010).

63. Zhou, M. & Robinson, C. V. When proteomics meets structural biology. *Trends Biochem. Sci.* **35,** 522–529 (2010).

64. Tang, K., Shvartsburg, A. A., Lee, H.-N., Prior, D. C., Buschbach, M. A., Li, F., Tolmachev, A. V., Anderson, G. A. & Smith, R. D. High-Sensitivity Ion Mobility Spectrometry/Mass Spectrometry Using Electrodynamic Ion Funnel Interfaces. *Anal. Chem.* **77,** 3330–3339 (2005).

65. Belov, M. E., Clowers, B. H., Prior, D. C., Danielson III, W. F., Liyu, A. V., Petritis, B. O. & Smith, R. D. Dynamically Multiplexed Ion Mobility Time-of-Flight Mass Spectrometry. *Anal. Chem.* **80,** 5873–5883 (2008).

66. Ruotolo, B. T., Gillig, K. J., Stone, E. G., Russell, D. H., Fuhrer, K., Gonin, M. & Schultz, J. A. Analysis of protein mixtures by matrix-assisted laser desorption ionization-ion mobility-orthogonal-time-of-flight mass spectrometry. *Int. J. Mass Spectrom.* **219,** 253–267 (2002).

67. Valentine, S. J., Kulchania, M., Barnes, C. A. S. & Clemmer, D. E. Multidimensional separations of complex peptide mixtures: a combined high-performance liquid chromatography/ion mobility/time-of-flight mass spectrometry approach. *Int. J. Mass Spectrom.* **212,** 97–109 (2001).

68. Kolakowski, B. M. & Mester, Z. Review of applications of high-field asymmetric waveform ion mobility spectrometry (FAIMS) and differential mobility spectrometry (DMS). *Analyst* **132,** 842–864 (2007).

69. Giles, K., Williams, J. P. & Campuzano, I. Enhancements in travelling wave ion mobility resolution. *Rapid Commun. Mass Spectrom.* **25,** 1559–1566 (2011).

70. Mason, E. A. & McDaniel, E. W. *Transport Properties of Ions in Gases*. (Wiley-VCH Verlag GmbH & Co. KGaA, 1988). at <http://onlinelibrary.wiley.com/book/10.1002/3527602852>

71. Henderson, S. C., Valentine, S. J., Counterman, A. E. & Clemmer, D. E. ESI/Ion Trap/Ion Mobility/Time-of-Flight Mass Spectrometry for Rapid and Sensitive Analysis of Biomolecular Mixtures. *Anal. Chem.* **71,** 291–301 (1999).

72. Myung, S., Lee, Y. J., Moon, M. H., Taraszka, J., Sowell, R., Koeniger, S., Hilderbrand, A. E., Valentine, S. J., Cherbas, L., Cherbas, P., Kaufmann, T. C., Miller, D. F., Mechref, Y., Novotny, M. V., Ewing, M. A., Sporleder, C. R. & Clemmer, D. E. Development of High-Sensitivity Ion Trap Ion Mobility Spectrometry Time-of-Flight Techniques: A High-Throughput Nano-LC-IMS-TOF Separation of Peptides Arising from a Drosophila Protein Extract. *Anal. Chem.* **75,** 5137–5145 (2003).

73. Wyttenbach, T., Kemper, P. R. & Bowers, M. T. Design of a new electrospray ion mobility mass spectrometer. *Int. J. Mass Spectrom.* **212,** 13–23 (2001).

74. Clowers, B. H., Siems, W. F., Hill, H. H. & Massick, S. M. Hadamard Transform Ion Mobility Spectrometry. *Anal. Chem.* **78,** 44–51 (2006).

75. Tarver, E. E. External Second Gate, Fourier Transform Ion Mobility Spectrometry: Parametric Optimization for Detection of Weapons of Mass Destruction. *Sensors* **4,** 1–13 (2004).

76. Vautz, W., Schwarz, L., Hariharan, C. & Schilling, M. Ion characterisation by comparison of ion mobility spectrometry and mass spectrometry data. *Int. J. Ion Mobil. Spectrom.* **13,** 121–129 (2010).

77. Tang, X., Bruce, J. E. & Hill, H. H. Characterizing Electrospray Ionization Using Atmospheric Pressure Ion Mobility Spectrometry. *Anal. Chem.* **78,** 7751–7760 (2006).

78. Baim, M. A. & Hill, H. H. Tunable selective detection for capillary gas chromatography by ion mobility monitoring. *Anal. Chem.* **54,** 38–43 (1982).

79. Snyder, A. P., Harden, C. S., Brittain, A. H., Kim, M. G., Arnold, N. S. & Meuzelaar, H. L. C. Portable hand-held gas chromatography/ion mobility spectrometry device. *Anal. Chem.* **65,** 299–306 (1993).

80. Eatherton, R. L., Morrissey, M. A., Siems, W. F. & Hill, H. H. Ion mobility detection after supercritical fluid chromatography. *J. High Resolut. Chromatogr.* **9,** 154–160 (1986).

81. Huang, M. X., Markides, K. E. & Lee, M. L. Evaluation of an ion mobility detector for supercritical fluid chromatography with solvent-modified carbon dioxide mobile phases. *Chromatographia* **31,** 163–167 (1991).

82. Jackson, S. N., Ugarov, M., Egan, T., Post, J. D., Langlais, D., Schultz, J. A. & Woods, A. S. MALDI-ion mobility-TOFMS imaging of lipids in rat brain tissue. *J. Mass Spectrom.* **42,** 1093–1098 (2007).

83. Weston, D. J., Bateman, R., Wilson, I. D., Wood, T. R. & Creaser, C. S. Direct analysis of pharmaceutical drug formulations using ion mobility spectrometry/quadrupole-time-of-flight mass spectrometry combined with desorption electrospray ionization. *Anal. Chem.* **77,** 7572–7580 (2005).

84. Hill, C. A. & Thomas, C. L. P. A pulsed corona discharge switchable high resolution ion mobility spectrometer-mass spectrometer. *Analyst* **128,** 55–60 (2003).

85. Shvartsburg, A. A., Tang, K., Smith, R. D., Holden, M., Rush, M., Thompson, A. & Toutoungi, D. Ultrafast Differential Ion Mobility Spectrometry at Extreme Electric Fields Coupled to Mass Spectrometry. *Anal. Chem.* **81,** 8048–8053 (2009).

86. Enders, J. R. & Mclean, J. A. Chiral and structural analysis of biomolecules using mass spectrometry and ion mobility-mass spectrometry. *Chirality* **21,** E253–E264 (2009).

87. Eiceman, G. A. & Karpas, Z. *Ion Mobility Spectrometry, Second Edition*. (CRC Press, 2004).

88. Matz, L. M. & Hill, H. H. Evaluating the Separation of Amphetamines by Electrospray Ionization Ion Mobility Spectrometry/MS and Charge Competition within the ESI Process. *Anal. Chem.* **74,** 420–427 (2002).

89. Covey, T. & Douglas, D. J. Collision cross sections for protein ions. *J. Am. Soc. Mass Spectrom.* **4,** 616–623 (1993).

90. Douglas, D. J. Applications of Collision Dynamics in Quadrupole Mass Spectrometry. *J. Am. Soc. Mass Spectrom.* **9,** 101–113 (1998).

91. Javahery, G. & Thomson, B. A segmented radiofrequency-only quadrupole collision cell for measurements of ion collision cross section on a triple quadrupole mass spectrometer. *J. Am. Soc. Mass Spectrom.* **8,** 697–702 (1997).

92. Guo, Y., Wang, J., Javahery, G., Thomson, B. A. & Siu, K. W. M. Ion Mobility Spectrometer with Radial Collisional Focusing. *Anal. Chem.* **77,** 266–275 (2004).

93. Shvartsburg, A. A., Tang, K. & Smith, R. D. Modeling the resolution and sensitivity of FAIMS analyses. *J. Am. Soc. Mass Spectrom.* **15,** 1487–1498 (2004).

94. FAIMS Interface - Thermo Scientific. at <http://www.thermoscientific.com/ecomm/servlet/productsdetail?productId=11961722&storeId=11152>

95. Hatsis, P., Brockman, A. H. & Wu, J.-T. Evaluation of high-field asymmetric waveform ion mobility spectrometry coupled to nanoelectrospray ionization for bioanalysis in drug discovery. *Rapid Commun. Mass Spectrom.* **21,** 2295–2300 (2007).

96. Cui, M., Ding, L. & Mester, Z. Separation of Cisplatin and Its Hydrolysis Products Using Electrospray Ionization High-Field Asymmetric Waveform Ion Mobility Spectrometry Coupled with Ion Trap Mass Spectrometry. *Anal. Chem.* **75,** 5847–5853 (2003).

97. Champarnaud, E., Laures, A. M.-F., Borman, P. J., Chatfield, M. J., Kapron, J. T., Harrison, M. & Wolff, J.-C. Trace level impurity method development with high-field asymmetric waveform ion mobility spectrometry: systematic study of factors affecting the performance. *Rapid Commun. Mass Spectrom.* **23,** 181–193 (2009).

98. Aksenov, A. A. & Kapron, J. T. Behaviour of tetraalkylammonium ions in high-field asymmetric waveform ion mobility spectrometry. *Rapid Commun. Mass Spectrom.* **24,** 1392–1396 (2010).

99. Smith, R. D., Prasad, S., Tang, K., Manura, D. & Papanastasiou, D. Simulation of Ion Motion in FAIMS through Combined Use of SIMION and Modified SDS. *Anal. Chem.* **81,** 8749–8757 (2009).

100. Nazarov, E. G., Coy, S. L., Krylov, E. V., Miller, R. A. & Eiceman, G. A. Pressure Effects in Differential Mobility Spectrometry. *Anal Chem* **78,** 7697–7706 (2006).

101. Levin, D. S., Vouros, P., Miller, R. A., Nazarov, E. G. & Morris, J. C. Characterization of Gas-Phase Molecular Interactions on Differential Mobility Ion Behavior Utilizing an Electrospray Ionization-Differential Mobility-Mass Spectrometer System. *Anal Chem* **78,** 96–106 (2011).

102. Prieto, M. & Yost, R. A. Spherical FAIMS: comparison of curved electrode geometries. *Int. J. Ion Mobil. Spectrom.* **14,** 61–69 (2011).

103. Guevremont, R. & Purves, R. W. Atmospheric pressure ion focusing in a high-field asymmetric waveform ion mobility spectrometer. *Rev. Sci. Instrum.* **70,** 1370 (1999).

104. Krylov, E. V. A method of reducing diffusion losses in a drift spectrometer. *Tech. Phys.* **44,** 113–116 (1999).

105. Purves, R. W. & Shvartsburg, A. A. Differential Ion Mobility Spectrometry: Nonlinear Ion Transport and Fundamentals of FAIMS, CRC Press, Taylor and Francis Group, Boca Raton, FL 33487-2742, USA (2009) ISBN 978-1-4200-5106-3 Hardcover, $159.95 US, 322 pp. *J. Am. Soc. Mass Spectrom.* **21,** R3–R3 (2010).

106. Gerlich, D. in *Advances in Chemical Physics* (eds. Ng, C.-Y., Baer, M., Prigogine, I. & Rice, S. A.) 1–176 (John Wiley & Sons, Inc., 1992). at <http://onlinelibrary.wiley.com/doi/10.1002/9780470141397.ch1/summary>

107. Shvartsburg, A. A. & Smith, R. D. Fundamentals of Traveling Wave Ion Mobility Spectrometry. *Anal. Chem.* **80,** 9689–9699 (2008).

108. Williams, J. P., Bugarcic, T., Habtemariam, A., Giles, K., Campuzano, I., Rodger, P. M. & Sadler, P. J. Isomer Separation and Gas-Phase Configurations of Organoruthenium Anticancer Complexes: Ion Mobility Mass Spectrometry and Modeling. *J. Am. Soc. Mass Spectrom.* **20,** 1119–1122 (2009).

109. D'Agostino, P. A. & Chenier, C. L. Desorption electrospray ionization mass spectrometric analysis of organophosphorus chemical warfare agents using ion mobility and tandem mass spectrometry. *Rapid Commun. Mass Spectrom.* **24,** 1617–1624 (2010).

110. Pringle, S. D., Giles, K., Wildgoose, J. L., Williams, J. P., Slade, S. E., Thalassinos, K., Bateman, R. H., Bowers, M. T. & Scrivens, J. H. An investigation of the mobility separation of some peptide and protein ions using a new hybrid quadrupole/travelling wave IMS/oa-ToF instrument. *Int. J. Mass Spectrom.* **261,** 1–12 (2007).

111. Knutson, E. O. & Whitby, K. T. Aerosol classification by electric mobility: apparatus, theory, and applications. *J. Aerosol Sci.* **6,** 443–451 (1975).

112. Stolzenburg, M. R. & McMurry, P. H. Equations Governing Single and Tandem DMA Configurations and a New Lognormal Approximation to the Transfer Function. *Aerosol Sci. Technol.* **42,** 421–432 (2008).

113. Hogan, C. J., Ruotolo, B. T., Robinson, C. V. & Fernandez de la Mora, J. Tandem Differential Mobility Analysis-Mass Spectrometry Reveals Partial Gas-Phase Collapse of the GroEL Complex. *J. Phys. Chem. B* **115,** 3614–3621 (2011).

114. de la Mora, J. F., Ude, S. & Thomson, B. A. The potential of differential mobility analysis coupled to MS for the study of very large singly and multiply charged proteins and protein complexes in the gas phase. *Biotechnol. J.* **1,** 988–997 (2006).

115. Ude, S., Fernández de la Mora, J. & Thomson, B. A. Charge-Induced Unfolding of Multiply Charged Polyethylene Glycol Ions. *J. Am. Chem. Soc.* **126,** 12184–12190 (2004).

116. Rus, J., Moro, D., Sillero, J. A., Royuela, J., Casado, A., Estevez-Molinero, F. & Fernández de la Mora, J. IMS–MS studies based on coupling a differential mobility analyzer (DMA) to commercial API–MS systems. *Int. J. Mass Spectrom.* **298,** 30–40 (2010).

117. Martínez-Lozano, P. & Rus, J. Separation of Isomers L-Alanine and Sarcosine in Urine by Electrospray Ionization and Tandem Differential Mobility Analysis-Mass Spectrometry. *J. Am. Soc. Mass Spectrom.* **21,** 1129–1132 (2010).

118. Shvartsburg, A. A., Danielson, W. F. & Smith, R. D. High-Resolution Differential Ion Mobility Separations Using Helium-Rich Gases. *Anal. Chem.* **82,** 2456–2462 (2010).

119. Methodologies for Metabolomics. *Cambridge University Press* at <http://www.cambridge.org/gb/academic/subjects/life-

sciences/biotechnology/methodologies-metabolomics-experimental-strategies-and-techniques?format=HB>

120. *Fundamentals of Mass Spectrometry*. (Springer New York, 2013). at <http://link.springer.com/10.1007/978-1-4614-7233-9>

121. Nazarov, E. G. A journey into DMS/FAIMS technology. *Int. J. Ion Mobil. Spectrom.* **15,** 83–84 (2012).

122. Williams, J. P., Grabenauer, M., Holland, R. J., Carpenter, C. J., Wormald, M. R., Giles, K., Harvey, D. J., Bateman, R. H., Scrivens, J. H. & Bowers, M. T. Characterization of simple isomeric oligosaccharides and the rapid separation of glycan mixtures by ion mobility mass spectrometry. *Int. J. Mass Spectrom.* **298,** 119–127 (2010).

123. Shvartsburg, A. A., Clemmer, D. E. & Smith, R. D. Isotopic Effect on Ion Mobility and Separation of Isotopomers by High-Field Ion Mobility Spectrometry. *Anal. Chem.* **82,** 8047–8051 (2010).

124. Siems, W. F., Wu, C., Tarver, E. E., Hill, H. H. J., Larsen, P. R. & McMinn, D. G. Measuring the Resolving Power of Ion Mobility Spectrometers. *Anal. Chem.* **66,** 4195–4201 (1994).

125. Koeniger, S. L., Merenbloom, S. I., Valentine, S. J., Jarrold, M. F., Udseth, H. R., Smith, R. D. & Clemmer, D. E. An IMS−IMS Analogue of MS−MS. *Anal. Chem.* **78,** 4161–4174 (2006).

126. Shelimov, K. B., Clemmer, D. E., Hudgins, R. R. & Jarrold, M. F. Protein Structure in Vacuo: Gas-Phase Conformations of BPTI and Cytochrome c. *J. Am. Chem. Soc.* **119,** 2240–2248 (1997).

127. Kemper, P. R., Dupuis, N. F. & Bowers, M. T. A new, higher resolution, ion mobility mass spectrometer. *Int. J. Mass Spectrom.* **287,** 46–57 (2009).

128. Clowers, B. H., Ibrahim, Y. M., Prior, D. C., Danielson, W. F., Belov, M. E. & Smith, R. D. Enhanced ion utilization efficiency using an electrodynamic ion funnel trap as an injection mechanism for ion mobility spectrometry. *Anal. Chem.* **80,** 612–623 (2008).

129. Valentine, S. J., Stokes, S. T., Kurulugama, R. T., Nachtigall, F. M. & Clemmer, D. E. Overtone Mobility Spectrometry: Part 2. Theoretical Considerations of Resolving Power. *J. Am. Soc. Mass Spectrom.* **20,** 738–750 (2009).

130. Bohrer, B. C., Merenbloom, S. I., Koeniger, S. L., Hilderbrand, A. E. & Clemmer, D. E. Biomolecule Analysis by Ion Mobility Spectrometry. *Annu. Rev. Anal. Chem.* **1,** 293–327 (2008).

131. Li, X., Stoll, D. R. & Carr, P. W. Equation for Peak Capacity Estimation in Two-Dimensional Liquid Chromatography. *Anal. Chem.* **81,** 845–850 (2009).

132. Griffin, G. W., Dzidic, I., Carroll, D. I., Stillwell, R. N. & Horning, E. C. Ion mass assignments based on mobility measuremets. Validity of plasma chromatographic mass mobility correlations. *Anal. Chem.* **45,** 1204–1209 (1973).

133. Dwivedi, P., Schultz, A. J. & Jr, H. H. H. Metabolic profiling of human blood by high-resolution ion mobility mass spectrometry (IM-MS). *Int. J. Mass Spectrom.* **298,** 78–90 (2010).

134. Guo, Y., Srinivasan, S. & Gaiki, S. Evaluation of The Peak Capacity of Various RP-Columns for Small Molecule Compounds in Gradient Elution. *Chromatographia* **70,** 1045–1054 (2009).

135. Wren, S. A. C. Peak capacity in gradient ultra performance liquid chromatography (UPLC). *J. Pharm. Biomed. Anal.* **38,** 337–343 (2005).

136. Canterbury, J. D., Yi, X., Hoopmann, M. R. & MacCoss, M. J. Assessing the Dynamic Range and Peak Capacity of Nanoflow LC−FAIMS−MS on an Ion Trap Mass Spectrometer for Proteomics. *Anal. Chem.* **80,** 6888–6897 (2008).

137. Schneider, B. B., Covey, T. R., Coy, S. L., Krylov, E. V. & Nazarov, E. G. Chemical Effects in the Separation Process of a Differential Mobility/Mass Spectrometer System. *Anal. Chem.* **82,** 1867–1880 (2010).

138. Liu, X., Valentine, S. J., Plasencia, M. D., Trimpin, S., Naylor, S. & Clemmer, D. E. Mapping the Human Plasma Proteome by SCX-LC-IMS-MS. *J. Am. Soc. Mass Spectrom.* **18,** 1249–1264 (2007).

139. Taraszka, J. A., Gao, X., Valentine, S. J., Sowell, R. A., Koeniger, S. L., Miller, D. F., Kaufman, T. C. & Clemmer, D. E. Proteome Profiling for Assessing Diversity: Analysis of Individual Heads of Drosophila melanogaster Using LC−Ion Mobility−MS. *J. Proteome Res.* **4,** 1238–1247 (2005).

140. Fenn, L. S. & McLean, J. A. Enhanced carbohydrate structural selectivity in ion mobility-mass spectrometry analyses by boronic acid derivatization. *Chem. Commun.* 5505 (2008).

141. Howdle, M. D., Eckers, C., Laures, A. M.-F. & Creaser, C. S. The Use of Shift Reagents in Ion Mobility-Mass Spectrometry: Studies on the Complexation of an Active Pharmaceutical Ingredient with Polyethylene Glycol Excipients. *J. Am. Soc. Mass Spectrom.* **20,** 1–9 (2009).

142. Clowers, B. H. & Hill, H. H. Influence of cation adduction on the separation characteristics of flavonoid diglycoside isomers using dual gate-ion mobility-quadrupole ion trap mass spectrometry. *J. Mass Spectrom.* **41,** 339–351 (2006).

143. Flick, T. G., Campuzano, I. D. G. & Bartberger, M. D. Structural Resolution of Proline Diastereomers with Ion Mobility Spectrometry via Alkali Metal Ion Cationization. *Anal. Chem.* (2015). doi:10.1021/ac5043285

144. Kurulugama, R. T., Darland, E., Kuhlmann, F., Stafford, G. & Fjeldsted, J. Evaluation of Drift Gas Selection in Complex Sample Analyses Using a High Performance Drift

Tube Ion Mobility-QTOF Mass Spectrometer. *Analyst* (2015). doi:10.1039/C5AN00991J

145. Fernández-Maestre, R., Wu, C. & Hill Jr., H. H. Using a buffer gas modifier to change separation selectivity in ion mobility spectrometry. *Int. J. Mass Spectrom.* **298,** 2–9 (2010).

146. Eiceman, G. A., Yuan-Feng, W., Garcia-Gonzalez, L., Harden, C. S. & Shoff, D. B. Enhanced selectivity in ion mobility spectrometry analysis of complex mixtures by alternate reagent gas chemistry. *Anal. Chim. Acta* **306,** 21–33 (1995).

147. Steiner, W. E., English, W. A. & Hill, H. H. Ion−Neutral Potential Models in Atmospheric Pressure Ion Mobility Time-of-Flight Mass Spectrometry IM(tof)MS. *J Phys Chem A* **110,** 1836–1844 (2006).

148. Wyttenbach, T., Bleiholder, C. & Bowers, M. T. Factors Contributing to the Collision Cross Section of Polyatomic Ions in the Kilodalton to Gigadalton Range: Application to Ion Mobility Measurements. *Anal. Chem.* **85,** 2191–2199 (2013).

149. Asbury, G. R. & Hill, H. H. Using Different Drift Gases To Change Separation Factors (α) in Ion Mobility Spectrometry. *Anal. Chem.* **72,** 580–584 (2000).

150. Krylov, E., Nazarov, E. G., Miller, R. A., Tadjikov, B. & Eiceman, G. A. Field Dependence of Mobilities for Gas-Phase-Protonated Monomers and Proton-Bound Dimers of Ketones by Planar Field Asymmetric Waveform Ion Mobility Spectrometer (PFAIMS). *J. Phys. Chem. A.* **106,** 5437–5444 (2002).

151. Krylov, E. V. & Nazarov, E. G. Electric field dependence of the ion mobility. *Int. J. Mass Spectrom.* **285,** 149–156 (2009).

152. Schneider, B. B., Covey, T. R., Coy, S. L., Krylov, E. V. & Nazarov, E. G. Control of chemical effects in the separation process of a differential mobility mass spectrometer system. *Eur. J. Mass Spectrom. Chichester Engl.* **16,** 57–71 (2010).

153. Coy, S. L., Krylov, E. V., Schneider, B. B., Covey, T. R., Brenner, D. J., Tyburski, J. B., Patterson, A. D., Krausz, K. W., Fornace, A. J. & Nazarov, E. G. Detection of Radiation-Exposure Biomarkers by Differential Mobility Prefiltered Mass Spectrometry (DMS-MS). *Int. J. Mass Spectrom.* **291,** 108–117 (2010).

154. Beegle, L. W., Kanik, I., Matz, L. & Hill, H. H. Electrospray Ionization High-Resolution Ion Mobility Spectrometry for the Detection of Organic Compounds, 1. Amino Acids. *Anal. Chem.* **73,** 3028–3034 (2001).

155. Budimir, N., Weston, D. J. & Creaser, C. S. Analysis of pharmaceutical formulations using atmospheric pressure ion mobility spectrometry combined with liquid chromatography and nano-electrospray ionisation. *Analyst* **132,** 34 (2007).

156. Karimi, A. & Alizadeh, N. Rapid analysis of captopril in human plasma and pharmaceutical preparations by headspace solid phase microextraction based on polypyrrole film coupled to ion mobility spectrometry. *Talanta* **79,** 479–485 (2009).

157. O'Donnell, R. M., Sun, X. & Harrington, P. de B. Pharmaceutical applications of ion mobility spectrometry. *TrAC Trends Anal. Chem.* **27,** 44–53 (2008).

158. Wang, Y., Nacson, S. & Pawliszyn, J. The coupling of solid-phase microextraction/surface enhanced laser desorption/ionization to ion mobility spectrometry for drug analysis. *Anal. Chim. Acta* **582,** 50–54 (2007).

159. Jafari, M. T., Khayamian, T., Shaer, V. & Zarei, N. Determination of veterinary drug residues in chicken meat using corona discharge ion mobility spectrometry. *Anal. Chim. Acta* **581,** 147–153 (2007).

160. Alonso, R., Rodríguez-Estévez, V., Domínguez-Vidal, A., Ayora-Cañada, M. J., Arce, L. & Valcárcel, M. Ion mobility spectrometry of volatile compounds from Iberian pig fat for fast feeding regime authentication. *Talanta* **76,** 591–596 (2008).

161. Jafari, M. T. Determination and identification of malathion, ethion and dichlorovos using ion mobility spectrometry. *Talanta* **69,** 1054–1058 (2006).

162. Keller, T., Keller, A., Tutsch-Bauer, E. & Monticelli, F. Application of ion mobility spectrometry in cases of forensic interest. *Forensic Sci. Int.* **161,** 130–140 (2006).

163. Tuovinen, K., Paakkanen, H. & Hänninen, O. Detection of pesticides from liquid matrices by ion mobility spectrometry. *Anal. Chim. Acta* **404,** 7–17 (2000).

164. Dussy, F. E., Berchtold, C., Briellmann, T. A., Lang, C., Steiger, R. & Bovens, M. Validation of an ion mobility spectrometry (IMS) method for the detection of heroin and cocaine on incriminated material. *Forensic Sci. Int.* **177,** 105–111 (2008).

165. Lawrence, A. H. Ion mobility spectrometry/mass spectrometry of some prescription and illicit drugs. *Anal. Chem.* **58,** 1269–1272 (1986).

166. Collins, D. C. & Lee, M. L. Electrospray ionization gas-phase electrophoresis under ambient conditions and it's potential or high-speed separations. *Fresenius J. Anal. Chem.* **369,** 225–233 (2001).

167. Zhao, W., Bhushan, A., Schivo, M., Kenyon, N. J. & Davis, C. E. in *Wearable and Autonomous Biomedical Devices and Systems for Smart Environment* **75,** 55–73 (Springer Berlin Heidelberg, 2010).

168. Covington, J. A., Schee, M. P. van der, Edge, A. S. L., Boyle, B., Savage, R. S. & Arasaradnam, R. P. The application of FAIMS gas analysis in medical diagnostics. *Analyst* **140,** 6775–6781 (2015).

169. Pris, A. D., Mondello, F. J., Wroczynski, R. J., Murray, A. J., Boudries, H., Surman, C. M. & Paxon, T. L. Improved Specific Biodetection with Ion Trap Mobility Spectrometry (ITMS): A 10-min, Multiplexed, Immunomagnetic ELISA. *Anal. Chem.* **81,** 9948–9954 (2009).

170. Snyder, A. P., Blyth, D. A. & Parsons, J. A. Ion mobility spectrometry as an immunoassay detection technique. *J. Microbiol. Methods* **27,** 81–88 (1996).

171. Dear, G. J., Munoz-Muriedas, J., Beaumont, C., Roberts, A., Kirk, J., Williams, J. P. & Campuzano, I. Sites of metabolic substitution: investigating metabolite structures utilising ion mobility and molecular modelling. *Rapid Commun. Mass Spectrom.* **24,** 3157–3162 (2010).

172. Cuyckens, F., Wassvik, C., Mortishire-Smith, R. J., Tresadern, G., Campuzano, I. & Claereboudt, J. Product ion mobility as a promising tool for assignment of positional isomers of drug metabolites. *Rapid Commun. Mass Spectrom.* **25,** 3497–3503 (2011).

173. Manard, M. J., Trainham, R., Weeks, S., Coy, S. L., Krylov, E. V. & Nazarov, E. G. Differential mobility spectrometry/mass spectrometry: The design of a new mass spectrometer for real-time chemical analysis in the field. *Int. J. Mass Spectrom.* **295,** 138–144 (2010).

174. Shvartsburg, A. A., Smith, R. D., Wilks, A., Koehl, A., Ruiz-Alonso, D. & Boyle, B. Ultrafast Differential Ion Mobility Spectrometry at Extreme Electric Fields in Multichannel Microchips. *Anal. Chem.* **81,** 6489–6495 (2009).

175. Weston, D. J. Ambient ionization mass spectrometry: current understanding of mechanistic theory; analytical performance and application areas. *Analyst* **135,** 661 (2010).

176. Dwivedi, P., Wu, C., Matz, L. M., Clowers, B. H., Siems, W. F. & Hill, H. H. Gas-Phase Chiral Separations by Ion Mobility Spectrometry. *Anal. Chem.* **78,** 8200–8206 (2006).

177. Mie, A., Jörntén-Karlsson, M., Axelsson, B.-O., Ray, A. & Reimann, C. T. Enantiomer Separation of Amino Acids by Complexation with Chiral Reference Compounds and

High-Field Asymmetric Waveform Ion Mobility Spectrometry: Preliminary Results and Possible Limitations. *Anal. Chem.* **79,** 2850–2858 (2007).

178. Campuzano, I., Bush, M. F., Robinson, C. V., Beaumont, C., Richardson, K., Kim, H. & Kim, H. I. Structural Characterization of Drug-like Compounds by Ion Mobility Mass Spectrometry: Comparison of Theoretical and Experimentally Derived Nitrogen Collision Cross Sections. *Anal. Chem.* **84,** 1026–1033 (2012).

179. Arthur, K. E., Wolff, J. & Carrier, D. J. Analysis of betamethasone, dexamethasone and related compounds by liquid chromatography/electrospray mass spectrometry. *Rapid Commun. Mass Spectrom.* **18,** 678–684 (2004).

180. Blech, S. & Laux, R. Resolving the microcosmos of complex samples: UPLC/travelling wave ion mobility separation high resolution mass spectrometry for the analysis of in vivo drug metabolism studies. *Int. J. Ion Mobil. Spectrom.* **16,** 5–17 (2012).

181. Harry, E. L., Bristow, A. W. T., Wilson, I. D. & Creaser, C. S. Real-time reaction monitoring using ion mobility-mass spectrometry. *Analyst* **136,** 1728 (2011).

182. Dwivedi, P., Bendiak, B., Clowers, B. H. & Hill, H. H. Rapid resolution of carbohydrate isomers by electrospray ionization ambient pressure ion mobility spectrometry-time-of-flight mass spectrometry (ESI-APIMS-TOFMS). *J. Am. Soc. Mass Spectrom.* **18,** 1163–1175 (2007).

183. Zhu, M., Bendiak, B., Clowers, B. & Hill, H. H. Ion mobility-mass spectrometry analysis of isomeric carbohydrate precursor ions. *Anal. Bioanal. Chem.* **394,** 1853–1867 (2009).

184. Likar, M. D., Cheng, G., Mahajan, N. & Zhang, Z. Rapid identification and absence of drug tests for AG-013736 in 1 mg Axitinib tablets by ion mobility spectrometry and DART(TM) mass spectrometry. *J. Pharm. Biomed. Anal.* **55,** 569–573 (2011).

185. Harry, E. L., Reynolds, J. C., Bristow, A. W. T., Wilson, I. D. & Creaser, C. S. Direct analysis of pharmaceutical formulations from non-bonded reversed-phase thin-layer chromatography plates by desorption electrospray ionisation ion mobility mass spectrometry. *Rapid Commun. Mass Spectrom.* **23,** 2597–2604 (2009).

186. Baker, E. S., Bushnell, J. E., Wecksler, S. R., Lim, M. D., Manard, M. J., Dupuis, N. F., Ford, P. C. & Bowers, M. T. Probing Shapes of Bichromophoric Metal−Organic Complexes Using Ion Mobility Mass Spectrometry. *J. Am. Chem. Soc.* **127,** 18222–18228 (2005).

187. Poornima, C. S. & Dean, P. M. Hydration in drug design. 1. Multiple hydrogen-bonding features of water molecules in mediating protein-ligand interactions. *J. Comput. Aided Mol. Des.* **9,** 500–512 (1995).

188. Pace, C. N., Treviño, S., Prabhakaran, E. & Scholtz, J. M. Protein structure, stability and solubility in water and other solvents. *Philos. Trans. R. Soc. Lond. B. Biol. Sci.* **359,** 1225–1234 (2004).

189. Homans, S. W. Water, water everywhere--except where it matters? *Drug Discov. Today* **12,** 534–539 (2007).

190. Momoh, P. O. & El-Shall, M. S. Stepwise hydration of ionized acetylene trimer. Further evidence for the formation of benzene radical cation. *Chem. Phys. Lett.* **436,** 25–29 (2007).

191. Momoh, P. O. & El-Shall, M. S. Gas phase hydration of organic ions. *Phys. Chem. Chem. Phys.* **10,** 4827 (2008).

192. Ibrahim, Y. M., Meot-Ner, M., Alshraeh, E. H., El-Shall, M. S. & Scheiner, S. Stepwise Hydration of Ionized Aromatics. Energies, Structures of the Hydrated Benzene Cation, and the Mechanism of Deprotonation Reactions. *J. Am. Chem. Soc.* **127,** 7053–7064 (2005).

193. Wyttenbach, T., Paizs, B., Barran, P., Breci, L., Liu, D., Suhai, S., Wysocki, V. H. & Bowers, M. T. The Effect of the Initial Water of Hydration on the Energetics, Structures, and H/D Exchange Mechanism of a Family of Pentapeptides: An Experimental and Theoretical Study. *J. Am. Chem. Soc.* **125,** 13768–13775 (2003).

194. Poully, J.-C., Nieuwjaer, N. & Pierre Schermann, J. Structure and dynamics of molecules of pharmaceutical interest in gas phase and in aqueous phase. *Phys. Scr.* **78,** 058123 (2008).

195. Foloppe, N. & Chen, I.-J. Conformational sampling and energetics of drug-like molecules. *Curr. Med. Chem.* **16,** 3381–3413 (2009).

196. Williams, J. P., Lough, J. A., Campuzano, I., Richardson, K. & Sadler, P. J. Use of ion mobility mass spectrometry and a collision cross-section algorithm to study an organometallic ruthenium anticancer complex and its adducts with a DNA oligonucleotide. *Rapid Commun. Mass Spectrom.* **23,** 3563–3569 (2009).

197. Heuvel, R. H. van den & Heck, A. J. Native protein mass spectrometry: from intact oligomers to functional machineries. *Curr. Opin. Chem. Biol.* **8,** 519–526 (2004).

198. Rand, K. D., Pringle, S. D., Murphy, J. P., Fadgen, K. E., Brown, J. & Engen, J. R. Gas-Phase Hydrogen/Deuterium Exchange in a Traveling Wave Ion Guide for the Examination of Protein Conformations. *Anal. Chem.* **81,** 10019–10028 (2009).

199. Ruotolo, B. T., Giles, K., Campuzano, I., Sandercock, A. M., Bateman, R. H. & Robinson, C. V. Evidence for Macromolecular Protein Rings in the Absence of Bulk Water. *Science* **310,** 1658–1661 (2005).

200. Schultz, S. G. & Solomon, A. K. Determination of the Effective Hydrodynamic Radii of Small Molecules by Viscometry. *J. Gen. Physiol.* **44,** 1189 –1199 (1961).

201. Shelimov, K. B. & Jarrold, M. F. Conformations, Unfolding, and Refolding of Apomyoglobin in Vacuum: An Activation Barrier for Gas-Phase Protein Folding. *J. Am. Chem. Soc.* **119,** 2987–2994 (1997).

202. Allen, F. H., Harris, S. E. & Taylor, R. Comparison of conformer distributions in the crystalline state with conformational energies calculated by ab initio techniques. *J. Comput. Aided Mol. Des.* **10,** 247–254 (1996).

203. Bastug, T. & Kuyucak, S. Role of the Dielectric Constants of Membrane Proteins and Channel Water in Ion Permeation. *Biophys. J.* **84,** 2871–2882 (2003).

204. Révész, Á., Schröder, D., Rokob, T. A., Havlík, M. & Dolenský, B. In-Flight Epimerization of a Bis-Tröger Base. *Angew. Chem. Int. Ed.* **50,** 2401–2404 (2011).

205. Maitra, U., Bag, B. G., Rao, P. & Powell, D. Asymmetric synthesis of steroidal Troger's base analogues. X-Ray molecular structure of methyl 3α,12α-{6H,12H-5,11-methanodibenzo[b,f][1,5]diazocine-2,8-bisacetoxy}-5β-cholan-24-oate. *J. Chem. Soc. [Perkin 1]* 2049 (1995).

206. Giles, K., Wildgoose, J. L., Langridge, D. J. & Campuzano, I. A method for direct measurement of ion mobilities using a travelling wave ion guide. *Int. J. Mass Spectrom.* **298,** 10–16 (2010).

207. Knapman, T. W., Berryman, J. T., Campuzano, I., Harris, S. A. & Ashcroft, A. E. Considerations in experimental and theoretical collision cross-section measurements of small molecules using travelling wave ion mobility spectrometry-mass spectrometry. *Int. J. Mass Spectrom.* **298,** 17–23 (2010).

208. Bush, M. F., Hall, Z., Giles, K., Hoyes, J., Robinson, C. V. & Ruotolo, B. T. Collision Cross Sections of Proteins and Their Complexes: A Calibration Framework and Database for Gas-Phase Structural Biology. *Anal. Chem.* **82,** 9557–9565 (2010).

209. Lavanant, H., Tognetti, V. & Afonso, C. Traveling Wave Ion Mobility Mass Spectrometry and Ab Initio Calculations of Phosphoric Acid Clusters. *J. Am. Soc. Mass Spectrom.* **25,** 572–580 (2014).

210. Hofmann, J., Struwe, W. B., Scarff, C. A., Scrivens, J. H., Harvey, D. J. & Pagel, K. Estimating Collision Cross Sections of Negatively Charged N-Glycans using Traveling Wave Ion Mobility-Mass Spectrometry. *Anal. Chem.* **86,** 10789–10795 (2014).

211. Lietz, C. B., Yu, Q. & Li, L. Large-Scale Collision Cross-Section Profiling on a Traveling Wave Ion Mobility Mass Spectrometer. *J. Am. Soc. Mass Spectrom.* **25,** 2009–2019 (2014).

212. Clemmer Group: Cross Section Database. at <http://www.indiana.edu/~clemmer/Research/Cross%20Section%20Database/cs_database.php>

213. Gelb, A. S., Jarratt, R. E., Huang, Y. & Dodds, E. D. A Study of Calibrant Selection in Measurement of Carbohydrate and Peptide Ion-Neutral Collision Cross Sections by Traveling Wave Ion Mobility Spectrometry. *Anal. Chem.* **86,** 11396–11402 (2014).

214. Kurulugama, R. T., Nachtigall, F. M., Lee, S., Valentine, S. J. & Clemmer, D. E. Overtone Mobility Spectrometry: Part 1. Experimental Observations. *J. Am. Soc. Mass Spectrom.* **20,** 729–737 (2009).

215. Baumketner, A., Bernstein, S. L., Wyttenbach, T., Lazo, N. D., Teplow, D. B., Bowers, M. T. & Shea, J.-E. Structure of the 21-30 fragment of amyloid β-protein. *Protein Sci.* **15,** 1239–1247 (2006).

216. von Helden, G., Wyttenbach, T. & Bowers, M. T. Conformation of Macromolecules in the Gas Phase: Use of Matrix-Assisted Laser Desorption Methods in Ion Chromatography. *Science* **267,** 1483–1485 (1995).

217. Hoaglund-Hyzer, C. S., Counterman, A. E. & Clemmer, D. E. Anhydrous Protein Ions. *Chem. Rev.* **99,** 3037–3080 (1999).

218. Jarrold, M. F. Peptides and proteins in the vapor phase. *Annu. Rev. Phys. Chem.* **51,** 179–207 (2000).

219. Kinnear, B. S., Hartings, M. R. & Jarrold, M. F. The Energy Landscape of Unsolvated Peptides: Helix Formation and Cold Denaturation in Ac-A4G7A4 + H$^+$. *J. Am. Chem. Soc.* **124,** 4422–4431 (2002).

220. Forsythe, J. G., Stow, S. M., Nefzger, H., Kwiecien, N. W., May, J. C., McLean, J. A. & Hercules, D. M. Structural Characterization of Methylenedianiline Regioisomers by Ion Mobility-Mass Spectrometry, Tandem Mass Spectrometry, and Computational Strategies: I. Electrospray Spectra of 2-Ring Isomers. *Anal. Chem.* **86,** 4362–4370 (2014).

221. Mao, Y., Ratner, M. A. & Jarrold, M. F. Molecular Dynamics Simulations of the Rehydration of Folded and Unfolded Cytochrome c Ions in the Vapor Phase. *J. Am. Chem. Soc.* **123,** 6503–6507 (2001).

222. Benigni, P., Marin, R. & Fernandez-Lima, F. Towards unsupervised polyaromatic hydrocarbons structural assignment from SA-TIMS –FTMS data. *Int. J. Ion Mobil. Spectrom.* **18,** 151–157 (2015).

223. Holmes, J. L. Assigning structures to ions in the gas phase. *Org. Mass Spectrom.* **20,** 169–183 (1985).

224. Wright, P., Alex, A., Nyaruwata, T., Parsons, T. & Pullen, F. Using density functional theory to rationalise the mass spectral fragmentation of maraviroc and its metabolites. *Rapid Commun. Mass Spectrom.* **24,** 1025–1031 (2010).

225. Alex, A., Harvey, S., Parsons, T., Pullen, F. S., Wright, P. & Riley, J. Can density functional theory (DFT) be used as an aid to a deeper understanding of tandem mass

spectrometric fragmentation pathways? *Rapid Commun. Mass Spectrom.* **23,** 2619–2627 (2009).

226. Klagkou, K., Pullen, F., Harrison, M., Organ, A., Firth, A. & Langley, G. J. Approaches towards the automated interpretation and prediction of electrospray tandem mass spectra of non-peptidic combinatorial compounds. *Rapid Commun. Mass Spectrom.* **17,** 1163–1168 (2003).

227. Galezowska, A., Harrison, M. W., Herniman, J. M., Skylaris, C.-K. & Langley, G. J. A predictive science approach to aid understanding of electrospray ionisation tandem mass spectrometric fragmentation pathways of small molecules using density functional calculations. *Rapid Commun. Mass Spectrom.* **27,** 964–970 (2013).

228. Shvartsburg, A. A. & Jarrold, M. F. An exact hard-spheres scattering model for the mobilities of polyatomic ions. *Chem. Phys. Lett.* **261,** 86–91 (1996).

229. Shvartsburg, A. A., Mashkevich, S. V., Baker, E. S. & Smith, R. D. Optimization of Algorithms for Ion Mobility Calculations. *J. Phys. Chem. A* **111,** 2002–2010 (2007).

230. Siu, C.-K., Guo, Y., Saminathan, I. S., Hopkinson, A. C. & Siu, K. W. M. Optimization of parameters used in algorithms of ion-mobility calculation for conformational analyses. *J. Phys. Chem. B* **114,** 1204–1212 (2010).

231. Fernandez-Lima, F. A., Wei, H., Gao, Y. Q. & Russell, D. H. On the Structure Elucidation Using Ion Mobility Spectrometry and Molecular Dynamics. *J. Phys. Chem. A* **113,** 8221–8234 (2009).

232. Wessel, M. D. & Jurs, P. C. Prediction of Reduced Ion Mobility Constants from Structural Information Using Multiple Linear Regression Analysis and Computational Neural Networks. *Anal. Chem.* **66,** 2480–2487 (1994).

233. Wessel, M. D., Sutter, J. M. & Jurs, P. C. Prediction of Reduced Ion Mobility Constants of Organic Compounds from Molecular Structure. *Anal. Chem.* **68,** 4237–4243 (1996).

234. Agbonkonkon, N., Tolley, H. D., Asplund, M. C., Lee, E. D. & Lee, M. L. Prediction of Gas-Phase Reduced Ion Mobility Constants (K0). *Anal. Chem.* **76,** 5223–5229 (2004).

235. Liu, H., Yao, X., Liu, M., Hu, Z. & Fan, B. Prediction of gas-phase reduced ion mobility constants (K(0)) based on the multiple linear regression and projection pursuit regression. *Talanta* **71,** 258–263 (2007).

236. Hariharan, C. B., Baumbach, J. I. & Vautz, W. Linearized Equations for the Reduced Ion Mobilities of Polar Aliphatic Organic Compounds. *Anal. Chem.* **82,** 427–431 (2010).

237. Wang, B., Valentine, S., Plasencia, M., Raghuraman, S. & Zhang, X. Artificial neural networks for the prediction of peptide drift time in ion mobility mass spectrometry. *BMC Bioinformatics* **11,** 182 (2010).

238. Kwasnik, M. & Fernández, F. M. Theoretical and experimental study of the achievable separation power in resistive-glass atmospheric pressure ion mobility spectrometry. *Rapid Commun. Mass Spectrom.* **24,** 1911–1918 (2010).

239. Kaplan, K., Graf, S., Tanner, C., Gonin, M., Fuhrer, K., Knochenmuss, R., Dwivedi, P. & Hill, H. H. Resistive Glass IM-TOFMS. *Anal. Chem.* **82,** 9336–9343 (2010).

240. Tabrizchi, M. & Jazan, E. Inverse Ion Mobility Spectrometry. *Anal. Chem.* **82,** 746–750 (2010).

241. Vonderach, M., Ehrler, O. T., Weis, P. & Kappes, M. M. Combining Ion Mobility Spectrometry, Mass Spectrometry, and Photoelectron Spectroscopy in a High-Transmission Instrument. *Anal. Chem.* **83,** 1108–1115 (2011).

242. Baykut, G., von Halem, O. & Raether, O. Applying a Dynamic Method to the Measurement of Ion Mobility. *J. Am. Soc. Mass Spectrom.* **20,** 2070–2081 (2009).

243. Creaser, C. S., Griffiths, J. R., Bramwell, C. J., Noreen, S., Hill, C. A. & Thomas, C. L. P. Ion mobility spectrometry: a review. Part 1. Structural analysis by mobility measurement. *Analyst* **129,** 984 (2004).

244. Karpas, Z., Stimac, R. M. & Rappoport, Z. Differentiating between large isomers and derivation of structural information by ion mobility spectrometry / mass spectrometry techniques. *Int. J. Mass Spectrom. Ion Process.* **83,** 163–175 (1988).

245. Karpas, Z., Berant, Z. & Stimac, R. M. An ion mobility spectrometry/mass spectrometry (IMS/MS) study of the site of protonation in anilines. *Struct. Chem.* **1,** 201–204 (1990).

246. Karpas, Z., Berant, Z. & Shahal, O. The effects of saturation and substitution on the mobility of protonated cyclic compounds. *Int. J. Mass Spectrom. Ion Process.* **96,** 291–297 (1990).

247. Karpas, Z. & Tironi, C. The mobility and ion structure of protonated aminoazoles. *Struct. Chem.* **2,** 655–659 (1991).

248. Karpas, Z. The structure and mobility in air of protonated ketones. *Int. J. Mass Spectrom. Ion Process.* **107,** 435–440 (1991).

249. Karpas, Z. The mobility of protonated aminoalcohols: Evidence for proton-induced cyclization. *Struct. Chem.* **3,** 139–141 (1992).

250. Asbury, G. R. & Hill, H. H. Separation of amino acids by ion mobility spectrometry. *J. Chromatogr. A* **902,** 433–437 (2000).

251. Pagel, K. & Harvey, D. J. Ion Mobility–Mass Spectrometry of Complex Carbohydrates: Collision Cross Sections of Sodiated N-linked Glycans. *Anal. Chem.* **85,** 5138–5145 (2013).

252. Huang, Y. & Dodds, E. D. Ion Mobility Studies of Carbohydrates as Group I Adducts: Isomer Specific Collisional Cross Section Dependence on Metal Ion Radius. *Anal. Chem.* **85,** 9728–9735 (2013).

253. Harvey, D. J., Edgeworth, M., Krishna, B. A., Bonomelli, C., Allman, S. A., Crispin, M. & Scrivens, J. H. Fragmentation of negative ions from N-linked carbohydrates: Part 6.

Glycans containing one N-acetylglucosamine in the core. *Rapid Commun. Mass Spectrom.* **28,** 2008–2018 (2014).

254. Hoffmann, W., Hofmann, J. & Pagel, K. Energy-Resolved Ion Mobility-Mass Spectrometry—A Concept to Improve the Separation of Isomeric Carbohydrates. *J. Am. Soc. Mass Spectrom.* **25,** 471–479 (2014).

255. Poyer, S., Loutelier-Bourhis, C., Coadou, G., Mondeguer, F., Enche, J., Bossée, A., Hess, P. & Afonso, C. Identification and separation of saxitoxins using hydrophilic interaction liquid chromatography coupled to traveling wave ion mobility-mass spectrometry. *J. Mass Spectrom.* **50,** 175–181 (2015).

256. May, J. C., Goodwin, C. R., Lareau, N. M., Leaptrot, K. L., Morris, C. B., Kurulugama, R. T., Mordehai, A., Klein, C., Barry, W., Darland, E., Overney, G., Imatani, K., Stafford, G. C., Fjeldsted, J. C. & McLean, J. A. Conformational Ordering of Biomolecules in the Gas Phase: Nitrogen Collision Cross Sections Measured on a Prototype High Resolution Drift Tube Ion Mobility-Mass Spectrometer. *Anal. Chem.* **86,** 2107–2116 (2014).

257. Struwe, W. B., Pagel, K., Benesch, J. L. P., Harvey, D. J. & Campbell, M. P. GlycoMob: an ion mobility-mass spectrometry collision cross section database for glycomics. *Glycoconj. J.* 1–6 (2015). doi:10.1007/s10719-015-9613-7

258. Fernandez-Maestre, R., Harden, C. S., Ewing, R. G., Crawford, C. L. & Hill Jr., H. H. Chemical standards in ion mobility spectrometry. *Analyst* **135,** 1433–1442 (2010).

Chapter 2: Can ion mobility spectrometry-mass spectrometry and density functional theory help elucidate protonation sites in 'small' molecules?

2.1 INTRODUCTION

Ion mobility spectrometry-mass spectrometry (IMS-MS) offers an opportunity to combine measurements and/or calculations of the collision cross-sections and subsequent mass spectra with computational modelling in order to derive the three-dimensional structure of ions. IMS-MS has previously been reported to separate two components for the compound norfloxacin[1], explained by protonation on two different protonation sites enabling the separation of protonated isomers (protomers) using ion mobility with distinguishable MS/MS data. This study reveals further insights into the specific example of norfloxacin and wider implications for ion mobility mass spectrometry.

The fragmentation of the protonated molecule forms the basis of many structural studies using electrospray mass spectrometry. The existence of isomers differing by protonation site (protomers) and/or tautomeric state can be important in interpretation of both ion mobility and mass spectrometry data. The protonation site can have a profound effect on the three-dimensional structure of an ion and subsequent fragmentation that determines the product spectrum observed. The prevalence of protomers in 'small molecule' chemical space is difficult to quantify accurately, for example, at the time of writing the ZINC database[2] of commercially available compounds for virtual screening contains data on 77,242,420 substances and 0.65 protomers per substance.

Using mass spectrometry alone it can be difficult to infer which site is protonated in the gas-phase and many recent studies aim to build general rules and methodologies to predict fragmentation. The use of ion mobility mass spectrometry to study the effect of protonation has been previously reported for norfloxacin[1]. In the aforementioned study the ion mobility stage was used to separate ions according to their ion mobilities; presumably with different protonation sites having slightly different ion mobilities. The resulting MS/MS spectra appear consistent with this explanation as two peaks are observed in the ion mobilogram and changing the cone voltage from between 10, 120 and 200 V changes the appearance of the mass spectrum, consistent with the proposed fragmentation pathway[1].
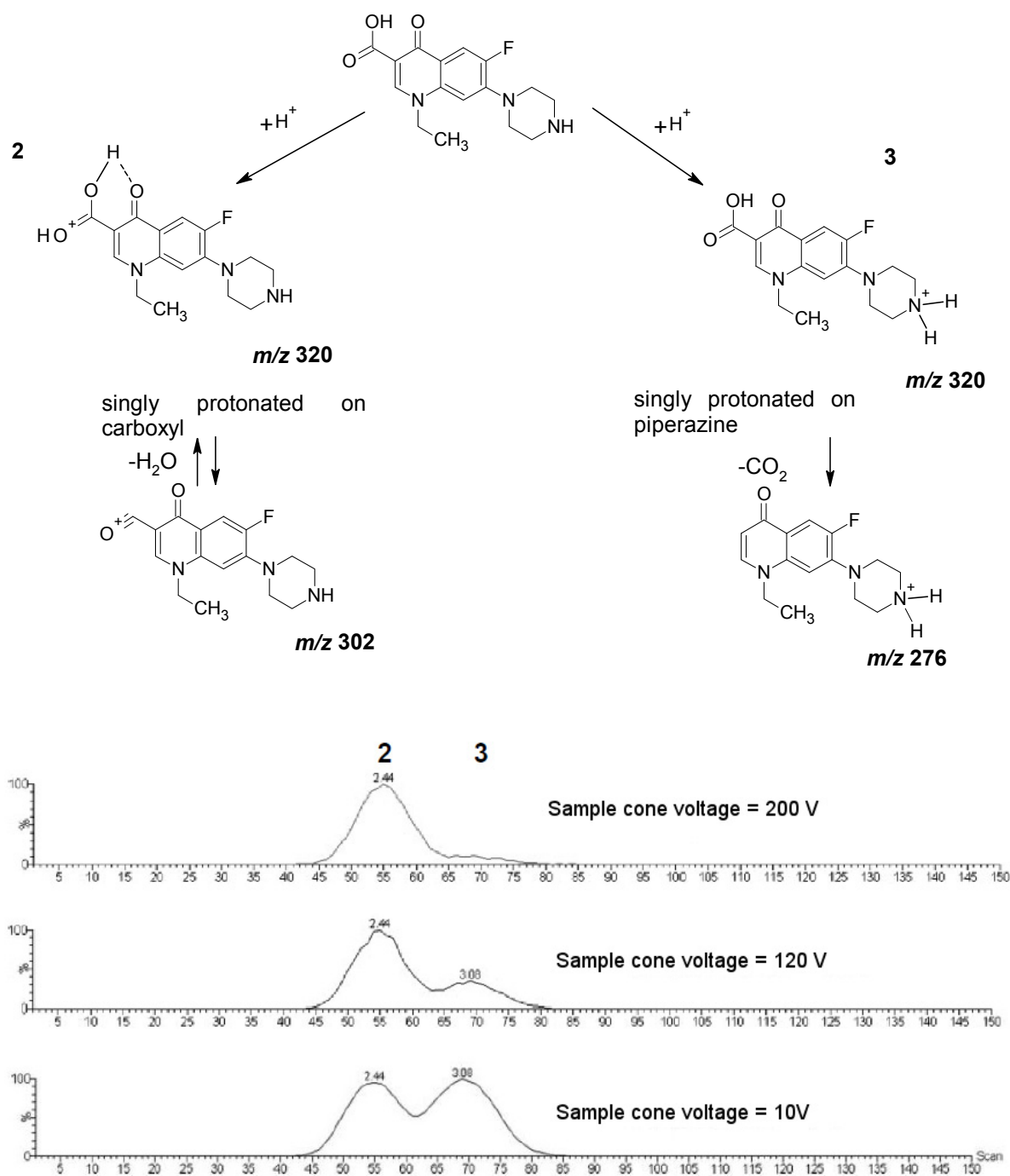
Figure 2-1. Proposed fragmentation pathway (adapted from reference 6) and effect of sample cone voltages on arrival time distributions (adapted from reference 2) with labelled components 2 and 3.

2.1.1 Understanding the site of protonation

Quinolones that are structurally similar to norfloxacin are known to exist as zwitterions in neutral solutions.[3] However, gas-phase proton transfer reactions can occur when a molecule with a high gas-phase proton affinity abstracts a proton from the protonated form of a molecule that has a lower gas-phase proton affinity. Thus an inversion in the order of basicity among a series of molecules proceeding from the solution phase to the gas-phase[4] can take place because solution-phase basicity (pKa) and gas-phase proton affinity are not necessarily related. This may be further complicated with different solvent composition, pH *etc*., indeed the site of protonation in norfloxacin has been proposed to be determined by the pH, aqueous-organic ratio or ionic strength of the mobile phase used in liquid chromatography-mass spectrometry studies[5]. The following sections highlight the important and characteristic losses from norfloxacin, which in turn enable more confident assignment of fragmentation pathways and protonation sites.

2.1.2 Loss of H_2O from norfloxacin, *m/z* 320

The protonated ions of the three compounds in Figure 2-2 with carboxyl groups undergo rapid loss of H_2O, and subsequent loss of CO or other species, but were reported to result in no detectable loss of CO_2.[6]

flumequine

nalidixic acid

4-Hydroxy-7-trifluoromethyl-3-quinolinecarboxylic acid
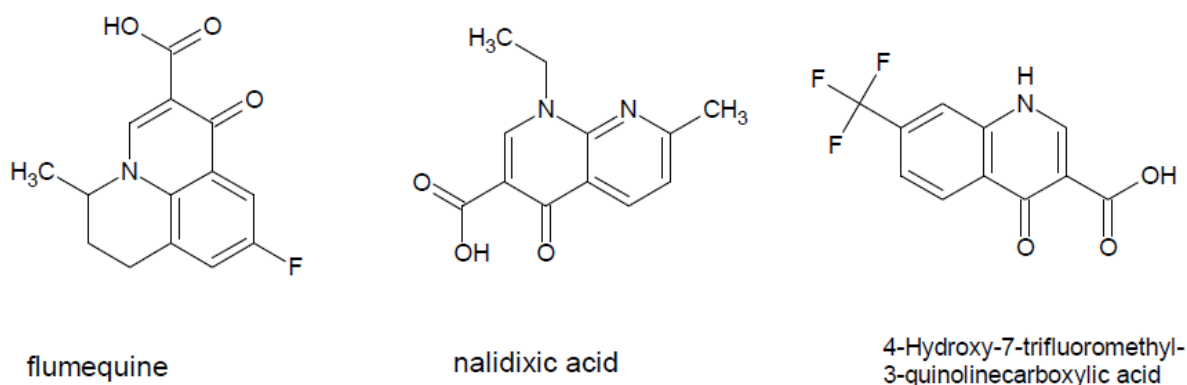
Figure 2-2. Three compounds related to norfloxacin lacking the piperazine ring.

It is not clear whether loss of H_2O occurs only when the proton is attached to the carboxyl group during the electrospray ionisation process, or whether it is possible for a proton attached to the oxygen or nitrogen of the quinolone ring to be collisionally activated and transferred to the carboxyl group[6].

2.1.3 Addition of H_2O to [norfloxacin + H - H_2O]$^+$, *m/z* 302

When norfloxacin was dissolved in methanol by Neta *et al.*, [6] in the absence of water, MS/MS/MS experiments on the [M + H$^+$ - H_2O]$^+$ ion (*m/z* 302) showed addition of H_2O (to form *m/z* 320) as well as addition of CH_3OH (to form *m/z* 334). Loss of H_2O from *m/z* 320 was postulated to lead to formation of an acyl species, which has high affinity for water or alcohols. This process is most pronounced at the lowest collision energies while at higher energies the [M + H]$^+$ ion undergoes fragmentation. Addition of a water molecule in the collision cell was reported for other compounds and was explained by the presence of water in the collision cell which is difficult to remove by standard pumping.[6] This process can, reportedly, take place in the collision cell as well as in the cone region (in-source) of the spectrometer[7] although the addition may be to form a water adduct rather than reversible fragmentation[8].

2.1.4 Loss of CO_2 from norfloxacin, *m/z* 320

The previous results reported indicate that *m/z* 320 undergoes loss of CO_2 when a positive charge or a proton is on the piperazine ring, an irreversible process based on their experimental data[6].

2.1.5 Addition of CO_2 to [norfloxacin + H - CO_2]$^+$, *m/z* 276

Loss of CO_2 leads to replacement of the CO_2H group with H, forming a relatively stable species, where addition of CO_2 appears unlikely. The relative intensities of the –CO_2 and -H_2O product ions are believed to change with cone voltage because their rate of formation and fragmentation are likely to be different.[6]

To further understand the fragmentation of norfloxacin, additional experimental studies and theoretical calculations were conducted, ultimately describing another feature present in the ion mobilogram that appears consistent with an additional third structure of gas-phase norfloxacin.

2.2 EXPERIMENTAL

2.1.1 Chemicals and materials

Norfloxacin, poly-(D/L)-alanine, sodium hydroxide, isopropanol and methanol were purchased from Sigma-Aldrich (Gillingham, UK), acetonitrile from Rathburn (Walkerburn,

UK) and high purity water from VWR International Ltd (West Chester, USA). Formic acid was supplied by Biosolve (Valkenswaard, Netherlands).

2.1.2 Mass spectrometry and liquid chromatography conditions

A solution of 0.1 mg/mL of norfloxacin was prepared in methanol and 2 μL of the 0.1 mg/mL solution was injected on to a Waters (Manchester, UK) Acquity reverse phase chromatography system using an ACQUITY UHPLC BEH C18 column (particle size:1.7 μm) in a mobile phase reverse phase gradient composition of A: water + 0.1% (v/v) formic acid and B: acetonitrile + 0.1% (v/v) formic acid. The flow rate was 0.5 mL/min to the electrospray ionisation source. The gradient conditions were an initial composition of 95.0% A, from 0.5 min to 4.5 min a gradient from 95% to 40% A, 5% A at 4.6 min to 5.4 min and a re-equilibration of 95% A from 5.5 min to 7 min. No splitter was used, so the entire flow was introduced to the electrospray ionisation source and the UHPLC column temperature was maintained at 30ºC throughout the analysis.

Experiments were performed using a Waters (Manchester, UK) Synapt G2 HDMS system with a hybrid quadrupole/traveling wave ion mobility/orthogonal acceleration time-of-flight configuration. Experiments were conducted using positive ion electrospray ionisation (ESI) with a capillary voltage of 3.2 kV and cone voltage of 30 V. An orthogonal LockSpray™ ESI probe was used with the protonated molecule for leucine enkephaline (m/z 556.2771) used as the internal mass correction calibrant. The TOF analyser was operated in resolution mode (a resolution of 18000 at m/z 556), acquiring 2 scans per second. The source temperature was 150ºC, desolvation temperature was 500ºC, cone gas flow rate of 80 L/h and desolvation gas flow rate of 1200 L/h. A mass calibration solution of sodium formate was prepared by mixing 0.05 mM sodium hydroxide solution with 0.05% formic acid in isopropanol/water (90/10; v/v) and infused at 10 μL/min.

2.1.3 Ion mobility conditions

The collision energy in the trap and transfer ion guide was set at 6 eV, and 0 eV, respectively. The mobility T-wave cell was operated at a nitrogen pressure of 2.8 mbar . The wave velocity was 600 m/s, and the wave height was fixed at 40 V, except where stated otherwise.

2.1.4 Data processing

Data acquisition and processing were carried out using Masslynx 4.1 and Driftscope 2.4 (Waters Ltd, Manchester, UK) software. The *m/z* range for the peak of interest was selected and Driftscope software was used to determine the collision cross-section (CCS) values of the analyte compounds by projecting their drift times onto a calibration curve. The T-wave instrument was calibrated using a well-established protocol[9] by plotting the drift time/cross-section function (Figure 2-3) following data acquisition of a 10 mM poly(DL-alanine) solution in methanol/water (50:50; v/v) under exactly the same ion mobility and mass spectrometric conditions as those used for the following analysis. The measured drift times of the poly-(D/L)-alanine clusters were plotted against the CCSs determined on a standard IMS drift tube instrument[10].
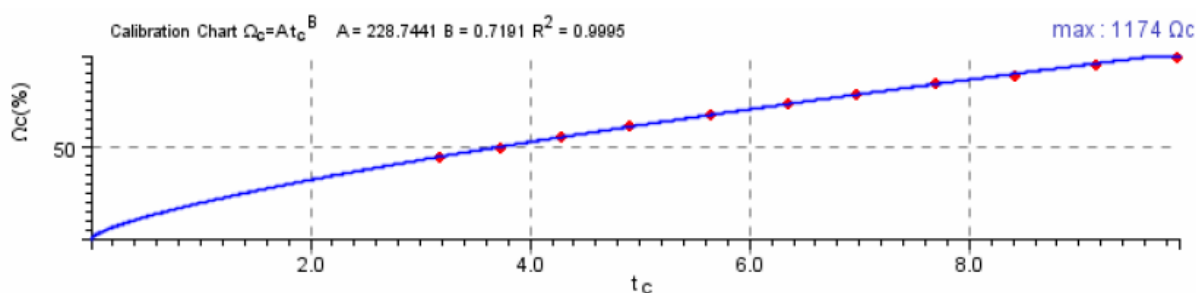
Figure 2-3. Traveling-wave ion mobility calibration curve of a typical drift-time versus adjusted collision cross-section of a series of poly-(D/L)-alanine clusters. A power curve of the form $y = ax^b$ is fitted to the data.

2.1.5 Density functional theory (DFT) calculations

DFT calculations of the structures, and associated energies, of norfloxacin and its protonated derivatives were carried out with the Gaussian 09 program[11] (using the hybrid SCF-DFT method B3LYP, which incorporates Becke's three parameter hybrid functional[12] and the Lee, Yang and Parr correlation functional.[13] All calculations were performed using the 6-311++G(d,p) basis set, which was considered to be large enough to provide reliable relative energies. The initial model for the geometry optimisation of norfloxacin was obtained from the most recent crystal structure.[14] Initial models for each of the protonated derivatives were constructed by placing a hydrogen atom at a distance of 1 Å from each putative protonation site, followed by geometry optimisation. In the case of protonation at the carboxyl oxygen

atom geometry optimisation resulted in transfer of the proton to the carbonyl oxygen atom; this representing an energetically more favourable structure, at least at this level of theory.

2.3 RESULTS AND DISCUSSION

2.3.1   Effect of conformation and protonation site on product ion spectra

It may be expected that the thermodynamically most favourable product ion would be generated, however it is feasible that the protonation site may be sterically hindered and thus protonation is kinetically determined.[15]

The conformation of ions has been demonstrated to be of importance in peptide and small molecule fragmentation patterns due to proton shifts that enable fragmentation pathways to be accessible. The effect of protonation on CID fragmentation pathways has been previously reported for species including even electron disassociations in 4-azasteroids,[16] voriconazole and fluconazole,[17] and in odd-electron disassociations in *N,N'*-dibenzylpiperazines and *N*-benzylpiperazines.[18] For example, where a fluconazole ion is protonated on one of the three possible basic sites[17] the hydrogen at the charge site and the hydroxyl oxygen are spatially arranged to accommodate the formation of a hydrogen bond; these two atoms being 1.787 Å apart, as predicted by DFT calculations. The resulting loss of H_2O (comprised of the hydroxyl and the proton; Figure 2-4) results in the production of a tertiary carbocation product ion, which is indeed observed in the product ion spectrum using electrospray.

Molecular Formula	= $C_{13}H_{13}F_2N_6O$
Monoisotopic Mass	= 307.1113 Da

Molecular Formula	= $C_{13}H_{11}F_2N_6$
Monoisotopic Mass	= 289.1008 Da
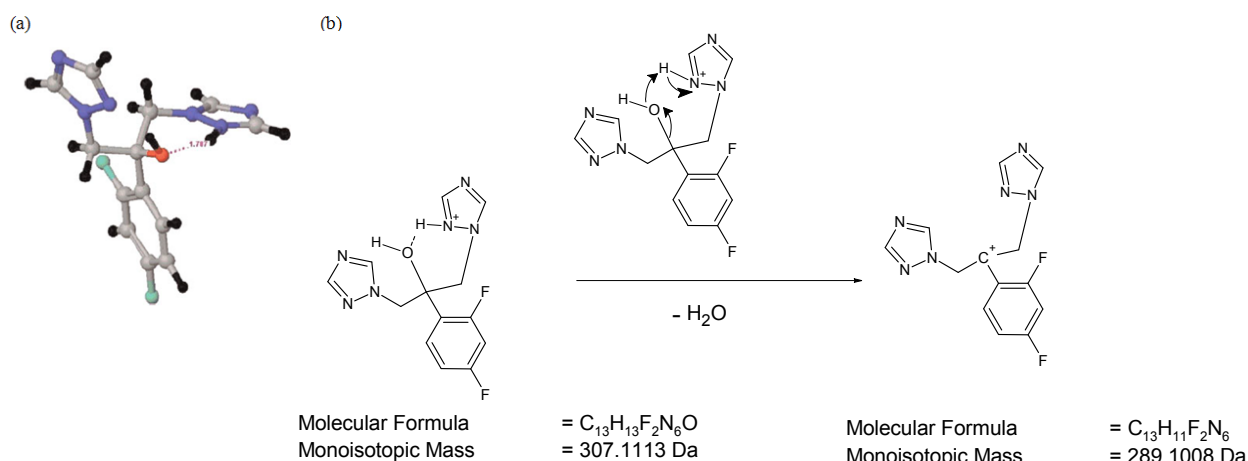
Figure 2-4. (a) Structure of protonated fluconazole molecule illustrating newly formed hydrogen bond, (b) Proposed reaction mechanism that enables elimination of H_2O via the formation of the hydrogen bond from the precursor at *m/z* 307 to form *m/z* 289.

In another example, the conformation of the rigid isomer pair *cis* and *trans* 3-pinanones affords a significant difference in the isobutane chemical ionisation (CI) mass spectrum (Figure 2-5) of the *cis* isomer which is dominated by the loss of H_2O (*m/z* 135) whereas the loss of C_2H_4O (*m/z* 109) is dominant in the *trans* isomer.[19] The loss of C_2H_4O is supported by analysis of the spectra obtained for the 2,4,4-deuterated compound which loses C_2HD_3O. They proposed that protonation, by isobutane CI, did not disturb the ground-state conformation of the isomers.

m/z 153

1 (cis)

133.41 kcal/mol
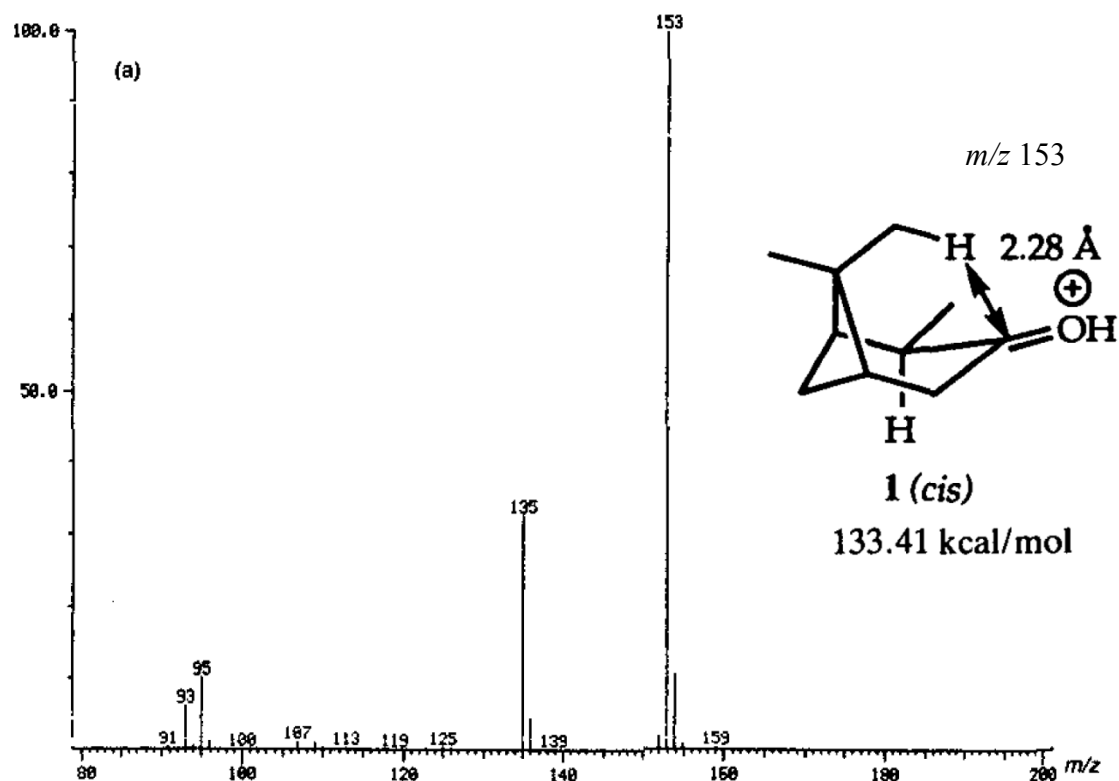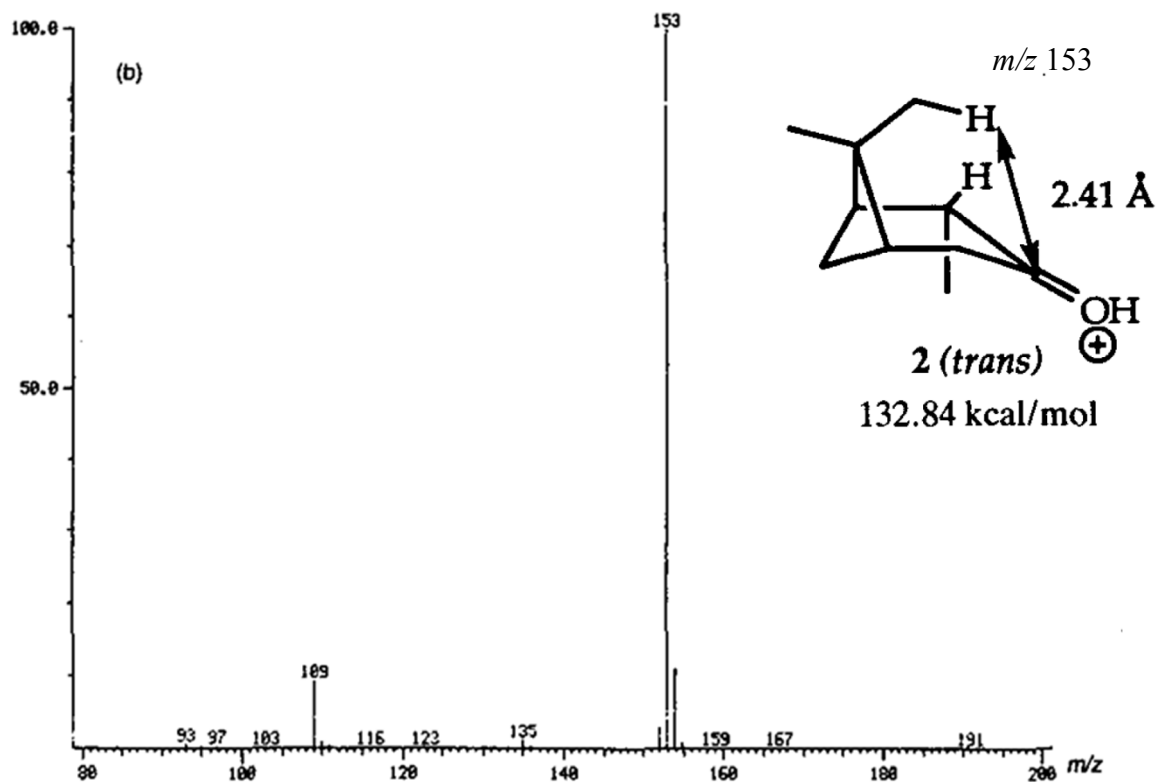
Figure 2-5. Structure and isobutane chemical ionisation mass spectrum of (a) *cis-* and (b) *trans-* 3-pinanone (adapted from reference 19).

The conformation of the ions involved in fragmentation pathways have been calculated for 3-pinanones using AM1 quantum chemical methods,[19] for protonated Voriconazole,[17] measured for ephedrine using high and low resolution UV spectroscopy[20] and compared to NMR spectroscopy assignments for *p*-benzoquinone and 1,1-bicycloalkenyls.[21] Thus there are important relationships proposed between conformers and the subsequent accessible fragmentation pathways.

2.3.2 Observation of multiple components in the ion mobilogram of norfloxacin

In contrast to the two components that have been previously reported in ion mobilograms of norfloxacin, this data shows three components when *m/z* 320 was selected as the precursor ion before ion mobility separation.

The ion mobility data were selected by retention time at T_R 1.7 min, initially to ensure that components from other retention times were not included in the analysis; this can be seen in the top trace in Figure 2-6 which shows a single peak, there are no significant peaks either side of the main peak at T_R 1.7 min.
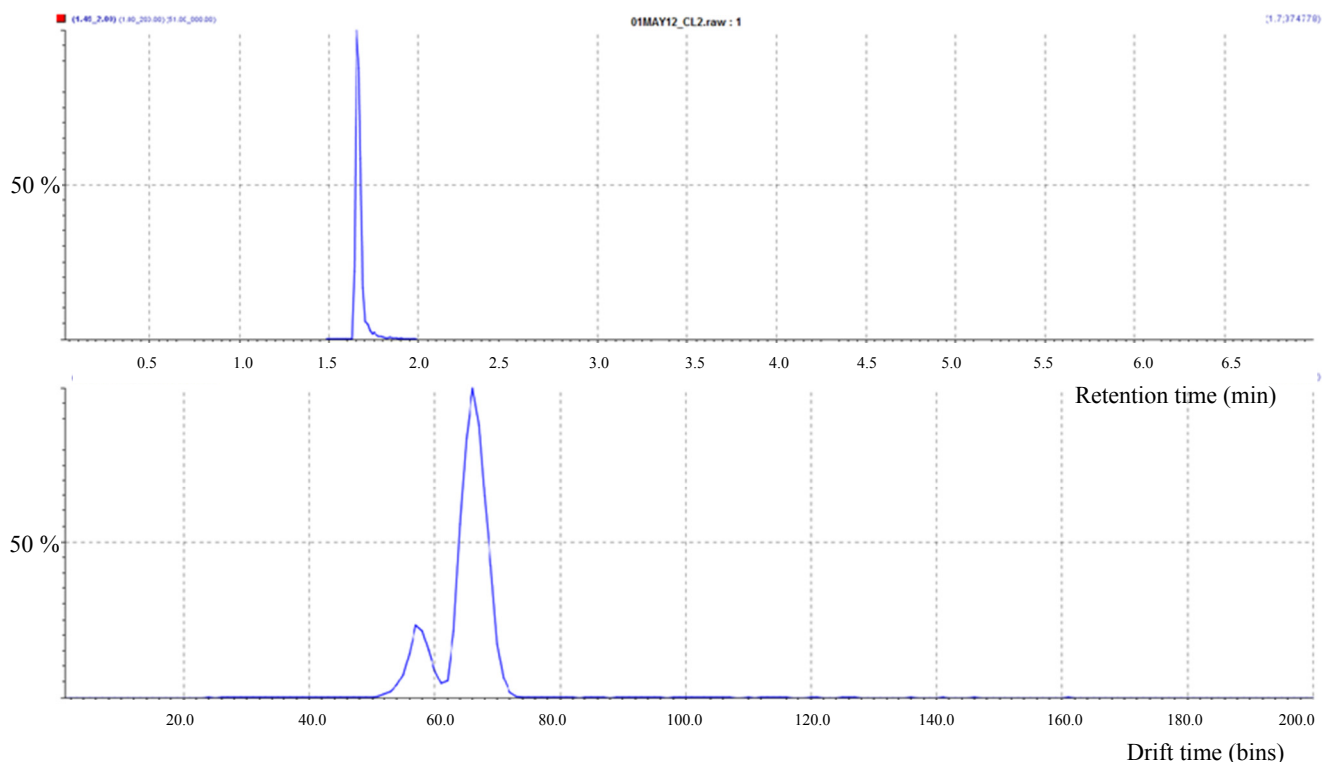
Figure 2-6. XIC chromatogram (top trace) and ion mobilogram (bottom trace) of *m/z* 320, consistent with norfloxacin.

The ion mobilogram (shown in the bottom trace in Figure 2-6) initially appears to show two major peaks. However, selecting a number of arbitrary IMS bins over the left hand side of the first peak (from 53 to 55 bins inclusive) or the right hand side of the first peak (from 57 to 59 bins inclusive) results in two discernibly different mass spectra (see Figure 2-7). This selection was achieved with the processing program Driftscope (Waters, Manchester UK) that allows users to select by drift-time and/or retention time.
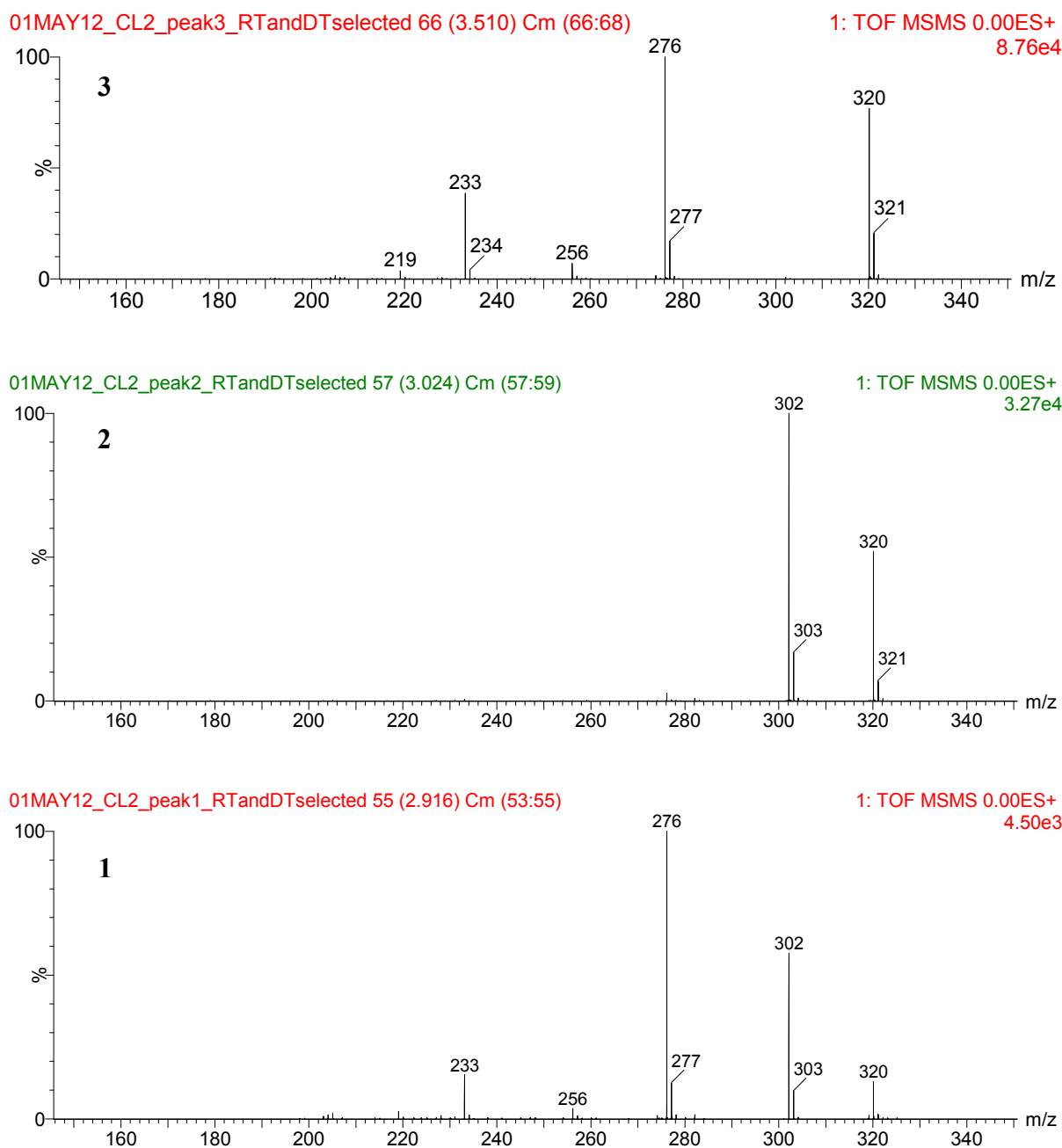
Figure 2-7. Positive ion ESI product ion spectra for main components observed for norfloxacin, processed from the drift-time selected mobilograms.

Interestingly component 1, which has not been described before, appears similar to a theoretical mixture of component 2 and component 3. The presence of ion *m/z* 302 in the MS/MS product ion spectrum of component 3 indicates a loss of H_2O from precursor *m/z* 320 (similar to component 2), however the presence of *m/z* 276 and *m/z* 256 indicates a loss of CO_2 and HF (similar to component 3). To further understand the composition of this mixture

of components in the drift-time dimension, extracted ion mobilograms are shown in Figure 2-8, which show the abundance of the *m/z* 302 ion and the *m/z* 276 ion.
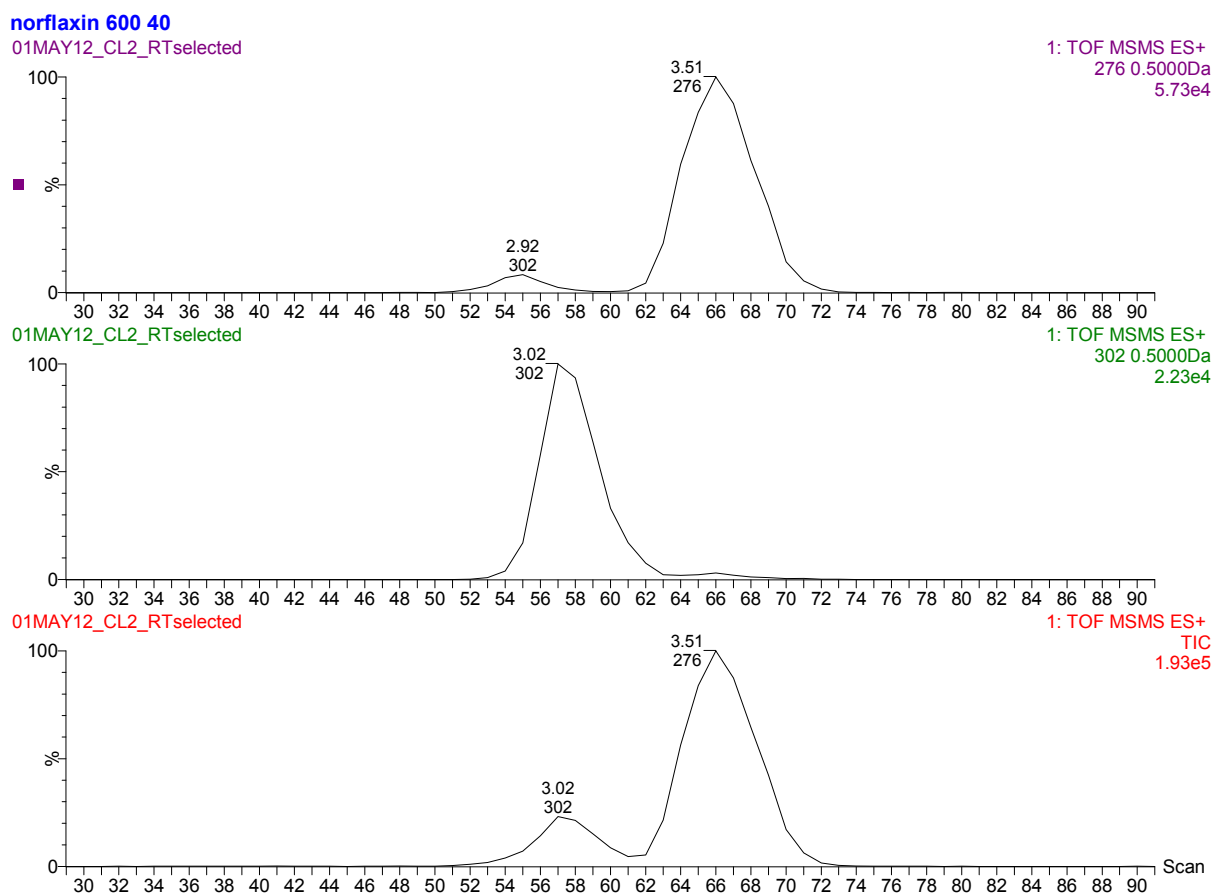
Figure 2-8. Bottom trace shows ion mobilogram for retention time 1.55 to 1.80 min, middle trace shows extracted ion mobilogram for *m/z* 302, top trace shows extracted ion mobilogram for *m/z* 276.

To understand the composition of the mixture further, the ion mobility measurements were repeated at 1400 m/s wave velocity and 40 V wave height (Figure 2-9). There appear to be three components, with component 1 observed from bin 118 to 128, component 2 observed from bin 128 to 143 and component 3 observed from 143 to bin 170. The bin is an arbitrary unit to capture the drift time dimension using the Waters Synapt G2 instrument. It is interesting to note that there appears to be not only better separation of the proposed components but also the peak shape of component 3 suggests a potential fourth conformation.
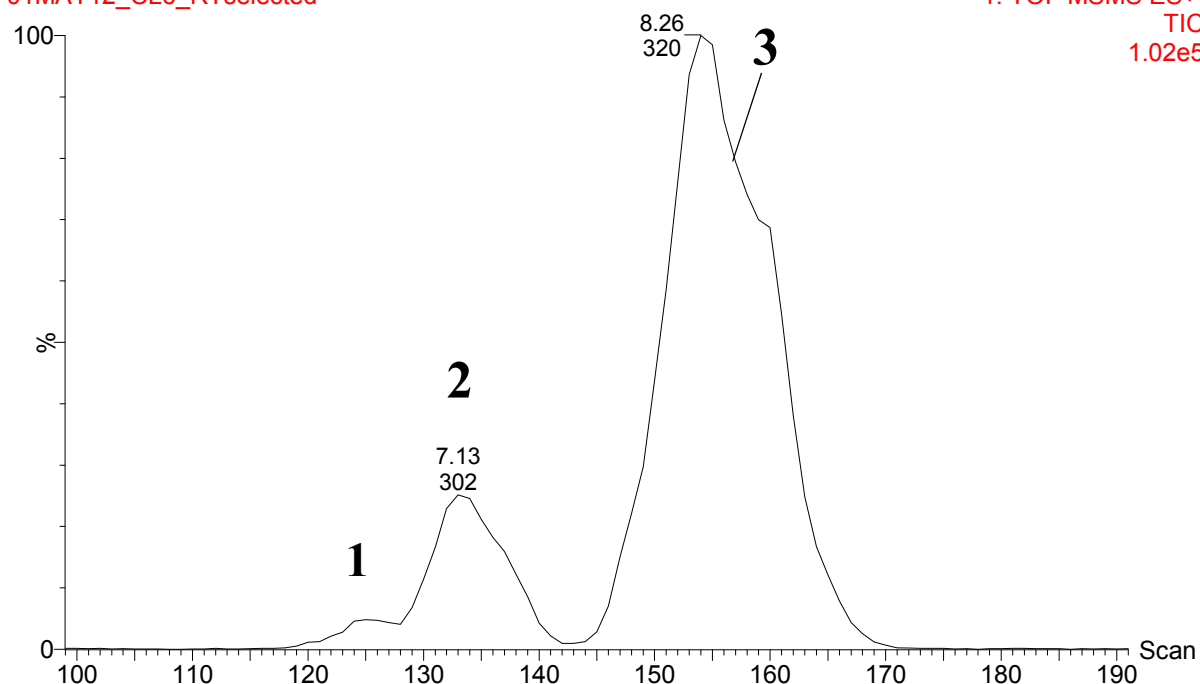
Figure 2-9. Ion mobilogram showing three main components and atypical peak shape in component 3.
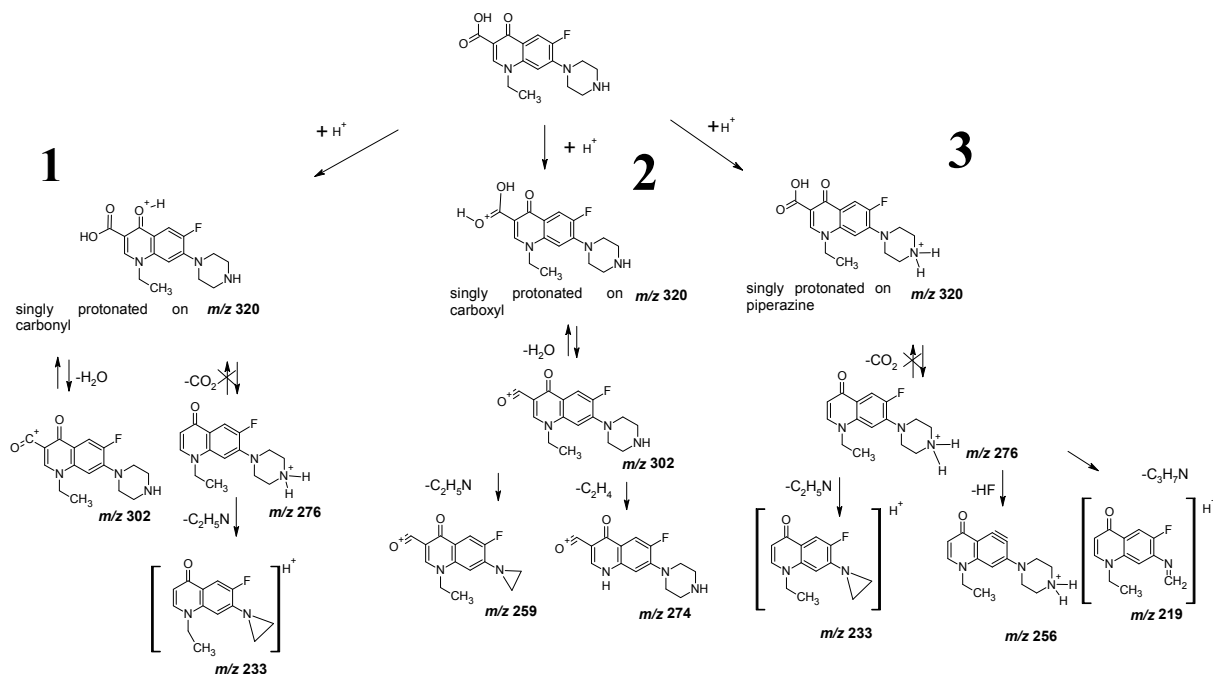
Scheme 1. Proposed fragmentation pathways for norfloxacin including all three components observed in this study (1, 2 and 3).

The peaks in the ion mobilogram for norfloxacin reported herein are consistent with a more complex mixture of more than two components, in contrast to what has been previously reported and a fragmentation pathway summary is presented in Scheme 1. It is especially interesting that component 1 is consistent with a loss of both CO_2 and H_2O, in contrast to what has previously been reported, where separate fragmentation pathways explain these individual losses[1].

In Scheme 2 mechanisms are proposed for the losses of both (A) H_2O and (B) CO_2 from the norfloxacin ion, protonated on the carbonyl group, component 1. It is interesting to note the degree of delocalisation possible for component 1, which appears to have a larger number of resonance structures than component 2 and component 3.
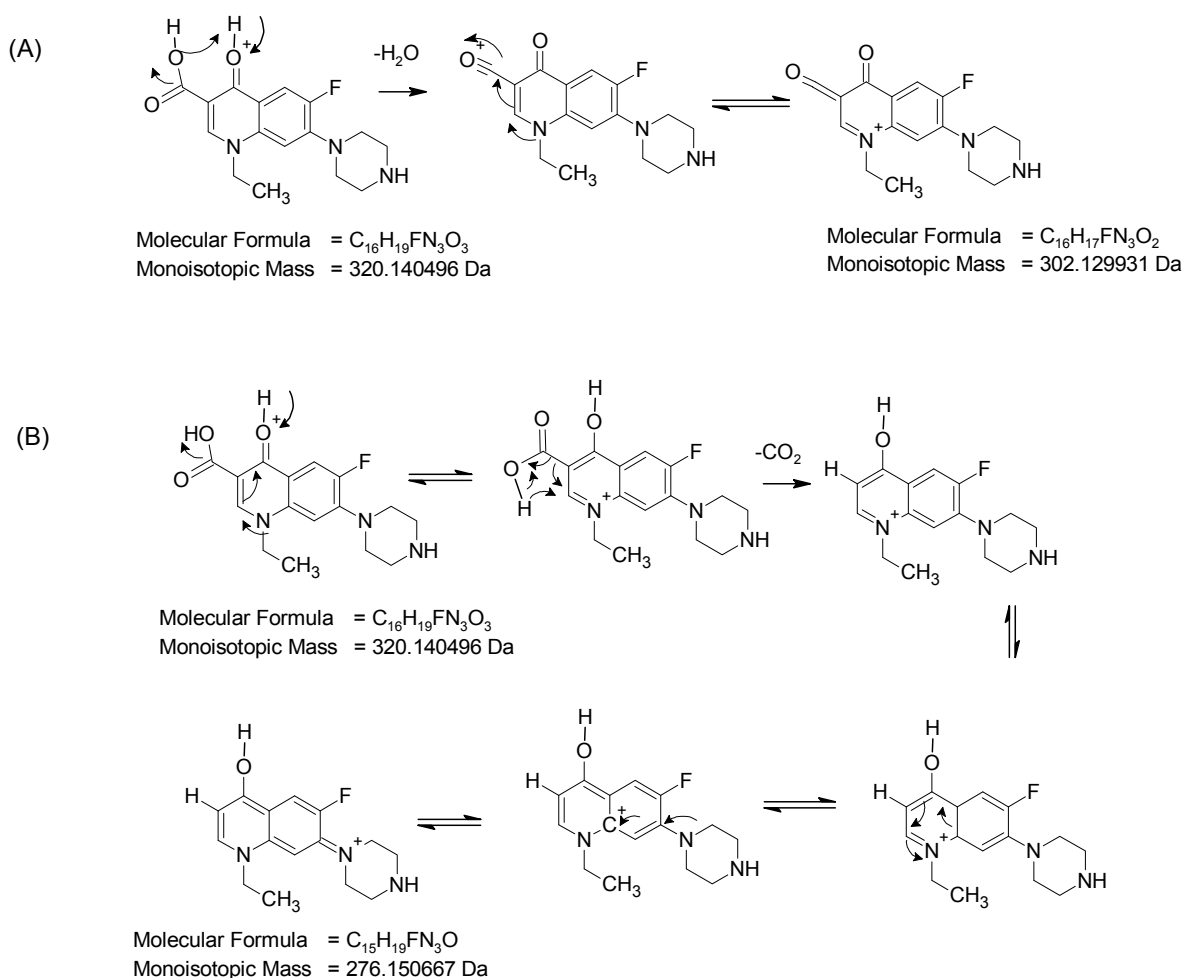
Scheme 2. Proposed scheme for losses of H_2O and CO_2 from component 1.

The use of a high efficiency UHPLC C18 separation increases confidence that it is not an impurity that is being observed, as positional isomers might be expected to be separated in the liquid chromatography dimension. It is also reported that the common synthetic impurities of norfloxacin do not include an isomer with the same *m/z* value.[22]

2.3.3 Molecular modelling using Density functional theory

To further understand the likely protonation sites in norfloxacin (Scheme 3) DFT calculations were undertaken using an initial geometry based on a recently obtained crystal structure[14] and are collected in Table 2-1. Norfloxacin structures with calculated minimum energies and proton affinities. The geometry was optimised at the B3LYP/6-311++G(d,p) level. It is noticeable that there is a hydrogen bond between the carboxyl group and carbonyl group which is consistent with several condensed phase studies including for the solvated neutral and zwitterion species using molecular modelling,[3] capillary electrophoresis,[23] potentiometric methods[24] and infra-red spectroscopy.[25]
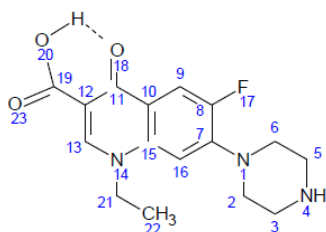
Scheme 3. Structure and atom numbering scheme for norfloxacin and dashed line highlighting the proposed hydrogen bond.

All of the initial protonation sites were considered in this study, ignoring any 'educated' prejudice, and the proton was constrained to the O23 protonation site such that proton migration did not occur, as it was considered this unlikely in the millisecond timescale of the IMS-MS experiment. The proton affinities in Table 2-1 contrast with those found by Neta *et al.*,[6] especially for protonation at O23 which they determined as the most favoured protonation site. Their calculations did not allow for possible protonation on the O18 position.

In this study the proton affinity for O18, which is reported here for the first time, is relatively favourable, and energetically more favourable than protonation at N4 which has important ramifications for understanding the ion mobility separation and subsequent product ion mass spectra.

2.3.4 Molecular modelling compared to IMS peak heights

The height of the peaks in the ion mobilogram (Figure 2-6) shows that component 3 (MS/MS product ion spectrum is consistent with protonation at N4) is more abundant than component 2 (MS/MS product ion spectrum is consistent with protonation at O23) in contrast to the thermodynamic data above suggesting component 2 should be more abundant due to the favourable proton affinity. This appears to indicate that it is not only the thermodynamics that determine the abundance of certain protomers, and that kinetics or steric effects may also be important.

2.3.5 Molecular modelling compared to IMS drift times

The CCS is experimentally determined from the drift time through the IMS cell. However, all the factors which contribute to ion mobility drift time are not clear, and in special cases (where electrostatic forces play a major role) traditional models of ion mobility may not be applicable. For example, the dipole moment is considered to be important in FAIMS ion mobility, and was considered to be an important factor in a six parameter regression model to predict ion mobility constants in a diverse set of 159 compounds.[26] The physical reasons for the dipole moment being important in ion mobility may be related to:
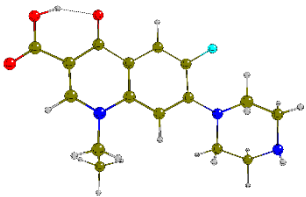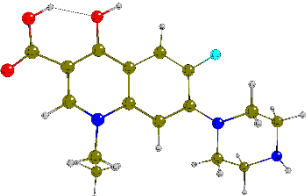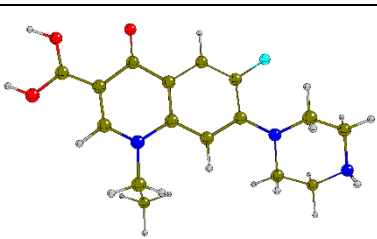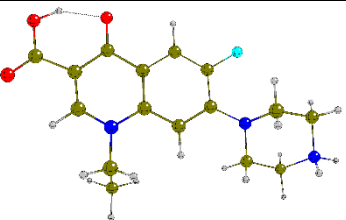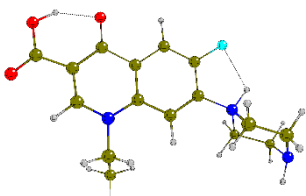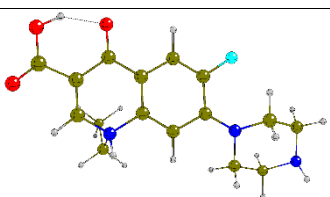
1. the polarisation interaction between an ion and neutral buffer gas and/or contaminant species in the IMS cell.[27]

2. interaction of the molecular dipole moment with the electric field of the ion mobility cell and any net alignment with the field which could reduce the effective CCS.[28]

The calculated dipole moment herein (obtained from the Gaussian output file) varies from ~4 to ~30 D when protonated at different sites, the theoretical calculations predicting a dipole moment for the ion protonated on the amine nearly ten times larger than that for the ion protonated on the carboxyl group, which may explain the unexpected magnitude of the peak separation observed between components 2 and 3.

Theoretical CCS values were initially calculated using the projection approximation (PA) algorithm in Waters Driftscope software[9] and are shown in Table 2-1. (Some caution must be taken with the use of MOBCAL for unusual atom types, since the original source code does not include sufficient data for molecules and ions containing some elements (including fluorine), although the code can be modified to suit), whilst Waters Driftscope includes fluorine by default.

Previous studies on *N*-protonated aniline and porphyrins[29] have highlighted that significant differences between theoretically determined CCS (^{t}CCS) values and experimental determined CCS (^{e}CCS) values may indicate a difference in charge distribution; ions with more localised charges may form longer-lived gas-phase interactions with the mobility buffer gas than delocalised charges. Currently these interactions do not appear to be modelled well using the main theoretical algorithms including projection approximation (PA), exact hard sphere scattering (EHSS) and trajectory method (TM), leading to poor agreement between theoretical and experimental CCS values.

Table 2-1. Norfloxacin structures with calculated minimum energies and proton affinities.

Protonation site	ΔE (kJ mol^{-1}) [a]	ΔE (kJ mol^{-1}) [b]	Structure	PA ^{t}CCS (Å^2)	^{e}CCS (Å^2)	Dipole moment (D)
n/a	0.0	0.0		111.14	n.d.	11.02
O18 (component 1)	-948.4 (1)	n.d.		111.60	100.58	4.37
O23 (component 2)	-871.0 (4)	-980.4 (1)		112.12	107.34	13.89
N4 (component 3)	-944.4 (2)	-905.8 (2)		111.85	118.38	30.67
N1	-929.2 (3)	-903.4 (3)		112.75	n.d.	18.42
N14	-799.8 (5)	-772.3 (4)		112.00	n.d	8.82

a Calculated in Gaussian 09 as described herein
b Adapted from reference 6
Parentheses describe the ranking in order of likely protonation sites

In general the large difference between the ^{t}CCS and ^{e}CCS indicates one or more factors other than purely the physical CCS is playing a critical role in the separation of these ions.

For example, the ^tCCS for norfloxacin protonated at the N4 position (111.85 $Å^2$) is slightly smaller than when protonated at the 023 position (112.12 $Å^2$), a difference in CCS between two theoretical CCSs (Δ^tCCS) of 0.27 $Å^2$. These species are observed to be well separated (shown in Figure 2-1 and Figure 2-9) which is surprising considering the small Δ^tCCS. Indeed the ^eCCS, calibrated using poly-(D/L)-alanine, for component 2 is 118.38 $Å^2 \pm 0.13$ and for component 1 a value of 107.3 $Å^2 \pm 0.24$, a difference in experimental CCS (Δ^eCCS) of 11.08 $Å^2$.

There is a very good correlation between the rank order of the molecular dipole (D) and the drift time, with the ions with larger dipoles also found to have a longer drift time, resulting in calculation of a larger ^eCCS. It is remains to be seen whether this example can be extrapolated to other compounds which exhibit a range of dipoles and a relatively small difference in ^tCCS, in effect whether dipole moment can be an important predictor for ^eCCS using TWIMS. Drift times were correlated with the dipole moment in the study of corrole isomers[30] using CO_2 as the drift gas, albeit this study uses the less polarisable N_2 drift gas.

There is also a general trend of larger ^tCCS than ^eCCS using PA for two of the three detected ions. This is surprising since any attractive electrostatic interactions present in the IMS cell, such as an induced dipole leading to a non-ideal collision between analyte and buffer gas, might be expected to generate a larger effective collision cross-section, leading to a larger ^eCCS, and an underestimation of ^tCCS. PA is also known to overestimate ^tCCS by up to 20% for concave structure.[31]

2.4 CONCLUSIONS

Mutiple protonation sites are not typically explicitly considered in interpretation of mass spectrometry and ion mobility data, indeed ions from different protonation sites may well be conflated to obscure relationships between structure and fragmentation pathways. It may be difficult to predict the site of protonation purely based on solution-phase pK_a or gas-phase basicity thermodynamics as kinetic effects also play a part in the process. The calculation of gas-phase basicities using DFT for all potential protonation sites in norfloxacin, without exclusion by 'educated' bias, reveals an unexpected protonation site that is thermodynamically favourable. The additional information from DFT and IMS-MS/MS adds confidence to assignment of the protonation site and thus fragmentation pathway.

In the case of norfloxacin reported herein, ion mobility mass spectrometry data are treated like liquid chromatography mass spectrometry data to deconvolute the data and reveal the presence of three components, albeit two components (1 and 2) are effectively eluted under one ion mobility peak under the initial experimental conditions. An improvement in separation was achieved by changing the ion mobility conditions, but this might not always be feasible so careful processing, taking into account the presence and absence of peaks in the mass spectra and their intensity, may reveal further information on mixtures analysed using ion mobility mass spectrometry.

The deconvolution of ion mobility mass spectrometry data may be especially useful where mass spectrometry and ion mobility spectrometry alone may not be able to distinguish between different components[32] and the extra dimension added by DFT should help with assignment of ion mobility and mass spectrometry data.

2.5 REFERENCES

1. Irwin, J. J., Sterling, T., Mysinger, M. M., Bolstad, E. S. & Coleman, R. G. ZINC: A Free Tool to Discover Chemistry for Biology. *J. Chem. Inf. Model.* **52,** 1757–1768 (2012).

2. Kaufmann, A., Butcher, P., Maden, K., Widmer, M., Giles, K. & Uría, D. Are liquid chromatography/electrospray tandem quadrupole fragmentation ratios unequivocal confirmation criteria? *Rapid Commun. Mass Spectrom.* **23,** 985–998 (2009).

3. Vitorino, G. P., Barrera, G. D., Mazzieri, M. R., Binning Jr., R. C. & Bacelo, D. E. A DFT study of hydration in neutral and zwitterionic norfloxacin. *Chem. Phys. Lett.* **432,** 538–544 (2006).

4. Kebarle, P. & Peschke, M. On the mechanisms by which the charged droplets produced by electrospray lead to gas phase ions. *Anal. Chim. Acta* **406,** 11–35 (2000).

5. Wang, J., Aubry, A., Bolgar, M. S., Gu, H., Olah, T. V., Arnold, M. & Jemal, M. Effect of mobile phase pH, aqueous-organic ratio, and buffer concentration on electrospray ionization tandem mass spectrometric fragmentation patterns: implications in liquid

chromatography/tandem mass spectrometric bioanalysis. *Rapid Commun. Mass Spectrom.* **24,** 3221–3229 (2010).

6. Neta, P., Godugu, B., Liang, Y., Simón-Manso, Y., Yang, X. & Stein, S. E. Electrospray tandem quadrupole fragmentation of quinolone drugs and related ions. On the reversibility of water loss from protonated molecules. *Rapid Commun. Mass Spectrom.* **24,** 3271–3278 (2010).

7. Tuytten, R., Lemière, F., Van Dongen, W., Esmans, E. L., Witters, E., Herrebout, W., Van Der Veken, B., Dudley, E. & Newton, R. P. Intriguing Mass Spectrometric Behavior of Guanosine Under Low Energy Collision-Induced Dissociation: H_2O Adduct Formation and Gas-Phase Reactions in the Collision Cell. *J. Am. Soc. Mass Spectrom.* **16,** 1291–1304 (2005).

8. Beuck, S., Schwabe, T., Grimme, S., Schlörer, N., Kamber, M., Schänzer, W. & Thevis, M. Unusual mass spectrometric dissociation pathway of protonated isoquinoline-3-carboxamides due to multiple reversible water adduct formation in the gas phase. *J. Am. Soc. Mass Spectrom.* **20,** 2034–2048 (2009).

9. Williams, J. P., Lough, J. A., Campuzano, I., Richardson, K. & Sadler, P. J. Use of ion mobility mass spectrometry and a collision cross-section algorithm to study an organometallic ruthenium anticancer complex and its adducts with a DNA oligonucleotide. *Rapid Commun. Mass Spectrom.* **23,** 3563–3569 (2009).

10. Clemmer Group: Cross Section Database. at <http://www.indiana.edu/~clemmer/Research/Cross%20Section%20Database/cs_database.php>

11. Frisch, M. J., Trucks, G. W., Schlegel, H. B., Scuseria, G. E., Robb, M. A., Cheeseman, J. R., Scalmani, G., Barone, V., Mennucci, B., Petersson, G. A., Nakatsuji, H., Caricato, M., Li, X., Hratchian, H. P., Izmaylov, A. F., Bloino, J., Zheng, G., Sonnenberg, J. L., Hada,

M., Ehara, M., Toyota, K., Fukuda, R., Hasegawa, J., Ishida, M., Nakajima, T., Honda, Y., Kitao, O., Nakai, H., Vreven, T., Montgomery Jr., J. A., Peralta, J. E., Ogliaro, F., Bearpark, M. J., Heyd, J., Brothers, E. N., Kudin, K. N., Staroverov, V. N., Kobayashi, R., Normand, J., Raghavachari, K., Rendell, A. P., Burant, J. C., Iyengar, S. S., Tomasi, J., Cossi, M., Rega, N., Millam, N. J., Klene, M., Knox, J. E., Cross, J. B., Bakken, V., Adamo, C., Jaramillo, J., Gomperts, R., Stratmann, R. E., Yazyev, O., Austin, A. J., Cammi, R., Pomelli, C., Ochterski, J. W., Martin, R. L., Morokuma, K., Zakrzewski, V. G., Voth, G. A., Salvador, P., Dannenberg, J. J., Dapprich, S., Daniels, A. D., Farkas, Ö., Foresman, J. B., Ortiz, J. V., Cioslowski, J. & Fox, D. J. *Gaussian 09*. (Gaussian, Inc., 2009).

12. Becke, A. D. Density-functional thermochemistry. III. The role of exact exchange. *J. Chem. Phys.* **98,** 5648–5652 (1993).

13. Lee, C., Yang, W. & Parr, R. G. Development of the Colle-Salvetti correlation-energy formula into a functional of the electron density. *Phys. Rev. B* **37,** 785–789 (1988).

14. Holstein, J. J., Hübschle, C. B. & Dittrich, B. Electrostatic properties of nine fluoroquinolone antibiotics derived directly from their crystal structure refinements. *CrystEngComm* **14,** 2520–2531 (2012).

15. Joyce, J. R. & Richards, D. S. Kinetic Control of Protonation in Electrospray Ionization. *J. Am. Soc. Mass Spectrom.* **22,** 360–368 (2011).

16. Burinsky, D. J., Williams, J. D., Thornquest, A. D. & Sides, S. L. Mass spectral fragmentation reactions of a therapeutic 4-azasteroid and related compounds. *J. Am. Soc. Mass Spectrom.* **12,** 385–398 (2001).

17. Alex, A., Harvey, S., Parsons, T., Pullen, F. S., Wright, P. & Riley, J. Can density functional theory (DFT) be used as an aid to a deeper understanding of tandem mass

spectrometric fragmentation pathways? *Rapid Commun. Mass Spectrom.* **23,** 2619–2627 (2009).

18. Chai, Y., Sun, H., Pan, Y. & Sun, C. N-Centered Odd-Electron Ions Formation from Collision-Induced Dissociation of Electrospray Ionization Generated Even-Electron Ions: Single Electron Transfer via Ion/Neutral Complex in the Fragmentation of Protonated N,N′-Dibenzylpiperazines and Protonated N-Benzylpiperazines. *J. Am. Soc. Mass Spectrom.* **22,** 1526–1533 (2011).

19. Joseph Youssefi, M., Boschung, A. F., Thomas, A. F. & McLafferty, F. W. Conformation dependence in the chemical ionization mass spectra of 3-pinanones. *Rapid Commun. Mass Spectrom.* **8,** 313–316 (1994).

20. Chervenkov, S., Wang, P. Q., Braun, J. E. & Neusser, H. J. Fragmentation and conformation study of ephedrine by low- and high-resolution mass selective UV spectroscopy. *J. Chem. Phys.* **121,** 7169–7174 (2004).

21. Deutsch, J. & Mandelbaum, A. Studies in mass spectrometry. Part XIV. The effect of conformation on the electron impact-induced fragmentation of adducts of *p*-benzoquinone and 1,1'-bicycloalkenyls. *J. Chem. Soc. B Phys. Org.* 886 (1971).

22. Nageswara Rao, R. & Nagaraju, V. Separation and determination of synthetic impurities of norfloxacin by reversed-phase high performance liquid chromatography. *J. Pharm. Biomed. Anal.* **34,** 1049–1056 (2004).

23. Lin, C.-E., Deng, Y.-J., Liao, W.-S., Sun, S.-W., Lin, W.-Y. & Chen, C.-C. Electrophoretic behavior and pKa determination of quinolones with a piperazinyl substituent by capillary zone electrophoresis. *J. Chromatogr. A* **1051,** 283–290 (2004).

24. Barbosa, J., Bergés, R., Toro, I. & Sanz-Nebot, V. Protonation equilibria of quinolone antibacterials in acetonitrile-water mobile phases used in LC. *Talanta* **44,** 1271–1283 (1997).

25. Jelikiċ, M., Veselinoviċ, D. & Djurdjeviċ, P. Acid—base equilibria in substituted 4-quinolone carboxylic acid solutions. *Talanta* **39,** 665–670 (1992).

26. Liu, H., Yao, X., Liu, M., Hu, Z. & Fan, B. Prediction of gas-phase reduced ion mobility constants (K(0)) based on the multiple linear regression and projection pursuit regression. *Talanta* **71,** 258–263 (2007).

27. Beegle, L. W., Kanik, I., Matz, L. & Hill, H. H. Effects of drift-gas polarizability on glycine peptides in ion mobility spectrometry. *Int. J. Mass Spectrom.* **216,** 257–268 (2002).

28. Ruotolo, B. T., Benesch, J. L. P., Sandercock, A. M., Hyung, S.-J. & Robinson, C. V. Ion mobility–mass spectrometry analysis of large protein complexes. *Nat. Protoc.* **3,** 1139–1152 (2008).

29. Lalli, P. M., Iglesias, B. A., Toma, H. E., de Sa, G. F., Daroda, R. J., Silva Filho, J. C., Szulejko, J. E., Araki, K. & Eberlin, M. N. Protomers: formation, separation and characterization via travelling wave ion mobility mass spectrometry. *J. Mass Spectrom.* **47,** 712–719 (2012).

30. Fasciotti, M., Gomes, A. F., Gozzo, F. C., Iglesias, B. A., Sá, G. F. de, Daroda, R. J., Toganoh, M., Furuta, H., Araki, K. & Eberlin, M. N. Corrole isomers: intrinsic gas-phase shapes via traveling wave ion mobility mass spectrometry and dissociation chemistries via tandem mass spectrometry. *Org. Biomol. Chem.* **10,** 8396–8402 (2012).

31. Shvartsburg, A. A. & Jarrold, M. F. An exact hard-spheres scattering model for the mobilities of polyatomic ions. *Chem. Phys. Lett.* **261,** 86–91 (1996).

32. Lee, S., Li, Z., Valentine, S. J., Zucker, S. M., Webber, N., Reilly, J. P. & Clemmer, D. E. Extracted fragment ion mobility distributions: A new method for complex mixture analysis. *Int. J. Mass Spectrom.* **309,** 154–160 (2012).

Chapter 3: Studies of fluoroquinolone charge location isomers using travelling wave ion mobility mass spectrometry and molecular modelling

3.1 INTRODUCTION

Fluoroquinolones are an important and widely used class of antimicrobial agents for clinical applications and in livestock for preventing and controlling infections and growth promotion. The U.S. Food and Drug Administration (FDA) banned enrofloxacin and ciprofloxacin in livestock production in 2005[1] and the European Union (EU) banned antibiotic growth promoting agents in animal husbandry in 2006[2]. Furthermore, overuse of antibiotics has led to antibiotic resistance and accumulation of antibiotics in foodstuffs[3]. Liquid chromatography-mass spectrometry is the most common method of determining the concentration of fluoroquinolones with E.U. maximum residue levels ranging from 10 to 1900 μg/kg, depending on the animal species and tissue type[4].

Fluoroquinolones have proved an interesting and relatively well-studied case for ion mobility mass spectrometry since investigations showed poor reproducibility of product ion ratios in biological samples depending on tissue type.[5] Ion mobility separation of two major components with distinct product ion profiles was demonstrated from experiments conducted with norfloxacin[6], which was rationalised by the existence of at least two charge location isomers. Charge location isomers typically have the same connectivity and stereochemistry and differ only in the location of the charge, for example when two ions differ only by the location of the proton in a protonated molecule. The product ion ratios was found to vary due to experimental conditions, including collisonally-induced dissociation (CID) activation energy and desolvation temperature. Variability was also observed in energy-resolved CID breakdown curves and product ion spectra with mobile phase composition, pH and ionic strength[7]. The unusual propensity of the $[M - H_2O + H]^+$ ion to gain H_2O post-quadrupole was later detected[8] and corroborated by experiments with an ion-trap mass spectrometer, again indicating that careful selection of experimental conditions is required for accurate quantitation with this class of compounds. In this research project structures for all protonation sites in norfloxacin were modelled and projection approximation calculation of theoretical collision cross-section (CCS) carried out. The theoretical collision cross-section (tCCS) results from the projection approximation method, which disregards descriptions of localised charge, were consistent with the hypothesis of charge location isomers as there was

little difference in calculated CCS of structures of protonated norfloxacin when effectively only size and geometry were considered[9].

There has been some scepticism regarding whether charge location isomers exist presumably because 1) conceivably many small molecules (<*m/z* 900) possess two or more thermodynamically favourable protonation sites yet charge location isomers have rarely been observed and reported and/or 2) alternative explanations involving molecular rearrangements could be used to rationalise the experimental observations. Only recently has instrumentation and software led to larger volumes of ion mobility data being acquired routinely so it is likely that potential charge location isomers have not been readily tested unless particularly problematic in routine assays and deemed worthy of investigation. There are now numerous articles from recent literature describing charge location isomers including, for example, benzocaine[10], para- and meta-isomers of meso-tetrapyridylporphyrin and meso-4-tetra(carboxyphenyl)porphyrin[11], anilines,[11,12] 4-aminobenzoic acid[13,14] and 4-(dimethylamino)benzoic acid[15] on differing ion mobility systems including travelling wave ion mobility spectrometry (TWIMS) and differential ion mobility spectrometry.[16] Evidence consistent with charge location isomers has also been presented utilising complementary techniques including infra-red multiphoton dissociation (IRMPD) spectroscopy,[10,13] atmospheric pressure chemical ionisation[15] and molecular modelling.[8–10,15] While this phenomenon is clearly detectable using ion mobility mass spectrometry it appears to result from typical inlet and mass spectrometer conditions so is likely to occur in mass spectrometers of various configurations, but often not be detectable on typical systems other than potentially through poor reproducibility of product ion ratios. While molecular rearrangements can be complex and difficult to determine, the evidence from direct gas-phase measurements such as IRMPD and consistency with molecular modelling adds weight to the charge location isomer hypothesis.

In the current study the protonated molecules of norfloxacin, ciprofloxacin and enrofloxacin (Figure 3-1), as a selected subset of the fluoroquinolone antibiotics, are examined to further explore the evidence relating to charge location isomers using a variety of methods.
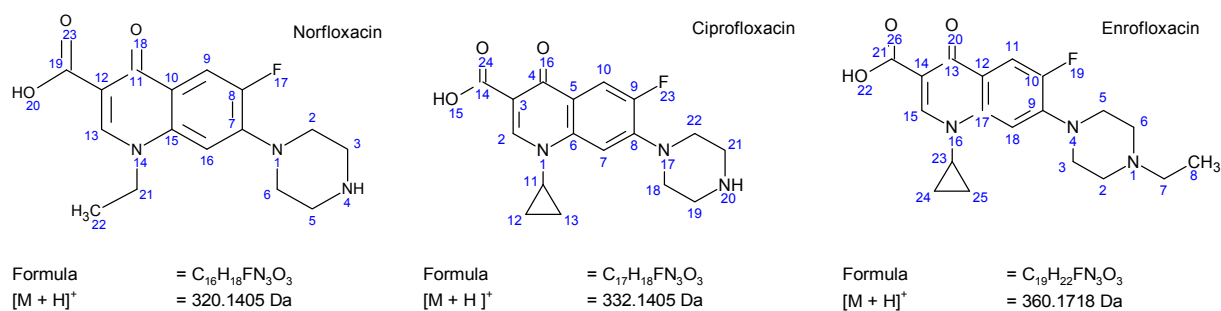
Figure 3-1. Structures of the fluoroquinolones investigated in this study.

3.2 EXPERIMENTAL

3.2.1 Reagents and materials

Norfloxacin, enrofloxacin, ciprofloxacin, poly-(D/L)-alanine, sodium hydroxide, isopropanol, methanol, acetonitrile, formic acid and high purity water were purchased from Sigma-Aldrich (Gillingham, UK).

3.2.2 Linear DT-IMS mass spectrometry conditions

Experiments were performed using a modified Waters (Manchester, UK) Synapt G2-S system with a hybrid quadrupole/DT-IMS/orthogonal acceleration time-of-flight configuration.[17] The TWIMS cell in this system has been replaced by a radio-frequency confining drift cell of 25.05 cm length in which a constant direct current electric field along the radial axis propels ions to the TOF analyser. Data were obtained by direct infusion of methanolic solutions at 3 µL/min at a concentration of 2 ng/mL. For experiments in nitrogen gas the mobility cell was operated at a pressure of 2.80 mbar of nitrogen and with a field range between 195-335 V. For experiments in helium gas the mobility cell was operated at a pressure of 2.36 mbar of helium and with a field range between 65-165 V. CCS values were calculated from the Mason-Schamp equation.[18]

Nitrogen gas was used as the nebulising gas. The capillary voltage was operated at 2.91 kV, source temperature at 120 ℃, sampling cone at 28 V, desolvation temperature at 250 ℃, cone gas flow 0 L/h and desolvation gas flow 655 L/h. Data was acquired over a range of *m/z* 50-600 units. The scan rate was 1 scan per second operating in resolution mode (~18,000 resolution at *m/z* 556). Argon was used as the CID gas. Alternating acquisition functions

116

initially set the transfer cell accelerating voltage at 4 eV to enable ion transmission while precursor ion data was collected, and a second function utilised an elevated-energy (collision energy ramp from 15 to 40 eV) to generate product ion data.

3.2.3 TWIMS mass spectrometry conditions

Experiments were also performed using a Waters (Manchester, UK) Synapt G2 HDMS system with a hybrid quadrupole/TWIMS/orthogonal acceleration time-of-flight configuration. The mobility T-wave cell was operated at a pressure of 2.8 mbar of nitrogen. The wave velocity was 800 m/s, and the wave height was fixed at 40 V. The CCS calibration was achieved using singly charged ions produced from a solution of poly-(D/L)-alanine (2 mg/mL in 1:1 H_2O:MeOH) with CCS previously determined using a DT-IMS instrument.[19] Data acquisition and processing were carried out using Masslynx 4.1 and Driftscope 2.4 (Waters Ltd, Manchester, UK) software. Collision cross-section (CCS) values of the analyte compounds were determined from a well-established calibration protocol[20] by plotting the drift time/CCS function following data acquisition of a poly-(D/L)-alanine solution.

Norfloxacin, enrofloxacin and ciprofloxacin were dissolved in 50:50 (v/v) of A: water + 0.1% formic acid and B: acetonitrile + 0.1 % formic acid to approximately 0.1 mg/mL concentration and 2 μL were introduced *via* a Waters (Manchester, UK) Acquity system without any chromatography. The flow rate was 0.5 mL/min to the electrospray source. No splitter was used, so the entire flow was introduced to the electrospray source throughout the run.

Nitrogen gas was used as the nebulising gas. The capillary voltage was operated at 1.5 kV, source temperature at 140 °C, sampling cone at 20 V, desolvation temperature at 350 °C, cone gas flow 90 L/h and desolvation gas flow 900 L/h. Data was acquired over a range of *m/z* 100-1000. The scan rate was 1 scan per second operating in resolution mode (~18,000 resolution at *m/z* 556).

3.2.4 Molecular modelling calculations

 Initial structures for protonated molecules were constructed by placing a hydrogen atom at a distance of 1 $Å^2$ from each putative protonation site. For enrofloxacin and ciprofloxacin a systematic rotor conformation search was conducted using the Open Babel 2.3.2 framework[21] as implemented in the software Avogadro v1.0.1[22] at the MMFF94[23] level of theory and low

energy conformers for each protonation site candidate selected as the starting geometry for *ab initio* geometry optimisation. For norfloxacin additional conformers were considered based on energy minimisation from the structure obtained from recent crystal data.[24]

DFT *ab initio* calculations of the structures, and associated energies of protonated norfloxacin, ciprofloxacin and enrofloxacin were then carried out with the Gaussian 09 program[25] using the hybrid SCF-DFT method B3LYP, incorporating Becke's three parameter hybrid functional[26] and the Lee, Yang and Parr functional.[27] All calculations were performed using the 6-31G(d,p) basis. The additional keywords *pop=(mk, dipole)* were included in the Gaussian input file to generate Merz–Singh–Kollman electrostatic potential partial atomic charges constrained to reproduce the molecular dipole. The nature of the stationary points were confirmed by frequency analysis with all structures having zero imaginary frequencies.

3.2.5 Theoretical CCS calculations

Output LOG files from the Gaussian 09 program were converted to the MOBCAL input MFJ file using the option to save Merz–Singh–Kollman partial atomic charges in the Chemcraft software[28]. In-house scripts were used to run calculations for all protonation sites using the trajectory method (T.M.) calculation method from a modified $N_{2(g)}$ parameterised version[29] of MOBCAL[30,31] and resulting typical standard deviations were typically 1% or less. MOBCAL code was compiled with the GNU Fortran 77 compiler packaged with Force 2.0.9 software[32].

3.3 RESULTS AND DISCUSSION

3.3.1 Comparison of fluoroquinolone ion mobilities in drift gases N_2 and He

Changing the mobility gas in ion mobility is a useful tool for separation and structure elucidation[33] since the mobility of an ion is predominantly based on shape, size and overall charge. Changing the mobility gas can manipulate the selectivity of the ion mobility separation.[34,35] The use of more polarisable gases such as $CO_{2(g)}$ has been explored to separate isomeric disaccharides (sucrose, lactose, maltose and cellobiose),[36] constitutional isomers of butyl-anilines,[37] protomers (charge location isomers resulting from protonation in different locations) of aniline and some porphyrins[11] and a series of carboxylic acids.[38] The use of differing drift gases including helium ($He_{(g)}$) and nitrogen ($N_{2(g)}$) with different polarisabilities (see Table 3-1) herein should therefore probe the drift times and arrival time distributions of proposed fluoroquinolone charge location isomers.

Table 3-1. Molecular weight, polarisability and radii for the two drift gases used in this study.

Drift gas	Molecular weight (g/mol)[39]	Polarisability[39] (Å³)	Van der Waals radii[40] (Å)	Rigid sphere radii[40] (Å)	Polarisation-limit model[40] (Å)
He$_{(g)}$	4.00260	0.205	1.40	1.03	3.38
N$_{2(g)}$	28.0134	1.740	n.d.	1.73	5.77

Helium is a small, inert, monatomic gas and has been considered as simpler to model and has historically provided better agreement between theoretical and experimental studies so became widely adopted. Nitrogen is diatomic, relatively cheap and commonly used as a gas for atmospheric pressure ionisation and has historically been the recommended mobility gas for TWIMS.
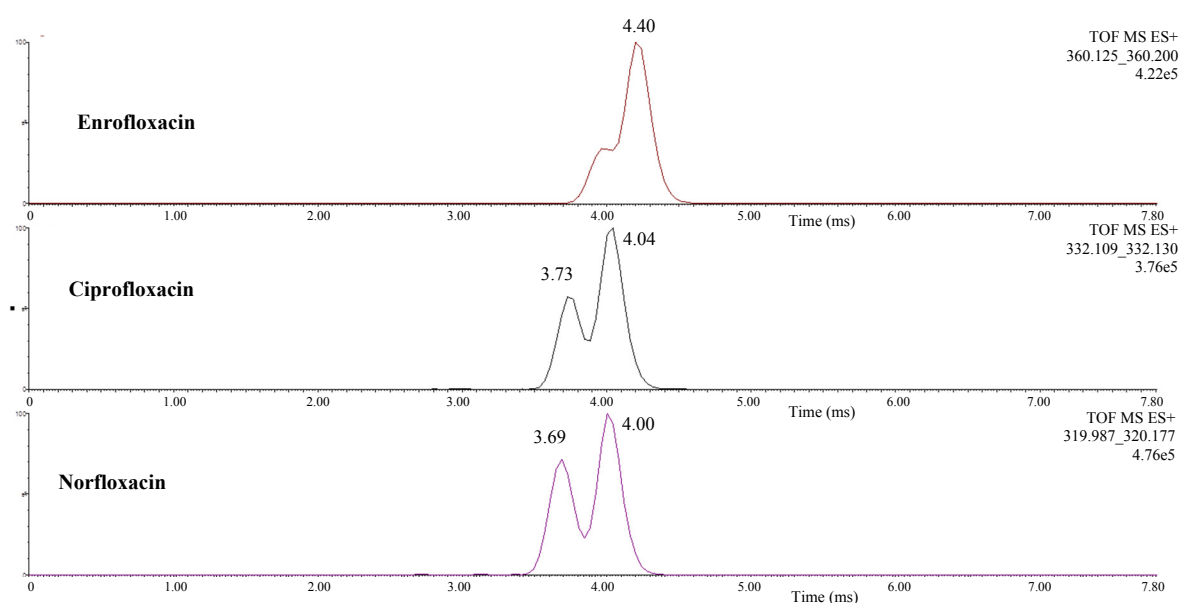
Figure 3-2. Linear DT-IMS ATDs for protonated enrofloxacin, ciprofloxacin and norfloxacin in the drift gas N$_2$.

The linear DT-IMS arrival time distributions (ATDs) for protonated enrofloxacin, ciprofloxacin and norfloxacin in the drift gas N$_2$ show two main peaks indicating two main components (Figure 3-2).

The extracted ion chromatograms for diagnostic product ions generated after the ion mobility cell also shows two main peaks with separation of diagnostic product ions (see Appendix A). The observation of multiple components in the linear DT-IMS separation of these

119

fluoroquinolones is in keeping with previous reports of charge location isomers with m/z consistent with the protonated molecule in TWIMS[9] and differential ion mobility spectrometry[16] systems.
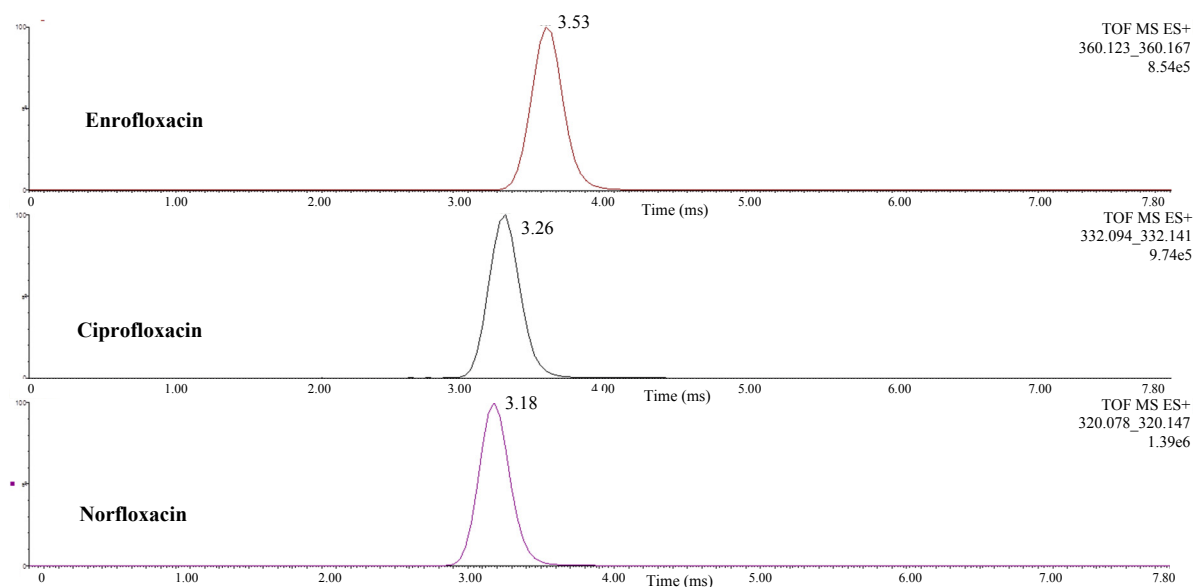
Figure 3-3. Linear DT-IMS ATDs for protonated enrofloxacin, ciprofloxacin and norfloxacin in the drift gas He.

The linear DT-IMS ATDs for protonated enrofloxacin, ciprofloxacin and norfloxacin in the drift gas He shows a single peak with no apparent separation between possible components (Figure 3-3). The extracted ion current chromatograms for diagnostic product ions (consistent with the loss of H_2O (18 m/z units) or CO_2 (44 m/z units) generated after the ion mobility cell are consistent with this finding, demonstrating no discernible separation for all three compounds. The observation of an apparent lack of separation in the drift gas He compared to the drift gas N_2 is consistent with the hypothesis that the separation is due to the charge distribution as the drift gas He is less polarisable and thus weaker interactions would be expected between the ion and the buffer gas resulting in less discrimination between ions that vary in terms of their charge distribution.

3.3.2 Comparison between CCS determined in linear DT-IMS and TWIMS

Investigation of protomers has typically either been performed on either DT-IMS systems[10,12] or commercial Waters Synapt TWIMS systems[5,9,11] so it is important to investigate whether this phenomenon is consistent between these two ion mobility regimes with different separation mechanisms. While DT-IMS and TWIMS share a general ion mobility separation

capability the mechanism by which they separate ions and the subsequent determination of CCS are different. In TWIMS, in the presence of an ion mobility gas, a travelling wave of transient dc voltage is superimposed on the rf voltage applied to a set of ring electrodes resulting in a travelling wave. Ions are propelled axially and lower mobility ions tend to roll over the travelling waves more frequently and experience longer drift-times.[41] As the motion of ions in TWIMS is less well understood[42] the CCS is typically calculated in TWIMS through calibration with known CCSs determined on DT-IMS instruments.[43] In contrast DT-IMS[33] uses a cell filled with a gas and a constant and relatively low-field is applied over the length allowing the CCS to be determined directly through the Mason-Schamp equation.[18]

A comparison of the directly derived CCS from a linear DT-IMS system and CCS calculated from TWIMS separation shows small differences in CCS (<3%, see Table 3-2), within typical experimental error. This demonstrates that, when comparing linear DT-IMS and TWIMS separations, the observed experimental CCS appears to be reasonably consistent and separation of different components is consistent so does not appear to be an artefact of TWIMS alone. The linear DT-IMS system utilised 195-335 V over the 25.05 cm cell length, which is a relatively low field strength, and the consistency with TWIMS CCSs suggests than any theoretical RF-heating effects postulated for TWIMS[44–46] have little apparent effect on the CCS for these compounds.

Table 3-2. Comparison of CCS in linear DT-IMS and TWIMS.

Protonation site	Linear DT-IMS Exp. CCS ($Å^2$) in $N_{2(g)}$	Waters Synapt G2 TWIMS Exp. CCS ($Å^2$) $N_{2(g)}$	% Difference
Norfloxacin			
N4	187.4	183.6	-2.0%
O18	172.3	171.5	-0.5%
Ciprofloxacin			
N20	188.8	185.4	-1.8%
O16	175.0	173.8	-0.7%
Enrofloxacin			
N1	198.3	192.8	-2.8%
O20	186.4	184.1	-1.2%

3.3.3 Comparison between experimental TWIMS CCS and theoretical CCS

Previous studies in this research project that were conducted to calculate CCS data from a Waters Driftscope (Manchester, UK) projection approximation method for norfloxacin showed a <2 $\mathring{A}^2$ CCS difference between structures compared to an observed experimental CCS difference >10 $\mathring{A}^2$.[7] Since the MOBCAL projection approximation method ignores the effect of charge the resultant tCCS indicates that the protonated norfloxacin structures have very similar cross-section areas and that another factor contributes significantly to the observed experimental CCS (eCCS).

Mechanistic investigations[6,29] have provided evidence to support the loss of 44 *m/z* units (-CO_2) from charge-remote fragmentation after protonation on the distal piperazine nitrogen (not connected to the quinolone, i.e. N14, N1 and N16 for norfloxacin, ciprofloxacin and enrofloxacin respectively), and loss of 18 *m/z* units (-H_2O) derives from charge-mediated fragmentation after protonation on the quinolone carbonyl (O18, O16 and O20 for norfloxacin, ciprofloxacin and enrofloxacin respectively). These assignments for sites of protonation are fully supported by the molecular modelling presented in Table 3-3, with those protonation sites ranked as the first and second most thermodynamically favoured.

The area of the second peak in the ion mobilogram (Figure 3-2) shows a significant increase in the order enrofloxacin>ciprofloxacin>norfloxacin. However, the relative energy differences in the gas-phase comparing the quinolone carbonyl oxygen and the distal piperazine nitrogen show a consistent >10 kcal/mol difference. Providing the DFT *ab initio* calculations give a reasonable estimate of the gas-phase stabilities leads to the conclusion that either there is an important effect in the transfer of the ion from solution to the gas-phase or the stability to activation in the mass spectrometer may be influencing the abundance of each component rather than the gas-phase thermodynamic stability alone. The influence of solution phase chemistry on the abundance of charge location isomers detected has been discussed previously[13,29] and this is clearly important in the case of fluoroquinolones where the abundance of components detected in the ion mobilogram is observed to change with factors including the pH and composition of the mobile phase.[7] The relative energies are useful in assessing the likelihood of ions existing in the gas-phase, but caution should be

exercised that ions may be kinetically trapped[10,47], and thus appear thermodynamically unfavourable, but exist in the gas-phase.

Table 3-3. Comparison of CCS from experimental DT-IMS measured in the drift gas N_2 and theoretical calculations.

Protonation site	tCCS ($Å^2$)	TWIMS eCCS ($Å^2$)	Percentage difference CCS	E (Ha)	Relative energy (kcal/mol)	Rank stability
Norfloxacin						
O18	176.4	171.5	2.8%	-1110.76298372	0.0	1
N4	192.6	187.4	2.7%	-1110.72952458	21.0	2
N1	189.0			-1110.72370353	24.6	3
N14	182.9			-1110.67620764	54.5	4
Ciprofloxacin						
O16	179.6	173.8	3.2%	-1148.830022669	0.0	1
N20	196.6	185.4	5.7%	-1148.79894386	19.6	2
N17	185.4			-1148.78727016	27.0	3
N1	184.0			-1148.73971121	56.8	4
Enrofloxacin						
O20	192.2	184.1	4.2%	-1227.456087	0.0	1
N1	204.9	192.8	5.9%	-1227-434439	13.6	2
N4	198.4			-1227.422359	21.2	3
N16	196.1			-1227.365514	56.8	4

The tCCS values are generally in good agreement with the eCCS values, with all values within ~6% of the eCCS values and predicting a significant difference (>10 $Å^2$) between CCS values for the two most thermodynamically favoured protonation sites. The data consistently show the ion with the proton located on the carbonyl oxygen exhibiting the lowest tCCS for all three compounds.

However, the tCCSs cannot be used to confirm the protonation site when used in isolation. For example the N16 tCCS for enrofloxacin (shown in Table 3-3) is 196.1 $Å^2$ which is one of

the closest predicted candidate tCCS to the eCCS value of 192.8 Å^2, but appears to be thermodynamically unfavourable. Discrepancies between eCCSs and tCCSs have been noted before for charge location isomers of benzocaine[10] where T.M. calculations underestimated the CCS by 10 Å^2. Conversely discrepancies between 'small molecule' tCCSs and eCCSs with an apparent systematic overestimation of tCCSs (calculated using DFT molecular modelling and trajectory method calculations) has been demonstrated in a reasonably large set of pharmaceutically relevant molecules,[35] metabolites in plasma and urine,[48] and for saxitoxins.[49] Norfloxacin and ciprofloxacin have only three rotatable bonds and there are four rotatable bonds for enrofloxacin it is reasonable to assume that valid geometries may be obtained using the computational methods selected.

3.4 CONCLUSIONS

The ability of the drift gases N$_2$ and He to separate components observed in the ion mobilograms of a subset of fluoroquinolones was investigated. Analyses performed in the drift gas N$_2$ led to resolution for components which appear to co-elute in the drift gas He. Utilising different ion mobility regimes (TWIMS and DT-TIMS) gave reasonably consistent CCSs using the same drift gas demonstrating that the separation observed is not an individual artefact of either DT-IMS or TWIMS. Some agreement between tCCSs and eCCSs were found, and using the trajectory method in MOBCAL successfully predicted significant differences in the tCCSs of protonated molecules of the fluroquinolones. However, tCCSs were not found to be close enough to eCCSs to enable unequivocal assignments for the fluoroquinolones studied, indicating that improvements potentially including better parameterisation of charge distribution and/or more sophisticated molecular modelling approaches for these charge location isomers are required.

Overall the combined evidence here is consistent with the hypothesis of charge distribution playing a significant role in the separation of components detected using ion mobility mass spectrometry for the fluoroquinolones norfloxacin, ciprofloxacin and enrofloxacin evidenced by 1) increasing peak-to-peak resolution values in ion mobility gases correlated with increasing drift gas polarisability 2) different tCCSs for charge location isomers calculated using the trajectory method and 3) consistent CCSs for components observed in ion mobility experiments conducted using different ion mobility regimes of TWIMS and DT-IMS.

Supplementary data can be found in Supplementary data, Appendix A.

3.5 ACKNOWLEDGEMENTS

3.6 REFERENCES

1. Medicine, C. for V. Recalls & Withdrawals - Withdrawal of Enrofloxacin for Poultry. at <http://www.fda.gov/AnimalVeterinary/SafetyHealth/RecallsWithdrawals/ucm042004.htm>

2. 62 FR 27944 - Extralabel Animal Drug Use; Fluoroquinolones and Glycopeptides; Order of Prohibition. at <http://www.gpo.gov/fdsys/granule/FR-1997-05-22/97-13677>

3. Spellberg, B., Guidos, R., Gilbert, D., Bradley, J., Boucher, H. W., Scheld, W. M., Bartlett, J. G., Edwards, J. & America, the I. D. S. of. The Epidemic of Antibiotic-Resistant Infections: A Call to Action for the Medical Community from the Infectious Diseases Society of America. *Clin. Infect. Dis.* **46,** 155–164 (2008).

4. EudraLex - Volume 5 - Pharmaceutical legislation Medicinal Products for veterinary use - European Commission. at <http://ec.europa.eu/health/documents/eudralex/vol-5/index_en.htm>

5. Kaufmann, A., Butcher, P., Maden, K., Widmer, M., Giles, K. & Uría, D. Are liquid chromatography/electrospray tandem quadrupole fragmentation ratios unequivocal confirmation criteria? *Rapid Commun. Mass Spectrom.* **23,** 985–998 (2009).

6. Pulkrabová, J. & Tomaniová, M. 6th International Symposium on Recent Advances in Food Analysis (RAFA). in (2013).

7. Wang, J., Aubry, A., Bolgar, M. S., Gu, H., Olah, T. V., Arnold, M. & Jemal, M. Effect of mobile phase pH, aqueous-organic ratio, and buffer concentration on electrospray ionization tandem mass spectrometric fragmentation patterns: implications in liquid

chromatography/tandem mass spectrometric bioanalysis. *Rapid Commun. Mass Spectrom.* **24,** 3221–3229 (2010).

8. Neta, P., Godugu, B., Liang, Y., Simón-Manso, Y., Yang, X. & Stein, S. E. Electrospray tandem quadrupole fragmentation of quinolone drugs and related ions. On the reversibility of water loss from protonated molecules. *Rapid Commun. Mass Spectrom.* **24,** 3271–3278 (2010).

9. Lapthorn, C., Dines, T. J., Chowdhry, B. Z., Perkins, G. L. & Pullen, F. S. Can ion mobility mass spectrometry and density functional theory help elucidate protonation sites in 'small' molecules? *Rapid Commun. Mass Spectrom.* **27,** 2399–2410 (2013).

10. Warnke, S., Seo, J., Boschmans, J., Sobott, F., Scrivens, J. H., Bleiholder, C., Bowers, M. T., Gewinner, S., Schöllkopf, W., Pagel, K. & von Helden, G. Protomers of Benzocaine: Solvent and Permittivity Dependence. *J. Am. Chem. Soc.* **137,** 4236–4242 (2015).

11. Lalli, P. M., Iglesias, B. A., Toma, H. E., de Sa, G. F., Daroda, R. J., Silva Filho, J. C., Szulejko, J. E., Araki, K. & Eberlin, M. N. Protomers: formation, separation and characterization via travelling wave ion mobility mass spectrometry. *J. Mass Spectrom.* **47,** 712–719 (2012).

12. Karpas, Z., Berant, Z. & Stimac, R. M. An ion mobility spectrometry/mass spectrometry (IMS/MS) study of the site of protonation in anilines. *Struct. Chem.* **1,** 201–204 (1990).

13. Schmidt, J., Meyer, M. M., Spector, I. & Kass, S. R. Infrared Multiphoton Dissociation Spectroscopy Study of Protonated *p* -Aminobenzoic Acid: Does Electrospray Ionization Afford the Amino- or Carboxy-Protonated Ion? *J. Phys. Chem. A* **115,** 7625–7632 (2011).

14. Tian, Z. & Kass, S. R. Does Electrospray Ionization Produce Gas-Phase or Liquid-Phase Structures? *J. Am. Chem. Soc.* **130,** 10842–10843 (2008).

15. Chai, Y., Weng, G., Shen, S., Sun, C. & Pan, Y. The Protonation Site of para-Dimethylaminobenzoic Acid Using Atmospheric Pressure Ionization Methods. *J. Am. Soc. Mass Spectrom.* **26,** 668–676 (2015).

16. Kovačević, B., Schorr, P., Qi, Y. & Volmer, D. A. Decay Mechanisms of Protonated 4-Quinolone Antibiotics After Electrospray Ionization and Ion Activation. *J. Am. Soc. Mass Spectrom.* **25,** 1974–1986 (2014).

17. Bush, M. F., Hall, Z., Giles, K., Hoyes, J., Robinson, C. V. & Ruotolo, B. T. Collision Cross Sections of Proteins and Their Complexes: A Calibration Framework and Database for Gas-Phase Structural Biology. *Anal. Chem.* **82,** 9557–9565 (2010).

18. McDaniel, E. W. & Martin, D. W. *Drift tube-mass spectrometer for studies of thermal-energy ion-molecule reactions. Technical Report No. 3.* (1960).

19. Collision Cross Section Database | Bush Lab. at <http://depts.washington.edu/bushlab/ccsdatabase/>

20. Williams, J. P., Lough, J. A., Campuzano, I., Richardson, K. & Sadler, P. J. Use of ion mobility mass spectrometry and a collision cross-section algorithm to study an organometallic ruthenium anticancer complex and its adducts with a DNA oligonucleotide. *Rapid Commun. Mass Spectrom.* **23,** 3563–3569 (2009).

21. O'Boyle, N. M., Banck, M., James, C. A., Morley, C., Vandermeersch, T. & Hutchison, G. R. Open Babel: An open chemical toolbox. *J. Cheminformatics* **3,** 33 (2011).

22. Hanwell, M. D., Curtis, D. E., Lonie, D. C., Vandermeersch, T., Zurek, E. & Hutchison, G. R. Avogadro: an advanced semantic chemical editor, visualization, and analysis platform. *J. Cheminformatics* **4,** 17 (2012).

23. Halgren, T. A. Merck molecular force field. I. Basis, form, scope, parameterization, and performance of MMFF94. *J. Comput. Chem.* **17,** 490–519 (1996).

24. Holstein, J. J., Hübschle, C. B. & Dittrich, B. Electrostatic properties of nine fluoroquinolone antibiotics derived directly from their crystal structure refinements. *CrystEngComm* **14,** 2520–2531 (2012).

25. Frisch, M. J., Trucks, G. W., Schlegel, H. B., Scuseria, G. E., Robb, M. A., Cheeseman, J. R., Scalmani, G., Barone, V., Mennucci, B., Petersson, G. A., Nakatsuji, H., Caricato, M., Li, X., Hratchian, H. P., Izmaylov, A. F., Bloino, J., Zheng, G., Sonnenberg, J. L., Hada, M., Ehara, M., Toyota, K., Fukuda, R., Hasegawa, J., Ishida, M., Nakajima, T., Honda, Y., Kitao, O., Nakai, H., Vreven, T., Montgomery Jr., J. A., Peralta, J. E., Ogliaro, F., Bearpark, M. J., Heyd, J., Brothers, E. N., Kudin, K. N., Staroverov, V. N., Kobayashi, R., Normand, J., Raghavachari, K., Rendell, A. P., Burant, J. C., Iyengar, S. S., Tomasi, J., Cossi, M., Rega, N., Millam, N. J., Klene, M., Knox, J. E., Cross, J. B., Bakken, V., Adamo, C., Jaramillo, J., Gomperts, R., Stratmann, R. E., Yazyev, O., Austin, A. J., Cammi, R., Pomelli, C., Ochterski, J. W., Martin, R. L., Morokuma, K., Zakrzewski, V. G., Voth, G. A., Salvador, P., Dannenberg, J. J., Dapprich, S., Daniels, A. D., Farkas, Ö., Foresman, J. B., Ortiz, J. V., Cioslowski, J. & Fox, D. J. *Gaussian 09*. (Gaussian, Inc., 2009).

26. Becke, A. D. Density-functional thermochemistry. III. The role of exact exchange. *J. Chem. Phys.* **98,** 5648–5652 (1993).

27. Lee, C., Yang, W. & Parr, R. G. Development of the Colle-Salvetti correlation-energy formula into a functional of the electron density. *Phys. Rev. B* **37,** 785–789 (1988).

28. Chemcraft - Download. at <http://www.chemcraftprog.com/download.html>

29. Campuzano, I., Bush, M. F., Robinson, C. V., Beaumont, C., Richardson, K., Kim, H. & Kim, H. I. Structural Characterization of Drug-like Compounds by Ion Mobility Mass Spectrometry: Comparison of Theoretical and Experimentally Derived Nitrogen Collision Cross Sections. *Anal. Chem.* **84,** 1026–1033 (2012).

30. Shvartsburg, A. A. & Jarrold, M. F. An exact hard-spheres scattering model for the mobilities of polyatomic ions. *Chem. Phys. Lett.* **261,** 86–91 (1996).

31. Mesleh, M. F., Hunter, J. M., Shvartsburg, A. A., Schatz, G. C. & Jarrold, M. F. Structural Information from Ion Mobility Measurements: Effects of the Long-Range Potential. *J. Phys. Chem.* **100,** 16082–16086 (1996).

32. Download | Force Fortran - The Force Project. at <http://force.lepsch.com/p/download.html>

33. Lapthorn, C., Pullen, F. & Chowdhry, B. Z. Ion mobility spectrometry-mass spectrometry (IMS-MS) of small molecules: Separating and assigning structures to ions. *Mass Spectrom. Rev.* **32,** 43–71 (2013).

34. Matz, L. M., Hill, H. H., Beegle, L. W. & Kanik, I. Investigation of drift gas selectivity in high resolution ion mobility spectrometry with mass spectrometry detection. *J. Am. Soc. Mass Spectrom.* **13,** 300–307 (2002).

35. Kurulugama, R. T., Darland, E., Kuhlmann, F., Stafford, G. & Fjeldsted, J. Evaluation of drift gas selection in complex sample analyses using a high performance drift tube ion mobility-QTOF mass spectrometer. *Analyst* **140,** 6834–6844 (2015).

36. Fasciotti, M., Sanvido, G. B., Santos, V. G., Lalli, P. M., McCullagh, M., de Sá, G. F., Daroda, R. J., Peter, M. G. & Eberlin, M. N. Separation of isomeric disaccharides by traveling wave ion mobility mass spectrometry using CO2 as drift gas. *J. Mass Spectrom.* **47,** 1643–1647 (2012).

37. Lalli, P. M., Corilo, Y. E., Fasciotti, M., Riccio, M. F., de Sa, G. F., Daroda, R. J., Souza, G. H. M. F., McCullagh, M., Bartberger, M. D., Eberlin, M. N. & Campuzano, I. D. G. Baseline resolution of isomers by traveling wave ion mobility mass spectrometry: investigating the effects of polarizable drift gases and ionic charge distribution. *J. Mass Spectrom.* **48,** 989–997 (2013).

38. Fasciotti, M., Lalli, P. M., Heerdt, G., Steffen, R. A., Corilo, Y. E., Sá, G. F. de, Daroda, R. J., Reis, F. de A. M., Morgon, N. H., Pereira, R. C. L., Eberlin, M. N. & Klitzke, C. F. Structure-drift time relationships in ion mobility mass spectrometry. *Int. J. Ion Mobil. Spectrom.* **16,** 117–132 (2013).

39. Handbook of Chemistry and Physics. at <http://www.hbcpnetbase.com/>

40. Steiner, W. E., English, W. A. & Hill, H. H. Ion−Neutral Potential Models in Atmospheric Pressure Ion Mobility Time-of-Flight Mass Spectrometry IM(tof)MS. *J. Phys. Chem. A* **110,** 1836–1844 (2006).

41. Pringle, S. D., Giles, K., Wildgoose, J. L., Williams, J. P., Slade, S. E., Thalassinos, K., Bateman, R. H., Bowers, M. T. & Scrivens, J. H. An investigation of the mobility separation of some peptide and protein ions using a new hybrid quadrupole/travelling wave IMS/oa-ToF instrument. *Int. J. Mass Spectrom.* **261,** 1–12 (2007).

42. Shvartsburg, A. A. & Smith, R. D. Fundamentals of Traveling Wave Ion Mobility Spectrometry. *Anal. Chem.* **80,** 9689–9699 (2008).

43. Clemmer Group: Cross Section Database. at <http://www.indiana.edu/~clemmer/Research/Cross%20Section%20Database/cs_database.php>

44. Merenbloom, S. I., Flick, T. G. & Williams, E. R. How Hot are Your Ions in TWAVE Ion Mobility Spectrometry? *J. Am. Soc. Mass Spectrom.* **23,** 553–562 (2012).

45. Morsa, D., Gabelica, V. & Pauw, E. D. Fragmentation and Isomerization Due to Field Heating in Traveling Wave Ion Mobility Spectrometry. *J. Am. Soc. Mass Spectrom.* **25,** 1384–1393 (2014).

46. Morsa, D., Gabelica, V. & De Pauw, E. Effective Temperature of Ions in Traveling Wave Ion Mobility Spectrometry. *Anal. Chem.* **83,** 5775–5782 (2011).

47. Joyce, J. R. & Richards, D. S. Kinetic Control of Protonation in Electrospray Ionization. *J. Am. Soc. Mass Spectrom.* **22,** 360–368 (2011).

48. Paglia, G., Williams, J. P., Menikarachchi, L., Thompson, J. W., Tyldesley-Worster, R., Halldórsson, S., Rolfsson, O., Moseley, A., Grant, D., Langridge, J., Palsson, B. O. & Astarita, G. Ion Mobility Derived Collision Cross Sections to Support Metabolomics Applications. *Anal. Chem.* **86,** 3985–3993 (2014).

49. Poyer, S., Loutelier-Bourhis, C., Coadou, G., Mondeguer, F., Enche, J., Bossée, A., Hess, P. & Afonso, C. Identification and separation of saxitoxins using hydrophilic interaction liquid chromatography coupled to traveling wave ion mobility-mass spectrometry. *J. Mass Spectrom.* **50,** 175–181 (2015).

Chapter 4: How useful is molecular modelling in combination with ion mobility mass spectrometry for small molecule ion mobility collision cross-sections?

Based on the paper: *Lapthorn, C., Pullen, F.S., Chowdhry, B.Z., Wright, P., Perkins, G.L., and Heredia, Y. How useful is molecular modelling in combination with ion mobility mass spectrometry for small molecule ion mobility collision cross-sections?*

Analyst, 140, 6814-6823 (2015)

4.1 INTRODUCTION

The workflow and computational time required for small molecules is such that it is feasible to calculate many theoretical collision cross-sections (tCCSs) in under 24 hours using commonly available computing resources. It is then possible to compare the tCCS and experimental CCS (eCCS) values to gain further information, as shown in Figure 4-1. The increase in computing resources available to scientists and consumers enable tCCSs of ions to be calculated relevant for large sets of molecules, in contrast to many large biomolecule challenges where molecular size and complexity often limits throughput.
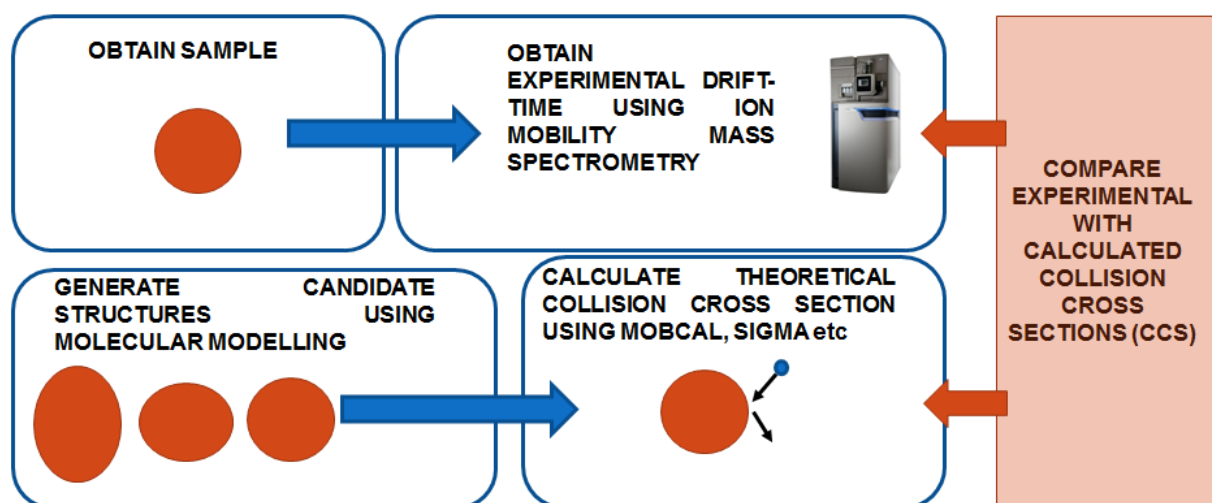
Figure 4-1 General workflow for combining molecular modelling with ion mobility mass spectrometry

However, there does not appear to be a consensus or evidence *via* blind trial to establish whether there is good agreement between eCCSs and tCCSs and which tCCS calculation methods provide the closest matches to eCCS values. Indeed, recent publications[1–8] on small molecules have utilised various and diverse approaches to calculate tCCSs, a summary of which is shown in Table 4-1.

Table 4-1. The approaches evaluated in this study are shown in italics, as well as alternative approaches to predicting tCCS values

Geometry optimisation	Mobility calculation	Software	Partial atomic charge
Density Functional Theory	*Trajectory Method (T.M.)*	*MOBCAL*	*Electrostatic potential*
Molecular dynamics	Exact Hard Sphere Scattering	Sigma	Mulliken
Semi-Empirical	Projection Approximation	Driftscope	-
Molecular mechanics	-	-	-

4.1.2 Experimental design

Overall the work reported in this study seeks to establish a baseline for comparing tCCS and eCCS values based on existing protocols. This study does not seek to optimise and improve on existing protocols, but instead to benchmark them. This study also seeks to provide evidence for practitioners to reflect on the results and accuracy from previous publications and may help understand which factors may exacerbate differences between tCCS and eCCS values. In all cases the eCCS of the singly charged ion is reported and the tCCS of the singly charged ion was calculated.

The compounds studied in this work are a diverse set of small molecule type compounds (see Figure 4-2). They are structurally diverse, and include pharmaceutically relevant compounds. The number of protonation sites, range of *m/z,* and sub-structures were varied, as shown in Figure 4-3. The compounds studied include pregabalin (Lyrica®) and sildenafil (Viagra®) hence this study is especially relevant to drug-like molecules.
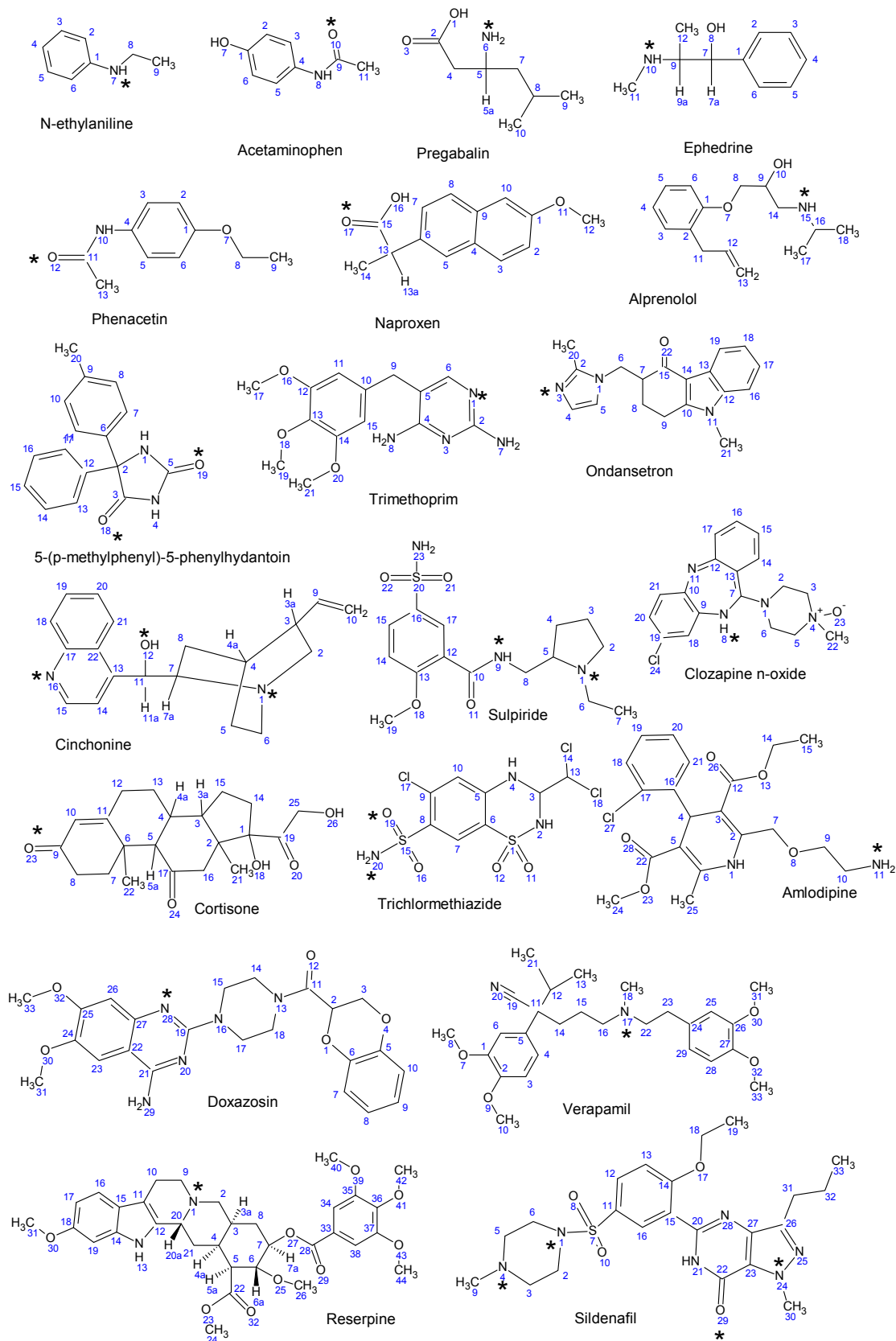
Figure 4-2. Structures of all compounds studied (* marks lowest energy structures or those within 5 kcal/mol of lowest energy structure, inferring most basic site(s)).

135

a)
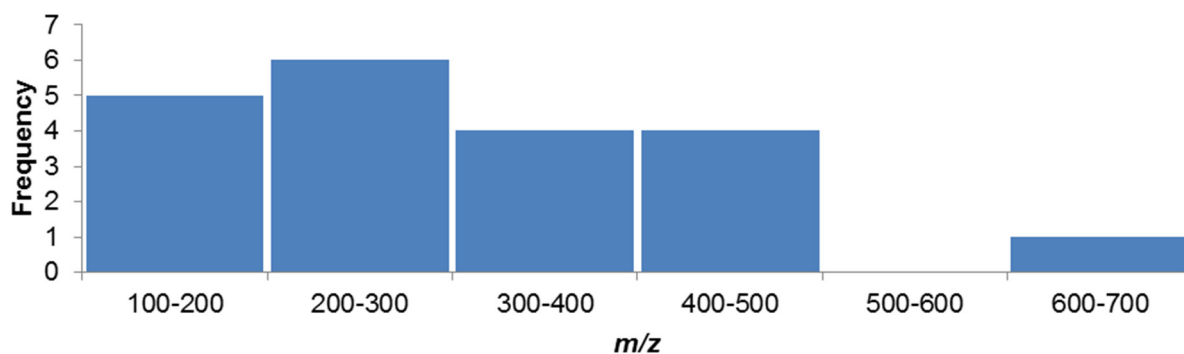
b)
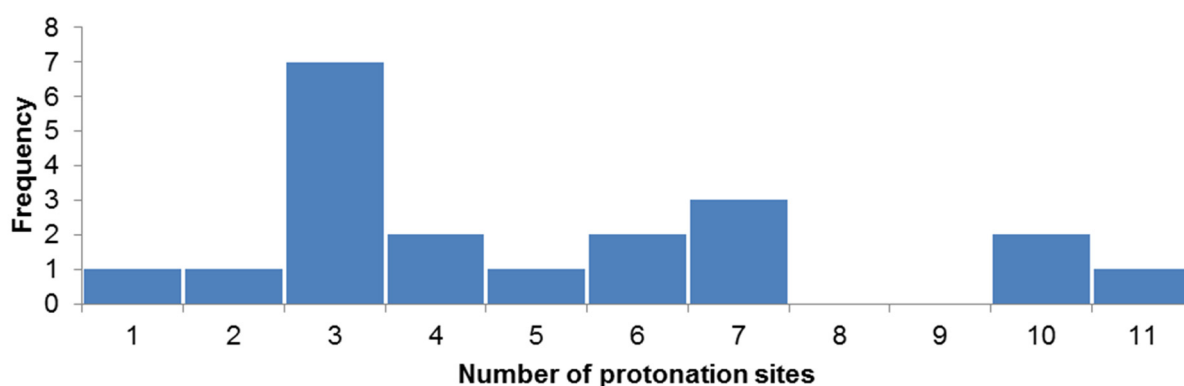
Figure 4-3. a) Histogram showing range of *m/z* values b) Histogram showing spread of number of protonation sites.

For calculations using the original He$_{(g)}$ MOBCAL code, it was not possible to calculate tCCS for nine of the compounds without modification to the original MOBCAL code or calibration protocol. Specifically the first six tCCSs data-points in Table 4-2 are omitted because the poly-(D/L)-alanine calibration does not cover that CCS range; so it may be questioned whether an experimental measurement is valid since it will be outside the eCCS calibration range. The remaining three tCCSs data-points were omitted because the original He$_{(g)}$ MOBCAL code does not include Cl. It is possible to modify the MOBCAL code before compilation to include Cl (and other atom types if desired), this would require either:

1) assuming that the Cl atom type has identical parameters to Si, which is unsupported by any direct experimental evidence and does not represent common past practice, or

2) measure and tune the MOBCAL parameters for Cl with representative compounds; which was felt to be outside of the scope of this study and does not represent common past practice.

The exclusion of some compounds using the original $He_{(g)}$ code highlights the usefulness of the drug-like calibration set and $N_{2(g)}$ MOBCAL code which includes parameterisation of elements including Cl and F and a larger range from 122 to 609 *m/z* units.[9]

Table 4-2 Summary of tCCS calculations conducted.

Identity	Protonated molecule *m/z*	Molecular formula	$He_{(g)}$ MOBCAL	$N_{2(g)}$ MOBCAL
N-Ethylaniline	122	$C_8H_{11}N$	n	y
Acetaminophen	152	$C_8H_9NO_2$	n	y
Pregabalin	160	$C_8H_{17}NO_2$	n	y
Ephedrine	166	$C_{10}H_{15}NO$	n	y
Phenacetin	180	$C_{10}H_{13}NO_2$	n	y
Naproxen	230	$C_{14}H_{14}O_3$	n	y
Alprenolol	250	$C_{15}H_{23}NO_2$	y	y
5-(*p*-Methylphenyl)-5-phenylhydantoin	267	$C_{16}H_{14}N_2O_2$	y	y
Trimethoprim	291	$C_{14}H_{18}N_4O_3$	y	y
Ondansetron	294	$C_{18}H_{19}N_3O$	y	y
Cinchonine	295	$C_{19}H_{22}N_2O$	y	y
Sulpiride	342	$C_{15}H_{23}N_3O_4S$	y	y
Clozapine *N*-oxide	343	$C_{18}H_{19}ClN_4O$	n	y
Cortisone	361	$C_{21}H_{28}O_5$	y	y
Trichlormethiazide	380	$C_8H_8Cl_3N_3O_4S_2$	n	y
Amlodipine	409	$C_{20}H_{25}ClN_2O_5$	n	y
Doxazosin	452	$C_{23}H_{25}N_5O_5$	y	y
Verapamil	455	$C_{27}H_{38}N_2O_4$	y	y
Sildenafil	475	$C_{22}H_{30}N_6O_4S$	y	y
Reserpine	609	$C_{33}H_{40}N_2O_9$	y	y
		count =	11	20
		% calculated	55%	100%

4.2 RESULTS AND DISCUSSION

4.2.1 Experimental compared to theoretical CCS for $N_{2(g)}$ calibration protocol

On plotting the tCCS values for the lowest energy structure, and those structures within 5 kcal/mol of the lowest energy structure, compared to eCCS, there is a linear correlation between the eCCS and tCCS with an R^2 value > 0.99 (see Figure 4-4) showing a good linear correlation. In contrast to previously described results[9] where the slope of the line is very close to 1 (*i.e. y = mx + c* where *m* is 1) these results demonstrate a linear correlation that has a defined slope of ~1.25, and a constant, derived from an apparent larger tCCS than eCCS for many ions. This study includes additional compounds to the *N*-ethylaniline, acetaminophen, alprenolol, ondansetron, clozapine *N*-oxide, verapamil and reserpine compared to previous results[20]. Using the same level of theory, basis set and parameters to calculate the optimised geometries using Gaussian 09, many of the of the same calibration compounds[9] and running the supplied MOBCAL script tCCS values are obtained that appear to be well described by a linear regression analysis with an excellent R^2 value of >0.99.
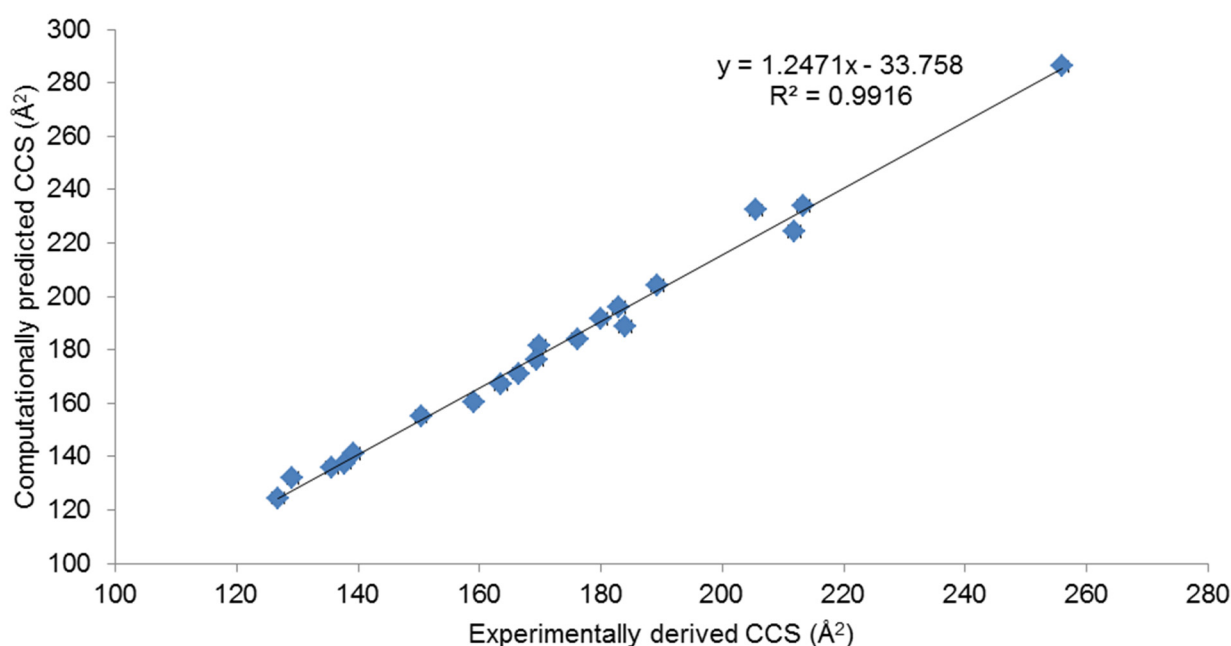
Figure 4-4. Linear regression of eCCS and tCCS for $N_{2(g)}$ MOBCAL with experimental standard deviation shown.

There may be two or more contributing factors for differences between tCCS and eCCS:

1) It is conceivable that the parameterisation of interactions in MOBCAL software versions has been sub-optimal as tuning was based on a limited dataset due to computing demands at the time when the software was written (c. 1997)[10,11] and on relatively small datasets since[9]. The slope of ~1.2 obtained herein is also corroborated by the slope of 1.2378 found in the computationally predicted CCS of 125 common metabolites[12] and slopes of up to ~1.2 obtained for saxitoxins[13] both using a similar $N_{2(g)}$ MOBCAL T.M. methodology.

A subset consisting of molecules from this dataset where the number of rotatable bonds were 3 or less (namely *N*-ethylaniline, acetaminophen, ephedrine, phenacetin, naproxen, *5*-(*p*-Methylphenyl)-*5*-phenylhydantoin, ondansetron, cinchonine, clozapine *N*-oxide, cortisone and trichlormethiazide) were selected and their tCCS values plotted against eCCS values (see Figure 4-5). For structures with smaller numbers of rotatable bonds (<6) these can be expected to have a relatively small distribution of conformational complexity and therefore it is reasonable to assume the global minimum potential energy structure could be found. A slope of ~1.15 is found for this subset in agreement with the hypothesis that the parameterisation in MOBCAL is sub-optimal and leads to overestimation of tCCS, demonstrated for this subset with limited conformational flexibility.
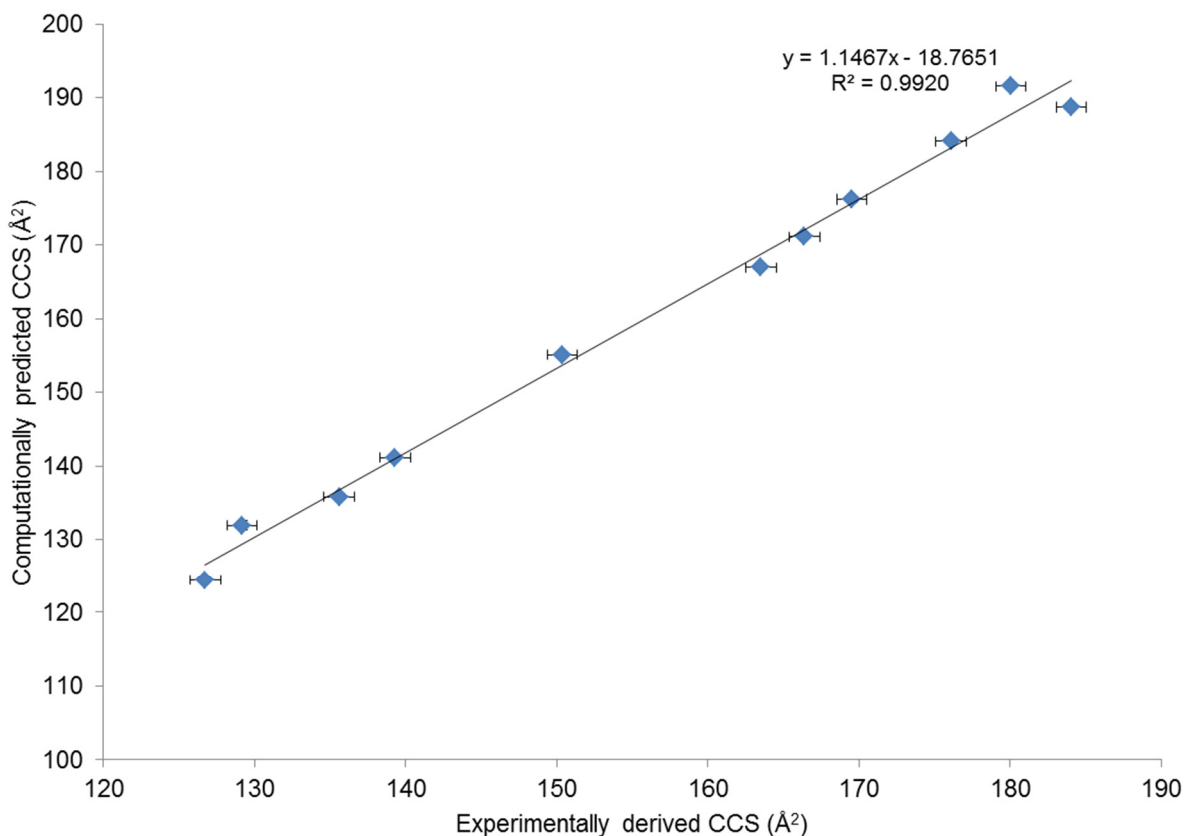
Figure 4-5. tCCS compared to eCCS for molecules where the number of rotatable bonds is three or less, with experimental standard deviation shown.

2) A stationary point consistent with a local minimum significantly different in conformational space to the eCCS structure may be obtained. However, it appears unlikely that systematically minimum energy geometries are obtained that result in tCCSs that are significantly larger than eCCSs.

3) The experimental errors include the standard deviation of the MOBCAL calculation which was typically 1% or less (Supplementary Data, Appendix B). The reproducibility of eCCS has been found to typically be between 0.5% and 1.3%.[9] In this study the standard deviation in percentage for the CCS measurement obtained using travelling wave ion mobility was less than 0.6% (see Appendix).

To compare the tCCS and eCCS on a per compound basis Figure 4-6 illustrates a 1) corrected tCCS compared to eCCS with a correction derived from the linear regression slope to account for potential sub-optimal parameterisation and 2) an uncorrected tCCS used without modification from the MOBCAL T.M. calculation result. The corrected tCCS was calculated

140

by subtracting the intercept of the slope (*c* from the general *y=mx + c*) and multiplying by the reciprocal of the slope of the regression (*m* from the general equation *y=mx + c*).

Figure 4-6. Comparison of % difference between and uncorrected tCCS and eCCS for $N_{2(g)}$ MOBCAL.

Summarising a comparison of tCCSs compared to eCCSs and binning the results into closeness of fit (see Figure 4-7) demonstrates that the majority of corrected tCCSs are within 2% of the eCCS, indeed ~90% of compounds exhibit a tCCS within 3% of the eCCS results and 45% of uncorrected tCCS values are within 3% of the eCCS results.
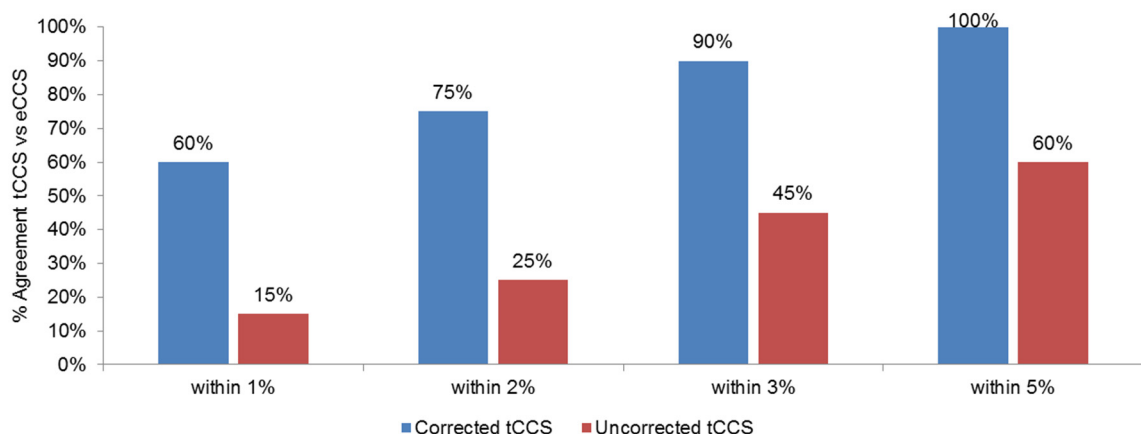
Figure 4-7. Agreement between corrected and uncorrected tCCS and eCCS for $N_{2(g)}$ MOBCAL.

141

4.2.2 Experimental compared to theoretical CCS for He$_{(g)}$ calibration protocol

On plotting the tCCS for the lowest energy structure, and those structures within 5 kcal/mol of the lowest energy structure, compared to eCCS there is a linear correlation between the eCCS and tCCS with an R^2 value ~ 0.99 (see Figure 4-8) showing a good linear correlation.
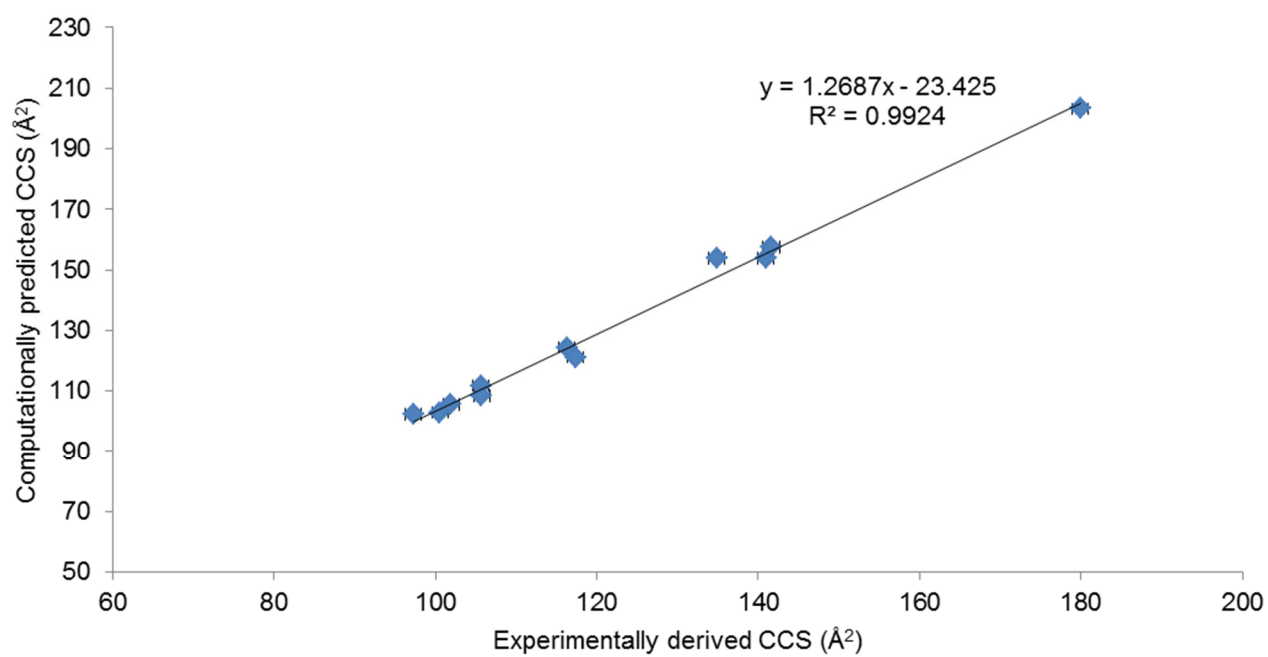
Figure 4-8. Linear regression of eCCS and tCCS for He$_{(g)}$ MOBCAL with experimental standard deviation shown.

To compare the tCCS and eCCS on a per compound basis see Figure 4-9 again illustrates 1) a corrected tCCS compared to the eCCS with a correction derived from the linear regression slope to account for potential sub-optimal parameterisation and 2) an uncorrected tCCS used without modification from the MOBCAL T.M. calculation result. The corrected tCCS was calculated by subtracting the intercept of the slope (*c* from the general *y=mx + c*) and multiplying by the reciprocal of the slope of the regression (*m* from the general equation *y=mx + c*).
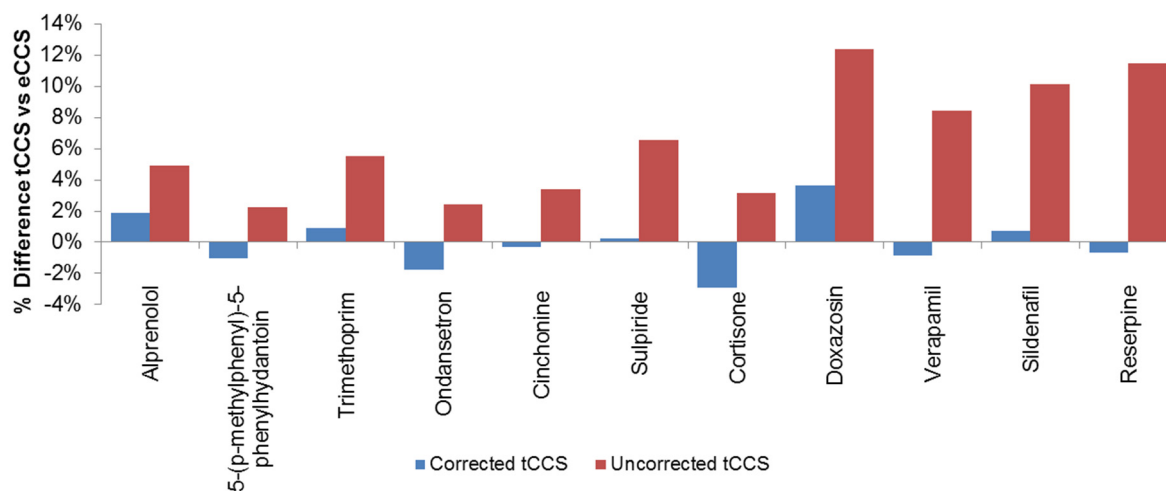
Figure 4-9. Comparison of % difference between corrected tCCS and eCCS for He$_{(g)}$ MOBCAL.

Comparing tCCSs and eCCSs by binning the results into closeness of fit (see Figure 4-10) demonstrates that the majority of corrected tCCSs are within 2% of the eCCS, indeed ~90% of compounds exhibit a tCCS within 3% of the eCCS result. Only 18% of uncorrected tCCSs are within 3% of the eCCS result and 45% within 5% of the eCCS result.
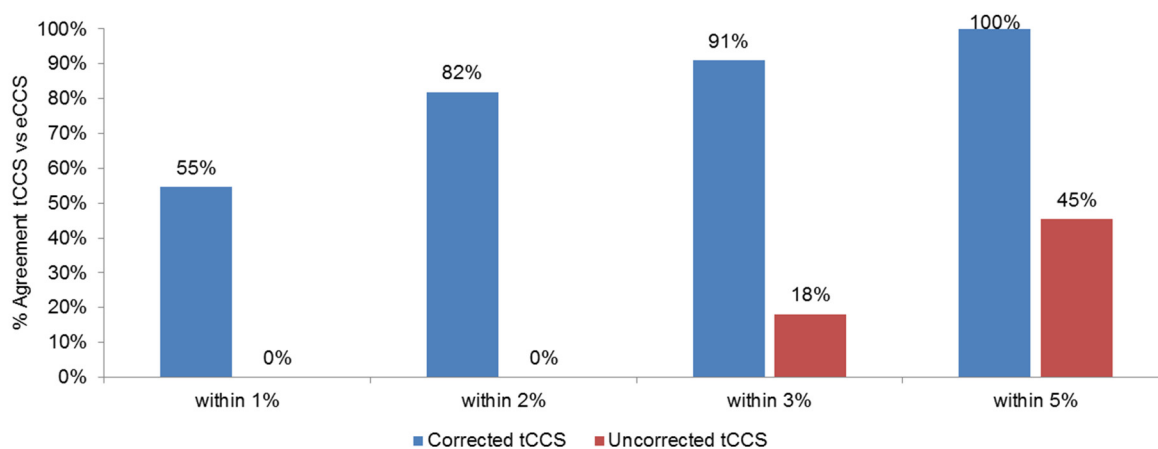
Figure 4-10. Agreement between corrected tCCS and eCCS for He$_{(g)}$ MOBCAL T.M. methods.

If tCCSs are able to accurately predict eCCSs within experimental error then this opens up powerful new opportunities for utilising ion mobility data. There are a number of applications where prediction of CCS may be especially useful including:

- generating libraries and thereafter utilising tCCSs as a confirmatory identification point for eCCSs

- to confirm the identity of an analyte *e.g.* a drug metabolite[14]

143

- to predict ion mobility of analytes[15,16] and determine, *in silico,* the degree of separation in a mixture

In terms of usefulness for structural identity, the absolute CCS prediction accuracy measured here may still be challenging, for example, to determine the site of metabolism on a molecule, so considering relative trends in CCS may also be useful. It has been demonstrated that one method of confirming the site of metabolism using ion mobility is to derivatise a single, or a collection of, functional group(s) and therefore increase the difference in CCS between closely related isomers so that they are clearly distinguishable. Derivatisation with 2-fluoro-*N*-methyl pyridinium *p*-toluenesulfonate allowed certain hydroxylated metabolites to be discerned in Atorvastatin, Warfarin and Imipraimine by increasing the CCS difference between ions with different sites of metabolism.[17] Other derivatisation studies have utilised *p*-toluenesulfonyl isocyanate for –OH groups in steroids[18] and boronic acids for the reducing end of cis-diols in carbohydrates[19] which sometimes achieved baseline resolution of isomers.

4.3 EXPERIMENTAL

4.3.1 Chemicals and materials

All test compounds, isopropanol and methanol were purchased from Sigma-Aldrich (Gillingham, UK), acetonitrile from Rathburn (Walkerburn, UK) and high purity water from VWR International Ltd (West Chester, PA, USA). Formic acid was supplied by Biosolve (Valkenswaard, The Netherlands).

4.3.2 Mass spectrometry conditions

Experiments were performed using a Waters Synapt G2 HDMS system (Waters, Manchester, UK) with a hybrid quadrupole/travelling wave ion mobility/orthogonal acceleration time-of-flight configuration. Experiments were conducted using an ESI source operated in the positive ion mode with a capillary voltage of 3.2 kV and cone voltage of 30 V. An orthogonal LockSpray™ ESI probe was used with the protonated molecule leucine-enkephaline ([M + H]$^+$ ion *m/z* 556.2771) as the internal mass correction calibrant. The TOF analyser was operated in resolution mode (a resolution of 18,000 at *m/z* 556), acquiring 2 scans per second. The trap was set at 4 eV and the transfer at 0 eV. The source temperature was 150°C, desolvation temperature was 500 °C, cone gas (N_2) flow rate of 80 L/h and desolvation gas

(N$_2$) flow rate of 1200 L/h. Mass calibration was achieved by mixing 0.05 mM sodium hydroxide solution with 0.05% formic acid in isopropanol/water (90:10 v/v), and infusing the resulting sodium formate solution at 10 μL/min.

4.3.3 Inlet conditions

A solution of 0.1 mg/mL of each compound was prepared in methanol:water (50:50) and 2 μL of that solution was introduced *via* direct injection. An Acquity UHPLC binary pump was used with a composition of 50:50 A: water + 0.1% (v/v) formic acid and B: acetonitrile + 0.1% (v/v) formic acid. The flow rate was 0.3 mL/min to the electrospray source. No splitter was used, so the entire flow was introduced into the electrospray source.

4.3.4 Ion mobility conditions

The mobility T-wave cell was operated at a pressure of 2.8 mbar of nitrogen. The wave velocity was 800 m/s and the wave height was fixed at 40 V.

4.3.5 Data processing and IMS calibration

Data acquisition and processing were carried out using MassLynx 4.1 and Driftscope 2.8 (Waters, Manchester, UK) software. The *m/z* range for the peak of interest was selected and Driftscope software was used to determine the CCS values of the analyte compounds by projecting their drift times onto a calibration curve. The T-wave instrument was calibrated using a well-established protocol[20] by plotting the drift time/CCS function following data acquisition of a suitable calibration set under exactly the same ion mobility and mass spectrometric conditions as those used for the following analysis.

Ion mobility eCCS results were calibrated with appropriate calibrants:

1. For comparison with MOBCAL calculations conducted in He$_{(g)}$ the experimental calibrants were ions with known CCS measured in drift-time instrument[21] from a 10 mM poly-(D/L)-alanine solution in methanol/water (50:50; v/v). These calibrants were chosen since historically many publications utilise the original MOBCAL He$_{(g)}$ code with poly-(D/L)-alanine drift-time calibration protocol.

2. For comparison with MOBCAL calculations conducted in N$_{2(g)}$ the experimental calibrants were ions with known CCS measured in a confining RF ion guide instrument[9] from a solution of drug-like compounds including *N*-ethylaniline,

acetaminophen, alprenolol, ondansetron, clozapine *N*-oxide, verapamil and reserpine. These calibrants were chosen since it reflects the new drug-like molecule drift-time calibration and updated MOBCAL $N_{2(g)}$ code.

4.3.6 Density functional theory (DFT) calculations

For metformin, ephedrine, desipramine, *5*-(*p*-Methylphenyl)-*5*-phenylhydantoin, trimethoprim, sulpiride, cortisone, trichlormethiazide, amlodipine, ziprasidone, doxazosin, sildenafil and reserpine the starting geometries were derived from previously conducted geometry optimisations[22] in Spartan '10[23]. Briefly, the starting geometry was obtained for each protonated derivative using molecular mechanics MMFF minimum energy geometry optimisation. All compounds were geometry optimised after protonation at all heteroatoms using DFT 6-31G(d,p) with the following preferences: maximum ligand distance 2.00 Å; polar area range 1000 kJ/mol; accessible area radius 1.000; 'converge' was selected.

For *N*-ethylaniline, acetaminophen, pregabalin, phenacetin, naproxen, alprenolol, ondansetron, cinchonine and clozapine *N*-oxide initial models for each of the protonated derivatives were constructed by placing a hydrogen atom at a distance of 1 Å from each putative protonation site. A systematic rotor conformation search was conducted using the Open Babel 2.3.2[24] as implemented in Avogadro v1.0.1[25] at the MMFF94 level of theory. The minimum energy conformer was selected as the starting geometry for further geometry optimisation.

Final DFT calculations of all the structures, and associated energies were then conducted with the Gaussian[26] 09 program using the hybrid SCF-DFT B3LYP method, which incorporates Becke's three parameter hybrid functional[27] and the Lee, Yang and Parr correlation functional[28]. All calculations were performed using the 6-31+G(d,p) basis set with geometry optimisation and additional keywords *pop=(mk,dipole)* to generate Merz-Singh-Kollman electrostatic potential partial atomic charges.

4.3.7 Theoretical collision cross-section MOBCAL calculations

The Chemcraft[29] software was used to convert from the Gaussian output LOG file to the MOBCAL input MFJ file using the option to save Merz-Singh-Kollman partial atomic charges. In-house scripts were used to run MOBCAL calculations for all protonation sites using the T.M. calculation method. Two versions of MOBCAL were used 1) the original $He_{(g)}$

parameterised MOBCAL[10,11] and 2) a $N_{2(g)}$ parameterised version[9]. The code for the original $He_{(g)}$ parameterised MOBCAL was altered on line 267 to 1000 imp, as recommended where only one structure exists[10,11], so that resulting typical standard deviations were typically 1% or less. MOBCAL code was compiled with the GNU Fortran 77 compiler packaged with Force 2.0.9 software.

4.4 CONCLUSIONS

This study represents the first quantitative evaluation of the agreement between tCCSs and eCCSs for a range of small pharmaceutically relevant molecules using travelling wave ion mobility mass spectrometry. Selecting a subset of molecules where the number of rotatable bonds is less than three builds confidence that sub-optimal parameterisation of interactions in MOBCAL is likely. Using the $N_{2(g)}$ parameterised calibration routine and MOBCAL calculation 1) 45% of the tCCS for the 20 small molecules studied are within 3% of the eCCS without correction and 2) 90% of the tCCSs are within 3% of the eCCS after a correction is applied.

For protein species a comparison of tCCSs and eCCSs may be derived, with some approximations, from the X-ray crystallography structures[30] but for small molecules the speed of molecular modelling allows high levels of computational theory to be utilised in timescales useful for structural determination. Many of the existing applications of IM-MS have been for biological challenges (*e.g.* conformational changes in proteins), so relatively little work has been carried out which explores the suitability of predictive tools for small molecule compounds[2]. Indeed this work also represents the first attempt at using MK partial atomic charges in Gaussian 09 optimised structures with $He_{(g)}$ MOBCAL. It is not clear from previous publications if Mulliken partial atomic charges were used or the influence of charge was disregarded altogether in the configuration of the MOBCAL calculation, and therefore potentially important charge distribution based interactions were missed. The presented results are based on established protocols, however further work using alternative modelling and calculation methods over a wide range of structures, conformers and molecular formulae is required to further evaluate and improve the general agreement between tCCSs and eCCSs.

4.5 REFERENCES

1. Rogers, R. A., Rodier, A. R., Stanley, J. A., Douglas, N. A., Li, X. & Brittain, W. J. A study of the spiropyran–merocyanine system using ion mobility-mass spectrometry: experimental support for the cisoid conformation. *Chem. Commun.* **50,** 3424–3426 (2014).

2. Knapman, T. W., Berryman, J. T., Campuzano, I., Harris, S. A. & Ashcroft, A. E. Considerations in experimental and theoretical collision cross-section measurements of small molecules using travelling wave ion mobility spectrometry-mass spectrometry. *Int. J. Mass Spectrom.* **298,** 17–23 (2010).

3. Fasciotti, M., Gomes, A. F., Gozzo, F. C., Iglesias, B. A., Sá, G. F. de, Daroda, R. J., Toganoh, M., Furuta, H., Araki, K. & Eberlin, M. N. Corrole isomers: intrinsic gas-phase shapes via traveling wave ion mobility mass spectrometry and dissociation chemistries via tandem mass spectrometry. *Org. Biomol. Chem.* **10,** 8396–8402 (2012).

4. Chan, Y.-T., Li, X., Yu, J., Carri, G. A., Moorefield, C. N., Newkome, G. R. & Wesdemiotis, C. Design, Synthesis, and Traveling Wave Ion Mobility Mass Spectrometry Characterization of Iron(II)– and Ruthenium(II)–Terpyridine Metallomacrocycles. *J. Am. Chem. Soc.* **133,** 11967–11976 (2011).

5. Zimnicka, M., Troć, A., Ceborska, M., Jakubczak, M., Koliński, M. & Danikiewicz, W. Structural Elucidation of Specific Noncovalent Association of Folic Acid with Native Cyclodextrins Using an Ion Mobility Mass Spectrometry and Theoretical Approach. *Anal. Chem.* **86,** 4249–4255 (2014).

6. Dear, G. J., Munoz-Muriedas, J., Beaumont, C., Roberts, A., Kirk, J., Williams, J. P. & Campuzano, I. Sites of metabolic substitution: investigating metabolite structures utilising ion mobility and molecular modelling. *Rapid Commun. Mass Spectrom.* **24,** 3157–3162 (2010).

7. Lalli, P. M., Iglesias, B. A., Toma, H. E., de Sa, G. F., Daroda, R. J., Silva Filho, J. C., Szulejko, J. E., Araki, K. & Eberlin, M. N. Protomers: formation, separation and characterization via travelling wave ion mobility mass spectrometry. *J. Mass Spectrom.* **47,** 712–719 (2012).

8. Lavanant, H., Tognetti, V. & Afonso, C. Traveling Wave Ion Mobility Mass Spectrometry and Ab Initio Calculations of Phosphoric Acid Clusters. *J. Am. Soc. Mass Spectrom.* **25,** 572–580 (2014).

9. Campuzano, I., Bush, M. F., Robinson, C. V., Beaumont, C., Richardson, K., Kim, H. & Kim, H. I. Structural Characterization of Drug-like Compounds by Ion Mobility Mass Spectrometry: Comparison of Theoretical and Experimentally Derived Nitrogen Collision Cross Sections. *Anal. Chem.* **84,** 1026–1033 (2012).

10. Mesleh, M. F., Hunter, J. M., Shvartsburg, A. A., Schatz, G. C. & Jarrold, M. F. Structural Information from Ion Mobility Measurements: Effects of the Long-Range Potential. *J. Phys. Chem.* **100,** 16082–16086 (1996).

11. Shvartsburg, A. A. & Jarrold, M. F. An exact hard-spheres scattering model for the mobilities of polyatomic ions. *Chem. Phys. Lett.* **261,** 86–91 (1996).

12. Paglia, G., Williams, J. P., Menikarachchi, L., Thompson, J. W., Tyldesley-Worster, R., Halldórsson, S., Rolfsson, O., Moseley, A., Grant, D., Langridge, J., Palsson, B. O. & Astarita, G. Ion Mobility Derived Collision Cross Sections to Support Metabolomics Applications. *Anal. Chem.* **86,** 3985–3993 (2014).

13. Poyer, S., Loutelier-Bourhis, C., Coadou, G., Mondeguer, F., Enche, J., Bossée, A., Hess, P. & Afonso, C. Identification and separation of saxitoxins using hydrophilic interaction liquid chromatography coupled to traveling wave ion mobility-mass spectrometry. *J. Mass Spectrom.* **50,** 175–181 (2015).

14. Cuyckens, F., Wassvik, C., Mortishire-Smith, R. J., Tresadern, G., Campuzano, I. & Claereboudt, J. Product ion mobility as a promising tool for assignment of positional isomers of drug metabolites. *Rapid Commun. Mass Spectrom.* **25,** 3497–3503 (2011).

15. Agbonkonkon, N., Tolley, H. D., Asplund, M. C., Lee, E. D. & Lee, M. L. Prediction of Gas-Phase Reduced Ion Mobility Constants (K0). *Anal. Chem.* **76,** 5223–5229 (2004).

16. Hariharan, C., Ingo Baumbach, J. & Vautz, W. Empirical prediction of reduced ion mobilities of secondary alcohols. *Int. J. Ion Mobil. Spectrom.* **12,** 59–63 (2009).

17. Shimizu, A. & Chiba, M. Ion Mobility Spectrometry–Mass Spectrometry Analysis for the Site of Aromatic Hydroxylation. *Drug Metab. Dispos.* **41,** 1295–1299 (2013).

18. Ahonen, L., Fasciotti, M., Gennäs, G. B. af, Kotiaho, T., Daroda, R. J., Eberlin, M. & Kostiainen, R. Separation of steroid isomers by ion mobility mass spectrometry. *J. Chromatogr. A* **1310,** 133–137 (2013).

19. Fenn, L. S. & McLean, J. A. Enhanced carbohydrate structural selectivity in ion mobility-mass spectrometry analyses by boronic acid derivatization. *Chem. Commun.* 5505–5507 (2008).

20. Williams, J. P., Lough, J. A., Campuzano, I., Richardson, K. & Sadler, P. J. Use of ion mobility mass spectrometry and a collision cross-section algorithm to study an organometallic ruthenium anticancer complex and its adducts with a DNA oligonucleotide. *Rapid Commun. Mass Spectrom.* **23,** 3563–3569 (2009).

21. Clemmer Group: Cross Section Database. at <http://www.indiana.edu/~clemmer/Research/Cross%20Section%20Database/cs_databas e.php>

22. Wright, P., Alex, A. & Pullen, F. Predicting collision-induced dissociation spectra: semi-empirical calculations as a rapid and effective tool in software-aided mass spectral interpretation. *Rapid Commun. Mass Spectrom.* **28,** 1127–1143 (2014).

23. Shao, Y., Molnar, L. F., Jung, Y., Kussmann, J., Ochsenfeld, C., Brown, S. T., Gilbert, A. T. B., Slipchenko, L. V., Levchenko, S. V., O'Neill, D. P., DiStasio Jr, R. A., Lochan, R. C., Wang, T., Beran, G. J. O., Besley, N. A., Herbert, J. M., Lin, C. Y., Voorhis, T. V., Chien, S. H., Sodt, A., Steele, R. P., Rassolov, V. A., Maslen, P. E., Korambath, P. P., Adamson, R. D., Austin, B., Baker, J., Byrd, E. F. C., Dachsel, H., Doerksen, R. J., Dreuw, A., Dunietz, B. D., Dutoi, A. D., Furlani, T. R., Gwaltney, S. R., Heyden, A., Hirata, S., Hsu, C.-P., Kedziora, G., Khalliulin, R. Z., Klunzinger, P., Lee, A. M., Lee, M. S., Liang, W., Lotan, I., Nair, N., Peters, B., Proynov, E. I., Pieniazek, P. A., Rhee, Y. M., Ritchie, J., Rosta, E., Sherrill, C. D., Simmonett, A. C., Subotnik, J. E., Iii, H. L. W., Zhang, W., Bell, A. T., Chakraborty, A. K., Chipman, D. M., Keil, F. J., Warshel, A., Hehre, W. J., Iii, H. F. S., Kong, J., Krylov, A. I., Gill, P. M. W. & Head-Gordon, M. Advances in methods and algorithms in a modern quantum chemistry program package. *Phys. Chem. Chem. Phys.* **8,** 3172–3191 (2006).

24. O'Boyle, N. M., Banck, M., James, C. A., Morley, C., Vandermeersch, T. & Hutchison, G. R. Open Babel: An open chemical toolbox. *J. Cheminformatics* **3,** 33 (2011).

25. Hanwell, M. D., Curtis, D. E., Lonie, D. C., Vandermeersch, T., Zurek, E. & Hutchison, G. R. Avogadro: an advanced semantic chemical editor, visualization, and analysis platform. *J. Cheminformatics* **4,** 17 (2012).

26. Frisch, M. J., Trucks, G. W., Schlegel, H. B., Scuseria, G. E., Robb, M. A., Cheeseman, J. R., Scalmani, G., Barone, V., Mennucci, B., Petersson, G. A., Nakatsuji, H., Caricato, M., Li, X., Hratchian, H. P., Izmaylov, A. F., Bloino, J., Zheng, G., Sonnenberg, J. L., Hada, M., Ehara, M., Toyota, K., Fukuda, R., Hasegawa, J., Ishida, M., Nakajima, T., Honda, Y., Kitao, O., Nakai, H., Vreven, T., Montgomery Jr., J. A., Peralta, J. E., Ogliaro, F., Bearpark, M. J., Heyd, J., Brothers, E. N., Kudin, K. N., Staroverov, V. N., Kobayashi, R., Normand, J., Raghavachari, K., Rendell, A. P., Burant, J. C., Iyengar, S. S., Tomasi, J.,

Cossi, M., Rega, N., Millam, N. J., Klene, M., Knox, J. E., Cross, J. B., Bakken, V., Adamo, C., Jaramillo, J., Gomperts, R., Stratmann, R. E., Yazyev, O., Austin, A. J., Cammi, R., Pomelli, C., Ochterski, J. W., Martin, R. L., Morokuma, K., Zakrzewski, V. G., Voth, G. A., Salvador, P., Dannenberg, J. J., Dapprich, S., Daniels, A. D., Farkas, Ö., Foresman, J. B., Ortiz, J. V., Cioslowski, J. & Fox, D. J. *Gaussian 09*. (Gaussian, Inc., 2009).

27. Becke, A. D. Density-functional thermochemistry. III. The role of exact exchange. *J. Chem. Phys.* **98,** 5648–5652 (1993).

28. Lee, C., Yang, W. & Parr, R. G. Development of the Colle-Salvetti correlation-energy formula into a functional of the electron density. *Phys. Rev. B* **37,** 785–789 (1988).

29. Chemcraft - Download. at <http://www.chemcraftprog.com/download.html>

30. Jurneczko, E. & Barran, P. E. How useful is ion mobility mass spectrometry for structural biology? The relationship between protein crystal structures and their collision cross sections in the gas phase. *Analyst* **136,** 20–28 (2010).

Chapter 5: The use of molecular modelling in ion mobility mass spectrometry to predict collision cross-sections for small molecules

5.1 INTRODUCTION

The rise of 'omics and challenges to identify and quantify analytes in complex matrices have, arguably, increased the desire for efficient pre-separation and identification strategies in combination with mass spectrometry (MS).[1] Mass spectrometry is often applicable to high-throughput challenges and ion mobility provides a rapid separation step, with the structural information derived from an ion's position in conformational space, sometimes able to rapidly classify analytes[2] and has been used to pinpoint the site of chemical substitution in drug degradation or metabolism.[3,4] The coupling of ion mobility spectrometry (IMS) to MS has also been shown to improve performance in selectivity, speed and limit of detection[5] for many types of analyte. Molecular modelling can be used to deduce the structures of gas-phase ions by calculating structures, computing their theoretical collision cross-sections (tCCSs) and comparing with their experimental CCSs (eCCSs).[6]

Molecular modelling is now routinely used to study compounds relevant for small molecule applications including drug metabolism, pharmaceutical, food and environmental and natural products. Density functional theory (DFT) has emerged as a particularly useful method for studying the structures of ions in the gas-phase and relevant to a wide range of mass spectrometry phenomena including matrix-assisted laser desorption/ionisation[7], collision-induced dissociation[8–11] and adduct formation[12]. Due to increasing computational processing power[13], improved computational methods and a better integration between computational and experimental studies there are increasingly lower barriers for conducting molecular modelling.

The target audience member is a practising mass spectrometrist who is utilising ion mobility to study and answer structural and separation challenges for small molecules. It is assumed that the reader either (i) works with colleagues who are experts in computational chemistry or (ii) has access to a range of free and commercial computational software packages (*e.g.* GAMESS, Gaussian, Avogadro, Gabedit, *etc.*). The reader should also have access to ion mobility mass spectrometry (IM-MS) data and be able to obtain eCCS data. The reader should have some basic familiarity with the Windows command shell interface. The objective of this protocol is to serve as a practical guide to tCCS calculations derived from DFT quantum mechanical calculations and for comparison of the resulting tCCS values with eCCS data to draw meaningful conclusions for structural determination.

A key advantage of IM-MS is that an ion mobility separation can be performed in the millisecond timeframe followed by mass spectrometry on a microsecond timeframe and give additional structural information, without compromising the speed of detection. The practical separating power in ion mobility is relatively low, typically comparable to a standalone peak capacity between 10 and 100 for IMS[14] depending on the type compared to ~400 for UHPLC[15], but data are acquired rapidly and ion mobility separations can be combined with other separation techniques including gas chromatography and liquid chromatography to further increase separating power without increasing the acquisition time as it is a nested data acquisition.

Alternative methods to obtain detailed structural information for gas-phase ions include using alternative fragmentation techniques *e.g.* photo-dissociation in combination with IM-MS to yield diagnostic ions[16,17]. Photo-dissociation can provide a selective means of fragmentation and structure elucidation where other chromatographic (*e.g.* GC or UHPLC) and ion mobility separation is not sufficient to resolve components so collision-induced dissociation (CID) provides a composite spectrum. Structural information on iso-mass gas-phase ions can readily be acquired using a combination of mass spectrometry and ion spectroscopy[18]. Action spectroscopy experiments have provided the most convenient ion spectroscopy approach to understanding small conformational or structural differences among iso-mass ions, using UV/Vis electronic[19] or IR spectroscopy[20,21]. However, these instruments are not commercially available so data are currently limited and interpretation can benefit from, and often relies on, comparisons of the measured spectral data with molecular modelling predictions.

Initially the sample is ionised, using ionisation techniques such as electrospray ionisation (ESI), atmospheric pressure chemical ionisation (APCI), matrix-assisted laser desorption/ionisation (MALDI), Direct Analysis in Real-Time (DART) or Atmospheric Solids Analysis Probe (ASAP). The analyte may be selected using a quadrupole mass analyser based on specified *m/z* values or a 'full scan' *m/z* range. In some instrument configurations a first 'trap' collision cell enables a selected collision energy to be applied in a neutral gas (typically argon gas) so that product ions can be generated prior to ion mobility separation. Ions can then be introduced into the ion mobility cell containing a neutral gas at a controlled pressure (*e.g.* 2.5 mbar nitrogen gas). Typically, more extended analyte ions experience more collisions with the neutral buffer gas and therefore experience a longer drift-time than less extended ions. In some instrument configurations a second 'transfer' collision

cell enables a selected collision energy to be applied in a neutral gas (typically argon gas) so product ions can be generated after ion mobility separation. While this protocol focusses on the practical steps required for travelling wave IM-MS on the Waters Synapt IM-MS systems many of these steps can be applied to low-field IM-MS instruments where eCCS determination is possible including the Agilent 6560 IM-MS (Agilent Technologies, Santa Clara, CA)[22–26] and the Bruker Trapped IM-MS (TIMS) (Bruker Daltonics Inc., MA.).[27]

The combination of IM-MS with molecular modelling is relatively well established for systems including peptides,[28,29] polymers[30] and petrochemicals.[31–33] However, there appears to be relatively few practitioners of small molecule IM-MS molecular modelling. IM-MS for peptides and proteins therefore appears to be increasingly accepted and tCCS modelling tools are often targeted and validated with proteins or peptides, potentially overlooking key data and opportunities regarding small molecules.

This protocol has been created to lower the barrier to users with limited experience of computational tools; in addition (in Supplementary Data, Appendix C) a Windows command shell script that is helpful in automating otherwise laborious and time-consuming parts of the procedure has been created. This script can be used to queue tCCS calculations and execute multiple instances of MOBCAL to maximise use of available processing power. On a modern consumer PC with an Intel Xeon CPU E5-2620 v2 2.10GHz with 12 logical processors this means tCCS results can be obtained between ~12 times faster than typical serial, manual execution based on the MOBCAL Fortran source code alone. The script also summarises the results from MOBCAL and tabulates them in order of the tCCS calculation method *e.g.* projection approximation (P.A.), exact hard sphere scattering (E.H.S.S.) and trajectory method (T.M.) to enable comparison between eCCS and tCCS. The script can be initiated in two different ways either (a) as a job when multiple MOBCAL MFJ input files are available, or (b) as a monitoring process that waits for MOBCAL MFJ input files, and when input files are deposited then manages the calculation of tCCSs and then resumes monitoring for new input files. The monitoring form of MultiMOBCAL allows workflows pipelines to be established from molecular modelling, and automation via email or website submission to a specified directory.

There have been a number of recent studies that illustrate the growing utility of CCS values to better understand fundamental mass spectrometry processes and to help with identification of isomers (see case studies below) for small molecules; this protocol is based on current approaches[34] and the methodology has been used in recent published studies.[35–37]

Case study 1: Prediction of separation of protomers and the effect on quantitation

For norfloxacin, IM-MS in nitrogen gas uniquely reveals at least two major components in the precursor ion mobilogram with near baseline IMS separation. The shape and overall charge of ions are the most commonly used factors to explain drift-time in ion mobility; long, extended ions typically drift slower than short, compact ions and increased overall charge (*e.g. z*=2) encourages the ion to migrate quicker in the electric field.
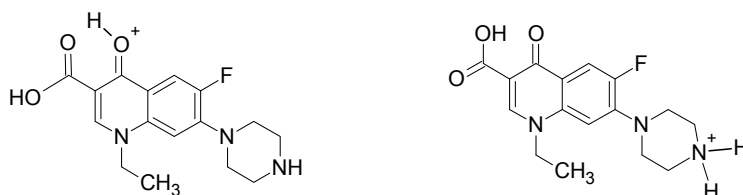
Figure 5-1. Scheme of norfloxacin with favoured protonation sites on the carbonyl oxygen and piperazine distal nitrogen.

However, for norfloxacin the appearance of at least two major peaks in the ion mobilogram with distinct product ion spectra is best rationalised by considering that the molecule can be protonated either on the carbonyl oxygen or the piperazine distal nitrogen (see Figure 5-1). This 'protomer' phenomenon has been increasingly explored using both ion mobility and molecular modelling[36,38–40] with important implications for quantitative applications where the reproducibility and abundance of product ions is critical.

157

Case study 2: Prediction of metabolite CCS in drug discovery and metabolism

Derivatisation of the 6, 7 and 8 hydroxylated metabolites of warfarin, (see **Figure 5-2**) with 2-fluoro-*N*-methyl pyridinium *p*-toluenesulfonate and calculation of the tCCS predicted[41] that the isomers can be distinguished and a rank order predicted for their drift-time. For the underivatised warfarin the tCCS values were 110.42, 110.23 and 109.84 $Å^2$ for the 6,7 and 8 substituted warfarins which does not provide specificity Derivatised analogues showed increased differentiation with tCCS values of 140.62, 142.60 and 135.90 $Å^2$ respectively.[41]
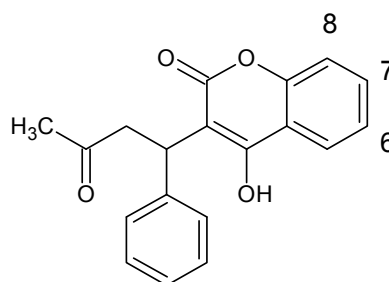
Figure 5-2. Structure of warfarin and hydroxylation sites.

Results from molecular modelling have, additionally, helped interpret eCCS data for ruthenium containing drug-like molecules,[42,43] product ions for elucidating structural isomers *e.g.* drug metabolites,[3,35] a series of drug-like molecules proposed for CCS calibration[34] and more general descriptions of drift-time and structure relationships[31] for a series of carboxylic acids relevant to small molecule drug discovery.

5.1.1 What types of small molecules can be analysed using travelling wave IM-MS?

The availability of a wide array of ionisation sources makes many analyte classes amenable to analysis by IM-MS, such that IM can be considered as a gas-phase separation device before MS. For drift-tube IMS systems the eCCS values can be derived directly from the drift-time using the Mason-Schamp equation.[44] However, for travelling wave ion mobility (TWIMS) the eCCS is not straightforward to derive from the drift-time[45] so a suitable calibration must be used, and typically calibrants in the same chemical class and molecular weight range have been recommended.[46] The most common calibrants include poly-(L/D)-alanine[47], denatured tryptic peptides[48] and a drug-like compound series.[34,49] There are three significant website databases[48,49,50] of eCCS values that may be used as either reference

158

points or to calibrate systems where required. Recently a number of chemical classes including lipids, carbohydrates and tetraalkyl-ammonium salts[25] and pesticides[22] were measured using a high-resolution drift-tube IM-MS system which may serve as suitable calibrants and provide relevant and comparable data for analysis.

5.1.2 What structural information can be obtained using small molecule IM-MS?

There are essentially four main types of mobility experiments that can be performed using Waters Synapt travelling wave IMS instrumentation (as illustrated in Table 5-1):

Table 5-1. Illustration of common types of IM-MS experiments.

Mode	Quadrupole	Trap Collision Cell	Transfer Collision Cell
1. Precursor ion IMS	RF and resolving DC (selective) or RF only (non-selective)	Low energy	Low energy
2. Product ion IMS	RF and resolving DC (selective) or RF only (non-selective)	High energy	Low energy
3(a) Fragmentation of precursor IMS	RF and resolving DC (selective)	Low energy	High energy
3(b) Fragmentation of precursor IMS	RF only (non-selective, MSE alternating between low and high energy CID)	Low energy	Low energy
		Low energy	High energy
4. Fragmentation of product ion IMS (Time Aligned Parallel (TAP) fragmentation[51])	RF and resolving DC (selective) or RF only (non-selective)	High energy	High energy

1. Precursor ion IMS - typically most suitable to determine the eCCS for a desired analyte for addition to a eCCS database and/or for comparison with CCS values obtained from reference materials or other structural data (*e.g.* molecular modelling). Utilising the quadrupole to selectively transmit ions with certain *m/z* improves confidence of the precursor identity at the quadrupole stage. In some cases post-quadrupole activation and ion-molecule reactions[12] may result in changes to the identity of precursor ions.

2. Product ion IMS - useful in cases where information on the ion substructure is required and/or may provide definitive information that helps distinguish between ions with similar precursor *m/z*[3,4], particularly when the precursor ion eCCS does not distinguish between structural isomers. There are currently few databases of product ion eCCS so they must be created in-house; their creation is highly desirable, however, and would assist in the assignment of product ion structures, and subsequent assignment for precursor structures.

3. Fragmentation of precursor IMS – useful to obtain product ion *m/z* information on precursor ion IMS separated ions. The MS[E] data acquisition mode may be combined with chromatographic and ion mobility separation and the MS[E] data viewer software (Waters Corp, Manchester) to provide an unbiased and untargeted approach. The advantages include eliminating i) a requirement for exclusion lists that can reduce the performance of MS/MS data-dependent acquisition (DDA) triggering and ii) the requirement for inclusion lists for MS/MS data-dependent acquisition that are not comprehensive and therefore biased.[52] Ion mobility can also be used to clean up the spectra by removing background (*e.g.* matrix) ions from the mass spectra, increasing the signal:noise ratio for analyte ions. Comprehensive data collected using this methodology may be stored and reviewed later to investigate 'unknowns' and key structural assignments. It has been suggested that this may be particularly valuable where complex samples are analysed *e.g.* preclinical samples for toxicological testing[52] as archived data may contain useful information that is critical to drug development, and reduces the likelihood that the sample(s) need(s) to be re-analysed.

4. Fragmentation of product ion IMS – useful to obtain product ion *m/z* information on product ion IMS separated ions (equivalent to second generation product ions). The second generation product ions are time-aligned with the first generation product ions which allows the user to collect a number of second generation product ions

simultaneously and remain confident of their precursors by utilising the ion drift time (see Figure 5-3).
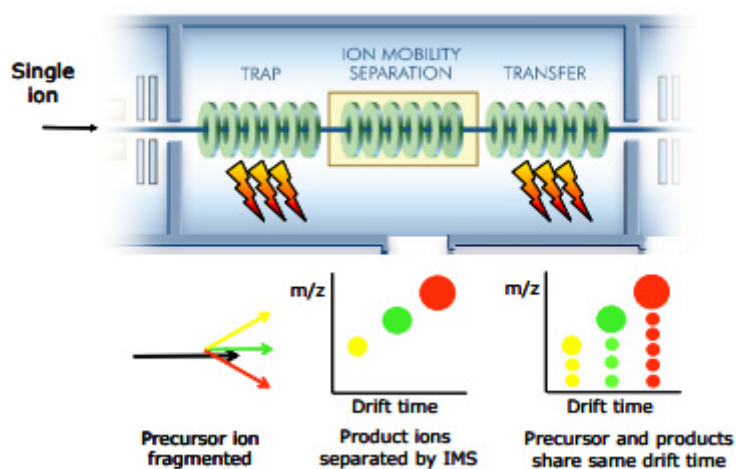
Figure 5-3. Illustration of time aligned parallel (TAP) fragmentation, equivalent to fragmentation of product ion IMS separated ions (adapted from reference 52).

5.1.3 How are drift time data used to calculate eCCS values in travelling wave ion mobility?

The motion of ions in the travelling wave ion mobility regime is currently not understood well enough to calculate the eCCS directly from the drift-time[45] so it has been recommended that a calibrant is utilised from the same chemical class as the analyte. The selection of the charge state of the calibrant has, perhaps unsurprisingly, been found to be critical to the accurate measurement of eCCS values, contributing on average 3.5% to the eCCS error[46]. Choosing the class of biomolecule calibrant, in measurements of carbohydrate and peptide ions was found to be less important, contributing 1.0% on average to the error and mismatching both calibrant class and charge states resulted in errors of around 4.7% on average.[46]

The instrument operator may manipulate parameters including both the wave speed and height to optimise a separation so it is important to use the same conditions for calibration that were used during collection of the experimental data. The proprietary Waters Driftscope software (Waters Corp., Manchester) incorporates a calibration protocol which is simple to use for the novice user. The Waters Driftscope software requires a comma separated value (CSV) file containing a list of *m/z*, eCCS and charge state for the respective calibrant ions (provided in Supplementary Data, Appendix C)

It is therefore recommended to use calibrant data of the same chemical class *e.g.* poly-(L/D)-alanine[53] or drug-like molecules[34] to calibrate travelling wave ion mobility data for small molecules acquired in the same drift-gas (typically $N_{2(g)}$) as the experimental data[53].

The drift-times are converted to eCCSs by calibration against ions with known eCCS values thus, rather than an absolute measurement, a relationship between the measured drift time t_D^X, where X is the proportionality constant derived from the calibration curve, and eCCS (Ω) is described[54] by:

$$\Omega \sim t_D^X$$

The proprietary Waters Driftscope software carries out the many of the functions below, simplifying processing for the novice user. (The *A* and *X* parameters described below are shown in Figure 5-4 as A and B. The Pearson co-efficient is calculated to show the fit). A large number of CCSs for ions may be interrogated using the graphical tools simply by holding the Ctrl key then 'hovering over' the *m/z* of interest. Selection tools, such as lasso, may be used to select region of ions according to their mobility or *m/z* and then exported as text files which may be useful to rapidly record multiple eCCS data points and build eCCS databases.
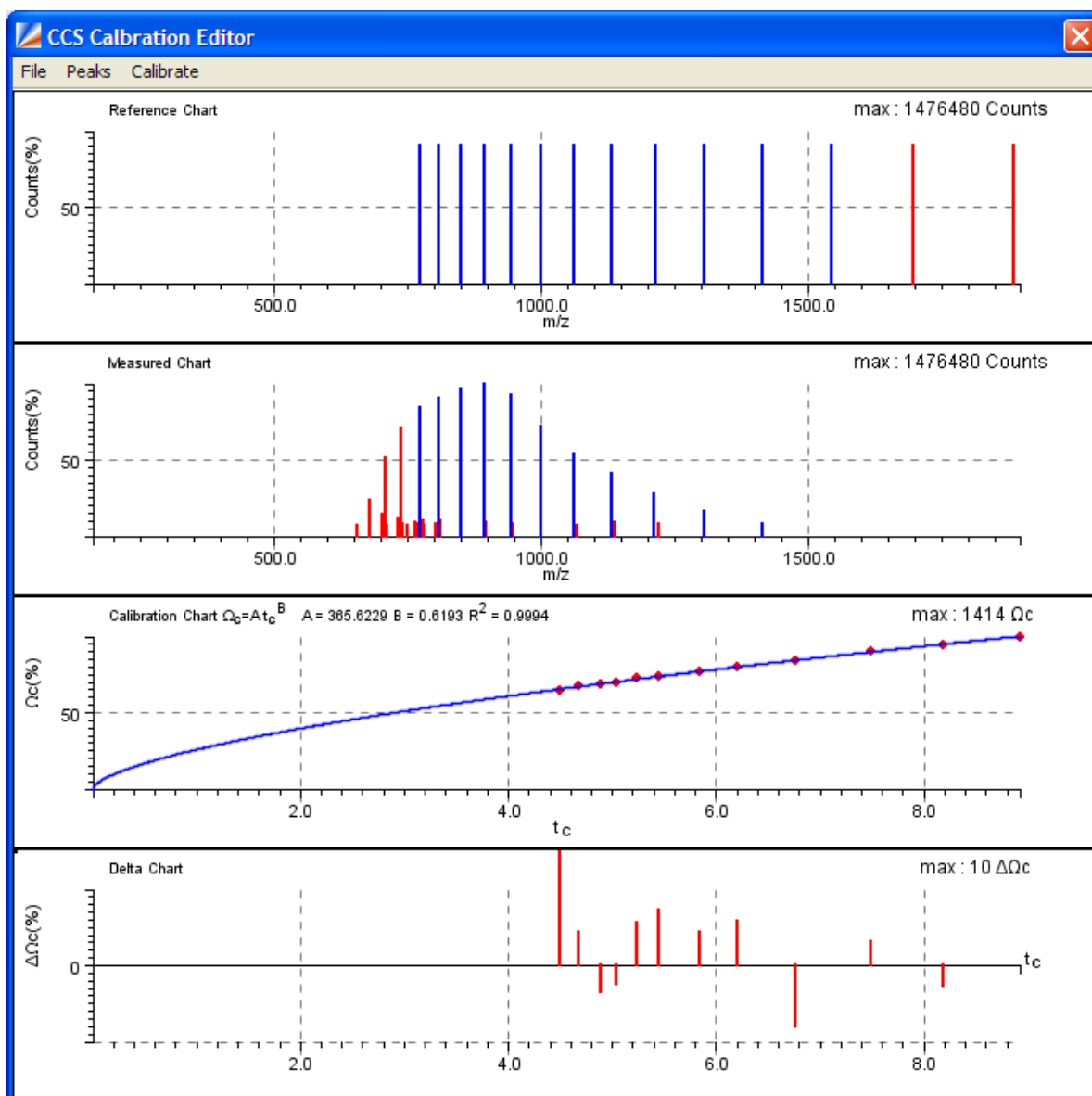
Figure 5-4. Illustration of drift-time calibration in Waters Driftscope software. Top pane shows reference chart with previously measured eCCS. Second pane shows measured CCS. Third pane shows calibration curve. Bottom pane shows the residuals highlighting the difference between the calibration curve and the raw datapoints.

The calibration procedure, as carried out in Waters Driftscope software or manually[55,56], is as follows:

1. Acquire IM-MS data for the calibrants under exactly the same conditions, especially the wave height and speed, voltage and pressure settings to maintain the separation, as used for the analyte data.

$$t'_D = t_D - \frac{c\sqrt{m/z}}{1000}$$

where t_D' is the corrected drift time in ms, t_D is the experimental drift time in ms, m/z is the mass to charge ratio for the ion and c is the enhanced duty cycle delay co-efficient constant (found under System, Settings, Acquisition Settings, Acquisition Setup for Waters Synapt instruments).

2. Correct each of the calibrant eCCS for charge state and reduced mass:

$$\Omega_C = \frac{\Omega}{z \sqrt{\dfrac{1}{m_{ion}} + \dfrac{1}{m_{gas}}}}$$

where Ω_C is the corrected eCCS, Ω is the literature eCCS,[34,48,49] z is the charge state of the observed ion, m_{ion} is the mass of the measured ion, m_{gas} is the mass of the IMS drift gas.

3. Plot $\ln(t_D')$ against $\ln(\Omega_C)$

4. Fit the plot to a linear relationship of the form $\ln(\Omega_C) = X \ln(t_D') + \ln A$ where X is found from the slope and A from the y intercept. The correlation co-efficient of fit (R^2) should be > 0.98.[55]

5. Correct the calibrant drift-time using the exponential factor, X as determined above.

$$t_D'' = z * t_D^X * \sqrt{\frac{1}{m_{ion}} + \frac{1}{m_{gas}}}$$

The correlation co-efficient of fit (R^2) should be > 0.98.[55]

6. Replot Ω_C against t_D'' to validate the results. The correlation co-efficient of fit (R^2) should be > 0.98.

7. Calculate the analyte drift-time using the expression:

$$t_D'' = t_D^X + z \sqrt{\frac{1}{m_{ion}} + \frac{1}{m_{gas}}}$$

8. Calculate Ω of the target analyte using the fit-determined constant $\Omega = At_D''$

5.1.4 What kind of useful information is made available using molecular modelling?

Molecular modelling for small molecule ions in the gas-phase suited to IM-MS has predominantly been performed using *ab initio*, semi-empirical or molecular dynamics methods. There is a growing field of publications that deal with isolated protonated small molecules in the gas phase, their geometries, thermodynamics and physiochemical properties, especially useful for IM-MS studies.

Molecular modelling can provide several useful types of information:

1) *Geometries* – the physical shape and size of ions that may help understand collisional effects and bond dissociation

2) *Partial atomic charges* – the distribution of charge on each atom that may help understand bond dissociation and induced dipole effects, especially in more polarisable gases like $CO_{2(g)}$ and $N_{2(g)}$ compared to a less polarisable gas like $He_{(g)}$.

3) *Thermodynamic stability* – the energy of an ion may be calculated and a rank order of relative energies generated, or the proton affinity may be calculated.

There are a number of software packages that are available that can help visualise or perform the functions above, and many more related functions, as shown in Table 5-2.

Table 5-2. Example molecular modelling software.

Name of software package	Typical primary function(s)	License
Avogadro[57]	Molecular mechanics, input file generation	Free/GNU Free DOC License
Gabedit[58]	Input file generation, visualisation of results	Free
Gaussview[59]	Input file generation, visualisation of results	Academic/Commercial
Gaussian[60]	Molecular mechanics, semi-empirical, *ab initio*	Academic/Commercial
GAMESS[61]	Molecular mechanics, semi-empirical, *ab initio*	Free
Spartan[62,63]	Molecular mechanics, semi-empirical, *ab initio*	Academic/Commercial

Some approaches to generate geometries and charge distributions for small molecule structures have explored the use of rapid, relatively computationally inexpensive techniques, such as MMFF94 or SYBYL molecular mechanics.[4,41,64,65] The popular MMFF94 force field has been parameterised based, partly, on studies of over 700 organic molecules[66] using higher levels of computational theory, and for analytes with limited molecular and conformational flexibility this approach may provide reasonably accurate geometries[66] but can give unrealistic energies and perform poorly for conformationally flexible molecules.

For geometry optimisation[67] of small molecules higher levels of computational theory, such as those used in this protocol *e.g.* density functional theory B3LYP methods, in combination with hybrid orbital basis sets such as 6-31G+(d,p) typically give more accurate geometries and energies.[68] Good numerical agreement with experimentally determined heats of formation can be achieved using higher levels of computational theory, which can then be used to determine the thermodynamically most stable protonated ion(s), and those that are relatively un-favoured. This capability is in contrast to existing large biomolecule IM-MS approaches where the complexities of biomolecule systems often require approximations to be made using approaches such as molecular mechanics, an approach that often provides inaccurate heats of formation[69]. Computational studies have also correlated protonation-induced bond elongation with bond cleavages in CID[9–11,70] so this may provide an additional benefit requiring little additional effort to inform both drift-time and fragmentation interpretation.

Partial atomic charges derived from gas-phase wavefunctions are typically calculated post-self-consistent field (SCF) calculations so do not alter the geometry of the analyte. Partial atomic charges describe the charge distribution on the ion, which may have important effects on ion mobility due to electrostatic interactions with the buffer gas, as shown in the separation of betamethasone and dexamethasone diastereomers,[34] and for proposed charge location isomers.[21,38,40,71–74] Mulliken partial atomic charges are most common partial atomic charge types in molecular modelling programs but are heavily dependent on the level of computational theory, especially the basis set, and values calculated with higher basis sets often give increasingly unrealistic values. The Merz-Singh-Kollman (MK) scheme[75,76] used in this protocol derives charges from a least squares fit to the electrostatic potential calculated to a large number of points, with a density of 1 point/Å on a Connolly surface for the analyte. However, one of the known limitations of the MK scheme is that charges for 'buried' atoms

(*e.g.* sp^3 carbons) are not well determined[77] so partial atomic charge assignment can be strongly dependent on the conformation.

5.1.5 How are tCCSs typically calculated?

The most widely used software packages are Waters Driftscope (Waters Corp., Manchester) and MOBCAL[78,79], typically in the original He$_{(g)}$ parameterised form. Waters Driftscope includes a highly optimised, rapid P.A. calculation tool that accepts the common '.PDB' 3D co-ordinate input, rather than the '.MFJ' input for MOBCAL. Waters Driftscope has the advantage of being highly integrated into Waters software and relatively simple to use to calculate the tCCS in He$_{(g)}$; however, Waters Driftscope lacks the flexibility of being finely tuneable to other gases[80] and omits the E.H.S.S. and T.M. calculation methods. In contrast MOBCAL is freely available and has been modified from its original form to calculate tCCSs in He$_{(g)}$, N$_{2(g)}$[34] and CO$_{2(g)}$[81] ion mobility gases and additionally calculates tCCS using E.H.S.S. and T.M. methods.

There are a number of calculation methods for tCCSs which are available in a number of software packages, see Table 5-3.

Table 5-3. Software available for calculating tCCS values.

Name of program	Calculation methods	Source
Waters Driftscope	Projection approximation	Available from Waters Corp.
He$_{(g)}$ parameterised MOBCAL[78,79]	1. Projection approximation 2. Exact hard sphere scattering 3. Trajectory Method	Prof. Jarrold http://www.indiana.edu/~nano/software.html
N$_{2(g)}$ parameterised MOBCAL[34]	Trajectory Method only	Request from author Iain Campuzano, iainc@amgen.com
Sigma	1. Hard sphere mode 2. Lennard-Jones mode 3. Ion size scaled Lennard-Jones mode.	http://bowers.chem.ucsb.edu/theory_analysis/cross-sections/index.shtml
IMoS Suite	1. Projection approximation 2. Trajectory Method 3. Diffuse Hard Sphere Scattering 4. Diffuse Trajectory Method	Request from author Carlos Larriba-Andaluz clarriba@umn.edu

The three calculation methods available in MOBCAL are:

1) *projection approximation (P.A.)* – the ion is modelled as a collection of overlapping hard spheres. All possible collision geometries are averaged to give an orientationally-averaged geometric cross-section.

2) *exact hard sphere scattering (E.H.S.S.)* – the ion is modelled by a collection of overlapping hard spheres. The momentum transfer cross-section is calculated by determining scattering angles between the incoming buffer gas and the departing buffer gas trajectory.

3) *trajectory method (T.M.)* – the ion is modelled as collection of atoms with their own 12-6-4 Lennard-Jones potential[82]. The effective ion potential is obtained by summing over individual atomic contributions, the scattering angles are obtained and an average collision integral determined by averaging over all collision geometries.

The trajectory method (T.M.) used in this protocol provides the most comprehensive treatment of the physical processes in ion mobility occurring as collisions; short and long-range interactions are all considered[78,79]. However, T.M. methods rely on a 12-6-4 Lennard-Jones potential[82] as approximations of the interactions between analytes and the buffer gas (typically nitrogen gas ($N_{2(g)}$) or helium gas ($He_{(g)}$). While the Lennard-Jones potential is commonly used in computing electrostatic interactions it also suffers from a number of limitations, including regarding the energy potential as spherically symmetrical, and has been criticised for not modelling interactions between charged particles well.[83] The projection approximation (P.A.) methods, by comparison, appear relatively simplistic and can be conceived as using the shadow presented by an average of all orientations for the analyte. So, whilst trajectory methods are undoubtedly more rigorous, errors from poor parameterisation and approximations may, in fact, reduce the agreement between eCCS and tCCS values using more complex treatments such as T.M..

5.1.6 What limitations are there in current approaches?

There are important limitations on which elements may be modelled in MOBCAL without modification (see Table 5-4); notably the Group I and Group II metals are missing and parameterisation of some halogens may be non-ideal since they may not be verified experimentally by appropriate model compounds. In some cases atoms with elements that

have not been parameterised can be substituted[84] with Si parameters but this is not ideal, and is arguably best validated by experiment.

Table 5-4. Main features of available MOBCAL codes.

Software name	Elements supported	Source
$He_{(g)}$ parameterised mobcal	H, C, N, O, Na, Si, S, Fe	http://www.indiana.edu/~nano/software.html
$N_{2(g)}$ parameterised mobcal	H, C, N, O, Na, Si, S, Fe, P, F, Cl, I, Br	iain.campuzano@amgen.com

The conformational landscape of fairly rigid small molecules may be reasonably described by conformer searching using molecular mechanics and energy minimisation/geometry optimisation using density functional theory, however for more flexible molecules molecular dynamics or a wider sampling of potential conformers may be more appropriate for determining an ensemble of populated conformers.[85–87]

How are instrument conditions modified for optimum separation and to obtain mass spectrometry data?

There have been reports of activation through RF heating at increasing wave heights and/or decreasing IMS cell pressure,[88,89] therefore it may be useful for cases where isomerisation is suspected that wave height is maintained below 35 V and IMS cell pressure is maintained at the standard pressure (~2.5 mbar) to minimise any heating effects.

5.2 MATERIALS

REAGENTS	EQUIPMENT
• Ar $_{(g)}$ (pureshield) • N_2 $_{(g)}$ ($\geqslant$ 99.9995%, vol/vol)	**Hardware requirements for collection of IM-MS data** IM-mass spectrometer (*e.g.*, Synapt G2 HDMS, Q-IM-o-ToF, Waters) **Software requirements for processing of IM-MS software** Waters MassLynx, Waters Driftscope or equivalent **Hardware requirements for calculations** A computer with at least 2 GB RAM and a dual-core processor is able to perform the

	necessary conformational searches and geometry optimisation. Use of a high performance computing cluster will reduce the timing estimates for many of the steps in the procedure. For more complex molecules access to more computing resources would reduce the timing estimates. A typical consumer PC is capable of executing multimobcal and file conversion and visualisation in Chemcraft. **Software requirements for molecular modelling, tCCS calculations and file conversion** • Avogadro software, http://avogadro.cc/ (open-source and free) • Gaussian software, http://www.gaussian.com/ (commercial and academic) • MOBCAL software, Jarrold Group, http://www.indiana.edu/~nano/Software.html (free) • Command Prompt in Microsoft Windows (free) • Gaussview 5 or equivalent (commercial and academic) • Chemcraft (commercial and academic) • Microsoft Excel or equivalent spreadsheet application

5.3 PROCEDURE

Ondansetron is recommended as a test compound; it is a serotonin 5-HT3 antagonist,[90] which as a protonated molecule contains forty-two atoms and has two rotatable bonds thus has limited conformational flexibility. This protocol for ondansetron provides a worked example that allows a novice user to familiarise themselves with the protocol and the tools required. A solution of ondansetron should be prepared to a concentration of approximately 0.1 mg/mL.

Compile MOBCAL source code to generate mobcal.exe ● TIMING 5 min

1. Edit the mobcal.f file for $He_{(g)}$ parameterised MOBCAL[91] and change line 267 to imp=1000, as recommended where only one structure exists, so that resulting typical standard deviations are typically 1% or less for $He_{(g)}$ parameterised MOBCAL.

2. Compile the mobcal.f file for He$_{(g)}$ MOBCAL and N$_{2(g)}$ MOBCAL using Force 2.09 by choosing File, Open then Run, Compile to produce an executable file. This executable file is created in the same directory as the mobcal.f source file.

▲ CRITICAL STEP Care should be taken to compile and optimise code as compilers can give differing results. A Fortran compiler is required to convert the MOBCAL source file into an executable program. Several Fortran compilers are available from free to commercial options. Fortran has been released in various versions the accompanying mobcal.txt states that '*Fortran 77 retains numbers in subroutines and functions while the newer compilers usually do not*'. The Force 2.0.9 IDE plus GNU Fortran 77 (G77)[92] delivers a graphical user interface to examine and modify the code and a built-in compiler to produce the executable and gives the expected result (a101.out) from the test a101.mfj file[91] using the He$_{(g)}$ parameterised MOBCAL so is recommended.

■ PAUSE POINT The compiled mobcal.exe may be reused for all subsequent calculations unless optimisations to the compilation or changes in the code are desired.

Create an input geometry and carry out a conformational search using molecular mechanics in Avogadro ● TIMING 2 - 60 min

3. Import a three-dimensional structure into, or create/edit using built-in tools in, Avogadro[57].

4. Add hydrogen atoms to each proposed protonation site and conduct conformer searching using Extensions, Molecular Mechanics, Conformer Search to generate lowest energy conformer(s) using an appropriate molecular forcefield *e.g.* MMFF94. A systematic rotor search will typically provide the most comprehensive, but tractable, search of conformational space. Go to View, Properties and Conformer Properties to view the resultant conformers and their respective energies by selecting appropriate rows. It is possible to sort the conformers based on their energies. It may be required to select and energy minimise a representative proportion of conformers to maximise chances of obtaining a representative low energy conformer. Save the resulting conformer(s) by selecting the appropriate row then choosing File, Save As and selecting the option for PDB (*.PDB) for the Protein Databank Format.

■ PAUSE POINT The '.PDB' files from Avogadro can be accessed at any time after conformational searching is complete.

Carry out geometry optimisation using Gaussian and Gaussview ● TIMING 1 h – 7 days

5. Open the PDB file and select the Job Type, Method, Title, Link 0 and General options to conduct geometry optimisation on the lowest energy conformer(s) from Avogadro with Additional Keywords *pop=(mk,dipole)* to calculate Merz-Kollman electrostatic potential partial atomic charges for all protonation sites. Calculations may be conducted individually or in batches, in serial or in parallel. There is discussion of the different options available for calculations on the Gaussian website http://www.gaussian.com/g_tech/g_ur/g09help.htm.

■ PAUSE POINT The '.LOG' or '.OUT' files from Gaussview can be accessed at any time after geometry optimisation is complete.

Convert Gaussian output file to tCCS calculation input file (MFJ) for MOBCAL ● TIMING 5 min

6. Convert from Gaussian output file to MOBCAL input file (MFJ) using Chemcraft[93] software choosing to save with Merz-Kollman electrostatic potential charges.

■ PAUSE POINT The '.MFJ' files from Chemcraft can be accessed at any time after file conversion is complete.

Calculate the lowest energy structures ● TIMING 10 min

7. The total energy for the structure calculated using Gaussian can be found in the Gaussian output file by searching for the last text string "SCF Done:". Using a spreadsheet application such as Microsoft Excel calculate the minimum energy and the difference in energy (relative energy) for each candidate structure.

▲ CRITICAL STEP When multiple structures are found that are energetically similar these may be worth retaining and calculating tCCS. For structures that are not energetically favourable these may rejected, thus saving tCCS calculation time.

Calculate tCCS with MOBCAL ● TIMING 6 h - 1 day

8. Move all the desired '.MFJ' files to a directory that also contains the multimobcal file. Execute MOBCAL calculations using MultiMOBCAL.

If multiple protonation sites are possible, or indeed different isomers are being evaluated, there may be a number of MFJ input files to be run. It is therefore useful to automate the running of MOBCAL so that calculations can be left unattended to run several MFJ files, and to run calculations in parallel. The Windows command shell script (MultiMOBCAL) requires no installation and can run on versions of Microsoft Windows including XP, Vista, Windows 7, 8 and 10.

Acquisition of IM drift times ● TIMING 1.5 h

9. Carry out data acquisition of analytes before calibrating eCCS. Experimental conditions that are appropriate starting conditions for small molecule IM-MS are shown Table 5.5 and some troubleshooting steps in Table 5-6.

▲ CRITICAL STEP Altering voltages that affect the recorded drift time (*i.e.*, any element of the IM separation stage or post-IM stage) between calibration runs and measurements of unknowns can cause significant errors in eCCS measurements. Ensure that the same experimental conditions are utilised for both the calibrant and analyte data acquisition. It is recommended that the instrument is switched into ion mobility mode (Go to MassLynx, Instrument, MS Tune, Acq, Mobility TOF) for at least 1 h before measurements are made to ensure gas pressures and electronics have settled for the most reproducible results. It is recommended that analyte data are collected before calibrating eCCS as calibration data acquired first can be invalidated by subsequent changes to instrument conditions to optimise a separation. Conversely it is relatively difficult to choose separation conditions for analytes that exclude the possibility of subsequently acquiring valid eCCS calibration data

Table 5-5. Approximate instrument conditions for Waters Synapt G2 for analyzing small molecule structures (adapted from reference 55).

Pressure		
Region	**Value (mbar)**	**Comment**
Backing	2.0	
Trap	$2.0e^{-2}$	Using $Ar_{(g)}$.
IMS	2.5	Using $N_{2(g)}$.
Transfer	$2.0e^{-4}$	
Voltage		
Region	**Value**	**Comment**
Trap collision energy	0-50 eV	This value may be increased to generate product ions and measure their CCSs.
Transfer collision energy	0-50 eV	This value may be increased to i) generate product ions from precursor

		drift-time selected ion or ii) generate second generation product ions for further structural information.
Bias voltage	30-55 V	Low voltage generally transmits ions intact but can result in poor sensitivity whereas high voltage increases transmission but can also increase activation/fragmentation.
Cone voltage	20-80 V	Low voltage generally transmits ions intact whereas high voltage increases transmission but can also increase activation/fragmentation.
Extractor cone voltage	0.3-10 V	
Capillary voltage	1000-3000 V	Higher capillary voltages are often suitable for lower flow rates (<0.1ml/min) and vice versa.
IM parameters	**Value**	
Wave Velocity	400-1000 (m/s)	Wave velocity can be changed to improve a separation.
Wave Height	20-40 (V)	Wave height has been postulated to increase energy transmitted to ion and induce RF heating so should be minimised where possible.

Calibration of travelling wave IM drift times ● TIMING 10 min

10. Select a desired calibration set, typically from either poly-(L/D)-alanine[48,53] or a drug-like compound series[34] .

11. Prepare calibrant solutions. For poly-(L/D)-alanine dilute in acetonitrile:water (50:50, v/v) to an approximate concentration of 2 mg/mL. For drug-like compound series dilute in 50% acetonitrile/50% water and formic acid (0.1% v/v) to an approximate concentration of 0.1 mg/mL.

  Start from the standard settings given in Table 5-5 for IM separation voltages. These settings gave separation of all ions in the drug-like calibrant series so should be sufficient for initial conditions for many analytes in this mass range.

12. Acquire a complete calibration set and carry out the calibration procedure in Driftscope.

Table 5-6. Troubleshooting guide for ion mobility experiments (adapted from reference 55).

Problem	Possible reason(s)	Solution(s)
MOBCAL stops before calculation ends.	Input file is formatted incorrectly or contains values that are outside acceptable boundaries.	Verify values and formatting in the input file. Carefully check the format of the file against the example provided in the MOBCAL download.[91]
The same *m/z* is observed at the start and the end of the ion mobilogram in the tune view.	A 'roll-over' effect can occur when the time taken for ions to traverse the ion mobility cell is slower than the interval between the injections of new ion packets into the device.	This effect can be eliminated by increasing the IMS wave height, and decreasing wave velocity and IMS pressure.
Artificial 'ripples' of anomalously high resolution present in the ion mobilogram.	The Transfer wave velocity and pusher frequency are partially synchronised.	Adjust either the pusher frequency or transfer wave velocity. The optimum wave velocity is typically $1/6^{th}$ of the pusher period of the ToF.
Cannot separate components.	IMS wave height/wave velocity set incorrectly.	For larger ions better separation is often achieved at higher wave heights and lower wave velocities
	Transfer wave set incorrectly.	The wave height/velocity must be set so that ions are carried along with each wave.
	IMS pressure set incorrectly.	Increase pressure to increase separation of components, balancing separation of components with loss of transmission.
Poor sensitivity in mobility mode compared to TOF mode.	Voltages are set incorrectly for optimum transmission.	Reduce trap bias to reduce activation/fragmentation. Increase trap bias to increase transmission. The trap entrance, trap exit, IMS entance, IMS exit and Transfer entrance may also be tuned for maximum sensitivity in mobility mode.

5.4 ANTICIPATED RESULTS

There are four protonation sites for the example molecule onadansetron (structure shown in Figure 5-5) and the tCCSs for the lowest energy structures for each protonation site and relative energies are shown Table 5-7. The difference after following this protocol between

the eCCS and the tCCS for the most energetically favourable protonation site is 1.8%, which is in good agreement with previous results[4].
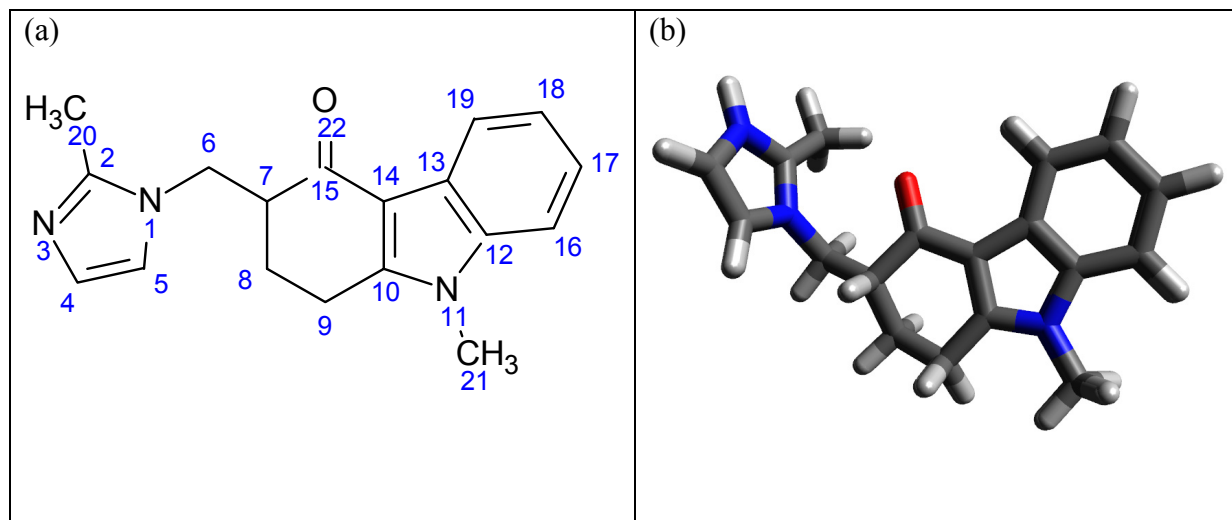
Figure 5-5. (a) Scheme for ondansetron and (b) the lowest energy protonated molecule structure.

Table 5-7. Relative energies and tCCSs for protonated molecules of ondansetron.

	tCCS ($Å^2$)	eCCS ($Å^2$)	Energy (H)	Relative energy (kcal/mol)
Experimental		106.5		
N3	108.4		-937.325947136	0.00
O22	109.6		-937.287900263	23.87
N11	100.0		-937.245699978	50.36
N1	109.3		-937.245041678	50.77

Comparing P.A. results with T.M. results can help differentiate contributions from the geometry or partial atomic charges. P.A. tCCS values are calculated from the average orientation based on a collection of hard spheres there is no contribution to drift-time from partial atomic charges. In contrast the T.M. tCCS values are calculated taking into account partial atomic charges and this method correctly predicts different eCCSs for norfloxacin and benzocaine ions[40] that give similar tCCS values from P.A.[36]

Good agreement between eCCS and tCCS for the calculation methods P.A., E.H.S.S. and T.M. may be specific to particular types of geometry or classes of compound. In this study on

a number of pharmaceutically relevant molecules there was a good correlation between the eCCS and tCCS using T.M. with an $R^2 > 0.99$ and agreement between experimental and tCCS could be obtained within 3% of eCCS for 90% of compounds with a correction factor) and 45% without a correction factor. Other studies have reported good correlations between eCCS and tCCS with E.H.S.S[31] and P.A. calculation methods[94] which have the advantage of far shorter calculation times compared to T.M..

5.5 REFERENCES

1. Di Girolamo, F., Lante, I., Muraca, M. & Putignani, L. The Role of Mass Spectrometry in the 'Omics' Era. *Curr. Org. Chem.* **17,** 2891–2905 (2013).

2. McLean, J. A. The mass-mobility correlation redux: the conformational landscape of anhydrous biomolecules. *J. Am. Soc. Mass Spectrom.* **20,** 1775–1781 (2009).

3. Cuyckens, F., Wassvik, C., Mortishire-Smith, R. J., Tresadern, G., Campuzano, I. & Claereboudt, J. Product ion mobility as a promising tool for assignment of positional isomers of drug metabolites. *Rapid Commun. Mass Spectrom.* **25,** 3497–3503 (2011).

4. Dear, G. J., Munoz-Muriedas, J., Beaumont, C., Roberts, A., Kirk, J., Williams, J. P. & Campuzano, I. Sites of metabolic substitution: investigating metabolite structures utilising ion mobility and molecular modelling. *Rapid Commun. Mass Spectrom.* **24,** 3157–3162 (2010).

5. Lanucara, F., Holman, S. W., Gray, C. J. & Eyers, C. E. The power of ion mobility-mass spectrometry for structural characterization and the study of conformational dynamics. *Nat. Chem.* **6,** 281–294 (2014).

6. Lapthorn, C., Pullen, F. & Chowdhry, B. Z. Ion mobility spectrometry-mass spectrometry (IMS-MS) of small molecules: Separating and assigning structures to ions. *Mass Spectrom. Rev.* **32,** 43–71 (2013).

7. Brancia, F. L., Stener, M. & Magistrato, A. A Density Functional Theory (DFT) Study on Gas-Phase Proton Transfer Reactions of Derivatized and Underivatized Peptide Ions

Generated by Matrix-Assisted Laser Desorption Ionization. *J. Am. Soc. Mass Spectrom.* **20,** 1327–1333 (2009).

8. Alex, A., Harvey, S., Parsons, T., Pullen, F. S., Wright, P. & Riley, J. Can density functional theory (DFT) be used as an aid to a deeper understanding of tandem mass spectrometric fragmentation pathways? *Rapid Commun. Mass Spectrom.* **23,** 2619–2627 (2009).

9. Wright, P., Alex, A., Nyaruwata, T., Parsons, T. & Pullen, F. Using density functional theory to rationalise the mass spectral fragmentation of maraviroc and its metabolites. *Rapid Commun. Mass Spectrom.* **24,** 1025–1031 (2010).

10. Wright, P., Alex, A., Harvey, S., Parsons, T. & Pullen, F. Understanding collision-induced dissociation of dofetilide: a case study in the application of density functional theory as an aid to mass spectral interpretation. *Analyst* **138,** 6869–6880 (2013).

11. Galezowska, A., Harrison, M. W., Herniman, J. M., Skylaris, C.-K. & Langley, G. J. A predictive science approach to aid understanding of electrospray ionisation tandem mass spectrometric fragmentation pathways of small molecules using density functional calculations. *Rapid Commun. Mass Spectrom.* **27,** 964–970 (2013).

12. Tuytten, R., Lemière, F., Van Dongen, W., Esmans, E. L., Witters, E., Herrebout, W., Van Der Veken, B., Dudley, E. & Newton, R. P. Intriguing Mass Spectrometric Behavior of Guanosine Under Low Energy Collision-Induced Dissociation: H2O Adduct Formation and Gas-Phase Reactions in the Collision Cell. *J. Am. Soc. Mass Spectrom.* **16,** 1291–1304 (2005).

13. Moore, G. E. Cramming More Components Onto Integrated Circuits. *Proc. IEEE* **86,** 82–85 (1998).

14. Canterbury, J. D., Yi, X., Hoopmann, M. R. & MacCoss, M. J. Assessing the Dynamic Range and Peak Capacity of Nanoflow LC−FAIMS−MS on an Ion Trap Mass Spectrometer for Proteomics. *Anal. Chem.* **80,** 6888–6897 (2008).

15. Wren, S. A. C. Peak capacity in gradient ultra performance liquid chromatography (UPLC). *J. Pharm. Biomed. Anal.* **38,** 337–343 (2005).

16. Bellina, B., Brown, J. M., Ujma, J., Murray, P., Giles, K., Morris, M., Compagnon, I. & Barran, P. E. UV photodissociation of trapped ions following ion mobility separation in a Q-ToF mass spectrometer. *Analyst* **139,** 6348–6351 (2014).

17. Zucker, S. M., Lee, S., Webber, N., Valentine, S. J., Reilly, J. P. & Clemmer, D. E. An Ion Mobility/Ion Trap/Photodissociation Instrument for Characterization of Ion Structure. *J. Am. Soc. Mass Spectrom.* **22,** 1477–1485 (2011).

18. Baer, T. & Dunbar, R. C. Ion Spectroscopy: Where Did It Come From; Where Is It Now; and Where Is It Going? *J. Am. Soc. Mass Spectrom.* **21,** 681–693 (2010).

19. Stearns, J. A., Guidi, M., Boyarkin, O. V. & Rizzo, T. R. Conformation-specific infrared and ultraviolet spectroscopy of tyrosine-based protonated dipeptides. *J. Chem. Phys.* **127,** 154322 (2007).

20. Oomens, J., Moore, D. T., von Helden, G., Meijer, G. & Dunbar, R. C. The Site of Cr+ Attachment to Gas-Phase Aniline from Infrared Spectroscopy. *J. Am. Chem. Soc.* **126,** 724–725 (2003).

21. Schmidt, J., Meyer, M. M., Spector, I. & Kass, S. R. Infrared Multiphoton Dissociation Spectroscopy Study of Protonated *p* -Aminobenzoic Acid: Does Electrospray Ionization Afford the Amino- or Carboxy-Protonated Ion? *J. Phys. Chem. A* **115,** 7625–7632 (2011).

22. Kurulugama, R. T., Darland, E., Kuhlmann, F., Stafford, G. & Fjeldsted, J. Evaluation of drift gas selection in complex sample analyses using a high performance drift tube ion mobility-QTOF mass spectrometer. *Analyst* **140,** 6834–6844 (2015).

23. D'Atri, V., Porrini, M., Rosu, F. & Gabelica, V. Linking molecular models with ion mobility experiments. Illustration with a rigid nucleic acid structure. *J. Mass Spectrom.* **50,** 711–726 (2015).

24. Belov, M. E., Buschbach, M. A., Prior, D. C., Tang, K. & Smith, R. D. Multiplexed Ion Mobility Spectrometry-Orthogonal Time-of-Flight Mass Spectrometry. *Anal. Chem.* **79,** 2451–2462 (2007).

25. May, J. C., Goodwin, C. R., Lareau, N. M., Leaptrot, K. L., Morris, C. B., Kurulugama, R. T., Mordehai, A., Klein, C., Barry, W., Darland, E., Overney, G., Imatani, K., Stafford, G. C., Fjeldsted, J. C. & McLean, J. A. Conformational Ordering of Biomolecules in the Gas Phase: Nitrogen Collision Cross Sections Measured on a Prototype High Resolution Drift Tube Ion Mobility-Mass Spectrometer. *Anal. Chem.* **86,** 2107–2116 (2014).

26. May, J. C., Dodds, J. N., Kurulugama, R. T., Stafford, G. C., Fjeldsted, J. C. & McLean, J. A. Broadscale resolving power performance of a high precision uniform field ion mobility-mass spectrometer. *Analyst* **140,** 6824–6833 (2015).

27. Fernandez-Lima, F., Kaplan, D. A., Suetering, J. & Park, M. A. Gas-phase separation using a trapped ion mobility spectrometer. *Int. J. Ion Mobil. Spectrom.* **14,** 93–98 (2011).

28. Fernandez-Lima, F. A., Wei, H., Gao, Y. Q. & Russell, D. H. On the Structure Elucidation Using Ion Mobility Spectrometry and Molecular Dynamics. *J. Phys. Chem. A* **113,** 8221–8234 (2009).

29. Wyttenbach, T., Pierson, N. A., Clemmer, D. E. & Bowers, M. T. Ion Mobility Analysis of Molecular Dynamics. *Annu. Rev. Phys. Chem.* **65,** 175–196 (2014).

30. Morsa, D., Defize, T., Dehareng, D., Jérôme, C. & De Pauw, E. Polymer Topology Revealed by Ion Mobility Coupled with Mass Spectrometry. *Anal. Chem.* **86,** 9693–9700 (2014).

31. Fasciotti, M., Lalli, P. M., Heerdt, G., Steffen, R. A., Corilo, Y. E., Sá, G. F. de, Daroda, R. J., Reis, F. de A. M., Morgon, N. H., Pereira, R. C. L., Eberlin, M. N. & Klitzke, C. F. Structure-drift time relationships in ion mobility mass spectrometry. *Int. J. Ion Mobil. Spectrom.* **16,** 117–132 (2013).

32. Lalli, P. M., Corilo, Y. E., Rowland, S. M., Marshall, A. G. & Rodgers, R. P. Isomeric Separation and Structural Characterization of Acids in Petroleum by Ion Mobility Mass Spectrometry. *Energy Fuels* **29,** 3626–3633 (2015).

33. Benigni, P., Marin, R. & Fernandez-Lima, F. Towards unsupervised polyaromatic hydrocarbons structural assignment from SA-TIMS –FTMS data. *Int. J. Ion Mobil. Spectrom.* **18,** 151–157 (2015).

34. Campuzano, I., Bush, M. F., Robinson, C. V., Beaumont, C., Richardson, K., Kim, H. & Kim, H. I. Structural Characterization of Drug-like Compounds by Ion Mobility Mass Spectrometry: Comparison of Theoretical and Experimentally Derived Nitrogen Collision Cross Sections. *Anal. Chem.* **84,** 1026–1033 (2012).

35. Thevis, M., Dib, J., Thomas, A., Höppner, S., Lagojda, A., Kuehne, D., Sander, M., Opfermann, G. & Schänzer, W. Complementing the characterization of in vivo generated N-glucuronic acid conjugates of stanozolol by collision cross section computation and analysis. *Drug Test. Anal.* **7,** 1050–1056 (2015).

36. Lapthorn, C., Dines, T. J., Chowdhry, B. Z., Perkins, G. L. & Pullen, F. S. Can ion mobility mass spectrometry and density functional theory help elucidate protonation sites in 'small' molecules? *Rapid Commun. Mass Spectrom.* **27,** 2399–2410 (2013).

37. Lapthorn, C., Pullen, F. S., Chowdhry, B. Z., Wright, P., Perkins, G. L. & Heredia, Y. How useful is molecular modelling in combination with ion mobility mass spectrometry for 'small molecule' ion mobility collision cross-sections? *Analyst* **140,** 6814–6823 (2015).

38. Lalli, P. M., Iglesias, B. A., Toma, H. E., de Sa, G. F., Daroda, R. J., Silva Filho, J. C., Szulejko, J. E., Araki, K. & Eberlin, M. N. Protomers: formation, separation and characterization via travelling wave ion mobility mass spectrometry. *J. Mass Spectrom.* **47,** 712–719 (2012).

39. Kaufmann, A., Butcher, P., Maden, K., Widmer, M., Giles, K. & Uría, D. Are liquid chromatography/electrospray tandem quadrupole fragmentation ratios unequivocal confirmation criteria? *Rapid Commun. Mass Spectrom.* **23,** 985–998 (2009).

40. Warnke, S., Seo, J., Boschmans, J., Sobott, F., Scrivens, J. H., Bleiholder, C., Bowers, M. T., Gewinner, S., Schöllkopf, W., Pagel, K. & von Helden, G. Protomers of Benzocaine: Solvent and Permittivity Dependence. *J. Am. Chem. Soc.* **137,** 4236–4242 (2015).

41. Shimizu, A. & Chiba, M. Ion Mobility Spectrometry–Mass Spectrometry Analysis for the Site of Aromatic Hydroxylation. *Drug Metab. Dispos.* **41,** 1295–1299 (2013).

42. Williams, J. P., Bugarcic, T., Habtemariam, A., Giles, K., Campuzano, I., Rodger, P. M. & Sadler, P. J. Isomer Separation and Gas-Phase Configurations of Organoruthenium Anticancer Complexes: Ion Mobility Mass Spectrometry and Modeling. *J. Am. Soc. Mass Spectrom.* **20,** 1119–1122 (2009).

43. Williams, J. P., Lough, J. A., Campuzano, I., Richardson, K. & Sadler, P. J. Use of ion mobility mass spectrometry and a collision cross-section algorithm to study an organometallic ruthenium anticancer complex and its adducts with a DNA oligonucleotide. *Rapid Commun. Mass Spectrom.* **23,** 3563–3569 (2009).

44. Mason, E. A. & McDaniel, E. W. *Transport Properties of Ions in Gases*. (Wiley-VCH Verlag GmbH & Co. KGaA, 1988). at <http://onlinelibrary.wiley.com/book/10.1002/3527602852>

45. Shvartsburg, A. A. & Smith, R. D. Fundamentals of Traveling Wave Ion Mobility Spectrometry. *Anal. Chem.* **80,** 9689–9699 (2008).

46. Gelb, A. S., Jarratt, R. E., Huang, Y. & Dodds, E. D. A Study of Calibrant Selection in Measurement of Carbohydrate and Peptide Ion-Neutral Collision Cross Sections by Traveling Wave Ion Mobility Spectrometry. *Anal. Chem.* **86,** 11396–11402 (2014).

47. Cross Section Database - Peptides - Miscellaneous. at <http://www.indiana.edu/~clemmer/Research/Cross%20Section%20Database/Peptides/polyaminoacid_cs.htm>

48. Clemmer Group: Cross Section Database. at <http://www.indiana.edu/~clemmer/Research/Cross%20Section%20Database/cs_database.php>

49. Collision Cross Section Database | Bush Lab. at <http://depts.washington.edu/bushlab/ccsdatabase/>

50. McLean Group - CCS Database. at <http://www.vanderbilt.edu/AnS/Chemistry/groups/mcleanlab/ccs.html>

51. Traditional Herbal Medicine Structural Elucidation using SYNAPT HDMS with Time-Aligned Parallel (TAP) Fragmentation - 720002542en.pdf. at <http://www.waters.com/webassets/cms/library/docs/720002542en.pdf>

52. Blech, S. & Laux, R. Resolving the microcosmos of complex samples: UPLC/travelling wave ion mobility separation high resolution mass spectrometry for the analysis of in vivo drug metabolism studies. *Int. J. Ion Mobil. Spectrom.* **16,** 5–17 (2012).

53. Bush, M. F., Campuzano, I. D. G. & Robinson, C. V. Ion Mobility Mass Spectrometry of Peptide Ions: Effects of Drift Gas and Calibration Strategies. *Anal. Chem.* **84,** 7124–7130 (2012).

54. Thalassinos, K., Grabenauer, M., Slade, S. E., Hilton, G. R., Bowers, M. T. & Scrivens, J. H. Characterization of Phosphorylated Peptides Using Traveling Wave-Based and Drift Cell Ion Mobility Mass Spectrometry. *Anal. Chem.* **81,** 248–254 (2009).

55. Ruotolo, B. T., Benesch, J. L. P., Sandercock, A. M., Hyung, S.-J. & Robinson, C. V. Ion mobility–mass spectrometry analysis of large protein complexes. *Nat. Protoc.* **3,** 1139–1152 (2008).

56. Michaelevski, I., Kirshenbaum, N. & Sharon, M. T-wave Ion Mobility-mass Spectrometry: Basic Experimental Procedures for Protein Complex Analysis. *J. Vis. Exp.* (2010). doi:10.3791/1985

57. Hanwell, M. D., Curtis, D. E., Lonie, D. C., Vandermeersch, T., Zurek, E. & Hutchison, G. R. Avogadro: an advanced semantic chemical editor, visualization, and analysis platform. *J. Cheminformatics* **4,** 17 (2012).

58. Allouche, A.-R. Gabedit—A graphical user interface for computational chemistry softwares. *J. Comput. Chem.* **32,** 174–182 (2011).

59. Dennington, R., Keith, T. & Millam, J. *GaussView.* (2009).

60. Frisch, M. J., Trucks, G. W., Schlegel, H. B., Scuseria, G. E., Robb, M. A., Cheeseman, J. R., Scalmani, G., Barone, V., Mennucci, B., Petersson, G. A., Nakatsuji, H., Caricato, M., Li, X., Hratchian, H. P., Izmaylov, A. F., Bloino, J., Zheng, G., Sonnenberg, J. L., Hada, M., Ehara, M., Toyota, K., Fukuda, R., Hasegawa, J., Ishida, M., Nakajima, T., Honda, Y., Kitao, O., Nakai, H., Vreven, T., Montgomery Jr., J. A., Peralta, J. E., Ogliaro, F., Bearpark, M. J., Heyd, J., Brothers, E. N., Kudin, K. N., Staroverov, V. N., Kobayashi, R., Normand, J., Raghavachari, K., Rendell, A. P., Burant, J. C., Iyengar, S. S., Tomasi, J., Cossi, M., Rega, N., Millam, N. J., Klene, M., Knox, J. E., Cross, J. B., Bakken, V., Adamo, C., Jaramillo, J., Gomperts, R., Stratmann, R. E., Yazyev, O., Austin, A. J., Cammi, R., Pomelli, C., Ochterski, J. W., Martin, R. L., Morokuma, K., Zakrzewski, V. G., Voth, G. A., Salvador, P., Dannenberg, J. J., Dapprich, S., Daniels, A. D., Farkas, Ö., Foresman, J. B., Ortiz, J. V., Cioslowski, J. & Fox, D. J. *Gaussian 09.* (Gaussian, Inc., 2009).

61. Schmidt, M. W., Baldridge, K. K., Boatz, J. A., Elbert, S. T., Gordon, M. S., Jensen, J. H., Koseki, S., Matsunaga, N., Nguyen, K. A., Su, S., Windus, T. L., Dupuis, M. & Montgomery Jr, J. A. General atomic and molecular electronic structure system. *J. Comput. Chem.* **14,** 1347–1363 (1993).

62. Shao, Y., Molnar, L. F., Jung, Y., Kussmann, J., Ochsenfeld, C., Brown, S. T., Gilbert, A. T. B., Slipchenko, L. V., Levchenko, S. V., O'Neill, D. P., DiStasio Jr, R. A., Lochan, R. C., Wang, T., Beran, G. J. O., Besley, N. A., Herbert, J. M., Lin, C. Y., Voorhis, T. V., Chien, S. H., Sodt, A., Steele, R. P., Rassolov, V. A., Maslen, P. E., Korambath, P. P., Adamson, R. D., Austin, B., Baker, J., Byrd, E. F. C., Dachsel, H., Doerksen, R. J., Dreuw, A., Dunietz, B. D., Dutoi, A. D., Furlani, T. R., Gwaltney, S. R., Heyden, A., Hirata, S., Hsu, C.-P., Kedziora, G., Khalliulin, R. Z., Klunzinger, P., Lee, A. M., Lee, M. S., Liang, W., Lotan, I., Nair, N., Peters, B., Proynov, E. I., Pieniazek, P. A., Rhee, Y. M., Ritchie, J., Rosta, E., Sherrill, C. D., Simmonett, A. C., Subotnik, J. E., Iii, H. L. W., Zhang, W., Bell, A. T., Chakraborty, A. K., Chipman, D. M., Keil, F. J., Warshel, A., Hehre, W. J., Iii, H. F. S., Kong, J., Krylov, A. I., Gill, P. M. W. & Head-Gordon, M. Advances in methods and algorithms in a modern quantum chemistry program package. *Phys. Chem. Chem. Phys.* **8,** 3172–3191 (2006).

63. Kong, J., White, C. A., Krylov, A. I., Sherrill, D., Adamson, R. D., Furlani, T. R., Lee, M. S., Lee, A. M., Gwaltney, S. R., Adams, T. R., Ochsenfeld, C., Gilbert, A. T. B., Kedziora, G. S., Rassolov, V. A., Maurice, D. R., Nair, N., Shao, Y., Besley, N. A., Maslen, P. E., Dombroski, J. P., Daschel, H., Zhang, W., Korambath, P. P., Baker, J., Byrd, E. F. C., Van Voorhis, T., Oumi, M., Hirata, S., Hsu, C.-P., Ishikawa, N., Florian, J., Warshel, A., Johnson, B. G., Gill, P. M. W., Head–Gordon, M. & Pople, J. A. Q-Chem 2.0: a high-performance ab initio electronic structure program package. *J. Comput. Chem.* **21,** 1532–1548 (2000).

64. Shimizu, A., Ohe, T. & Chiba, M. A Novel Method for the Determination of the Site of Glucuronidation by Ion Mobility Spectrometry-Mass Spectrometry. *Drug Metab. Dispos.* **40,** 1456–1459 (2012).

65. Chan, E. C. Y., New, L. S., Yap, C. W. & Goh, L. T. Pharmaceutical metabolite profiling using quadrupole/ion mobility spectrometry/time-of-flight mass spectrometry. *Rapid Commun. Mass Spectrom.* **23,** 384–394 (2009).

66. Halgren, T. A. Merck molecular force field. I. Basis, form, scope, parameterization, and performance of MMFF94. *J. Comput. Chem.* **17,** 490–519 (1996).

67. Schlegel, H. B. Optimization of equilibrium geometries and transition structures. *J. Comput. Chem.* **3,** 214–218 (1982).

68. Butler, K. T., Luque, F. J. & Barril, X. Toward accurate relative energy predictions of the bioactive conformation of drugs. *J. Comput. Chem.* **30,** 601–610 (2009).

69. *Energetics of Stable Molecules and Reactive Intermediates*. (Springer Netherlands, 1999). at <http://link.springer.com/10.1007/978-94-011-4671-5>

70. Wright, P., Alex, A. & Pullen, F. Predicting collision-induced dissociation spectra: semi-empirical calculations as a rapid and effective tool in software-aided mass spectral interpretation. *Rapid Commun. Mass Spectrom.* **28,** 1127–1143 (2014).

71. Lalli, P. M., Corilo, Y. E., Fasciotti, M., Riccio, M. F., de Sa, G. F., Daroda, R. J., Souza, G. H. M. F., McCullagh, M., Bartberger, M. D., Eberlin, M. N. & Campuzano, I. D. G. Baseline resolution of isomers by traveling wave ion mobility mass spectrometry: investigating the effects of polarizable drift gases and ionic charge distribution. *J. Mass Spectrom.* **48,** 989–997 (2013).

72. Kovačević, B., Schorr, P., Qi, Y. & Volmer, D. A. Decay Mechanisms of Protonated 4-Quinolone Antibiotics After Electrospray Ionization and Ion Activation. *J. Am. Soc. Mass Spectrom.* **25,** 1974–1986 (2014).

73. Benassi, M., Corilo, Y. E., Uria, D., Augusti, R. & Eberlin, M. N. Recognition and Resolution of Isomeric Alkyl Anilines by Mass Spectrometry. *J. Am. Soc. Mass Spectrom.* **20,** 269–277 (2009).

74. Karpas, Z., Berant, Z. & Stimac, R. M. An ion mobility spectrometry/mass spectrometry (IMS/MS) study of the site of protonation in anilines. *Struct. Chem.* **1,** 201–204 (1990).

75. Bayly, C. I., Cieplak, P., Cornell, W. & Kollman, P. A. A well-behaved electrostatic potential based method using charge restraints for deriving atomic charges: the RESP model. *J. Phys. Chem.* **97,** 10269–10280 (1993).

76. Chirlian, L. E. & Francl, M. M. Atomic charges derived from electrostatic potentials: A detailed study. *J. Comput. Chem.* **8,** 894–905 (1987).

77. Sigfridsson, E. & Ryde, U. Comparison of methods for deriving atomic charges from the electrostatic potential and moments. *J. Comput. Chem.* **19,** 377–395 (1998).

78. Shvartsburg, A. A. & Jarrold, M. F. An exact hard-spheres scattering model for the mobilities of polyatomic ions. *Chem. Phys. Lett.* **261,** 86–91 (1996).

79. Mesleh, M. F., Hunter, J. M., Shvartsburg, A. A., Schatz, G. C. & Jarrold, M. F. Structural Information from Ion Mobility Measurements: Effects of the Long-Range Potential. *J. Phys. Chem.* **100,** 16082–16086 (1996).

80. Siu, C.-K., Guo, Y., Saminathan, I. S., Hopkinson, A. C. & Siu, K. W. M. Optimization of parameters used in algorithms of ion-mobility calculation for conformational analyses. *J. Phys. Chem. B* **114,** 1204–1212 (2010).

81. Bataglion, G. A., Souza, G. H. M. F., Heerdt, G., Morgon, N. H., Dutra, J. D. L., Freire, R. O., Eberlin, M. N. & Tata, A. Separation of glycosidic catiomers by TWIM-MS using CO2 as a drift gas. *J. Mass Spectrom.* **50,** 336–343 (2015).

82. Jones, J. E. On the Determination of Molecular Fields. II. From the Equation of State of a Gas. *Proc. R. Soc. Lond. Ser. A* **106,** 463–477 (1924).

83. Cherkaoui, M. & Capolungo, L. *Atomistic and Continuum Modeling of Nanocrystalline Materials*. **112,** (Springer US, 2009).

84. Faull, P. A., Korkeila, K. E., Kalapothakis, J. M., Gray, A., McCullough, B. J. & Barran, P. E. Gas-phase metalloprotein complexes interrogated by ion mobility-mass spectrometry. *Int. J. Mass Spectrom.* **283,** 140–148 (2009).

85. Zakharova, N. L., Crawford, C. L., Hauck, B. C., Quinton, J. K., Seims, W. F., Jr, H. H. H. & Clark, A. E. An Assessment of Computational Methods for Obtaining Structural Information of Moderately Flexible Biomolecules from Ion Mobility Spectrometry. *J. Am. Soc. Mass Spectrom.* **23,** 792–805 (2012).

86. Forsythe, J. G., Stow, S. M., Nefzger, H., Kwiecien, N. W., May, J. C., McLean, J. A. & Hercules, D. M. Structural Characterization of Methylenedianiline Regioisomers by Ion Mobility-Mass Spectrometry, Tandem Mass Spectrometry, and Computational Strategies: I. Electrospray Spectra of 2-Ring Isomers. *Anal. Chem.* **86,** 4362–4370 (2014).

87. Stow, S. M., Goodwin, C. R., Kliman, M., Bachmann, B. O., McLean, J. A. & Lybrand, T. P. Distance Geometry Protocol to Generate Conformations of Natural Products to Structurally Interpret Ion Mobility-Mass Spectrometry Collision Cross Sections. *J. Phys. Chem. B* **118,** 13812–13820 (2014).

88. Morsa, D., Gabelica, V. & Pauw, E. D. Fragmentation and Isomerization Due to Field Heating in Traveling Wave Ion Mobility Spectrometry. *J. Am. Soc. Mass Spectrom.* **25,** 1384–1393 (2014).

89. Merenbloom, S. I., Flick, T. G. & Williams, E. R. How Hot are Your Ions in TWAVE Ion Mobility Spectrometry? *J. Am. Soc. Mass Spectrom.* **23,** 553–562 (2012).

90. Ye, J.-H., Ponnudurai, R. & Schaefer, R. Ondansetron: A Selective 5-HT3 Receptor Antagonist and Its Applications in CNS-Related Disorders. *CNS Drug Rev.* **7,** 199–213 (2001).

91. Martin Jarrold Research Group. at <http://www.indiana.edu/~nano/software.html>

92. Download | Force Fortran - The Force Project. at <http://force.lepsch.com/p/download.html>

93. Chemcraft - Download. at <http://www.chemcraftprog.com/download.html>

94. Troć, A., Zimnicka, M. & Danikiewicz, W. Separation of catechin epimers by complexation using ion mobility mass spectrometry. *J. Mass Spectrom.* **50,** 542–548 (2015).

Chapter 6: Overall conclusions and further work

6.1 OVERALL CONCLUSIONS

In an initial study ion mobility mass spectrometry was used to separate at least two apparent components in the ion mobility separation of ions consistent with the protonated molecule of norfloxacin (m/z 320). The tandem mass spectra showed distinct and mutually exclusive losses of -18 m/z units (-H_2O) and -44 m/z units (-CO_2) for ion mobility separated components. Modelling ion mobility CCSs using the popular projection approximation method appears insufficient to differentiate between candidate structures based on their predicted CCSs (**see Chapter 2**). These results have important implications for the use of tandem mass spectrometry for quantitation of small molecules where multiple protonation sites exist since the results suggest a mass spectrum may be a composite of more than one fragmentation pathway derived from different charge location isomers and prone to variation depending on experimental conditions. A further study was undertaken to measure the drift-times of potential charge location isomers in different drift gases, using both DT-IMS and TWIMS regimes, and comparing experimental with predicted CCSs from molecular modelling (**Chapter 3**). The separation of components consistent with the protonated molecules of fluoroquinolones was noticeably better in the more polarisable gas N_2 than He. More sophisticated modelling, using the relatively computationally expensive trajectory method, shows little difference in geometry but significant differences in charge distribution between charge location isomers resulting in significant difference in predicted CCSs. The calculated experimental CCSs were consistent within 3% for the DT-IMS and TWIMS measurements, which is within typical experimental error. The predicted CCSs were also typically within 6% of the experimental CCS and correctly predicted the rank order of elution in the ion mobility dimension. Together these results are consistent with the hypothesis of charge location isomers for the fluoroquinolones studied. The fluoroquinolone class of compounds, including norfloxacin, are a particularly useful model since they are easily available and relatively rigid molecules, with a number of related structural analogues useful for investigations.

A further study presented in this research project tested current state-of-the-art approaches using molecular mechanics to search for conformers and density functional theory to energy minimise the geometry and derive relative energies (see **Chapter 4)**. The CCS was then

predicted using the original and modified version of the MOBCAL program for a relatively wide range of drug-like structures (n=20). The results for this study demonstrate that with a simple linear correction ~90% of predicted CCSs are within 3% of their experimentally calculated values, which is close to reported experimental error This benchmark result enables an assessment of the utility of predicted CCSs and whether they can be used to make assignments based on experimental data, and serves as a foundation on which to seek improvements and understand the benefits and drawbacks of using CCS data for structural assignments. Current gold standards for assigning positional isomers include nuclear magnetic resonance (NMR) spectroscopy, which is often limited in terms of sensitivity. It is conceivable that CCSs may be calculated from experimental measurements or predicted for common substructures and enable confirmation of positional isomers where mass spectrometry alone cannot discern between candidates. This confirmatory step eliminates the need for synthesis or purification of positional isomers to generate sufficient material for NMR measurements and, when the substructure CCS is known, it enables a high-throughput confirmation on the same timescales as mass spectrometry workflows (including liquid or gas chromatography).

Some software code, named MultiMOBCAL, has been developed for release to the scientific community during this study, and is capable of significantly increasing the throughput of MOBCAL calculations. MultiMOBCAL is particularly useful for 'small molecules', since it enables many CCS calculations to be queued and processed unattended (see **Chapter 5**). The code acts as a framework around the MOBCAL program (and published modifications) to carry out CCS calculations, so changes can still be made to introduce and tune atomic interaction potentials, or compare CCSs to previous studies. The release of software to the scientific community assists in accelerating current research efforts and demonstrates that automation and investigation of larger datasets may prove beneficial in future research. One instance of MultiMOBCAL is capable of running calculations ~3-12 times faster than current manual workflows, and several instances spread over a multi-processor server or several workstations could increase throughput by over 100 times.

6.2 FUTURE RESEARCH

This research project has demonstrated that there is room for improvement in our understanding of ion mobility separations for 'small molecules'. While computational chemistry approaches are increasingly used to interpret the outcome of experimental studies there is room for refinement of both modelling and workflows to tackle common analytical challenges in timeframes that are useful for academic research and commercial activities. Future work to identify model chemical standards for ion mobility would help probe ion mobility behaviour and molecular modelling and reduce ambiguity due to approximations and uncertainties in molecular modelling approaches. Fairly rigid structures with well-defined charge locations, e.g. supra-molecular assemblies, could help tune interaction potentials and understand long-range and short-range effects for a variety of ion mobility conditions including different gases, temperatures, pressures etc.

The future development of complementary hyphenated techniques, particularly spectroscopic techniques, could help further inform both mass spectrometry and computational chemistry. For example, infra-red and ultraviolet spectroscopy approaches in IMS/TOF mass spectrometers appear ideally suited to studying the conformation and activating ions to obtain diagnostic product ions (fragments) that are not produced by widely available activation techniques. The structure of gas-phase ions can be elucidated by comparing the experimental UV/IR spectrum with the predicted spectrum from molecular modelling. It has been demonstrated that ion mobility can be added to mass spectrometry systems while maintaining robust operation and has been well adopted by the mass spectrometry community, both academic and commercial. The addition of tunable laser sources and optical detectors to mass spectrometer systems appears a viable next step with significant benefits to the scientific community.

Overall, future work should recognise that a multi-disciplinary approach incorporating ion mobility, mass spectrometry, computational approaches and gas-phase spectroscopies provides a virtuous circle to obtain and interpret rich data, with increasing confidence, about gas-phase ion structures.

APPENDICES

APPENDIX A: SUPPLEMENTARY DATA FOR CHAPTER 3

Geometry optimized structures obtained for norfloxacin, ciprofloxacin and enrofloxacin

Norfloxacin	
O18	N1
N4	N14
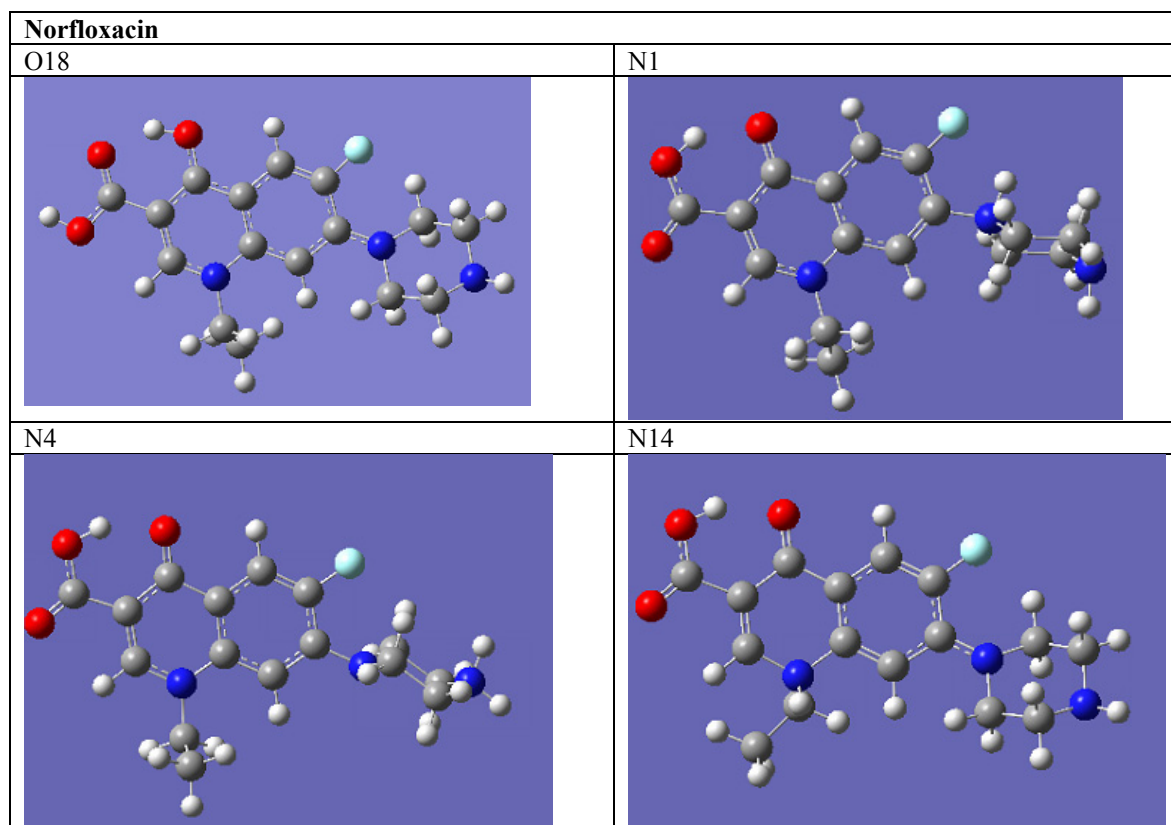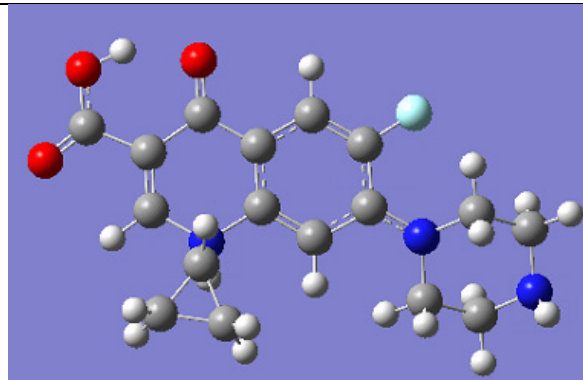
Ciprofloxacin

N1	O16
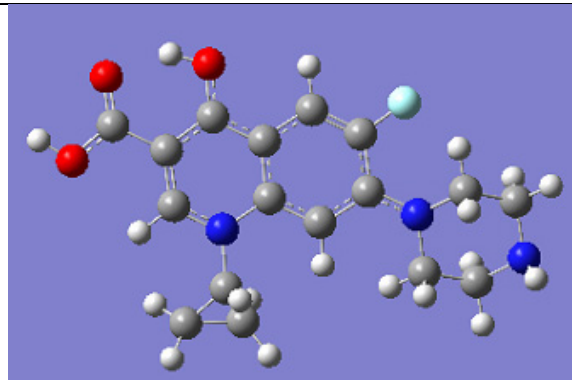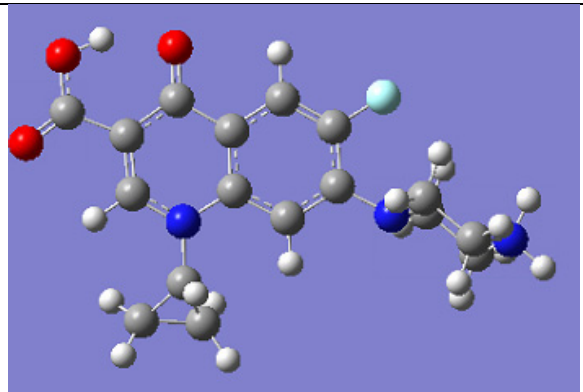
N20	N17
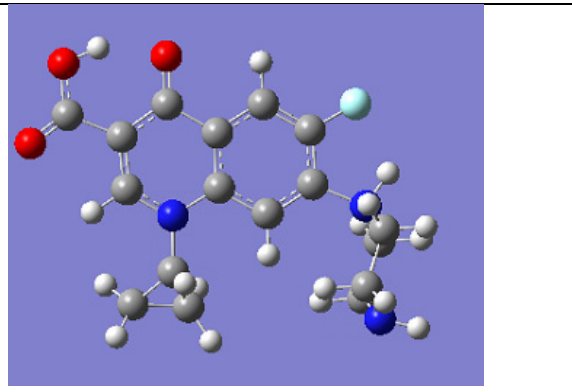
Enrofloxacin
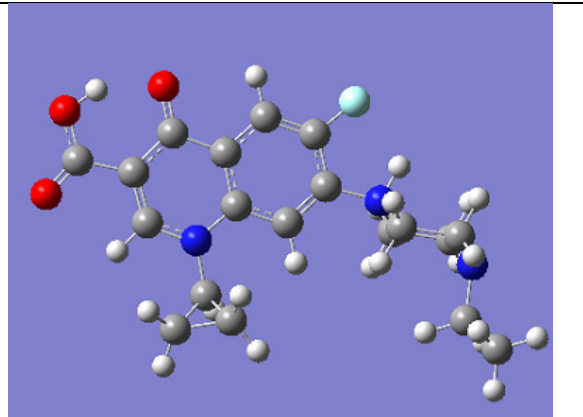
N4	O26
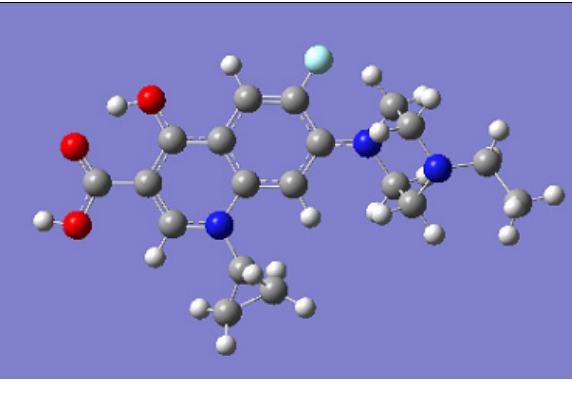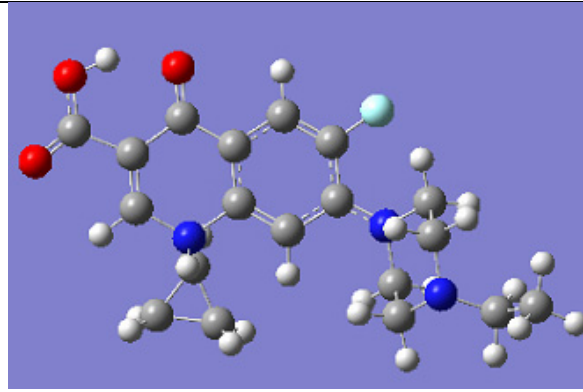
N16	N1
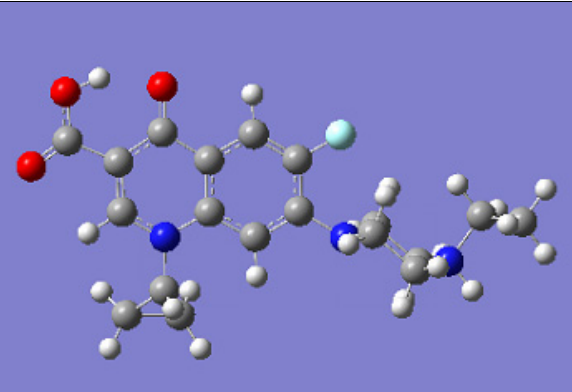
Linear Drift Tube He/N₂ comparison for MS/MS of ciprofloxacin (top = He, middle = N₂ peak 1, bottom = N₂ peak 2)
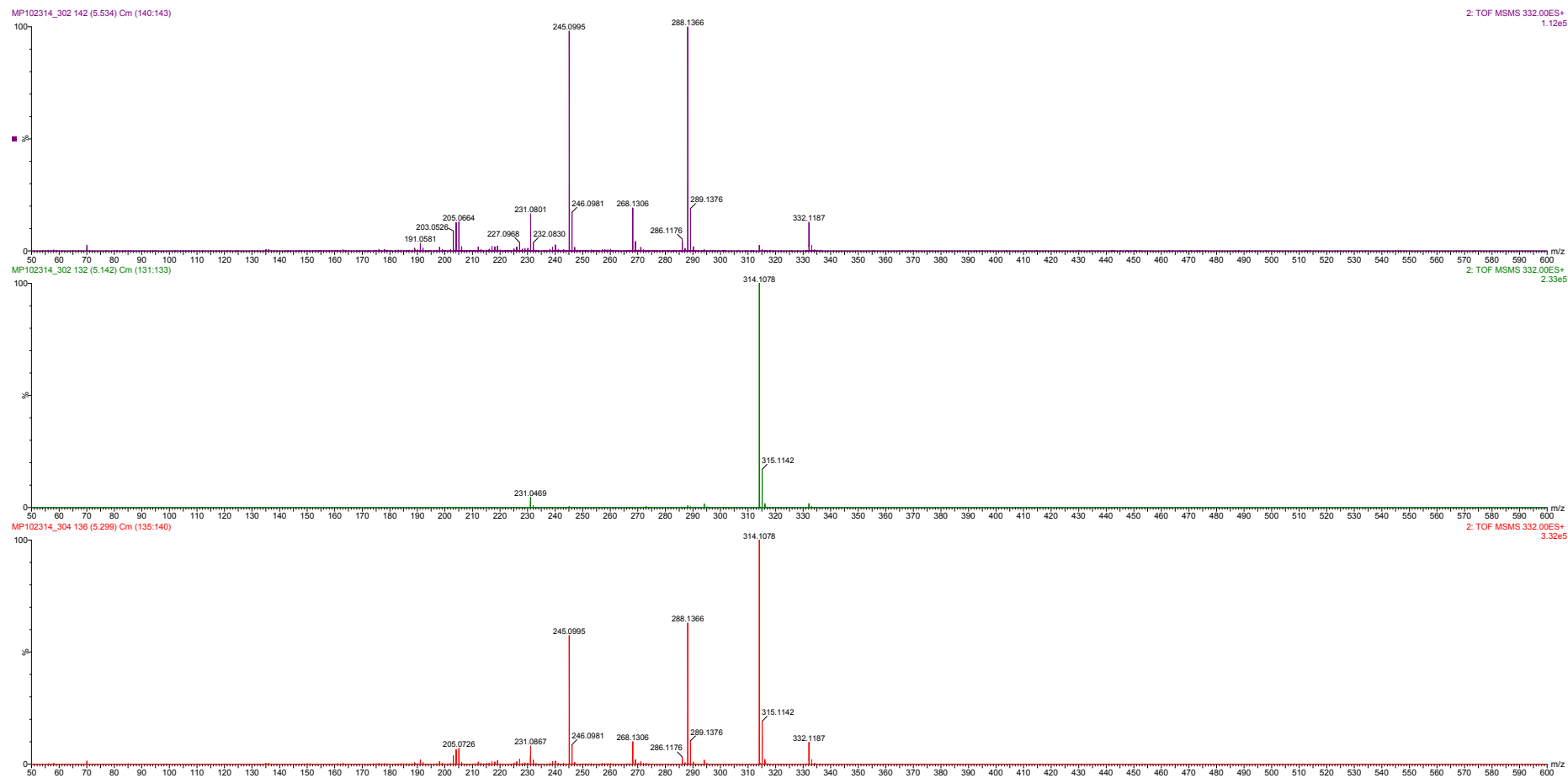
Linear Drift Tube He/N₂ comparison for MS/MS of norfloxacin (top = He, middle = N₂ peak 1, bottom = N₂ peak 2)
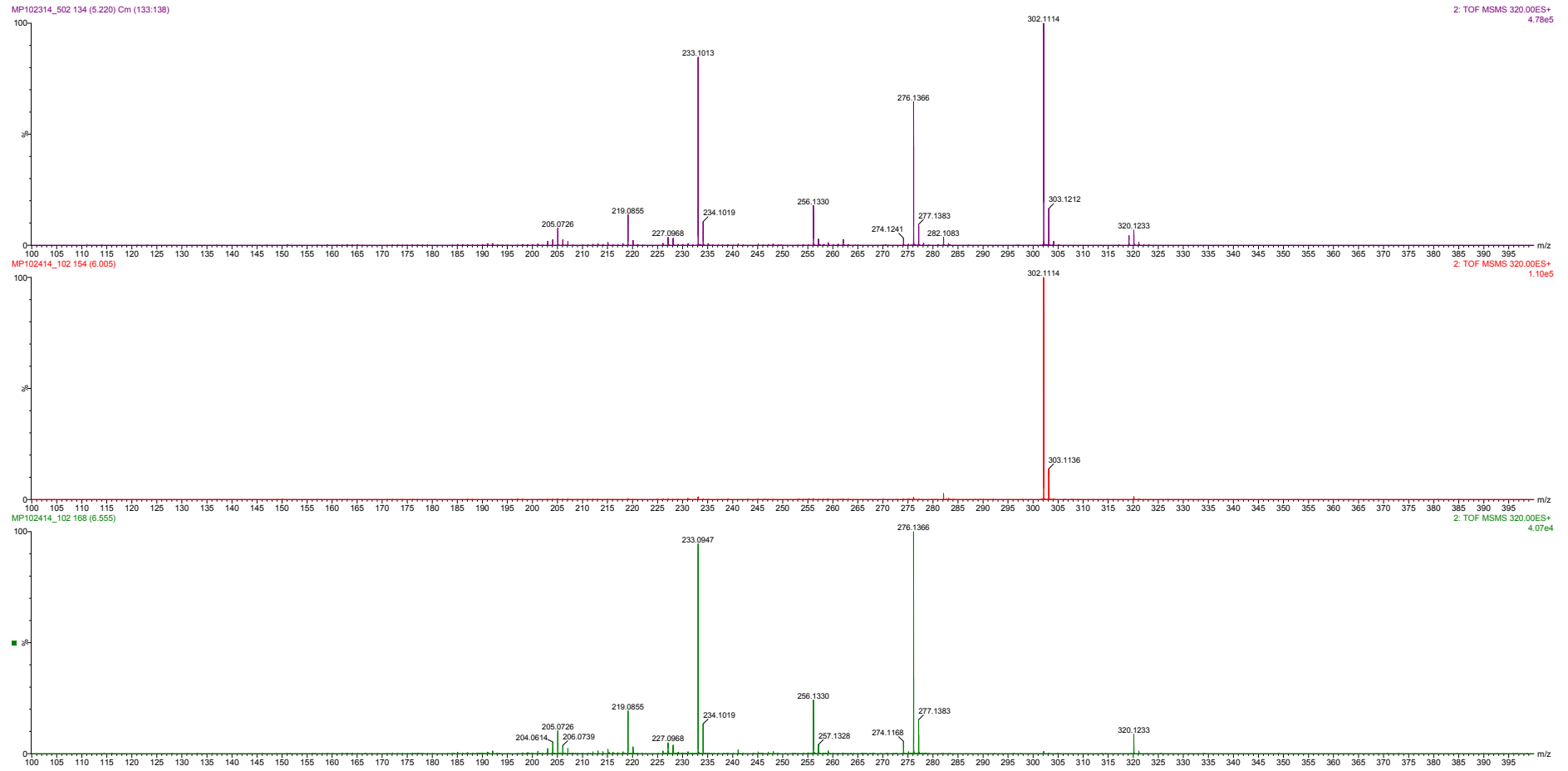
Linear Drift Tube He/N₂ comparison for MS/MS of enrofloxacin (top = He, middle = N₂ peak 1, bottom = N₂ peak 2)
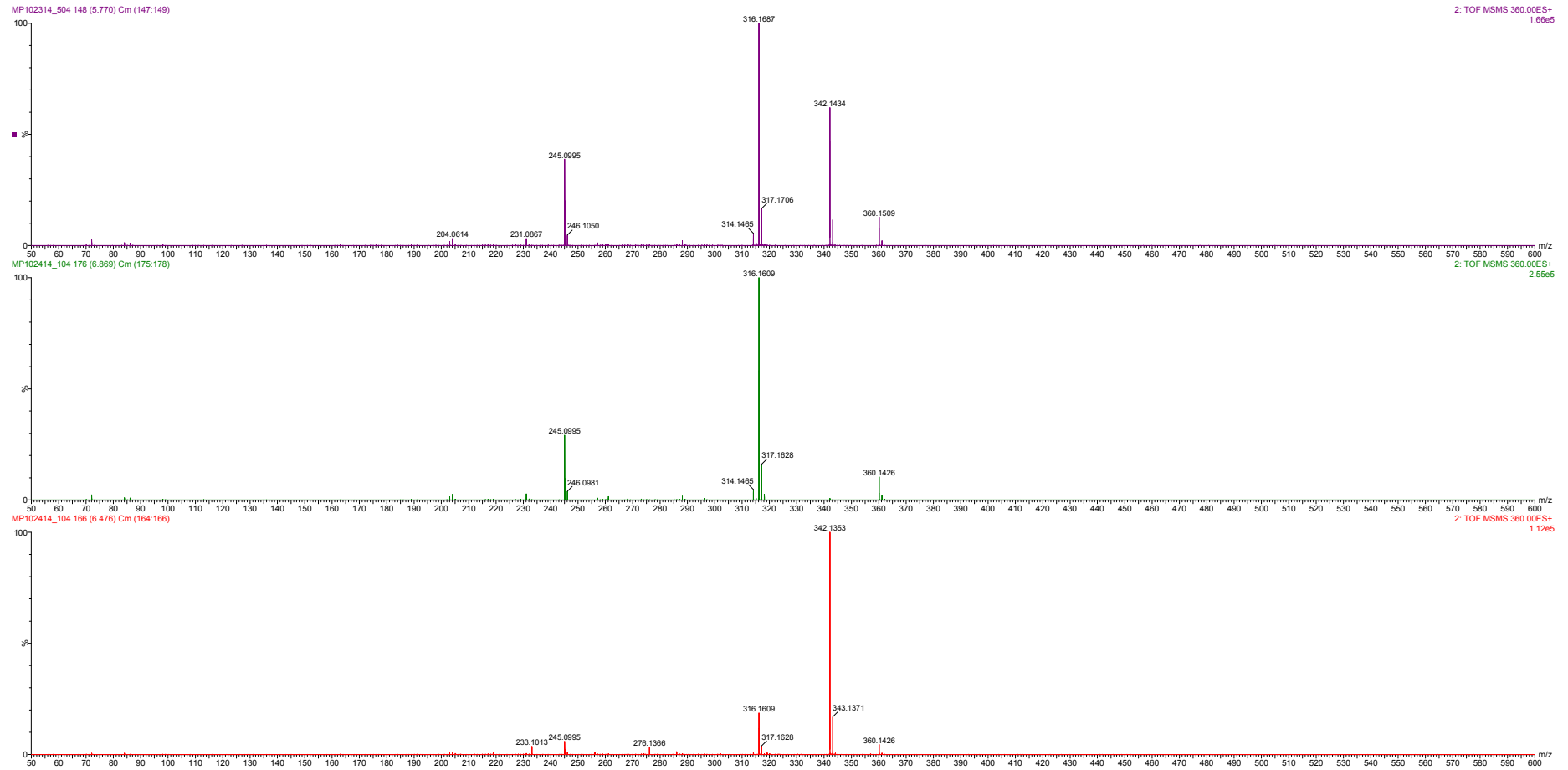
Extracted ion mobilograms for ciprofloxacin product ions in He(g)
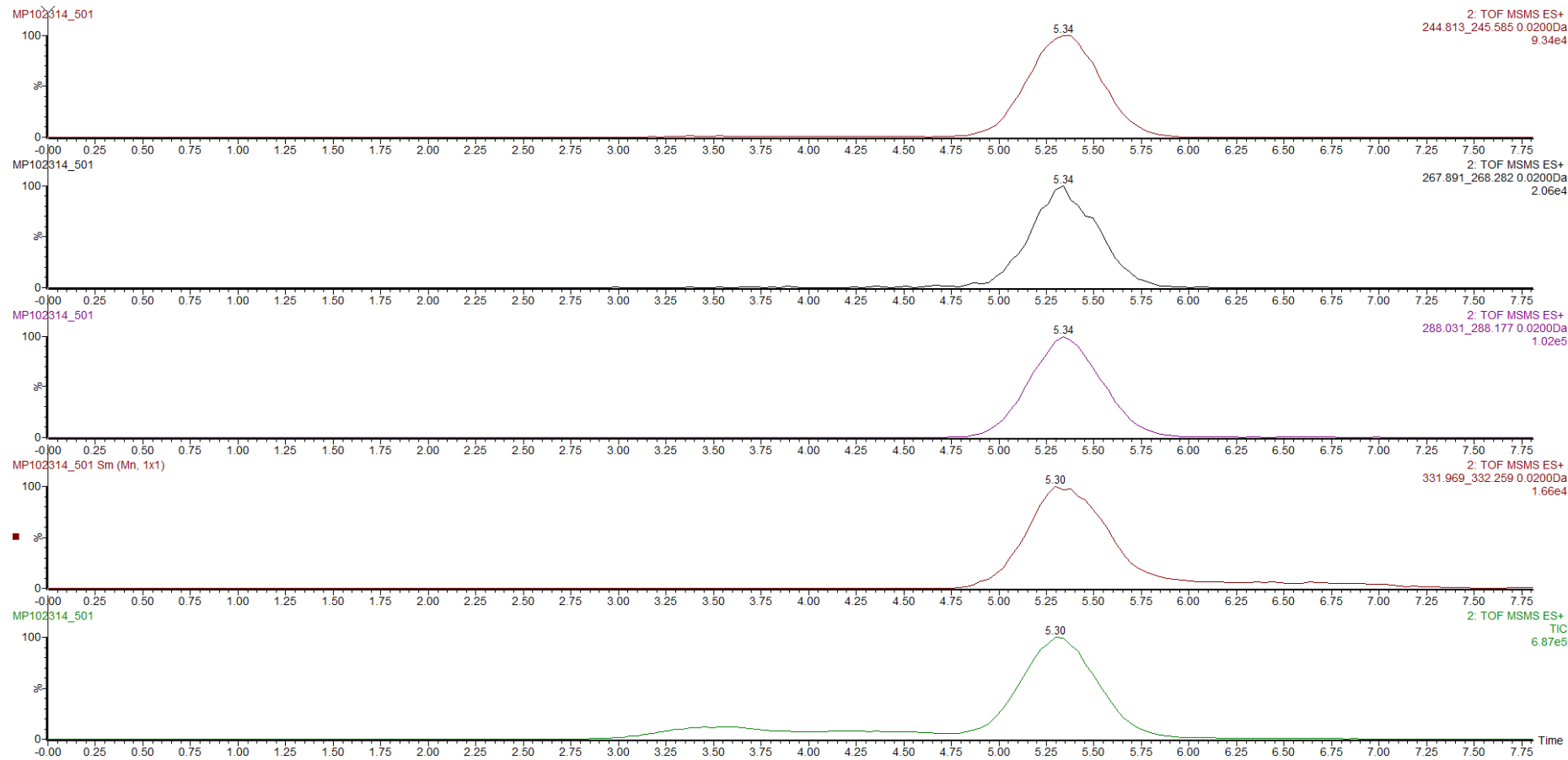
Extracted ion mobilograms for norfloxacin product ions in He(g)
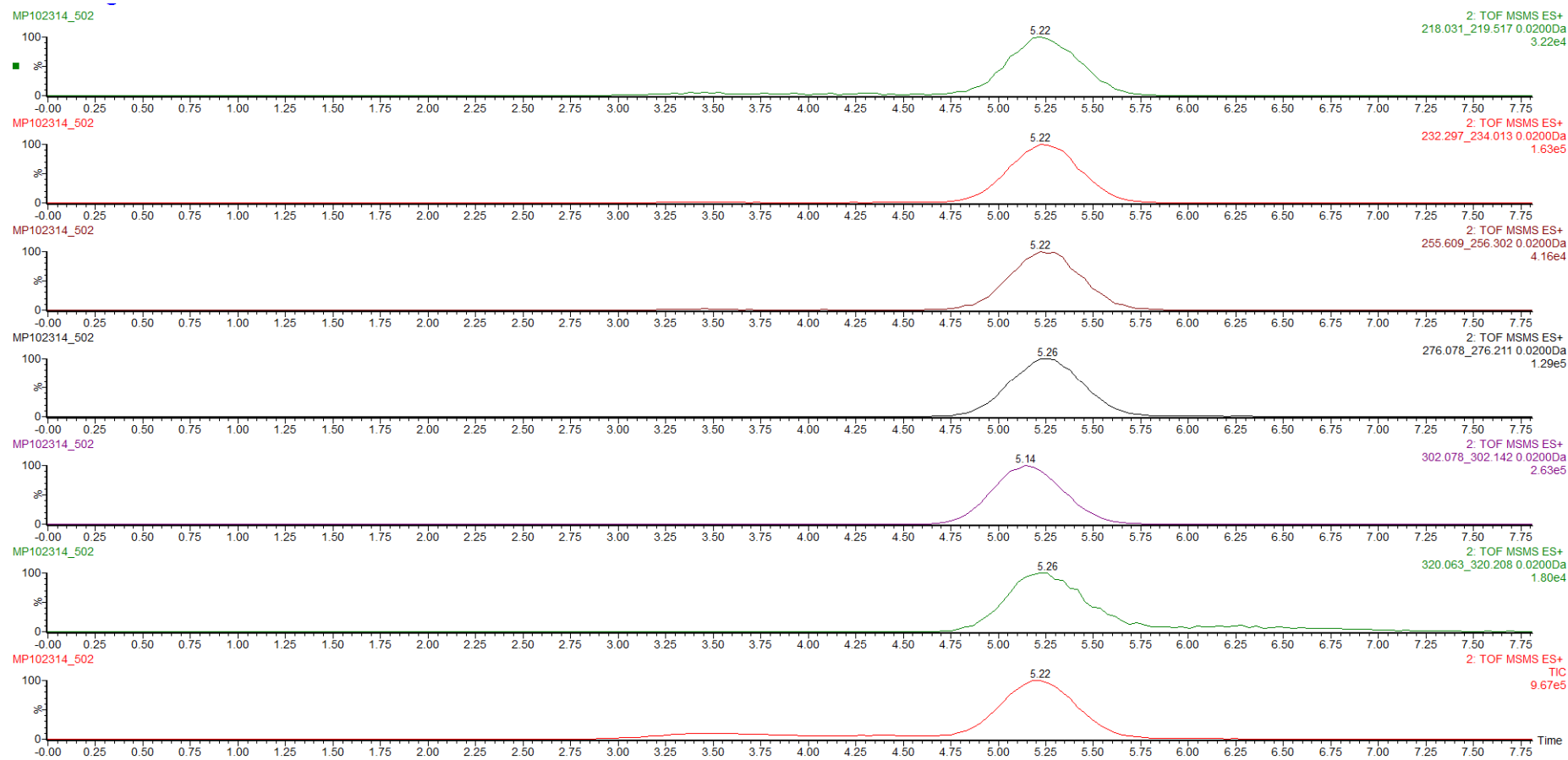
Extracted ion mobilograms for enrofloxacin product ions in He(g)
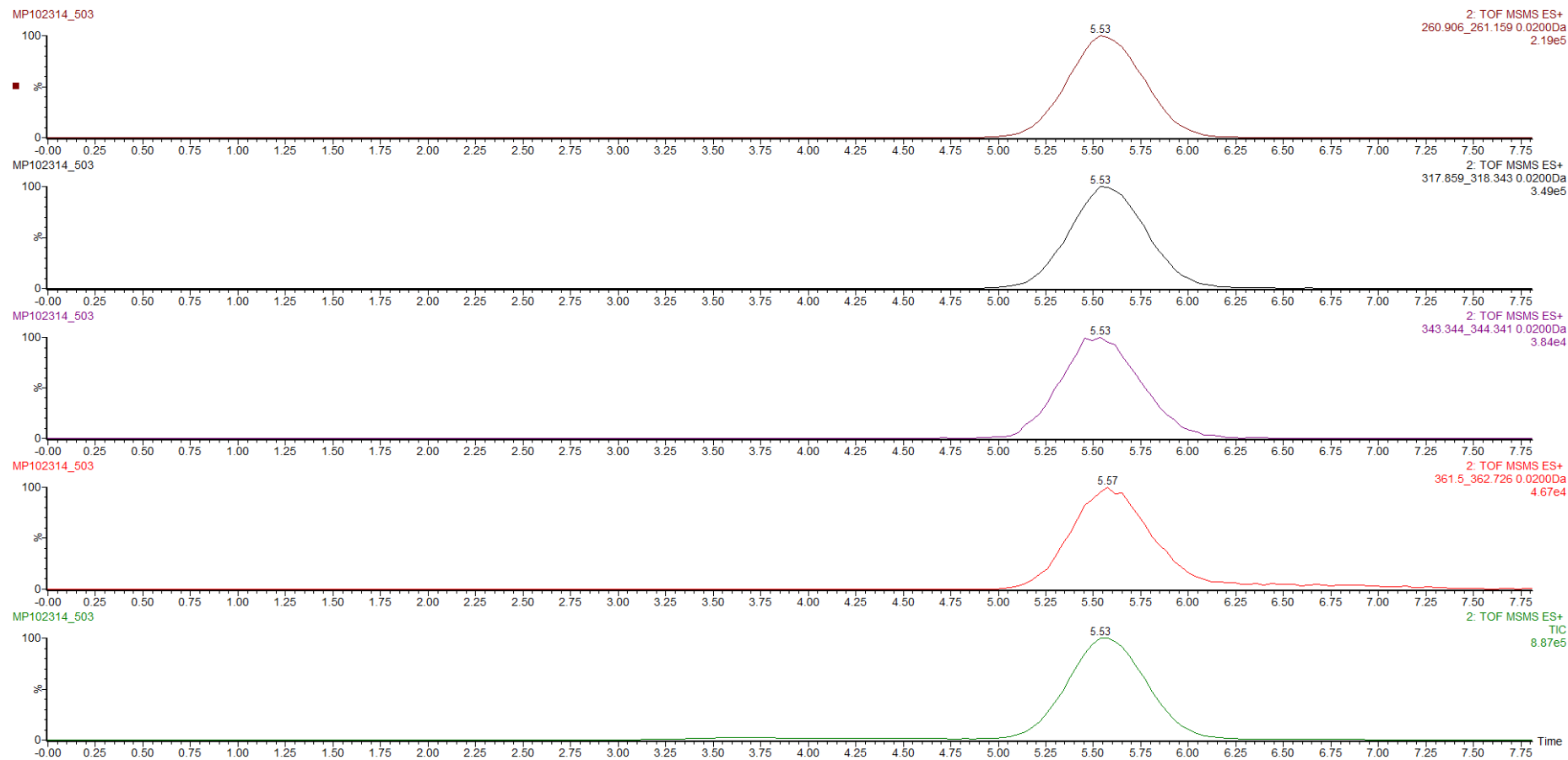
Ciprofloxacin
C17H19FN3O3
[M+H]$^+$

Single Mass Analysis
Tolerance = 5.0 PPM   /   DBE: min = -1.5, max = 50.0
Element prediction: Off
Number of isotope peaks used for i-FIT = 3
Monoisotopic Mass, Odd and Even Electron Ions
206 formula(e) evaluated with 2 results within limits (up to 1 closest results for each mass)
Elements Used:
C: 17-100   H: 0-100   N: 3-10   O: 0-10   F: 1-1   Na: 0-1

Mass	Calc. Mass	mDa	PPM	DBE	Formula	i-FIT	i-FIT Norm	Fit Conf %	C	H	N	O	F	Na
332.1403	332.1410	-0.7	-2.1	9.5	C17 H19 N3 O3 F	561.3	n/a	n/a	17	19	3	3	1	

cip
19Nov2015_CL8 2 (0.103) Cm (2:4)

2: TOF MSMS 332.00ES+
3.16e+005

C17H17FN3O2

[M+H-H₂O]⁺

Single Mass Analysis
Tolerance = 5.0 PPM   /   DBE: min = -1.5, max = 50.0
Element prediction: Off
Number of isotope peaks used for i-FIT = 3
Monoisotopic Mass, Odd and Even Electron Ions
183 formula(e) evaluated with 1 results within limits (up to 1 closest results for each mass)
Elements Used:
C: 17-100   H: 0-100   N: 3-10   O: 0-10   F: 1-1   Na: 0-1

Mass	Calc. Mass	mDa	PPM	DBE	Formula	i-FIT	i-FIT Norm	Fit Conf %	C	H	N	O	F	Na
314.1300	314.1305	-0.5	-1.6	10.5	C17 H17 N3 O2 F	618.7	n/a	n/a	17	17	3	2	1	

cip
19Nov2015_CL8 2 (0.103) Cm (2:4)

2: TOF MSMS 332.00ES+
3.16e+005

C16H19FN3O

[M+H-CO$_2$]$^+$

Single Mass Analysis
Tolerance = 5.0 PPM / DBE: min = -1.5, max = 50.0
Element prediction: Off
Number of isotope peaks used for i-FIT = 3
Monoisotopic Mass, Odd and Even Electron Ions
165 formula(e) evaluated with 1 results within limits (up to 1 closest results for each mass)
Elements Used:
C: 16-100   H: 0-100   N: 3-10   O: 0-10   F: 1-1   Na: 0-1

Mass	Calc. Mass	mDa	PPM	DBE	Formula	i-FIT	i-FIT Norm	Fit Conf %	C	H	N	O	F	Na
288.1510	288.1512	-0.2	-0.7	8.5	C16 H19 N3 O F	645.1	n/a	n/a	16	19	3	1	1	

cip
19Nov2015_CL8 2 (0.103) Cm (2:4)   2: TOF MSMS 332.00ES+
                                                                                                                      3.16e+005

Enrofloxacin
C19H23FN3O3
[M+H]+

Single Mass Analysis
Tolerance = 5.0 PPM   /   DBE: min = -1.5, max = 50.0
Element prediction: Off
Number of isotope peaks used for i-FIT = 3
Monoisotopic Mass, Odd and Even Electron Ions
284 formula(e) evaluated with 4 results within limits (up to 1 closest results for each mass)
Elements Used:
C: 16-100   H: 0-100   N: 3-10   O: 0-10   F: 1-1   Na: 0-1

Mass	Calc. Mass	mDa	PPM	DBE	Formula	i-FIT	i-FIT Norm	Fit Conf %	C	H	N	O	F	Na
360.1717	360.1723	-0.6	-1.7	9.5	C19 H23 N3 O3 F	587.3	n/a	n/a	19	23	3	3	1	

enr
19Nov2015_CL9 2 (0.103) Cm (2:4)

2: TOF MSMS 360.00ES+
7.93e+005

C19H21FN3O2

[M+H-H$_2$O]$^+$

Single Mass Analysis
Tolerance = 5.0 PPM / DBE: min = -1.5, max = 50.0
Element prediction: Off
Number of isotope peaks used for i-FIT = 3
Monoisotopic Mass, Odd and Even Electron Ions
244 formula(e) evaluated with 2 results within limits (up to 1 closest results for each mass)
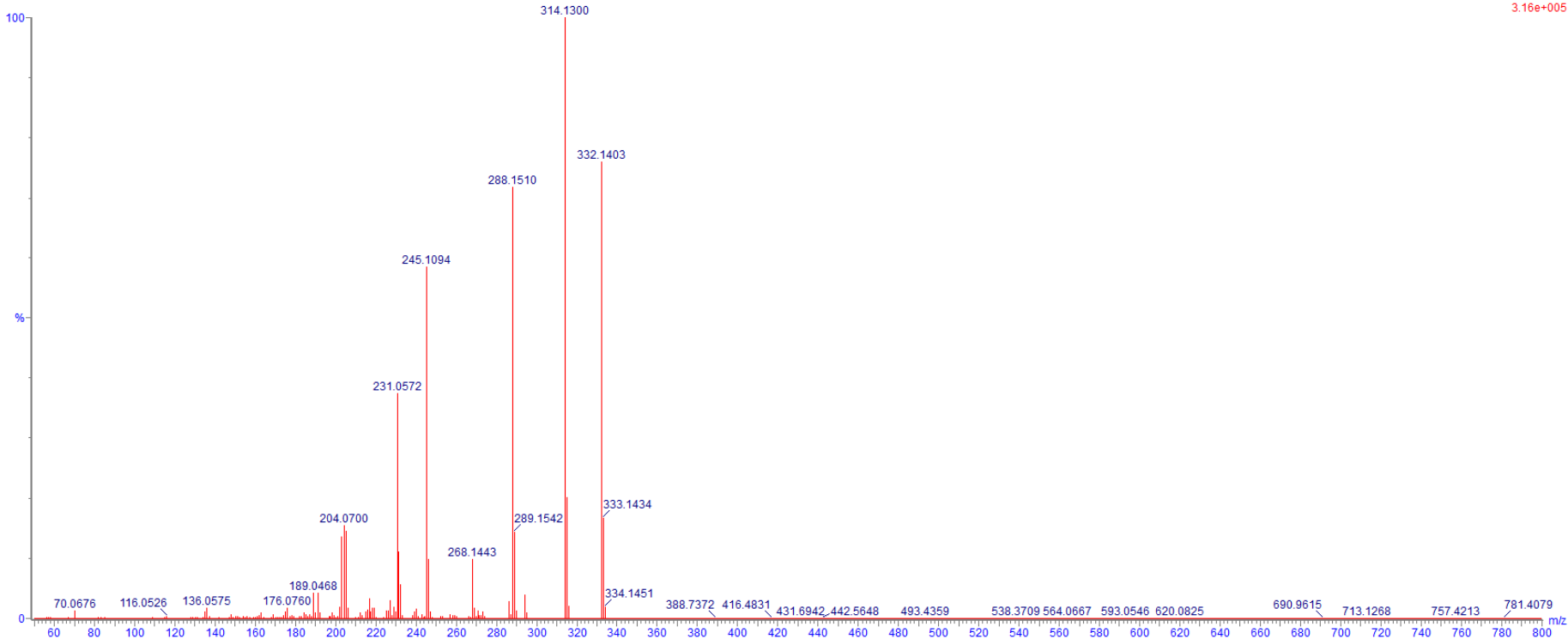Elements Used:
C: 16-100   H: 0-100   N: 3-10   O: 0-10   F: 1-1   Na: 0-1

Mass	Calc. Mass	mDa	PPM	DBE	Formula	i-FIT	i-FIT Norm	Fit Conf %	C	H	N	O	F	Na
342.1616	342.1618	-0.2	-0.6	10.5	C19 H21 N3 O2 F	702.4	n/a	n/a	19	21	3	2	1	

enr
19Nov2015_CL9 2 (0.103) Cm (2:4)

2: TOF MSMS 360.00ES+
7.93e+005

C18H23FN3O1

$[M+H-CO_2]^+$

Single Mass Analysis
Tolerance = 5.0 PPM   /   DBE: min = -1.5, max = 50.0
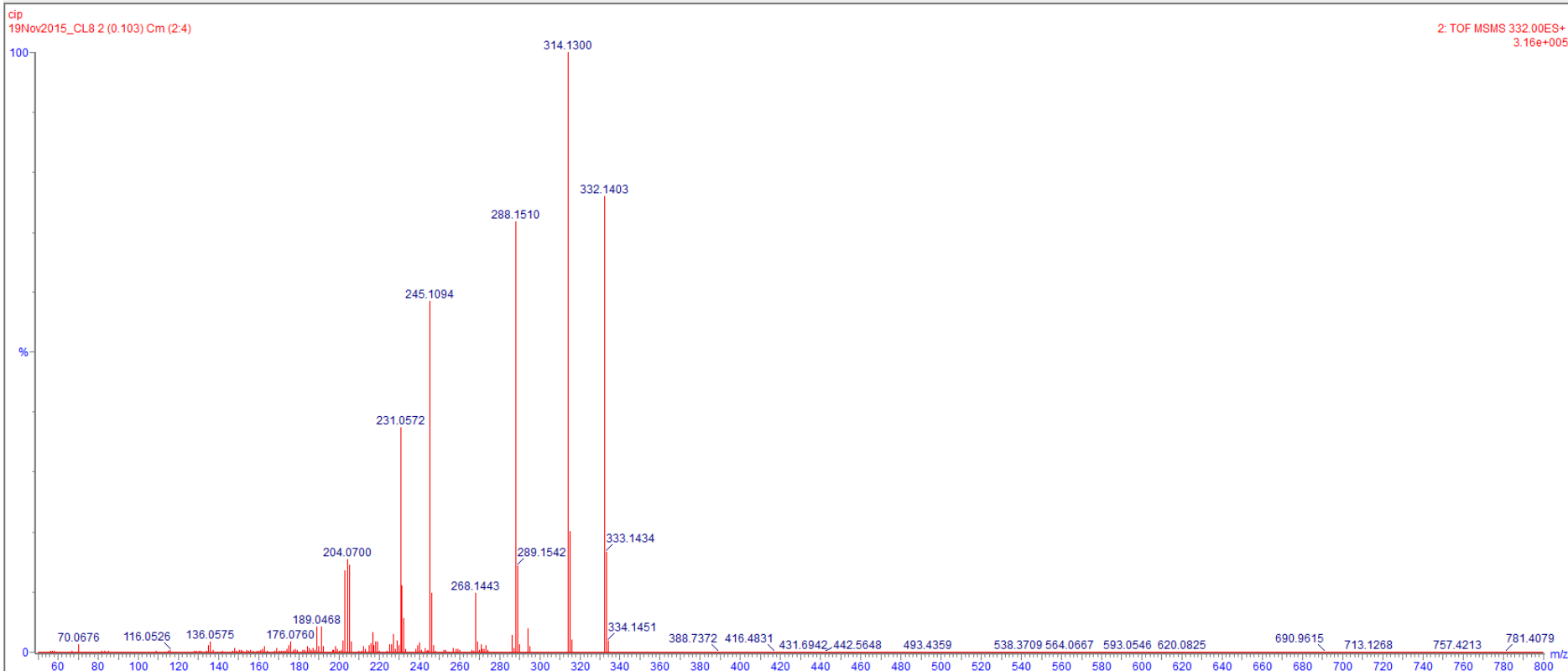Element prediction: Off
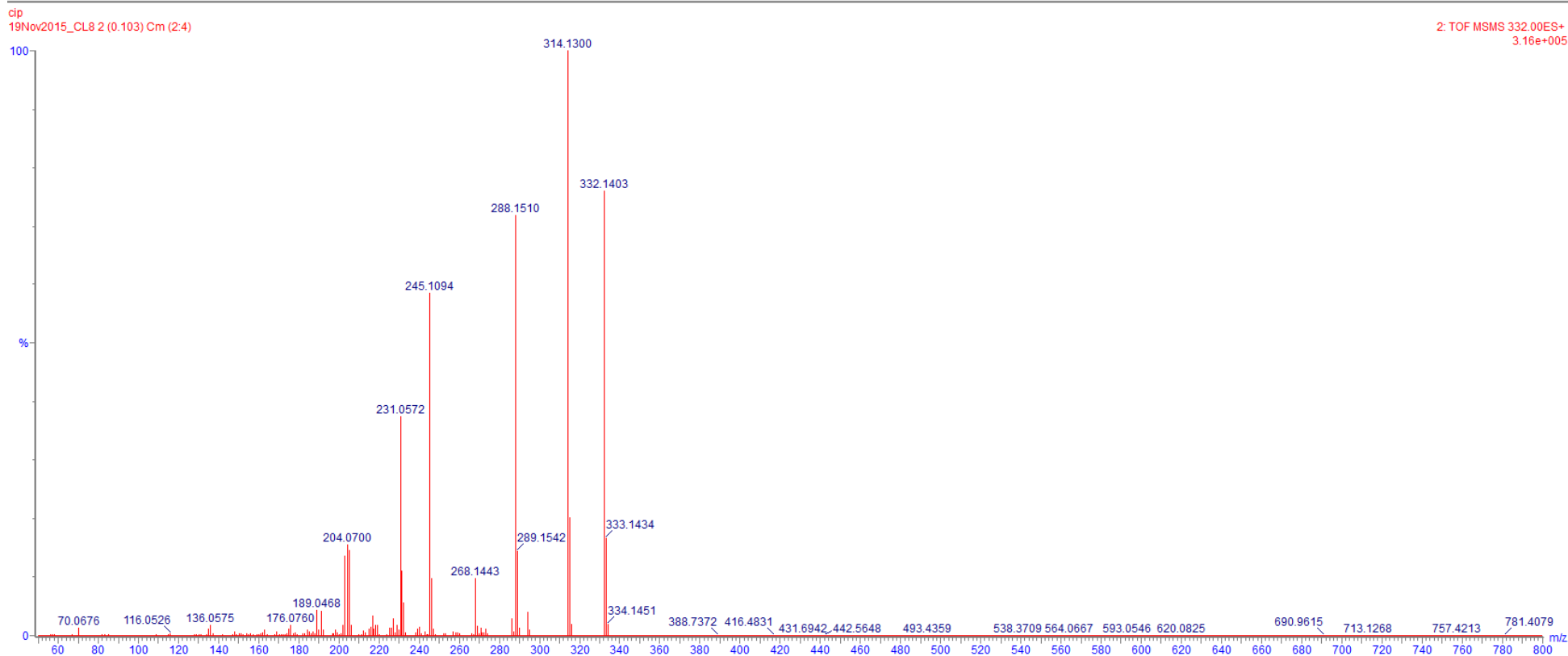Number of isotope peaks used for i-FIT = 3
Monoisotopic Mass, Odd and Even Electron Ions
197 formula(e) evaluated with 2 results within limits (up to 1 closest results for each mass)
Elements Used:
C: 16-100   H: 0-100   N: 3-10   O: 0-10   F: 1-1   Na: 0-1

Mass	Calc. Mass	mDa	PPM	DBE	Formula	i-FIT	i-FIT Norm	Fit Conf %	C	H	N	O	F	Na
316.1819	316.1825	-0.6	-1.9	8.5	C18 H23 N3 O F	739.6	n/a	n/a	18	23	3	1	1	

enr
19Nov2015_CL9 2 (0.103) Cm (2:4)

2: TOF MSMS 360.00ES+
7.93e+005
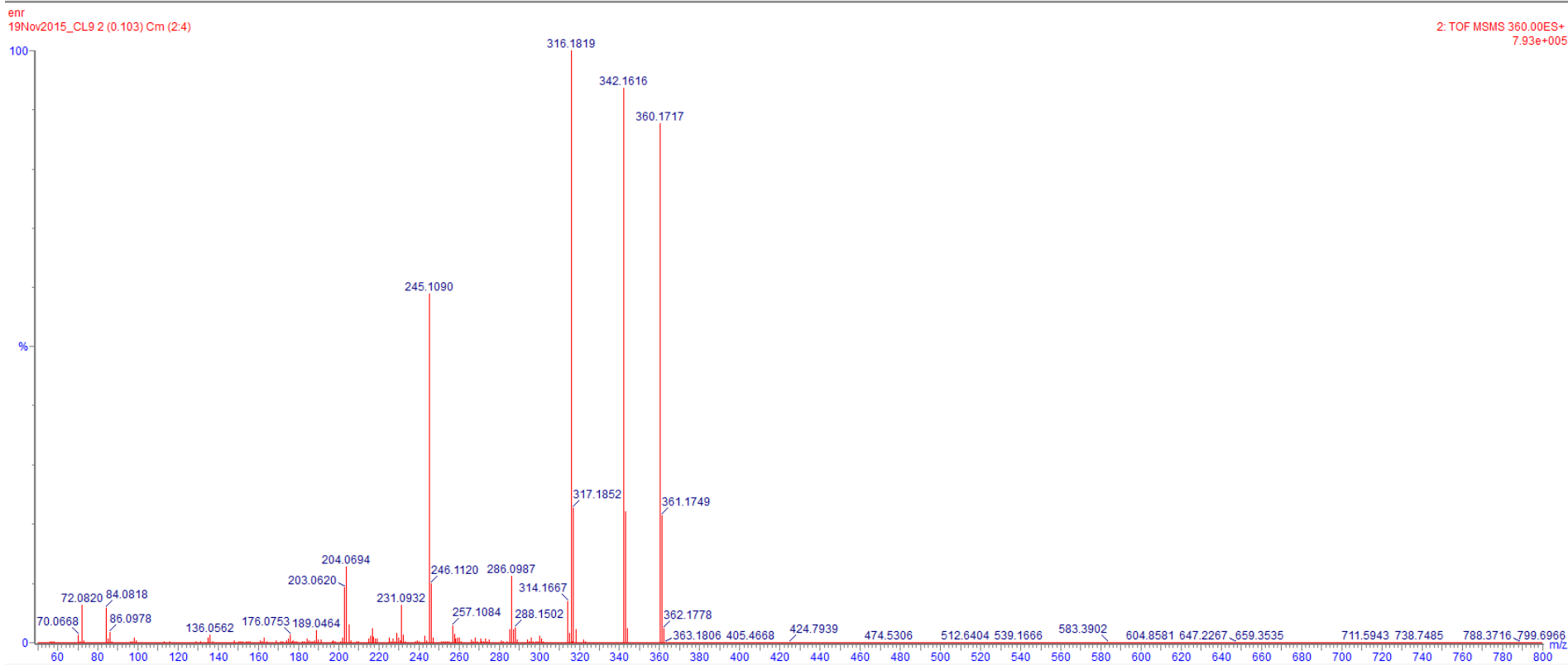
Norfloxacin
C16H19FN3O3
[M+H]$^+$
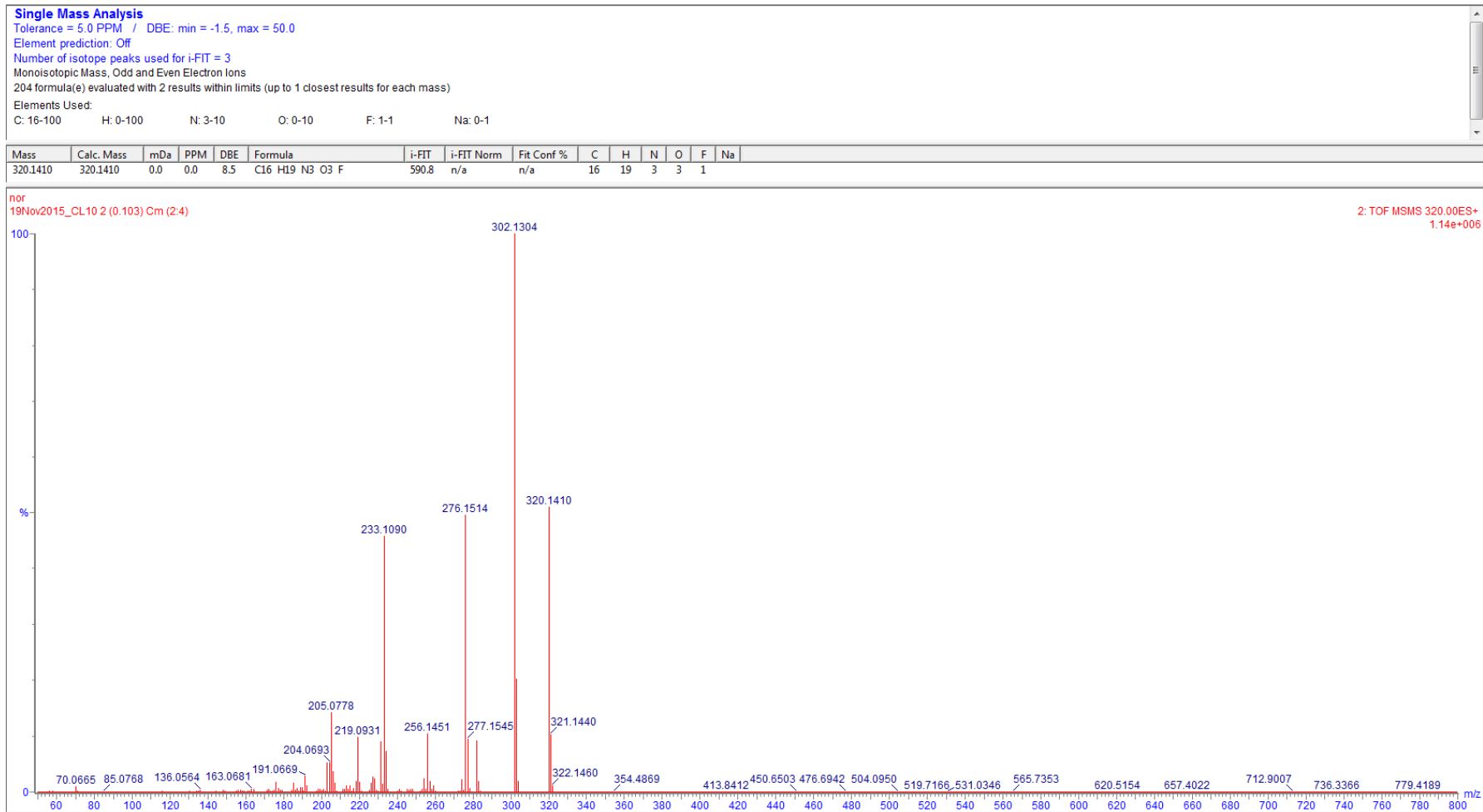
C16H17FN3O3

[M+H-H₂O]⁺

Single Mass Analysis
Tolerance = 5.0 PPM   /   DBE: min = -1.5, max = 50.0
Element prediction: Off
Number of isotope peaks used for i-FIT = 3
Monoisotopic Mass, Odd and Even Electron Ions
178 formula(e) evaluated with 1 results within limits (up to 1 closest results for each mass)
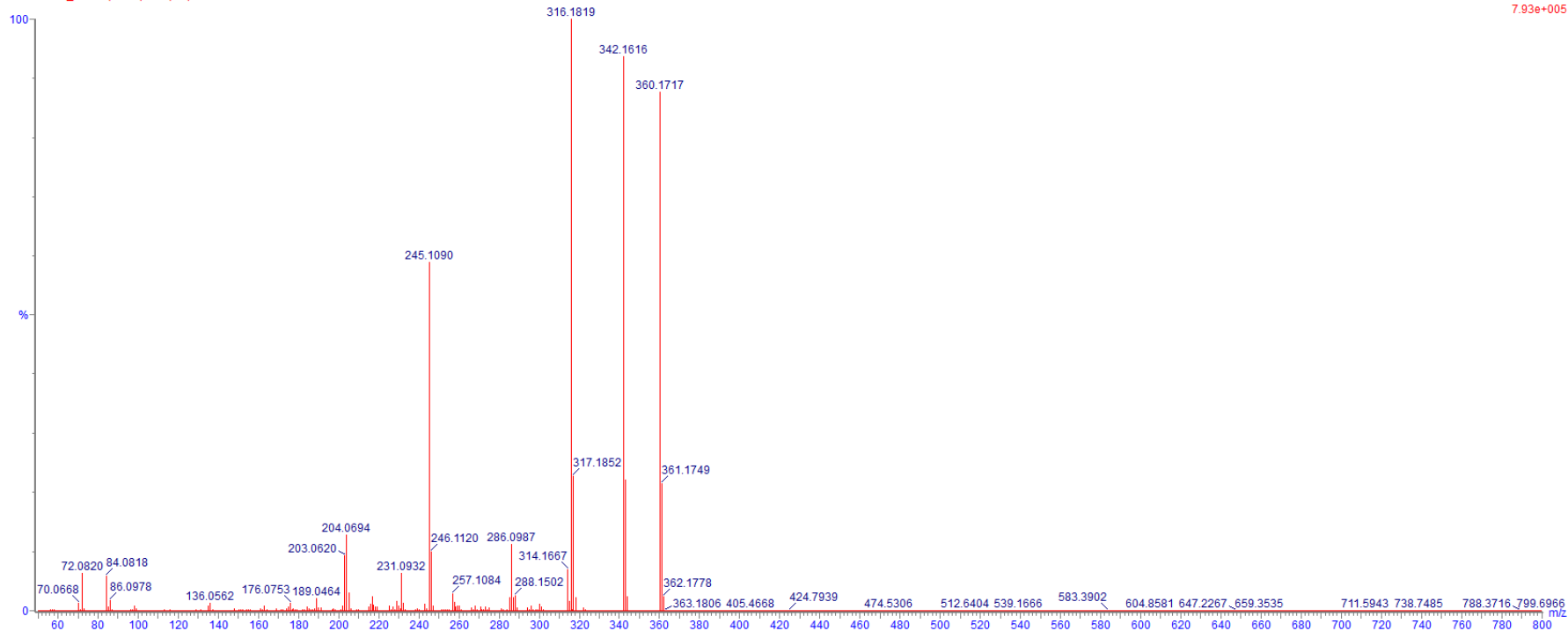Elements Used:
C: 16-100   H: 0-100   N: 3-10   O: 0-10   F: 1-1   Na: 0-1

Mass	Calc. Mass	mDa	PPM	DBE	Formula	i-FIT	i-FIT Norm	Fit Conf %	C	H	N	O	F	Na
302.1304	302.1305	-0.1	-0.3	9.5	C16 H17 N3 O2 F	730.9	n/a	n/a	16	17	3	2	1	

nor
19Nov2015_CL10 2 (0.103) Cm (2:4)

2: TOF MSMS 320.00ES+
1.14e+006
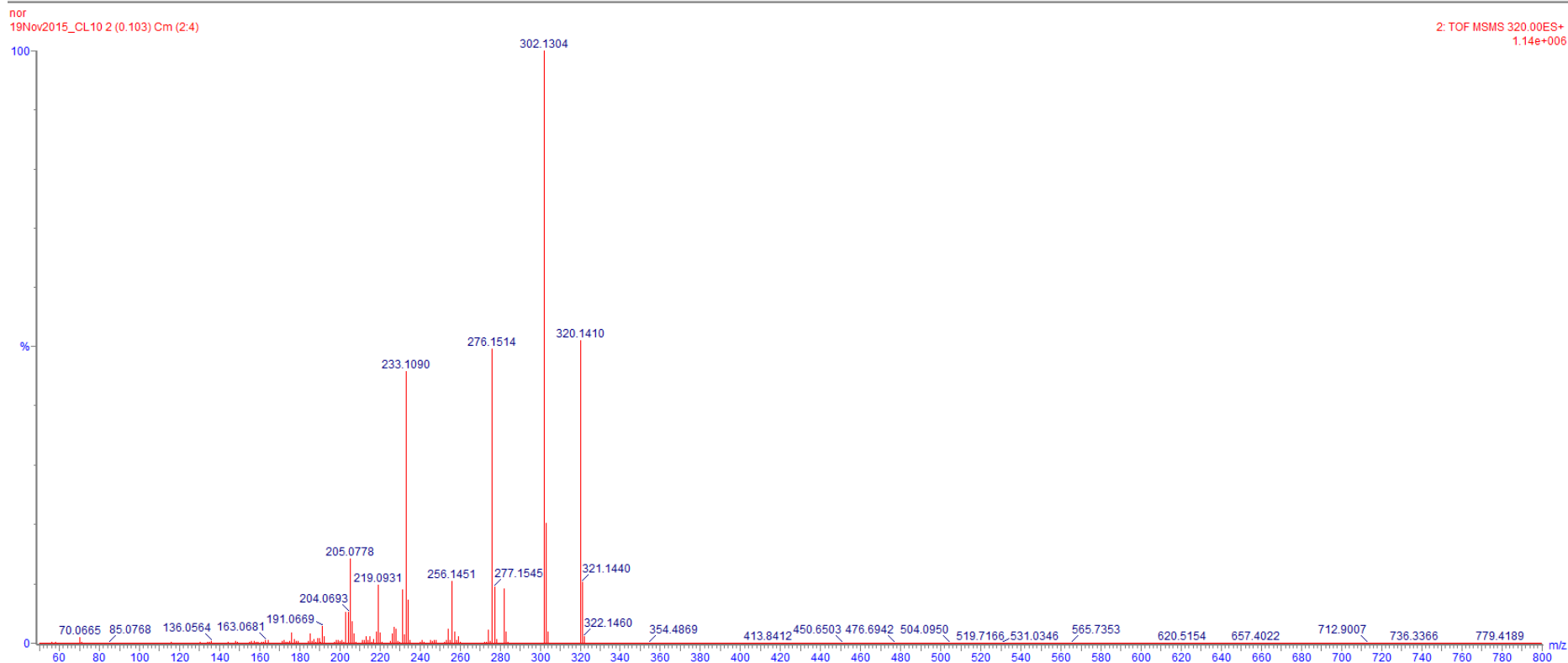
C15H19FN3O

[M+H-CO$_2$]$^+$

Single Mass Analysis
Tolerance = 5.0 PPM   /   DBE: min = -1.5, max = 50.0
Element prediction: Off
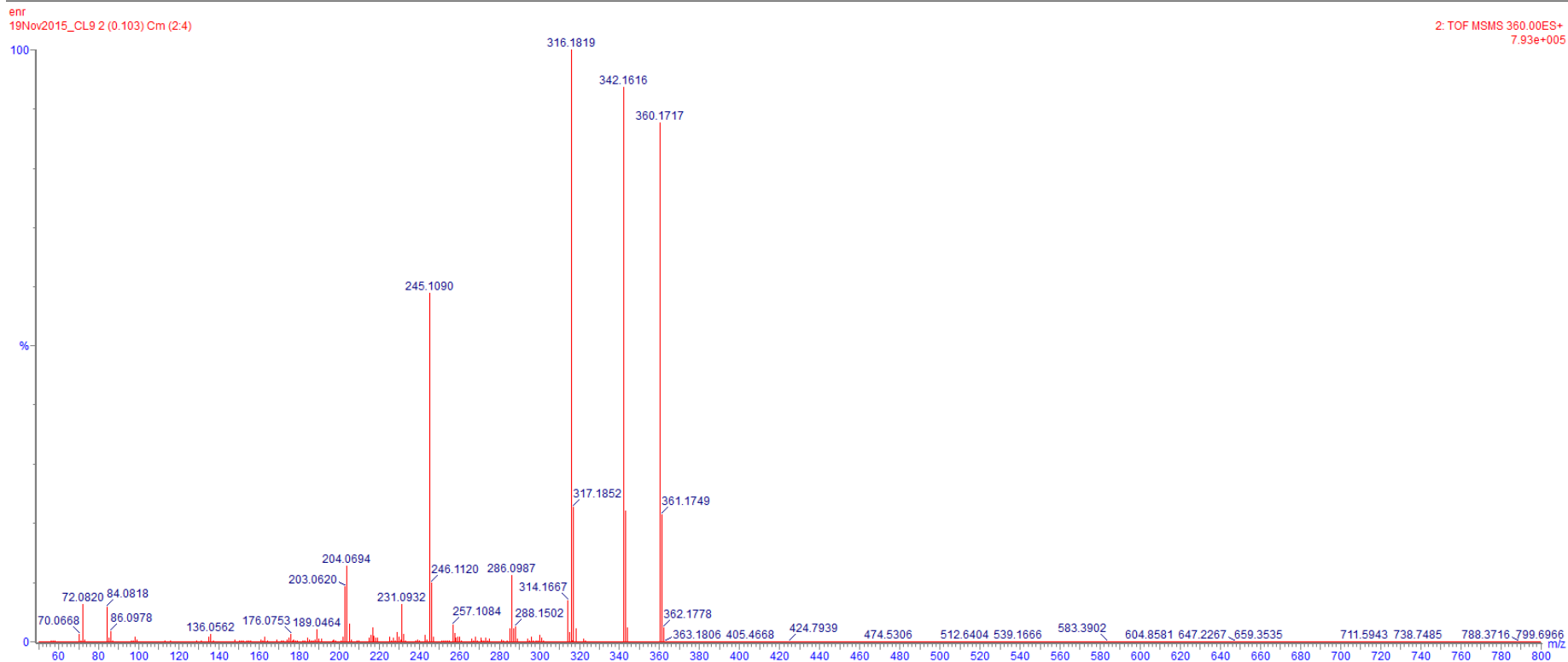Number of isotope peaks used for i-FIT = 3
Monoisotopic Mass, Odd and Even Electron Ions
158 formula(e) evaluated with 1 results within limits (up to 1 closest results for each mass)
Elements Used:
C: 15-100   H: 0-100   N: 3-10   O: 0-10   F: 1-1   Na: 0-1

Mass	Calc. Mass	mDa	PPM	DBE	Formula	i-FIT	i-FIT Norm	Fit Conf %	C	H	N	O	F	Na
276.1514	276.1512	0.2	0.7	7.5	C15 H19 N3 O F	707.6	n/a	n/a	15	19	3	1	1	

nor
19Nov2015_CL10 2 (0.103) Cm (2:4)

2: TOF MSMS 320.00ES+
1.14e+006
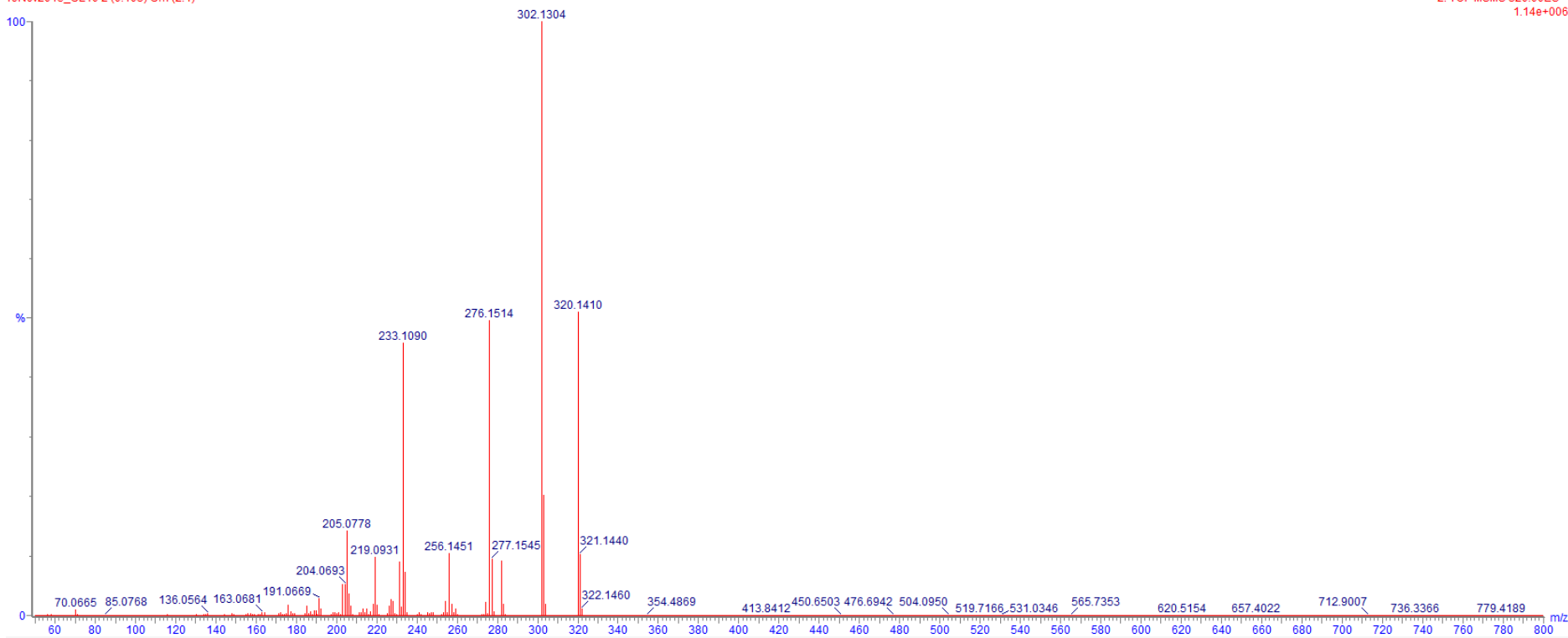
APPENDIX B: SUPPLEMENTARY DATA FOR CHAPTER 4

Experimental data for nitrogen-parameterised calibration set

	Name	eCCS1	eCCS2	eCCS3	Mean	Std Dev	% RSD
1	*N*-ethylaniline	126.81	126.84	126.64	126.76	0.11	0.09%
2	Acetaminophen	129.89	128.76	128.94	129.20	0.61	0.47%
3	Pregabalin	137.85	137.88	137.85	137.86	0.02	0.01%
4	Ephedrine	135.59	135.60	135.67	135.62	0.04	0.03%
5	Phenacetin	139.34	139.31	139.30	139.32	0.02	0.01%
6	Naproxen	150.32	150.37	150.42	150.37	0.05	0.03%
7	Alprenolol	159.58	158.68	158.77	159.01	0.50	0.31%
8	*5-(p-methylphenyl)-5*-phenylhydantoin	163.54	163.52	163.54	163.53	0.01	0.01%
9	Trimethoprim	169.87	169.78	169.93	169.86	0.08	0.04%
10	Ondansetron	170.06	169.26	169.29	169.54	0.45	0.27%
11	Cinchonine	166.54	166.46	166.19	166.40	0.18	0.11%
12	Sulpiride	182.91	182.84	183.07	182.94	0.12	0.06%
13	Clozapine *N*-oxide	180.31	179.95	179.91	180.06	0.22	0.12%
14	Cortisone	184.04	184.19	183.90	184.04	0.15	0.08%
15	Trichlormethiazide	176.05	176.28	175.96	176.10	0.17	0.09%
16	Amlodipine	189.48	189.33	189.06	189.29	0.21	0.11%
17	Doxazosin	205.68	205.69	205.31	205.56	0.22	0.11%
18	Verapamil	212.14	211.59	211.75	211.83	0.28	0.13%
19	Sildenafil	213.57	213.43	213.01	213.34	0.29	0.14%
20	Reserpine	255.93	255.98	256.18	256.03	0.13	0.05%

Experimental data for helium-parameterised calibration set

	Name	eCCS1	eCCS2	eCCS3	Mean	Std Dev	% RSD
1	*N*-ethylaniline	71.93	71.95	71.81	71.90	0.08	0.11%
2	Acetaminophen	74.54	73.72	73.85	74.04	0.44	0.60%
4	Ephedrine	78.46	78.47	78.51	78.48	0.03	0.03%
5	Phenacetin	80.22	80.21	80.19	80.21	0.02	0.02%
3	Pregabalin	80.26	80.28	80.26	80.27	0.01	0.01%
6	Naproxen	90.23	90.26	90.30	90.26	0.04	0.04%
7	Alprenolol	97.69	96.99	97.06	97.25	0.39	0.40%
8	*5-(p-methylphenyl)-5*-phenylhydantoin	100.55	100.53	100.55	100.54	0.01	0.01%
11	Cinchonine	102.04	101.97	101.76	101.92	0.15	0.14%
9	Trimethoprim	105.98	104.89	106.03	105.63	0.64	0.61%
10	Ondansetron	106.15	105.51	105.53	105.73	0.36	0.34%
15	Trichlormethiazide	110.01	110.21	109.95	110.06	0.14	0.12%
13	Clozapine *N*-oxide	114.45	114.26	114.22	114.31	0.12	0.11%
12	Sulpiride	115.97	116.35	116.53	116.28	0.29	0.25%
14	Cortisone	117.38	117.51	117.28	117.39	0.12	0.10%
16	Amlodipine	122.06	121.94	121.72	121.91	0.17	0.14%
17	Doxazosin	134.96	134.96	134.64	134.85	0.19	0.14%
18	Verapamil	141.22	140.75	140.89	140.95	0.24	0.17%
19	Sildenafil	141.80	141.68	141.32	141.60	0.25	0.18%
20	Reserpine	179.86	179.90	180.09	179.95	0.12	0.07%

APPENDIX C: SUPPLEMENTARY DATA FOR CHAPTER 5

Drug-like calibration He$_{(g)}$ CSV file for Waters Driftscope software
```
CCS (Lit.),m/z,z,,
63,122.1,1,,
67,152.1,1,,
96.9,250.2,1,,
105.9,294.2,1,,
112.5,393.2,1,,
130.8,400.3,1,,
142.6,455.3,1,,
178.8,609.4,1,,
Delete this and all content below this line then save this file as CSV.,,,,
The following lines are for info only .,,,,
,,,,
CCS (Lit.),m/z,z,name,molecular formula
63,122.1,1,N-ethylaniline,C8H11N
67,152.1,1,acetaminophen,C8H9NO2
96.9,250.2,1,alprenolol       ,C15H23NO2
105.9,294.2,1,ondansetron       ,C18H19N3O
112.5,393.2,1,clozapine N-oxide       ,C18H19ClN4
130.8,400.3,1,colchicine       ,C22H25NO6
142.6,455.3,1,verapamil,C27H38N2O4
178.8,609.4,1,reserpine       ,C33H40N2O9
,,,,
Structural Characterization of Drug-like Compounds by Ion Mobility Mass
Spectrometry: Comparison of Theoretical and Experimentally Derived Nitrogen
Collision Cross Sections,,,,
"Iain Campuzano, Matthew F. Bush, Carol V. Robinson, Claire Beaumont, Keith
Richardson, Hyungjun Kim, and Hugh I. Kim",,,,
"Analytical Chemistry 2012 84 (2), 1026-1033",,,,
http://pubs.acs.org/doi/abs/10.1021/ac202625t,,,,
http://depts.washington.edu/bushlab/ccsdatabase/,,,,
```

Drug-like calibration N$_{2(g)}$ CSV file for Waters Driftscope software

```
CCS (Lit.),m/z,z,,
124.5,122.1,1,,
130.4,152.1,1,,
157.5,250.2,1,,
172.7,294.2,1,,
180.6,393.2,1,,
196.2,400.3,1,,
210.0,455.3,1,,
254.3,609.4,1,,
Delete this and all content below this line then save this file as CSV.,,,,
The following lines are for info only.,,,,
,,,,
CCS (Lit.),m/z,z,name,molecular formula
124.5,122.1,1,N-ethylaniline,C8H11N
130.4,152.1,1,acetaminophen,C8H9NO2
157.5,250.2,1,alprenolol       ,C15H23NO2
172.7,294.2,1,ondansetron       ,C18H19N3O
180.6,393.2,1,clozapine N-oxide       ,C18H19ClN4
196.2,400.3,1,colchicine       ,C22H25NO6
210.0,455.3,1,verapamil,C27H38N2O4
254.3,609.4,1,reserpine       ,C33H40N2O9
,,,,
```

Structural Characterization of Drug-like Compounds by Ion Mobility Mass Spectrometry: Comparison of Theoretical and Experimentally Derived Nitrogen Collision Cross Sections,,,,
"Iain Campuzano, Matthew F. Bush, Carol V. Robinson, Claire Beaumont, Keith Richardson, Hyungjun Kim, and Hugh I. Kim",,,,
"Analytical Chemistry 2012 84 (2), 1026-1033",,,,
http://pubs.acs.org/doi/abs/10.1021/ac202625t,,,,
http://depts.washington.edu/bushlab/ccsdatabase/,,,,

Polyalanine calibration He(g) CSV file for Waters Driftscope software

```
CCS (Lit.),m/z,z,,,
89,232.1,1,,,
100,303.2,1,,,
114,374.2,1,,,
128,445.2,1,,,
141,516.3,1,,,
157,587.3,1,,,
170,658.4,1,,,
181,729.4,1,,,
194,800.4,1,,,
206,871.5,1,,,
217,942.5,1,,,
228,1013.5,1,,,
197,400.7,2,,,
208,436.2,2,,,
220,471.8,2,,,
232,507.3,2,,,
243,542.8,2,,,
255,578.3,2,,,
265,613.8,2,,,
276,649.3,2,,,
287,684.9,2,,,
297,720.4,2,,,
308,755.9,2,,,
317,791.4,2,,,
327,826.9,2,,,
337,862.5,2,,,
348,898.0,2,,,
358,933.5,2,,,
338,456.9,3,,,
348,480.6,3,,,
361,504.3,3,,,
373,527.9,3,,,
386,551.6,3,,,
399,575.3,3,,,
412,599.0,3,,,
425,622.7,3,,,
438,646.3,3,,,
452,670.0,3,,,
465,693.7,3,,,
479,717.4,3,,,
490,741.1,3,,,
502,764.7,3,,,
516,788.4,3,,,
Delete this and all content below this line then save file as CSV.,,,,,
The following lines are for info only.,,,,,
,,,,,
CCS (Lit.),m/z,z,number of oligomers,m,mass of polyalanine repeat unit
89,232.1,1,3,232.1297,71.0371
```

```
100,303.2,1,4,303.1668,
114,374.2,1,5,374.2039,
128,445.2,1,6,445.2410,
141,516.3,1,7,516.2781,
157,587.3,1,8,587.3152,
170,658.4,1,9,658.3523,
181,729.4,1,10,729.3894,
194,800.4,1,11,800.4265,
206,871.5,1,12,871.4636,
217,942.5,1,13,942.5007,
228,1013.5,1,14,1013.5378,
197,400.7,2,11,800.4265,
208,436.2,2,12,871.4636,
220,471.8,2,13,942.5007,
232,507.3,2,14,1013.5378,
243,542.8,2,15,1084.5749,
255,578.3,2,16,1155.6120,
265,613.8,2,17,1226.6491,
276,649.3,2,18,1297.6862,
287,684.9,2,19,1368.7233,
297,720.4,2,20,1439.7604,
308,755.9,2,21,1510.7975,
317,791.4,2,22,1581.8346,
327,826.9,2,23,1652.8717,
337,862.5,2,24,1723.9088,
348,898.0,2,25,1794.9459,
358,933.5,2,26,1865.9830,
338,456.9,3,19,1368.7233,
348,480.6,3,20,1439.7604,
361,504.3,3,21,1510.7975,
373,527.9,3,22,1581.8346,
386,551.6,3,23,1652.8717,
399,575.3,3,24,1723.9088,
412,599.0,3,25,1794.9459,
425,622.7,3,26,1865.9830,
438,646.3,3,27,1937.0201,
452,670.0,3,28,2008.0572,
465,693.7,3,29,2079.0943,
479,717.4,3,30,2150.1314,
490,741.1,3,31,2221.1685,
502,764.7,3,32,2292.2056,
516,788.4,3,33,2363.2427,
,,,,,
```

Ion Mobility Mass Spectrometry of Peptide Ions: Effects of Drift Gas and
Calibration Strategies,,,,,

Polyalanine calibration N$_{2(g)}$ CSV file for Waters Driftscope software

```
CCS (Lit.),m/z,z,,,
151,232.1,1,,,
166,303.2,1,,,
181,374.2,1,,,
195,445.2,1,,,
211,516.3,1,,,
228,587.3,1,,,
243,658.4,1,,,
256,729.4,1,,,
271,800.4,1,,,
282,871.5,1,,,
294,942.5,1,,,
306,1013.5,1,,,
296,400.7,2,,,
309,436.2,2,,,
320,471.8,2,,,
333,507.3,2,,,
344,542.8,2,,,
357,578.3,2,,,
369,613.8,2,,,
380,649.3,2,,,
393,684.9,2,,,
404,720.4,2,,,
416,755.9,2,,,
428,791.4,2,,,
437,826.9,2,,,
448,862.5,2,,,
458,898.0,2,,,
470,933.5,2,,,
482,456.9,3,,,
491,480.6,3,,,
501,504.3,3,,,
518,527.9,3,,,
532,551.6,3,,,
545,575.3,3,,,
561,599.0,3,,,
576,622.7,3,,,
592,646.3,3,,,
606,670.0,3,,,
621,693.7,3,,,
634,717.4,3,,,
649,741.1,3,,,
666,764.7,3,,,
674,788.4,3,,,
Delete this and all content below this line then save file as CSV.,,,,,,
The following lines are for info only.,,,,,,
,,,,,
CCS (Lit.),m/z,z,number of oligomers,m,mass of polyalanine repeat unit
151,232.1,1,3,232.1297,71.0371
166,303.2,1,4,303.1668,
181,374.2,1,5,374.2039,
195,445.2,1,6,445.2410,
211,516.3,1,7,516.2781,
228,587.3,1,8,587.3152,
243,658.4,1,9,658.3523,
256,729.4,1,10,729.3894,
271,800.4,1,11,800.4265,
282,871.5,1,12,871.4636,
294,942.5,1,13,942.5007,
```

306,1013.5,1,14,1013.5378,
296,400.7,2,11,800.4265,
309,436.2,2,12,871.4636,
320,471.8,2,13,942.5007,
333,507.3,2,14,1013.5378,
344,542.8,2,15,1084.5749,
357,578.3,2,16,1155.6120,
369,613.8,2,17,1226.6491,
380,649.3,2,18,1297.6862,
393,684.9,2,19,1368.7233,
404,720.4,2,20,1439.7604,
416,755.9,2,21,1510.7975,
428,791.4,2,22,1581.8346,
437,826.9,2,23,1652.8717,
448,862.5,2,24,1723.9088,
458,898.0,2,25,1794.9459,
470,933.5,2,26,1865.9830,
482,456.9,3,19,1368.7233,
491,480.6,3,20,1439.7604,
501,504.3,3,21,1510.7975,
518,527.9,3,22,1581.8346,
532,551.6,3,23,1652.8717,
545,575.3,3,24,1723.9088,
561,599.0,3,25,1794.9459,
576,622.7,3,26,1865.9830,
592,646.3,3,27,1937.0201,
606,670.0,3,28,2008.0572,
621,693.7,3,29,2079.0943,
634,717.4,3,30,2150.1314,
649,741.1,3,31,2221.1685,
666,764.7,3,32,2292.2056,
674,788.4,3,33,2363.2427,
,,,,,
Ion Mobility Mass Spectrometry of Peptide Ions: Effects of Drift Gas and Calibration Strategies,,,,
"Matthew F. Bush, Iain D. G. Campuzano, and Carol V. Robinson",,,,,
"Analytical Chemistry 2012 84 (16), 7124-7130",,,,,
http://pubs.acs.org/doi/abs/10.1021/ac3014498,,,,,

Code for MultiMOBCAL.bat written in Microsoft Windows command shell interface

```
@echo off

echo This script queues and runs multiple instances of MOBCAL
echo Calculations run faster and unattended
echo mobcal.run is suitable for original helium MOBCAL
echo mobcal.in is suitable for modified nitrogen MOBCAL
echo Programmed by Cris Lapthorn
echo ====================================
echo.
TITLE MultiMOBCAL control

echo. >>batch_mobcal.txt
setlocal disableDelayedExpansion
for /f "tokens=1* delims=:" %%A in ('dir *.mfj /o:s /b^|findstr /n "^"') do
(
set "file.%%A=%%B"
set "filecount=%%A"
)

setlocal enableDelayedExpansion
set /a ncpus=%NUMBER_OF_PROCESSORS%
echo There are !ncpus! processors available for MOBCAL
echo.
echo It is best to leave 1 or 2 processors free if other work is required
on this PC
set /p ccpus="Enter number of processors you wish to use for MOBCAL: " %=%
set /a ncpus=ccpus
echo.
echo Started %DATE% %TIME%>>batch_mobcal.txt
echo.%ncpus% processors selected for MOBCAL>>batch_mobcal.txt
dir *.mfj /o:-s /b>>batch_mobcal.txt
set /a b=%filecount%

:loop
echo Number of files to run is %b%
if not exist !file.%b%! goto skip
echo !file.%b%!>mobcal.run
set str=!file.%b%!
set str=%str:mfj=out%
echo.%str%>>mobcal.run
set /A RND=!RANDOM! %% 999999 + 111111
echo.%RND%>>mobcal.run
echo.%str%>>batch_mobcal.txt

for /f "tokens=1,*" %%a in ('tasklist ^| find /I /C "mobcal.exe"') do set
/a mobcalsrunning=%%a
set /a cpusfree=%ncpus%-%mobcalsrunning%
echo Number of processors free for running MOBCAL is !cpusfree!

if /i !cpusfree! LEQ 1 (
set /a b=%b%-1
echo Started %str%
echo.
mobcal

) else (
echo Spawned %str%
echo.
start /min mobcal
```

```
set /a b=%b%-1
ping 192.0.2.2 -n 1 -w 1000 > nul
)
if %b%==-1 goto skip
goto loop

:skip
timeout /t 1 >nul
tasklist|find "mobcal.exe" >nul 2>&1
if errorlevel 1 (
  goto nomobcals
) else (
  echo MOBCAL is still running
  timeout /t 1 >NUL
  goto skip
)

:nomobcals
if not exist doneoutfiles mkdir doneoutfiles >NUL
if not exist donemfjfiles mkdir donemfjfiles >NUL
cls
echo No more MFJ files, last file was %str%
echo Ended %DATE% %TIME%>>batch_mobcal.txt
echo Calculations have finished. Moving .mfj input files...
echo.
move /-y *.mfj donemfjfiles
cls
call show_ccs_results.bat
echo.
pause
echo Calculations have finished. Moving .out output files...
echo.
move /-y *.out doneoutfiles
cls
echo All done

pause
```

Code for MultiMOBCAL_monitor.bat written in Microsoft Windows command shell interface

```bat
@echo off

echo This script queues and runs multiple instances of MOBCAL
echo Calculations run faster and unattended
echo mobcal.run is suitable for original helium MOBCAL
echo mobcal.in is suitable for modified nitrogen MOBCAL
echo Programmed by Cris Lapthorn
echo ===================================
echo.
TITLE MultiMOBCAL control
echo. >>batch_mobcal.txt
setlocal disableDelayedExpansion
for /f "tokens=1* delims=:" %%A in ('dir *.mfj /o:s /b^|findstr /n "^"') do (
set "file.%%A=%%B"
set "filecount=%%A"
)

setlocal enableDelayedExpansion
set /a ncpus=%NUMBER_OF_PROCESSORS%-1
echo There are %NUMBER_OF_PROCESSORS% processors available for MOBCAL
echo.%ncpus% processors selected for MOBCAL
echo.
:: The format of %TIME% is HH:MM:SS,CS for example 23:59:59,99
set STARTTIME=%TIME%
echo Started %DATE% %TIME%>>batch_mobcal.txt
echo.%ncpus% processors selected for MOBCAL>>batch_mobcal.txt
dir *.mfj /o:-s /b>>batch_mobcal.txt
set /a b=%filecount%
:loop
echo Number of files to run is %b%
if not exist !file.%b%! goto skip
echo !file.%b%!>mobcal.run
set str=!file.%b%!
set str=%str:mfj=out%
echo.%str%>>mobcal.run
set /A RND=!RANDOM! %% 999999 + 111111
echo.%RND%>>mobcal.run
echo.%str%>>batch_mobcal.txt
for /f "tokens=1,*" %%a in ('tasklist ^| find /I /C "mobcal.exe"') do set /a mobcalsrunning=%%a
set /a cpusfree=%ncpus%-%mobcalsrunning%
echo Number of processors free for running MOBCAL is !cpusfree!
if /i !cpusfree! LEQ 1 (
set /a b=%b%-1
echo Started %str%
echo.
mobcal
) else (
echo Spawned %str%
echo.
start /min mobcal
set /a b=%b%-1
ping 192.0.2.2 -n 1 -w 1000 > nul
)
if %b%==-1 goto skip
goto loop

:skip
```

```
timeout /t 1 >nul
tasklist|find "mobcal.exe" >nul 2>&1
if errorlevel 1 (
  goto nomobcals
) else (
  echo MOBCAL is still running
  timeout /t 1 >NUL
  goto skip
)

:nomobcals
if not exist doneoutfiles mkdir doneoutfiles >NUL
if not exist donemfjfiles mkdir donemfjfiles >NUL
cls
echo No more MFJ files, last file was %str%
echo Ended %DATE% %TIME%>>batch_mobcal.txt
echo Calculations have finished. Moving .mfj input files...
echo.
move /y *.mfj donemfjfiles
cls
call show_ccs_results.bat
echo.
echo Calculations have finished. Moving .out output files...
echo.
move /y *.out doneoutfiles
cls
echo All done

:checkfornewmfj
call Run_MultiMOBCAL_monitor.bat
```

Code for Run_MOBCAL_monitor.bat written in Microsoft Windows command shell interface

```
@echo off
: CHECKMFJ
IF EXIST drop_mfj_files_here_for_MultiMOBCAL_monitor\*.mfj (
echo MFJ files exist
cd drop_mfj_files_here_for_MultiMOBCAL_monitor
move /y *.mfj ..
cd ..
GOTO CHECKMOBCAL
) ELSE (
echo MFJ files don't exist
TIMEOUT 10 >NUL
GOTO CHECKMFJ
)
pause

: CHECKMOBCAL
timeout 10 >NUL
tasklist|find "mobcal.exe" >nul 2>&1
IF ERRORLEVEL 1 (
  GOTO CALLMOBCAL
) ELSE (
  ECHO MOBCAL is still running
  TIMEOUT 1 >NUL
  GOTO CHECKMFJ
)

: CALLMOBCAL
call MultiMOBCAL_monitor.bat
GOTO CHECKMFJ
```

Code for show_ccs_results.bat written in Microsoft Windows command shell interface

```
@echo off
echo Average PA Cross Sections =========================== >>
mobcal_summary_duplicates.txt
findstr /I /C:"average PA cross section" *.out >>
mobcal_summary_duplicates.txt

echo Average EHSS Cross Sections =========================== >>
mobcal_summary_duplicates.txt
findstr /I /C:"average EHS cross section" *.out >>
mobcal_summary_duplicates.txt

echo Average TM Cross Sections =========================== >>
mobcal_summary_duplicates.txt
findstr /I /C:"average TM cross section" *.out >>
mobcal_summary_duplicates.txt

@echo off > mobcal_summary.txt
for /f "tokens=* delims= " %%a in (mobcal_summary_duplicates.txt) do (
find "%%a" < mobcal_summary.txt > nul
if errorlevel 1 echo %%a >> mobcal_summary.txt
)

del mobcal_summary_duplicates.txt
echo A summary from .out files in this folder was created in
mobcal_summary.txt
echo.
type mobcal_summary.txt
```